

Abishek Shrestha

Evaluation of deformation pressure on shotcrete lining at the headrace tunnels caused by squeezing and swelling of rocks

Master's thesis in Hydropower Development

Supervisor: Krishna Kanta Panthi

June 2021

Abishek Shrestha

Evaluation of deformation pressure on shotcrete lining at the headrace tunnels caused by squeezing and swelling of rocks

Master's thesis in Hydropower Development
Supervisor: Krishna Kanta Panthi
June 2021

Norwegian University of Science and Technology
Faculty of Engineering
Department of Geoscience and Petroleum





Your ref.: MS/I21T60/IGP/ASKP

Date: 14.01.2021

**TGB4945 Engineering Geology - MSc thesis
for
HPD student Abishek Shrestha**

Evaluation of deformation pressure on shotcrete lining at the headrace tunnels caused by squeezing and swelling of rocks

Background

The Norwegian principle of hydropower design is to exploit self-supporting capacity of the rock mass maximum possible. The water tunnels built for hydropower projects are therefore either unlined or shotcrete lined, which means the rock mass in the periphery of the tunnel is in direct contact with water. In a water tunnel aligned through weak rocks, there exists risk of failures caused by developed plastic deformation due to schistosity, swelling and water pressure variation. Especially, the clay-bearing rocks consisting swelling minerals like montmorillonite (smectite) are sensitive to degradation once exposed to water, which may lead to expansion of the tunnel wall leading to additional support pressure. Statkraft has experienced problems of tunnel collapses in some of the international projects built in Andes Mountains and elsewhere. Hence, Statkraft through HydroCen is directly involved in the research on potential swelling and slaking extent of weak rocks such as flysch, serpentinite, andesite, and clay rich sedimentary rocks. A PhD research that addresses slake durability and swelling behavior of some such rocks.

MSc thesis task

This MSc thesis is the continuation of the PhD research completed in November 2020 and will have following main tasks:

- Critical review of the Norwegian design principles for unlined or shotcrete lined waterway systems of hydropower project.
- Literature review on the engineering geological and mechanical properties of rock mass including swelling and slaking properties of weak rocks, and stability assessment methodologies practiced worldwide.
- Present cases of tunnels associated to the collapses caused by squeezing, swelling and slaking.
- Briefly discuss about the case projects used in the assessment in this MSc thesis. Describe engineering geological and rock mass quality conditions along the headrace tunnels.

- Describe geological condition of the collapsed area and instrumented area of tunnels, present measured deformation at various tunnel chainages.
- Collect laboratory test results of the rock and shotcrete samples of the headrace tunnels.
- Evaluate in-situ stress condition based on analytical and measured stress sources and the flat-jack measurement during instrumentation.
- Carry out stability assessment of the collapsed cases by considering both plastic deformation and rock swelling. Evaluate extent of pressure built-up on the applied rock support consisting systematic bolting and reinforced shotcrete including reinforced ribs of sprayed concrete. Both analytical and numerical methods should be used for this analysis.
- Discuss long-term impacts on the stability of headrace tunnels due to deformation, swelling and dynamic water pressure.
- Conclude the work with recommendations.

Relevant computer software packages

Candidate shall use *roc-science package* and other relevant computer software for the master study.

Background information for the study

- Relevant information about the project such as reports, maps, information and data received from the supervisors and collected by the candidate.
- The information provided by the professor about rock engineering and hydropower.
- Scientific papers and books related to international tunnelling cases.
- Literatures in rock engineering, rock support principles, rock mechanics and tunnelling.

Cooperating partner

Statkraft International is the cooperating partner. Dr. Siri Stokseth and MSc Thomas Schönborn are the contact persons and co-supervisors from the Statkraft.

The thesis work is to start on January 15, 2021 and to be completed by June 11, 2021.

The Norwegian University of Science and Technology (NTNU)
Department of Geoscience and Petroleum

January 14, 2021



Dr. Krishna K. Panthi
Professor of geological engineering, main supervisor

Preface

This master thesis titled “**Evaluation of the deformation pressure on shotcrete lining caused by rock swelling and deformation at the headrace tunnel**” is submitted to the Department of Geoscience and Petroleum at the Norwegian University of Science and Technology (NTNU) as the final requirement for fulfillment of Master of Science in Hydropower Development Program (2019-2021).

The thesis focuses on the evaluation of the deformation pressure on the shotcrete lining due to rock swelling. The semi-empirical, analytical, and numerical methods have been used for the plastic deformation analysis and stability analysis for two projects: La-Higuera hydropower plant, Chile, and Moglice hydropower project, Albania. The thesis work started during the spring semester of 2021 and is submitted at the end of the spring semester of 2021 and is supervised by Prof. Dr. Krishna Kanta Panthi.



Abishek Shrestha
NTNU, Trondheim, Norway
24.06.2021

Acknowledgement

I would like to express my deepest gratitude to my supervisor Prof. Dr. Krishna Kanta Panthi and thank him especially for always being there to help and teach me. His theoretical and technical knowledge along with the valuable guidance and advice offered by him during this thesis has been valuable and motivating which helped me to keep my morale and spirit high. I would like to extend my thanks and express my appreciation towards Dr. Siri Stokseth and Mr. Thomas Schönborn from Statkraft for believing in me and for their collaboration in this thesis by providing valuable input. I am grateful to Mr. Bibek Neupane (Ph.D. fellow NTNU) who take his time from his busy schedule to help me with numerical modeling.

I am very grateful to my loving family who has always support and encouraged me. I especially like to thank my mother Ranjika Devi Shrestha for being my role model and will always be grateful for her unconditional love and support. At this moment, I also like to remember my late father, who definitely would have been proud of me. My siblings have always been my strength, who always believed in me, so I like to thank my younger brother and three elder sisters and their family for their love, trust, support, and inspiration.

It has been an unusual time as the whole world is facing a pandemic which undoubtedly has hit us hard mentally and emotionally. It is the love and support from my friends residing in different parts of the world that helped me to overcome those stressful moments. Therefore, I would like to thank all my friends for cheering me up and motivating and encouraging me to pass this hard time during my thesis. A special thanks to my Nepalese friends and Ph.D. fellow and their families in Norway, who never let me feel alone and miss my family back home.

I am grateful to the Department of Geoscience and Petroleum under which this master thesis has been carried out. I would also like to extend my thanks to the Department of Civil and Environmental Engineering and the Norwegian Agency for Development Cooperation (NORAD) for providing the opportunity and scholarship to me for pursuing my master's in Hydropower Development.

Abstract

The underground excavation in the weak rock mass is challenging as many stability problems may be encountered during the construction and operation of the underground structure. The stability problem in weak rock may occur due to high induced stress, which results in compressive failure in the underground structure known as squeezing or plastic deformation. The water tunnels constructed in sedimentary rocks with clays, clay shales, or anhydritic shales undergo the swelling phenomenon. During construction, the rock mass is exposed to a dry condition which is later filled with water during operation. In addition during the operation of the hydropower tunnels, they are often drained and then filled after inspection and maintenance which causes the cycling drying and wetting of rock mass. This process of cyclic wetting and drying in water tunnels passing through weak and heterogeneous rock mass poses is associated with stability problems due to slaking and disintegration. This work is based on the study of the methods to evaluate the stability of the tunnels constructed in weak rock mass containing swelling minerals. The headrace tunnels of two projects La-Higuera hydropower plant, Chile, and Moglice headrace tunnel, Albania are considered for the study.

The La-Higuera hydropower headrace tunnel collapsed after 9 months of operation at the area where the tunnel passes through the weakness zone and rock mass containing swelling minerals. The rock samples collected from the tunnel contain a rich amount of Laumontite of zeolite group ranging from 8.6% to 42.1%. The maximum swelling pressure obtained from the laboratory test of the rock sample was 2.7 MPa which then varied from 5% to 55% to represent the in-situ swelling pressure. The semi-empirical and analytical methods used to evaluate long-term deformation due to rock swelling pressure shows that there is a substantial increase in deformation with the increase in the magnitude of swelling pressure. The numerical modeling carried out using RS2 shows a better extent of the impact of swelling pressure on rock support. The in-situ swelling pressure exceeding 10% of the maximum swelling pressure measured at the laboratory causes a significant increase in deformation suggesting the installed rock support is under-designed to sustain the deformation which eventually leads to the tunnel collapse.

The Moglice headrace tunnel passes through the rock mass containing flysch which is susceptible to swelling and slaking which may cause tunnel instability. The maximum swelling pressure was found to be 0.24 MPa from a swelling test performed at the laboratory on the rock samples collected from the Moglice headrace tunnel. For the stability assessment of the Moglice headrace tunnel, the in-situ swelling pressure is varied from 25% to 55% of the maximum lab swelling pressure to incorporate the possible worst-case scenario. Similar methods used in the La-Higuera project assessment have been used to carry out the stability assessment of the Moglice headrace tunnel. The results of the analyses from all methods show that the deformations due to swelling pressure are very less which is unlikely to cause damage to the installed rock support. The numerical modeling performed using RS2 shows that there is no significant increase in the number of yielded liner and bolts assuring the stability of the tunnel.

Contents

1	Introduction	1
1.1	Background	1
1.2	Objective and scope	2
1.3	Methodology of the study	2
1.3.1	Literature Review	2
1.3.2	Study of the Moglice Hydropower project	3
1.3.3	Assessment of La Higuera Tunnel Collapse	3
1.3.4	Plastic deformation Analysis	3
1.3.5	Evaluation of stability and long term deformation due to swelling rock	3
1.3.6	Comparison and discussion of results	3
1.4	Limitation of the study	4
2	Norwegian design principles for hydropower tunnels	5
2.1	Introduction	5
2.2	Norwegian design principles	6
2.2.1	Updated Rule-of -Thumb	6
2.2.2	Minimum principle stress criteria	7
2.2.3	Limitations of criteria and possible improvements	8
3	Rock Mass Quality Evaluation	11
3.1	Introduction	11
3.2	Mechanical Properties of intact rock	11
3.2.1	Intact rock strength	12
3.2.2	Deformability of intact rock material	16
3.3	Failure Criteria	16
3.3.1	Generalized Hoek and Brown Criteria	16
3.3.2	Mohr-Colulomb Criteria	18
3.3.3	Relationship between Mohr-Coulomb and Hoek and Brown	18
3.3.4	Post failure behaviour	19
3.4	Discontinuities	20
3.5	Rock mass classification	21
3.5.1	The Q-system	21
3.5.2	Geological Strength Index (GSI)	22
3.6	Rock mass strength	23
3.7	Rock mass deformability	23
3.8	Rock Stresses	24
3.9	Stress distribution around tunnel	26
4	Stability Assessment Methods	28
4.1	Weak Rock Mass	28
4.2	Problems Associated with Weak Rock	29
4.2.1	Squeezing or plastic deformation	29
4.2.2	Swelling	30
4.2.3	Slaking	34

4.3	Review of stability assessment methods	35
4.3.1	Empirical methods	36
4.3.2	Semi-empirical method	36
4.3.3	Analytical Method	38
4.3.4	Numerical Modeling	45
5	Cases of failure with Tunnels in a weak rock mass	51
5.1	Laodongshan Tunnel	51
5.1.1	Project description	51
5.1.2	Project Geology	51
5.1.3	Failure due to long term deformation	52
5.2	Chacabuquito Hydropower Plant Project	53
5.2.1	Project description	53
5.2.2	Project Geology	53
5.2.3	Failure due to swelling	54
6	Assessment of La Higuera Tunnel Collapse	56
6.1	Project Description	56
6.2	Project Layout	56
6.3	Engineering Geology condition of failure zone	57
6.4	Tunnel cross section and installed Rock support	59
6.5	Mineral Content of La Higuera Rock sample	60
6.6	Mechanical Properties of Intact rock sample	60
6.7	Rock Mass Properties	61
6.8	Laboratory results of Swelling Test	62
6.9	In situ stress Assessment	62
6.10	Assessment of La-Higuera Tunnel Collapse due to Swelling Pressure	65
6.10.1	Semi-empirical and Analytical method	65
6.10.2	Numerical Modeling	69
6.10.3	Elastic analysis	70
6.10.4	Plastic analysis	71
7	Moglice Hydropower Project	82
7.1	Project description	82
7.2	Project Layout	83
7.3	Regional Geology	84
7.3.1	Project Geology	85
7.4	Instrumentation carried out in the tunnel	86
7.4.1	Geological condition of the location of Flatjacks installation	88
7.5	Rock Support	89
7.6	Assessment of Norwegian design Principle	90
7.6.1	Analysis of Norwegian Confinement criteria	90
7.6.2	Analysis of Minimum principle stress criteria	91
8	Input parameter assessment for Moglice headrace tunnel	94
8.1	Engineering geological properties	94
8.2	Mechanical properties of intact rock	95

8.2.1	Laboratory Tests Results of Moglice Rock Sample	95
8.3	Determination of Mineral content by use of XRD	97
8.4	Mechanical Properties Laboratory Testing	98
8.4.1	Uniaxial Compression Strength Test and Deformability	98
8.4.2	Point Load Test	99
8.4.3	Brazil Test	100
8.4.4	Swelling Test and Slake Durability Index (SDI)	101
8.5	Conclusion on Laboratory results	101
8.6	Mechanical Properties of clay stone	102
9	Estimation of rock mass parameters for Moglice headrace tunnel	103
9.1	Input data	103
9.2	Back calculation	104
9.3	Rock mass strength	105
9.4	Rock mass deformation modulus	106
9.5	Tectonic Stress	106
9.5.1	Model setup and Input parameters	108
9.5.2	Definition of misfit	109
9.5.3	Existence of tectonic stresses	110
9.6	Estimation of In situ stress condition	113
9.6.1	Model Setup	114
10	Plastic Deformation Analysis of Moglice headrace tunnel	117
10.1	Convergence confinement method (CCM)	117
10.2	Hoek and Marinos (2000) method	120
10.3	Pantheni and Shrestha (2018) method)	121
10.4	Numerical Modeling	123
10.4.1	Elastic Analysis	123
10.4.2	Plastic Analysis	127
11	Stability Assessment of Moglice headrace tunnel due to Swelling Pressure	135
11.1	Convergence Confinement Method (CCM)	135
11.2	Hoek and Marinos (2000) method	136
11.3	Pantheni and Shrestha (2018) method	137
11.4	Numerical Modeling	138
12	Discussion	144
12.1	Discussion on Norwegian Design Principle	144
12.2	Discussion on La-Higuera Failure Assessment	144
12.3	Discussion on Plastic deformation Analysis	144
12.4	Discussion on impact of swelling pressure on rock support	147
12.5	Discussion on long term deformation due to rock swelling	147
13	Conclusion and Recommendation	151
13.1	Conclusion	151
13.2	Recommendation	152

References	161
A Standard Charts and Figures	162
A.1 Determination of mi Hoek and Marinos (2000)	162
A.2 GSI for Jointed Rock Hoek and Marinos (2000)	163
A.3 GSI for Heterogeneous masses such as flysch Hoek and Marinos (2000) .	164
A.4 Disturbance factor Hoek et al. (2002)	165
B Numerical Modeling Results	166
B.1 Plastic deformation and long-term deformation due to swelling pressure at Chainage 7+064	166
B.2 Plastic deformation and long-term deformation due to swelling pressure at Chainage 7+092	167
B.3 Plastic deformation and long-term deformation due to swelling pressure at Chainage 7+136	168
B.4 Plastic deformation and long-term deformation due to swelling pressure at Chainage 7+168	169
B.5 Plastic deformation and long-term deformation due to swelling pressure at Chainage 7+194	170
B.6 Plastic deformation and long-term deformation due to swelling pressure at Chainage 7+218	171
B.7 Plastic deformation and long-term deformation due to swelling pressure at Chainage 7+266	172
B.8 Plastic deformation and long-term deformation due to swelling pressure at Chainage 7+291	173
B.9 Plastic deformation and long-term deformation due to swelling pressure at Chainage 7+316	174
B.10 Plastic deformation and long-term deformation due to swelling pressure at Chainage 7+342	175

1 Introduction

1.1 Background

The stability of the underground structure highly depends on the properties of the rock mass. The stability of the underground structure in weak rock mass depends predominantly on the materials themselves whereas in hard rock mass the stability is controlled by the major discontinuities (Ulusay et al., 2013; Selen, 2020). The study for this Master's thesis focuses on the stability problem of hydropower tunnels in a weak rock mass. The construction of especially the hydropower tunnels in rock mass containing the swelling minerals is prone to face stability problems due to swelling and slaking. The tunnels constructed in sedimentary rocks with clays, clay shales, or anhydritic shales undergo the swelling phenomenon (Steiner, 1993) as these minerals when came in contact with water result in an increase in volume and the expansion will then increase the stress in rock (Vergara and Triantafyllidis, 2016). The hydropower tunnels are filled and emptied at regular intervals for maintenance, which causes cyclic wetting and drying of the surrounding rock mass of the tunnel. The tunnel faces the stability problem due to slaking which is associated with the weakening and disintegration because of wetting and drying of weak and clay-bearing rock (Panthi, 2006). Therefore, this master thesis is carried out to evaluate the impact of rock swelling pressure on the shotcrete lining of the hydropower tunnel. The study is carried out on two hydropower projects, La-Higuera hydropower plant tunnel, Chile, and Moglice hydropower tunnel, Albania.

La-Higuera hydropower project is a run-of-river hydropower plant of capacity 156 MW located within the Tinquirrica valley approximately 170 km south of Santiago, Chile which generates average annual energy of 811 GWh. The La-Higuera headrace tunnel collapses in 2011 after some time of power production (Broch and Palmstrom, 2017). At the location of collapse, it was found that the tunnel passes through the weakness zone and the rock mass has swelling potential as it contains the swelling minerals which are associated with zeolite group (Broch and Palmstrom, 2017). Therefore, the assessment is carried out on the La-Higuera headrace tunnel collapse to evaluate how the rock swelling pressure impacts the installed rock support that leads to a tunnel collapse. For this, the evaluation of the deformation of tunnel cross-section due to swelling of surrounding the rock mass is carried out.

Statkraft has completed construction of the Moglice Moglice hydropower project which is located at Korce and Elbasan districts in Albania and started the operation in the year 2020. The Moglicë plant is the upper and biggest of the three plants constructed in Devoll river with an installed capacity of 197 MW and generates average annual energy of 450GWh (Statkraft, 2021). The length of the Moglice headrace tunnel is 10.7 km which passes through the rock formation consisting of ophiolite, serpentinite, and flysch. The area where the headrace tunnel passes through the rock mass containing flysch is susceptible to possess the tunnel stability problem due to swelling and slaking. The flysch rock mass is relatively weak, deformed, thinly layered, laminated, and folded and is composed of swelling minerals. Skatkraft in past has experienced the problem of tunnel collapses in some of the international projects built in the Andes Mountains and other parts of the world. Hence, Statkraft through HydroCen has funded Ph.D. research which

was completed in November 2020 addressing slake durability and swelling behavior of such rocks and this MSc thesis is the continuation of the same completed Ph.D. research.

1.2 Objective and scope

The MSc thesis is the continuation of the completed Ph.D. research in November 2020 and the main objectives of the study are as follows:

- Evaluation of the deformation pressure on shotcrete lining caused by rock swelling
- Evaluation of the long-term deformation at the headrace tunnel of Møglice Hydropower Project due to rock swelling

The scope of the study is determined by the task assigned for the master's thesis. Following are the main tasks for the study of this Master thesis:

- A review of the Norwegian design principles practiced design of unlined or shotcrete lined waterway systems
- Literature review on the swelling and slaking properties of different rocks, engineering geological and mechanical properties of weak rock mass, and stability assessment methodologies practiced
- A case study of tunnel collapses caused by squeezing, swelling, and slaking
- A brief description of the Moglice Hydropower Project and engineering geological conditions along the headrace tunnel alignment along with the geological condition of the instrumented area and tunnels section where deformation measurement was carried out
- Collection of previously conducted laboratory test results of the rock and shotcrete samples brought from the headrace tunnel
- Assessment of in-situ stress condition based on measured stress sources and the flat-jack measurement during instrumentation
- Extensive assessment on the impact of swelling pressure on the applied rock support consisting of reinforced ribs of sprayed concrete and systematic bolting
- Evaluation of extent of deformation and discuss the long-term impact on the stability of headrace tunnel due to deformation caused by swelling

1.3 Methodology of the study

For conducting this MSc thesis to fulfill the objectives and to deliver the scopes as mentioned in Chapter 1.2, a methodology has been followed. The applied methodology has been described as follows:

1.3.1 Literature Review

A literature review of literature related to Norwegian design principles for hydropower tunnels, rock mechanical properties, tunnel stability problem, methods to evaluate rock

mass properties, stability problem in weak rock mass, and stability assessment methods has been considered. In addition, numerical investigation methodology is also reviewed. The materials for the literature review are considered from scientific papers, doctoral thesis, lecture notes and books, and previous studies related to the research topic.

1.3.2 Study of the Moglice Hydropower project

A review on the Moglice Moglice Hydropower Project and its engineering geological conditions along the headrace tunnel alignment along with the geological condition of the instrumented area and tunnels section where deformation measurement was carried out based on the project reports and relevant sources.

1.3.3 Assessment of La Higuera Tunnel Collapse

The headrace tunnel of the La Higuera hydropower plant located in Chile has collapsed after almost 9 months of operation. The failure is associated with the swelling rock mass present in the project location. A detailed assessment of tunnel collapse due to swelling pressure has been carried out.

1.3.4 Plastic deformation Analysis

The plastic deformation analysis of the Moglice headrace tunnel passing through the flysch rock mass has been done using various methods are described below:

- Semi empirical method: Hoek and Marinos (2000) method
- Analytical methods: Convergence Confinement method (CCM) (Carranza-Torres and Fairhurst, 2000) and Panthi and Shrestha (2018) method
- Numerical Modeling

1.3.5 Evaluation of stability and long term deformation due to swelling rock

The stability assessment due to deformation pressure on shotcrete lining caused by rock swelling and the evaluation of long-term deformation at the headrace tunnel of Mógica Hydropower Project have been done using following methods:

- Semi empirical method: Hoek and Marinos (2000) method (modified for introducing swelling pressure from rock mass)
- Analytical methods: Convergence Confinement method (CCM) (Carranza-Torres and Fairhurst, 2000) and Panthi and Shrestha (2018) method (modified for introducing swelling pressure from rock mass)
- Numerical Modeling

1.3.6 Comparison and discussion of results

The results from the analyses of plastic deformation and stability assessment due to swelling rock pressure using different methods have been compared and interpreted. The discussion is made on the applicability, limitations, and estimated results of each method.

1.4 Limitation of the study

The main limitation of the study is to establish input parameters for the analysis. For the La-Higuera hydropower project, the availability of information was limited. The available geological maps, laboratory test results are used to establish the input parameters. Due to the unavailability of information regarding the measured deformation at La-Higuera, the verification of the results on plastic deformation analysis was not possible. In the case of the Moglice headrace tunnel, the study focuses on the part of the headrace tunnel passing through the flysch rock mass. Flysch rock mass is defined as a rock mass with a sequence of varying alternations of clastic sedimentary rocks (Peranić and Arbanas, 2020). The study area of the headrace tunnel passes through layers containing weak rock masses containing claystone and siltstone and a variable proportion of hard rock. The weak rock content is dominating in the study area but the content varies from section to section. Because of the presence of dominating weak rock content, the weighted input parameters are needed to be established based on the proportion of weak rock content which is harder to measure. The weak rock content is thus considered based on Almenara (2021) article on "Analysis of plastic deformations in weak rock masses of flysch an evaluation based on a hydropower tunnel in Albania".

2 Norwegian design principles for hydropower tunnels

2.1 Introduction

In unlined tunnels, there is direct contact of water with the rock where limited parts that are in significance to collapses due to various factors are either lined with concrete or shotcrete to prevent local collapse or rock falls (Broch and Palmstrom, 2017). In over 100 years, Norway has constructed more than 4000 km length unlined pressure shafts and tunnels with the maximum static head of 1047 m reached at unlined pressure tunnel of Nye Tyin project where stress is equivalent to 10.5 MPa (Basnet and Panthi, 2018). According to Panthi and Basnet (2016), about 95% of the waterway length of Norwegian hydropower schemes is unlined. Herlandsfoss hydro plant constructed in the 1920s, is the first experience of unlined pressure tunnel (Broch and Palmstrom, 2017). Over more than 100 unlined tunnels and shafts have been constructed and are in operation with a static head of higher than 150 m (Hveding et al., 1992). Figure 2.1 shows the generalized layout of successful unlined shafts and pressure shafts implemented by Norway for different net hydropower schemes (Basnet and Panthi, 2018).

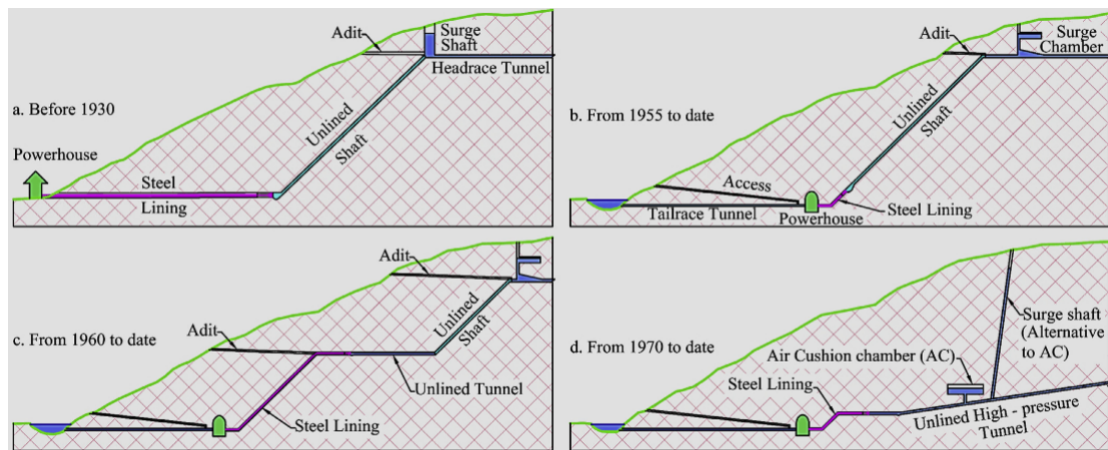


Figure 2.1: Layout of unlined pressure tunnels and shafts in different hydropower schemes of Norway (extracted from Panthi and Basnet (2016))

The construction of unlined pressure tunnels is also practiced all over the world as it provides cost-effective solutions for hydropower schemes (Panthi and Basnet, 2021). Lower Kihansi hydropower in Tanzania, as Lajas project in Chile project, Venda Nova II and Venda Nova III in Portugal, and Upper Tamakoshi Hydro-electric project in Nepal have implemented the Norwegian design principle in the design of unlined pressure tunnels and shafts (Basnet and Panthi, 2018).

The rock mass itself is a natural concrete and can resist the load exerted on it if it is massive with no significant fracturing. However, this exception cannot be met in the field due to the presence of various weakness zones (Panthi, 2014). For the construction of an unlined waterway, good geological conditions are required. Therefore it is important to avoid karstic areas, heavily jointed rock masses and open, inter-communicating joints, weakness zones and faults with unfavorable orientation, and impermeable rock layers or clay zones between the tunnel or shaft and the surface (Nilsen and Thidemann, 1993). If

the normal stresses across all discontinuities in the rock masses is lower than the water pressure, hydraulic jacking of the discontinuities may take place leading to the leakage from tunnel or shaft (Nilsen and Thidemann, 1993). Hence it is important to make sure that due to water pressure no deformation occurs in the surrounding rock masses.

2.2 Norwegian design principles

Design criteria have been continuously revised during the development over the years. The first rule of thumb used for the design of unlined hydropower tunnels before 1968 is shown in Equation 2.1. According to this rule of thumb for every point in the tunnel, the vertical rock cover (h) from the tunnel should be greater than the hydrostatic head (H) multiplied by a factor c (Basnet and Panthi, 2020). The constant c ranges from 0.6 to 1.0, where 0.6 for valley sides with inclinations up to 35° and increased 1.0 for the valley sides of 60° . The inclination of unlined shafts may be varied from 31° to 47° and 45° being most common because of construction reasons (Broch, 1984).

$$h > c.H \quad (2.1)$$

Later, the failure occurred in Byrte hydropower plant unlined tunnel which flooded the underground powerhouse in 1968, demands the new approach for the design (Broch and Palmstrom, 2017). The rule of thumb is then updated as explained in Chapter 2.2.1.

2.2.1 Updated Rule-of -Thumb

With the experience gained from the completed projects and failure of the Byrte hydropower plant in 1968, a new rule of thumb was introduced which will also cover steeper shafts than commonly used 45° (Selmer-Olsen, 1969). According to Selmer-Olsen (1969), the new rule of thumb is developed with the concept that the ground pressure given by vertical rock cover should be greater than the water pressure to avoid hydraulic jacking. In reference to the parameters shown in Figure 2.2, the new rule of thumb is defined by the Equation B and corresponding factor of safety (FoS_1) is given by Equation 2.3. According to Basnet and Panthi (2020), the rule of thumb set by Equation B is based on the principle that vertical pressure from rock mass above the tunnel is sufficient to prevent the tunnel from water pressure acting on it. The rule of thumb is limited to the application at relatively flat surface which may not always the case for every hydropower tunnel rather depends on the topography of the location.

$$h > \frac{\gamma_w.H}{\gamma_r.\cos \alpha} \quad (2.2)$$

$$FoS_1 = h \times \left(\frac{\gamma_r.\cos \alpha}{\gamma_w.H} \right) \quad (2.3)$$

Where h is the vertical rock cover above the tunnel, H is the hydrostatic head acting in the tunnel, γ_w is density of water, γ_r = density of rock mass, and α is the inclination of the shaft/tunnel with respect to the horizontal as shown in Figure 2.2.

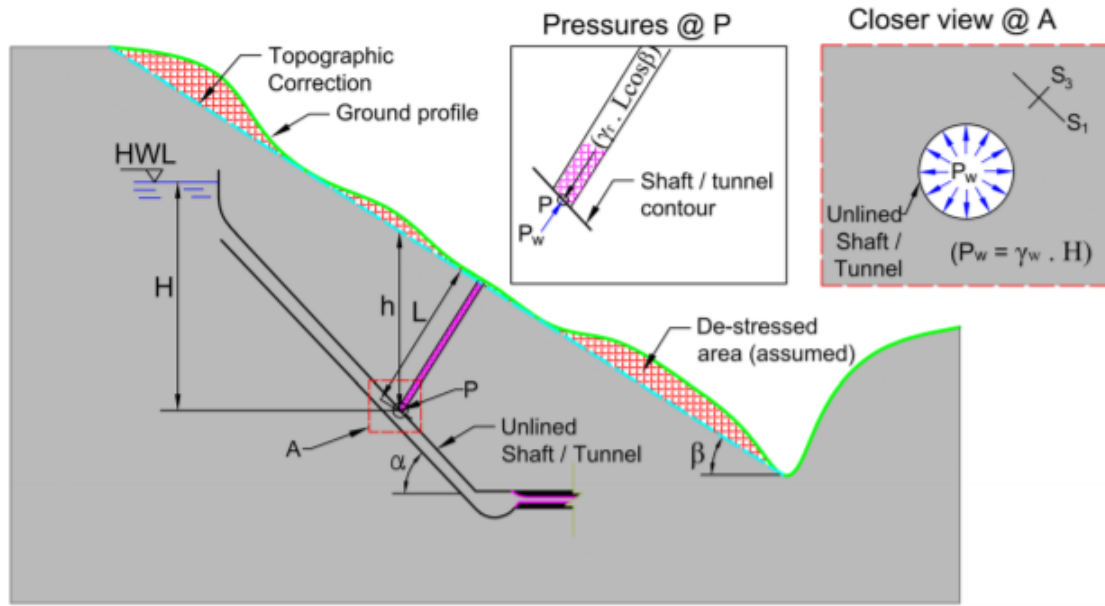


Figure 2.2: Different parameters used in different design criteria for unlined shaft/tunnel. S_3 is the minimum principal stress (Basnet and Panthi, 2020)

In 1970, the unlined pressure tunnel at the Åskora plant designed using criteria defined by Equation B failed due to hydraulic splitting. After this failure new rule of thumb was introduced where the inclination of the valley side was directly taken into account (Broch, 1984). The rule of thumb can be expressed as Equation A.4 and corresponding factor of safety (FoS_2) is represented by Equation 2.5. According to Basnet and Panthi (2020), the rule of thumb defined by Equation A.4 incorporates the slope of topography and calculates the resisting ground pressure against water pressure.

$$L > \frac{\gamma_w \cdot H}{\gamma_r \cdot \cos \beta} \tag{2.4}$$

$$FoS_2 = L \times \left(\frac{\gamma_r \cdot \cos \beta}{\gamma_w \cdot H} \right) \tag{2.5}$$

where, L is the shoretrest distance between the surface and the point of study (in m), and β is average inclination of valley side as shown in Figure 2.2.

The rule of thumb defined by Equation B and Equation A.4 are known as the the Norwegian criteria for confinement (Selmer-Olsen, 1969). In Basnet and Panthi (2020), it has been highlighted that all over the world the Norwegian criteria for confinement have been accepted and are widely used for the planning and design of the unlined pressure shafts and tunnel.

2.2.2 Minimum principle stress criteria

Norwegian confinement criteria are developed based on two-dimensional geometry of terrain which fails to fully represent the engineering geology of project location and in-situ stress condition induced in unlined pressure tunnels or shafts (Basnet and Panthi,

2020). In 1984, a new criterion has been introduced which incorporates the topographic correction which was required to refine the geometric parameters represented by a de-stressed area in Figure 2.2 (Broch, 1983). The criteria defined by Equation 2.6 is the state-of-art and the corresponding factor of safety is represented by Equation 2.8. The principle for criteria defined by Equation is based on the concept that the rock mass lying outside the topographic correction i.e. the de-stressed area as shown in Figure 2.2 have no contribution to the confinement (Basnet and Panthi, 2020). To prevent the hydraulic jacking, the in-situ minimum principal stress (S_3) should always be greater than the water pressure inside the tunnel ((Selmer-Olsen, 1974);(Broch, 1983); (Basnet and Panthi, 2018)). According to (Basnet and Panthi, 2020)), the criteria set by Equation A.4 was not adequate to incorporate the requirement of minimum principal in-situ stress to prevent hydraulic jacking in some Norwegian projects, which require a new concept of minimum principal stress criteria as represented by Equation 2.6 is made after the 1970s.

$$S_3 > P_w \tag{2.6}$$

$$FoS_3 = \frac{S_3}{P_w} \tag{2.7}$$

2.2.3 Limitations of criteria and possible improvements

The use of state-of-art criteria requires the assessment of minimum principal stress that can be established either by the field measurement or by numerical modeling but during the planning phase the assessment using either of these methods is not possible (Panthi et al., 2018). Therefore, Norwegian confinement criteria can be used during planning. However, Panthi et al. (2018) describe the favorable and unfavorable conditions for the application of Norwegian confinement criteria as presented in Table 7.6 and for the application even for unfavorable conditions, preliminary design criteria are needed.

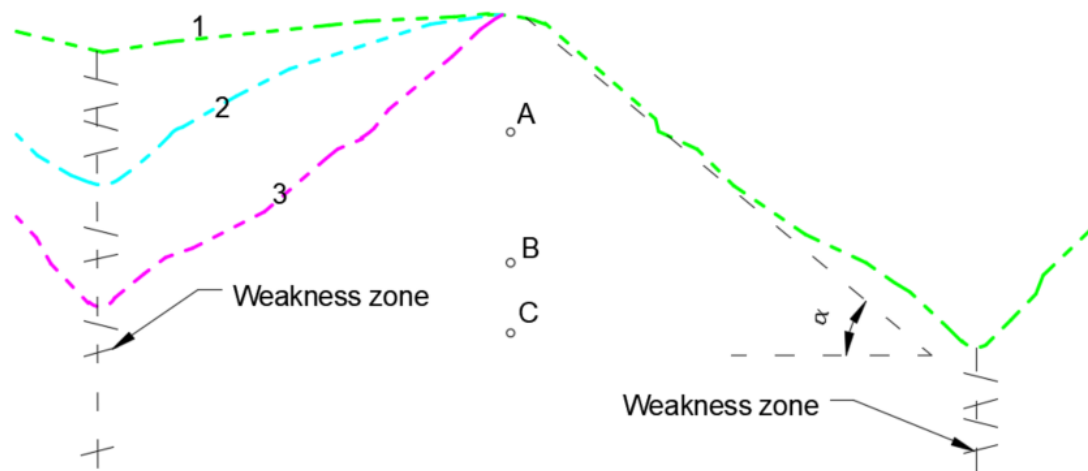


Figure 2.3: Different topographical conditions and tunnel locations and weakness zone[(Redrawn after Panthi et al. (2018)]

Table 2.1: Favorable and unfavorable ground conditions for the applicability of Norwegian confinement criteria (Panthi et al., 2018)

Category	Favorable conditions	Unfavorable conditions
Topography	Relatively gentle valley slope topography	Deep, steep and complex valley slope topography
Rock mass and Jointing	Homogeneous and strong rock mass formations with no or single joint set having tight joint wall, wide spacing and anti-dip against valley slope	Weak rock mass with high degree of schistosity; Highly porous rock mass of volcanic and sedimentary origin; Jointed rock mass having more than two systematic and long persisting joint sets with one or more joint sets dipping steeply towards valley slope; Pre-existing open joints or the joints filled with sand and silt, which could easily be washed away; Sub-horizontal joints at low overburden area
Faults and weakness/ crushed zones	No nearby major faults and weakness zones	Nearby fault and weakness zones that are parallel or cross-cutting to the valley slope
In situ stress state	The minimum principal stress always higher than the static water head	De-stressed area and location not far away from steep valley slope topography; Not sufficiently far away from the locally overstressed areas
Hydrogeology	Hydrostatic water line below natural groundwater table or tunnel aligned deep into the rock mass and far away from the steep valley slope restricting flow paths to reach valley slope topography	Hydro-static line above the groundwater table and relatively near from the valley side slope; Highly permeable and communicating joint sets

Hence this according to Panthi et al. (2018) can be done by the analysis of stress state and the fluid flow at different topography, geology, and geo-tectonic condition with considerations providing to every possible factor affecting the results of existing confinement criteria. In Figure 2.3, different geological conditions are shown that can be found while planning unlined tunnels around the world. Topography 1 and 2 are most common for the Scandinavia whereas 2 and 3 are topography which is usually found in the Himalayan region and most cases a deep river valley is present as shown in Figure 2.3 of slope α . The slope in the Himalayas varies from 35° to 40° (Panthi et al., 2018). In addition the location of the tunnel represented by A, B, and C may vary which will then depending on the location will affect the static water head. Panthi et al. (2018) has therefore proposed a state-of-art modification in the Norwegian confinement criteria as represented by Equation 2.8, that can be used for preliminary design of an unlined pressure tunnel /shaft in the geological and geotectonic environment as in the Himalayan region represented by topography 2 and 3. The Norwegian confinement criteria is multiplied by a factor (f_g) which varies from 1.6 to 3 to address another additional valley in comparison to a single valley that prevails in Scandinavia.

$$L > f_g \times \frac{\gamma_w \times H}{\gamma_r \times \cos\beta} \quad (2.8)$$

3 Rock Mass Quality Evaluation

3.1 Introduction

In engineering geology, rock and rock mass are two different terms. It is important to distinguish between rock and rock mass for the further discussion of their mechanical and physical properties. Rock also term as an intact rock is the part of the rock mass. A rock is a heterogeneous material composed of minerals. Hence, the properties of rock depend on its mineral composition. In terms of mineral composition, rock can be termed as homogeneous material but as the properties of the rock are different in different directions, it is an an-isotropic material. The physical and mechanical properties of rock depend on mineral composition, size, shape, orientation of the minerals, and also the mineral binding forces (Nilsen and Thidemann, 1993). The rock mass on the other hand is the in-situ material that contains intact rock along with all joints and discontinuities. Hence, the rock mass properties are slightly different than intact rock due to the presence of weakness zones (Nilsen and Thidemann, 1993).

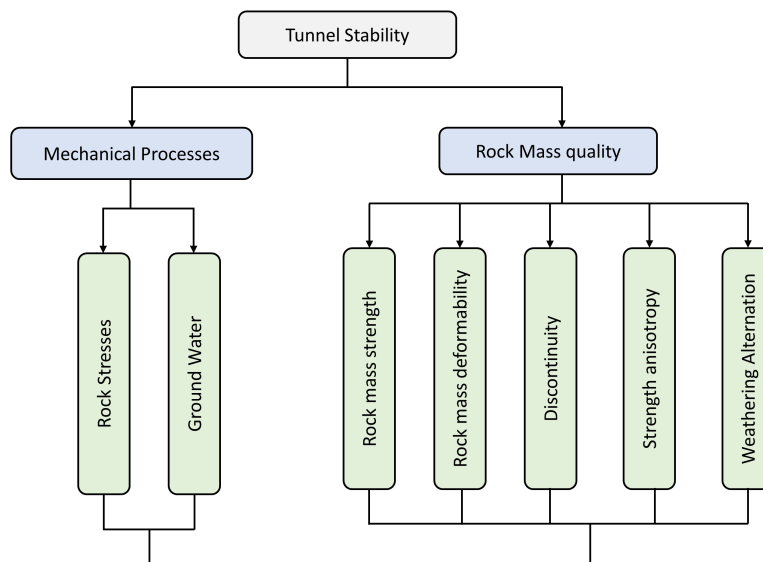


Figure 3.1: Factors affecting tunnel stability.[Extracted and redrawn after Panthi (2006)]

A rock mass can be characterized with two main features; rock mass quality and mechanical processes acting on the rock mass (Panthi, 2006). According to Panthi (2006), these two features are interlinked with each other. The stability of underground structure is the function of of these features as shown in Figure 3.1. Also, shape, size, location and orientation of an underground structure which are project specific influence on the stability of tunnel.

3.2 Mechanical Properties of intact rock

The main mechanical properties of an intact rock are strength, elasticity, and deformability. Laboratory experiments can be performed on a rock sample to quantify its mechanical properties. The determination of the various type of strengths such as compressive and

tensile are intended for the classification and characterization of intact rock. Compressive strength can be determined using the laboratory methods like the uniaxial compressive strength (UCS) test and point load test. The triaxial test on the other hand is used to find the uniaxial tensile strength of rock specimen.

3.2.1 Intact rock strength

The uniaxial compressive strength (UCS) represented as σ_{ci} of a rock specimen can be determined using the uniaxial compressive strength (UCS) test in a laboratory. A cylindrical test specimen is subjected to axial load until the failure occurs. The maximum load that is applied on the specimen before the failure occurs is then divided with the original cross-sectional area to determine the uniaxial compressive strength (Bieniawski and Bernede, 1979).

The point load test is used as an index test for the strength classification of rock materials as shown in Table 3.1. By using the correlation other strength parameters such as uniaxial compressive strength can be computed. The point Load Strength Index ($I_{S(50)}$) can be measured from the test (Franklin, 1985) and to compute UCS point load index is multiplied with correlation factor (K_{50}) as suggested by Table 3.2. The Strength anisotropy Index (I_a) of rock specimen can be computed as the ratio of greatest and least Point Load Strengths in directions (Franklin, 1985).

Table 3.1: Classification of Intact Rock based on Strength (Hoek and Brown, 1997)

Term	Uniaxial Compressive Strength UCS (MPa)	Point Load Index (MPa)
Extremely Weak	<1	-
Very Weak	1-5	-
Weak	5-25	-
Medium Strong	25-50	1-2
Strong	50-100	2-4
Very Strong	100-250	4-10
Extremely Strong	>250	>10

Table 3.2: Correlation between UCS and Point Load Index (Nilsen and Palmstrom, 2000)

Compressive Strength σ_{ci} (MPa)	Point Load Strength $I_{S(50)}$ (MPa)	Suggested value of K_{50}
25-50	1.8-3.5	14
50-100	3.5-6	16
100-200	6-10	20
>200	>10	25

The uniaxial tensile strength σ_t can be measured using Brazil Test. This is an indirect test for the measurement of tensile strength. The test is based on the fact that in the biaxial field stress fields, rock specimen fails in tension at their uniaxial tensile strength when one principal stress is tensile and the other one is compressive principal stress with a magnitude which does not exceed three times of tensile stress (ISRM, 1977).

The UCS of intact rock (σ_{ci}) is very useful to compute the rock mass strength. Many authors over the year have provided various relations that relate the intact rock strength with rock mass strength as discussed in Chapter 3.6. Various factors affect the strength of intact rock. The factors that affect the intact rock strength are the Size of a specimen, strength anisotropy, water effect, and weathering & alteration.

Effect of size

Intact rock is part of rock mass and specimen prepared from that intact rock is smaller. Rock in general composed of crystals and grains in a fabric that includes cracks and fissures. When a small specimen is used to estimate strength, they contain relatively few cracks. New crack growth occurs as they are subjected to failure load. But, the rock mass in the field is loaded with larger stresses and preexisting cracks may be present in a critical location. Thus, rock strength is size-dependent (Goodman, 1989).

The study by Hoek and Brown (1997) for the strength of different rock samples concerning varying sample sizes shows the decrease in strength with increase in sample size as shown in Figure 3.2. According to Panthi (2006), the size effect on on crystalline unweathered rocks is relatively small in comparsion to highly schistose, foliated, and deformed sedimentary and metamorphic rocks.

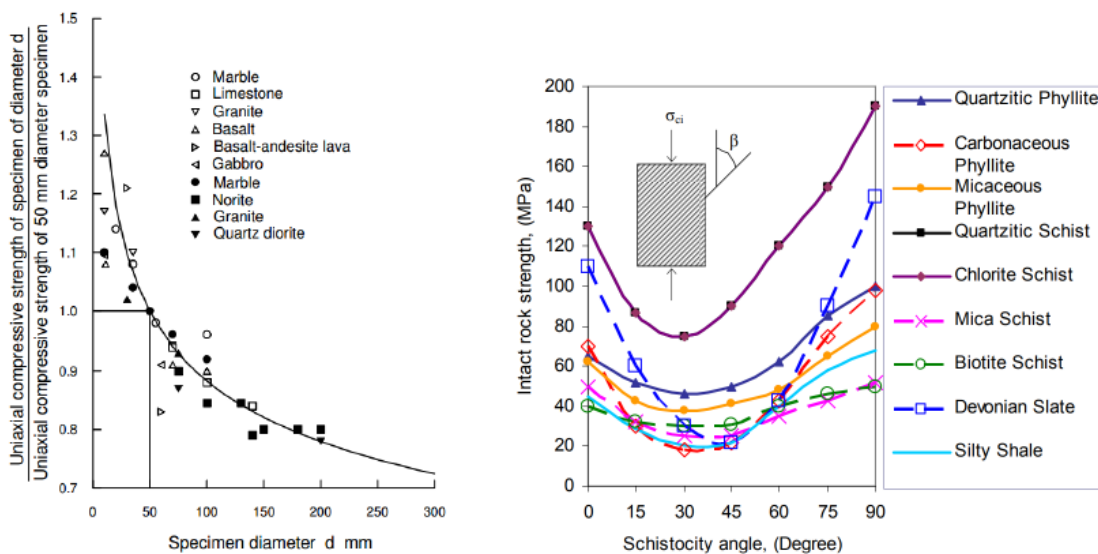


Figure 3.2: Size effect on the strength of an Intact rock extracted from Hoek and Brown (1997) (left) and Uniaxial compressive strength at different angle of Schistosity extracted from Panthi (2006) (right)

Effect of anisotropy

Strength anisotropy is defined as the variation of compressive strength according to the direction of principal stress. The composition of rocks with parallel arrangements of flat minerals like mica, chlorite, and clay or long minerals like hornblende is indicated by strength anisotropy (Goodman, 1989). As per Panthi (2006), the rock can be clasified into five categories as shown in Table 3.3, based on the strength anisotropy index (I_a). The

classification shows that the degree of anisotropy depends on the quantity and arrangement of flaky and prismatic or anisotropic minerals like mica, chlorite, talc, etc.

Table 3.3: Classification of rock strength anisotropy (Panthi, 2006)

Class	Descriptive Class	Strength anisotropy Index (I_a)	Typical rock types
I	Isotropic or close to Isotropic	1.0 – 1.2	Rocks having platy/prismatic minerals <10% with shape factors <2 and platy minerals in random orientation. Rock Types: Most of the igneous rocks and very high-grade metamorphic rocks, i.e. diorite, granite, gabbro, quartzite, granitic gneiss, granulite, etc.
II	Slightly anisotropic	1.2 – 1.5	Rocks having platy/prismatic minerals 0 – 20% with shape factors 2-4 and platy minerals in compositional layering. Rock Types: High-grade metamorphic rocks and some strong sedimentary rock, i.e. quartz-feldspatic gneiss, marble, migmatite, sandstone, limestone, etc.
III	Moderately anisotropic	1.5 – 2.5	Rocks having platy/prismatic minerals 20 – 40 % with shape factors 4-8 and foliation plane distinctly visible. Rock Types: Medium-high grade metamorphic rocks, i.e. mica gneiss, quartzitic schist, mica schist, biotite schist, etc.
IV	Highly anisotropic	2.5 – 4.0	Rocks having platy/prismatic minerals 40 – 60% with shape factors 8-12 and very closely foliated. Rock Types: Low - medium grade metamorphic rocks such as phyllite, silty slate, etc.
V	Extremely anisotropic	>4.0	Rocks having platy/prismatic minerals >60% with shape factors >12 and fissile rocks. Rock Types: Low grade metamorphic and argillaceous sedimentary rock, i.e. slate, carbonaceous phyllite, shale, etc.

The UCS of intact rock is greatest when the schistosity plane is perpendicular ($\beta = 90^\circ$) to the direction of loading and smallest when the plane is inclined at an angle 30° as shown in Figure 3.2 (Panthi, 2006). The measurement of UCS done diametrically and axially to weakness plane give approximately same maximum strength giving false impression of an isotropic material (Broch, 1983). According to Panthi (2006), the schistose rock consisting of minerals like mica, biotite/muscovite, chlorite, graphite, and talc have considerable strength anisotropy.

Effect of water

The sensitivity of water content is highly variable for different types of rock. The in-

fluence of moisture content is significant on the strength of rock. According to (Dyke and Dobereiner, 1991), the reduction in strength with an increase in moisture content involves the variation in cohesion angle and friction of granular material. The experiments on three quartz on arenites ranging the UCS from 34 to 70 MPa by Dyke and Dobereiner (1991), for the moisture content effect shows the reduction of strength varied from 24 to 34 % of dry strength. The sensitivity to moisture content variation for weaker sandstone is found to be more. (Hawkins and McConnell, 1992) experiments on the thirty-five different sandstones sampled from 21 localities within the British Isles show that for most cases, strength reduction occurs for the moisture content of 0 to 1%. Also, secant Young’s modulus decreases from the dry state showing the effect of moisture content on deformability. The statistical analysis done by Vásárhelyi (2003) to see the relation between saturated strength and dry UCS of sandstone on the Hawkins and McConnell (1992) data shows the overall best fit linear regression is represented by Equation 3.1.

$$\sigma_{ci,sat} = 0.759\sigma_{ci,dry} \tag{3.1}$$

Effect of weathering

Weathering causes the reduction in strength, deformability, slaking durability, and frictional resistance of rock mass, whereas at the same time increases the permeability. The weathering shows a reducing effect on rock mass properties as porosity, density, tensile strength, UCS, and elasticity modulus (Panthi, 2006). According to Panthi (2006), there is considerable variation in UCS with weathering grade as shown in Figure 3.3 (Left) and reduction of the strength of intact rock strength as shown in Figure 3.3 (Right). The 40% of strength reduction may occur by moderate weathering in sedimentary and meta-sedimentary rocks and 80% in crystalline rocks. Barton et al. (1978) classifies the weathering in six categories as shown in Table 3.4.

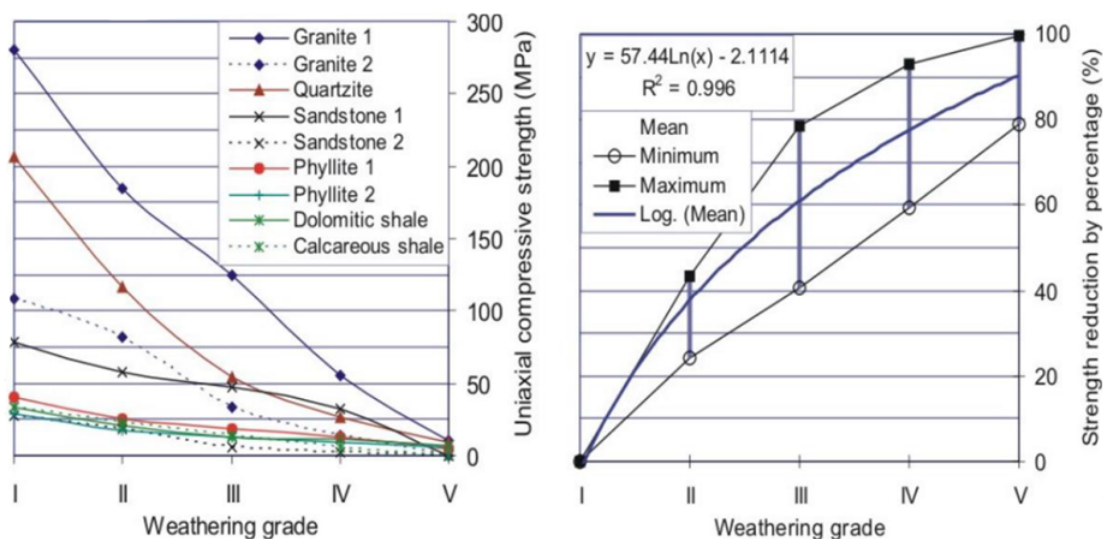


Figure 3.3: Compressive strength of rock (Left) and Strength reduction in % (Right) for different weathering grade (Panthi (2006))

Table 3.4: Classification of Weathering according to ISRM, 1978 (Panthi (2006))

Term	Description of mass condition	Weathering grade
Fresh rock	No visible sign of rock material weathering; perhaps slight discolouration on major discontinuity surfaces.	I
Slightly weathered	Discolouration indicates weathering of rock material and discontinuity surfaces. All the rock material may be discoloured by weathering and may be somewhat weaker externally than in its fresh condition.	II
Moderately weathered	Less than half of the material is decomposed and/or disintegrated into the soil. Fresh or discolored rock is present either as a continuous framework or as corestones.	III
Highly weathered	More than half of the rock material is decomposed and/or disintegrated into the soil. Fresh or discolored rock is present either as a discontinuous framework or as corestones.	IV
Completely weathered	All rock material is decomposed and/or disintegrated into the soil. The original mass structure is still largely intact.	V
Residual soil	All rock material is converted to the soil. The mass structure and material fabric are destroyed. There is a large change in volume, but the soil has not been significantly transported.	VI

3.2.2 Deformability of intact rock material

The deformability of intact rock is described by the elastic modulus (E_{ci}) also known as Young's Modulus. The modulus of elasticity of intact rock (E_{ci}) is defined as the ratio of stress to strain corresponding to load imposed. The elastic modulus is the gradient of the stress-strain curve obtained from the UCS test. The secant Young's Modulus consider as Young's modulus of intact rock is measured from the zero stress some fixed percentage of ultimate strength usually at 50% (Bieniawski and Bernede, 1979).

3.3 Failure Criteria

The failure of rock mass indicates the loss in integrity of rock mass causing its collapse. As failure occurs rock mass losses the load-carrying capacity. The variation of peak stress σ_3 with the confining pressure σ_3 is known as a criterion of failure (Goodman, 1989). Various failure criteria have been introduced over the year such as Mohr-Coulomb; Hoek and Brown; Modified Lade; Modified Wiebols and Cook; Mogi and Drucker- Prager. The Mohr-Coulomb and Hoek and Brown are the most used failure criteria. The reason is the simplicity of methods and their extensibility (Mehranpour and Kulatilake, 2016). Hence Mohr-Coulomb and Hoek and Brown Criteria have been discussed in this chapter.

3.3.1 Generalized Hoek and Brown Criteria

Generalized Hoek and Brown criteria is a nonlinear failure criterion that shows the empirical relationship based on fitting of parabolic curves in a triaxial test data (Nilsen and Thidemann, 1993) developed to provide input data for stability assessment of tunnel in a jointed and schistose rock mass (Hoek et al., 2002). The Generalized Hoek- Brown

criteria for jointed rock mass is defined as Equation 3.2 (Hoek and Brown, 1997).

$$\sigma_1' = \sigma_3' + \sigma_{ci} \left(m_b \frac{\sigma_3'}{\sigma_{ci}} + s \right)^a \tag{3.2}$$

Where σ_1' and σ_3' are the maximum and minimum effective stresses at failure respectively, m_b is the value of Hoek-Brown constant m for the rock mass, s and a are constants depend upon the characteristics of rock mass and σ_{ci} is the uniaxial compressive strength.

To use this approach the value of Hoek-Brown constant m_i , Geological Strength index GSI along with σ_{ci} of intact rock needs to be estimated. GSI can be described based on geological description and once GSI is estimated Hoek-Brown constant can be estimated using Equation 3.3.

$$m_b = m_i \exp \left(\frac{GSI - 100}{28 - 14D} \right) \tag{3.3}$$

$$s = \exp \left(\frac{GSI - 100}{9 - 3D} \right) \tag{3.4}$$

$$a = \frac{1}{2} + \frac{1}{6} \left(e^{-GSI/15} - e^{-20/3} \right) \tag{3.5}$$

D is the disturbance factor depending upon the degree of disturbance of the rock mass as shown in Appendix A.4. For the intact rock from the rock mass Generalized Hoek-Brown criteria simplifies to (Hoek and Brown, 1997) Equation 3.6 .

$$\sigma_1' = \sigma_3' + \sigma_{ci} \left(m_b \frac{\sigma_3'}{\sigma_{ci}} + 1 \right)^{0.5} \tag{3.6}$$

The relationship between effective principal stresses depends only on two constants the uniaxial compressive strength σ_{ci} and m_i .

Flysch rock is a heterogeneous sedimentary facies containing strong rock like sandstone and weak rocks such as claystone, siltstone, and conglomerates dominated by weak rock content. Thus, to use the material value of sandstone is not appropriate neither using the properties of weak rock is justifiable (Marinos and Hoek, 2001). Since both strong and weak rock contributes to the strength, Marinos and Hoek (2001) suggest a Table 3.5 to be used to estimate parameters of sandstone and siltstone. The flysch type is categorized based on GSI values by Marinos and Hoek (2001) and chart is presented in Appendix . Further, for rock mass parameters weighted average values should be used.

Table 3.5: Suggested Proportions of values for each rock type for estimating rock mass property of flysch (Marinos and Hoek (2001))

Flysch type	Proportions of values for each rock type to be included in rock mass property determination
A and B	Use value of sandstone beds
C	Reduce sandstone values by 20% and use full values for siltstone
D	Reduce sandstone values by 40% and use full values for siltstone
E	Reduce sandstone values by 40% and use full values for siltstone
F	Reduce sandstone values by 60% and use full values for siltstone
G	Use values for siltstone or shale
H	Use values for siltstone or shale

3.3.2 Mohr-Coulomb Criteria

Mohr-Coulomb is the simplest failure criteria. It consists of a linear envelope touching all Mohr's circle, those representing critical combination of principal stresses as shown in Figure 3.4 (Goodman, 1989). Mohr-Coulomb criteria is developed to assess the stability of tunnels in isotropic, unjointed and elastic rock mass.

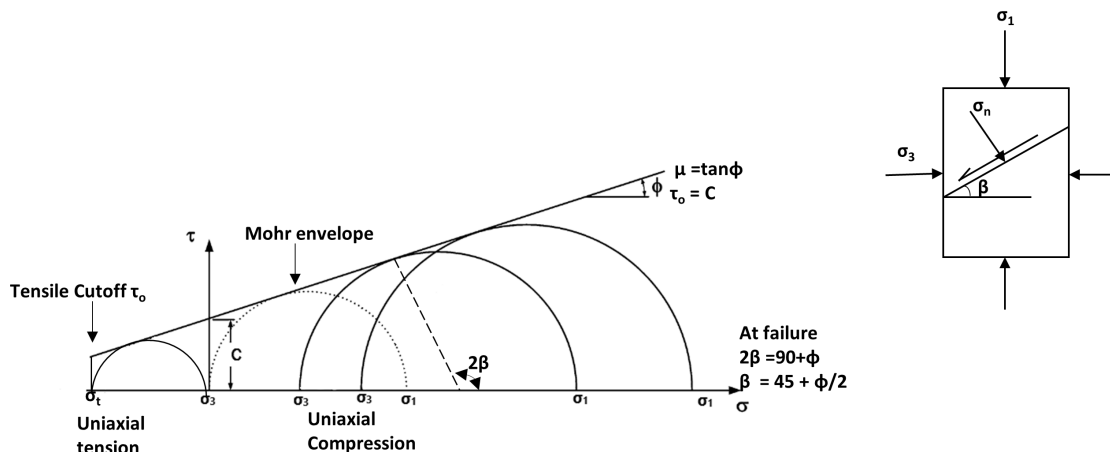


Figure 3.4: Mohr-Coulomb Failure Criteria (Extracted and redrawn after (Hudson and Harrison, 2000))

In terms of normal stress (σ) and shear stress (τ), the plane represented by the point of tangency for Mohr circle can be stated as Equation 3.7. Mohr- Column failure criteria for the rock mass strength is defined by cohesive strength c' and the angle of friction ϕ (Hoek and Brown, 1997). The linear relationship is defined as Equation 3.8.

$$\tau = C + \sigma \tan \phi \tag{3.7}$$

$$\sigma_1' = \sigma_{cm} + k \sigma_3' \tag{3.8}$$

Where σ_1' and σ_3' are the major and minor principal stresses respectively, σ_{cm} is the UCS of rock mass a rock mass k is the slope of line relating σ_1' and σ_3' .

3.3.3 Relationship between Mohr-Coulomb and Hoek and Brown

Most of geotechnical software uses the Mohr- Coulomb failure criteria. It is therefore necessary to determine by cohesive strength c' and the effective angle of friction ϕ . This is done by curve fitting. The Generalized Hoek- Brown criteria is solved for a range of minor principal stress value defined by $\sigma_1 < \sigma_3 < \sigma_{3max}'$ (Hoek et al., 2002) as shown in Figure 3.5 (right).

Hoek-Brown failure criteria assumes isotropic rock and rock mass behavior. Hence should only be used for rock masses in which there are sufficient number of closely spaced discontinuities and should not be used where the block size is same order as of structure being analyzed (Hoek and Brown, 1997). Figure 3.5 (left) shows that transition from an isotropic intact rock specimen, through a highly anisotropic rock mass in which failure is controlled by one or two discontinuities, to an isotropic heavily jointed rock

mass. In such case only for Intact rock and heavily jointed rock mass Hoek and Brown to be used and for remaining analysis of joints Mohr-Coulomb criteria to be used.

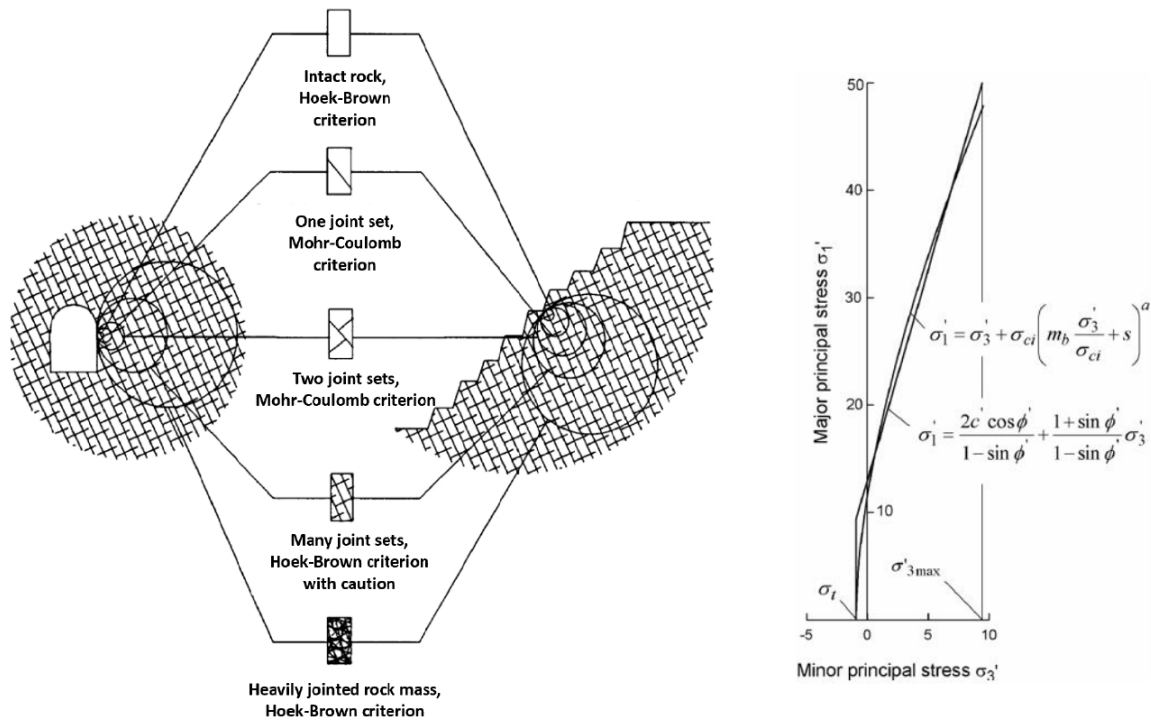


Figure 3.5: Idealized diagram showing the transition from intact rock to a heavily jointed rock mass (left) (Hoek and Brown, 1997) and Relationship between major and minor principal stresses for Hoek - Brown and equivalent Mohr-Coulomb criteria (right) (Hoek et al., 2002)

3.3.4 Post failure behaviour

Post-peak behavior for rock mass will be different depending on the quality of rock mass. As presented in Figure 3.6 a, the good quality rock loses strength quickly when maximum strength is exceeded resulted in elastic brittle nature. For medium quality rock as shown in Figure 3.6 b will result in strain-softening and for poor quality, rock masses show nearly plastic behavior as shown in Figure 3.6 (c) (Hoek and Diederichs, 2006).

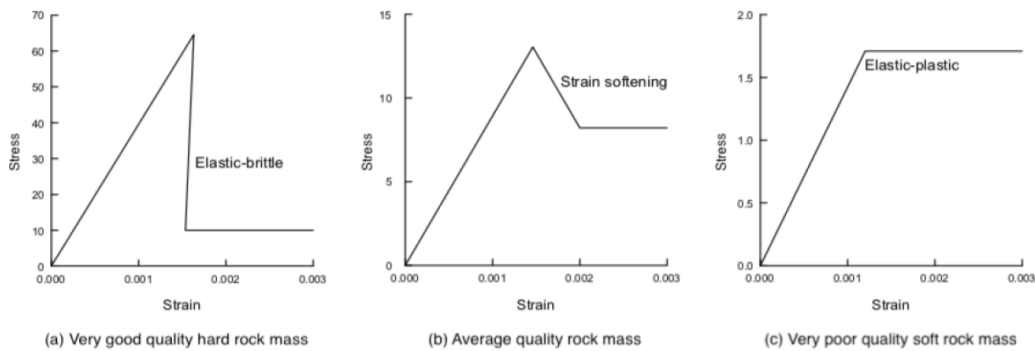


Figure 3.6: Suggested post failure characteristics for (a) Good quality (b) Average quality (c) Poor quality rock masses (Hoek and Diederichs, 2006)

Cai et al. (2007) characterized the post-failure characteristics based on the GSI system using block volume and joint conditions. According to Cai et al. (2007), residual strength can be quantified from residual GSI which is dependent on new failure surfaces and blocks interlocking using Equation 3.9.

$$GSI_r = GSI * e^{-0.0134GSI} \tag{3.9}$$

Initially, modeling is carried out using residual GSI using the relation suggested by Cai et al. (2007). But, using this value while performing numerical modeling provides results that are not conclusive. Hence, after discussion with professor Panthi, the residual parameters are assumed to be 25% of the peak value.

3.4 Discontinuities

Discontinuities are structural features that alter the homogeneity of the rock mass (Nilsen and Palmström, 2000). These structural features are the weakness planes within rock mass that tend to have zero or nearly zero tensile strength. Bedding plane, joints, folds, faults, shear zones and dykes are the major structural features of the rock mass (Brady and Brown, 2007). Figure 3.7 shows the different discontinuities that occur in rock mass according to the extent of their length that can be found in the field. Faults range in size from decimeter to hundreds of meters as shown in Figure 3.7. According to Panthi (2006), faults are tectonically formed minor and measure structures in the rock mass. They can be identified in the field as the occurrence of shear displacement. Minor faults range from decimeter to meter in thickness while major faults range from several meters to hundreds of meters.

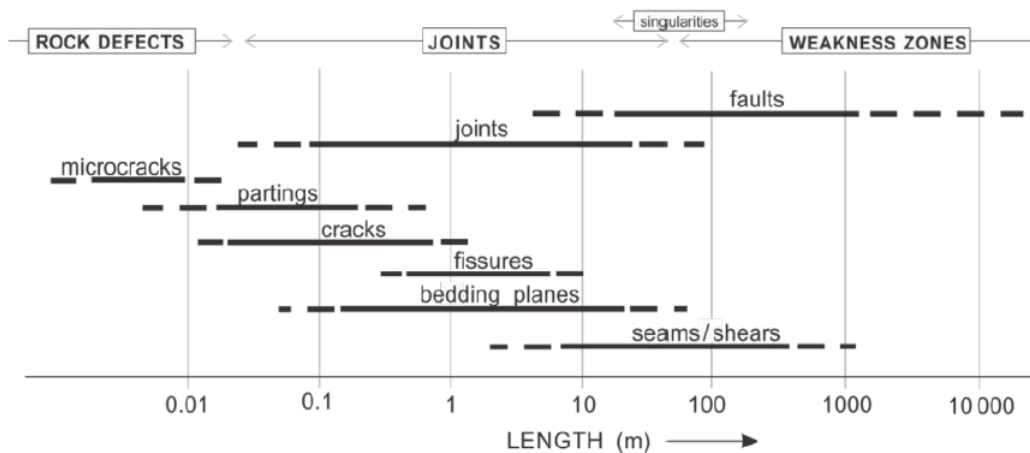


Figure 3.7: Distribution of discontinuities according to length according to Grimstad (1993)

Weakness zones are the part of rock mass, where in comparison to the surrounding rock mass have lower mechanical properties (Nilsen and Palmström, 2000). According to Panthi (2006), faults are tectonically formed minor and measure weakness zones in the rock mass. Faults range in size from decimeter to hundreds of meters as shown in Figure 3.7. They can be identified in the field as the occurrence of shear displacement.

Minor faults range from decimeter to meter in thickness while major faults range from several meters to hundreds of meters. Gouge materials are the filling materials that are found within weakness zones. The materials are often coarse rock fragments but sometimes clay materials like smectites are present in weakness zones. The smectites have a swelling potential after interaction with water which may cause stability problems in the underground structure.

The fracture in the rock with no noticeable shift is defined as joints (Mandl, 2005). These are the most common structural features found in the rock mass. A joint system is formed when joint sets intersect. A joint set is the group of parallel joints present in the rock mass. Nilsen and Palmström (2000) categorized joints in five categories according to their origin as tectonic joint, exfoliation joint, bedding stress, foliation stress, and sheet stress.

3.5 Rock mass classification

Many classification systems have been developed over the year and are widely being used. The objective for the classification of rock masses is to obtain a general rating of rock mass quality or classification of special engineering properties like drillability and blastability (Nilsen and Thidemann, 1993).

Previously, quantitative classifications were done based on single parameter such as compressive strength, Rock Quality Designation (RQD). RQD are still common in use. RQD is based on core drilling. RQD is the sum of core pieces greater than 10 cm per total drill run expressed in percentage. The RQD classifies very poor rock for RQD<25% and Excellent rock quality for RQD index 90-100% (Nilsen and Thidemann, 1993). Other classification systems used today are based on more than one parameter. Most of this system are also used for estimating rock support (Nilsen and Thidemann, 1993). Following are some common rock classification systems in use:

- Terzaghi's rock load theory
- Rock Mass Rating (RMR)
- Q-method
- Geological Strength Index (GSI)
- Rock Mass Index (RMi)

This chapter will only discuss the systems like Q-system and GSI in brief.

3.5.1 The Q-system

The Q-system was initially published in 1974 by (Barton et al., 1974). After the analysis of around 200 tunnel case records, correlation between the amount and type of support and the rock mass quality Q, with respect to tunnel stability was established. The numerical value of the Quality index (Q-value) is defined by Equation 3.10.

$$Q = \frac{RQD}{J_n} \cdot \frac{J_r}{J_a} \cdot \frac{J_w}{SRF} \quad (3.10)$$

Where RQD = Rock Quality Designation, J_n = joint set number, J_r = joint roughness number, J_a = joint alternation number, J_w = joint water reduction factor and SRF = Stress reduction factor.

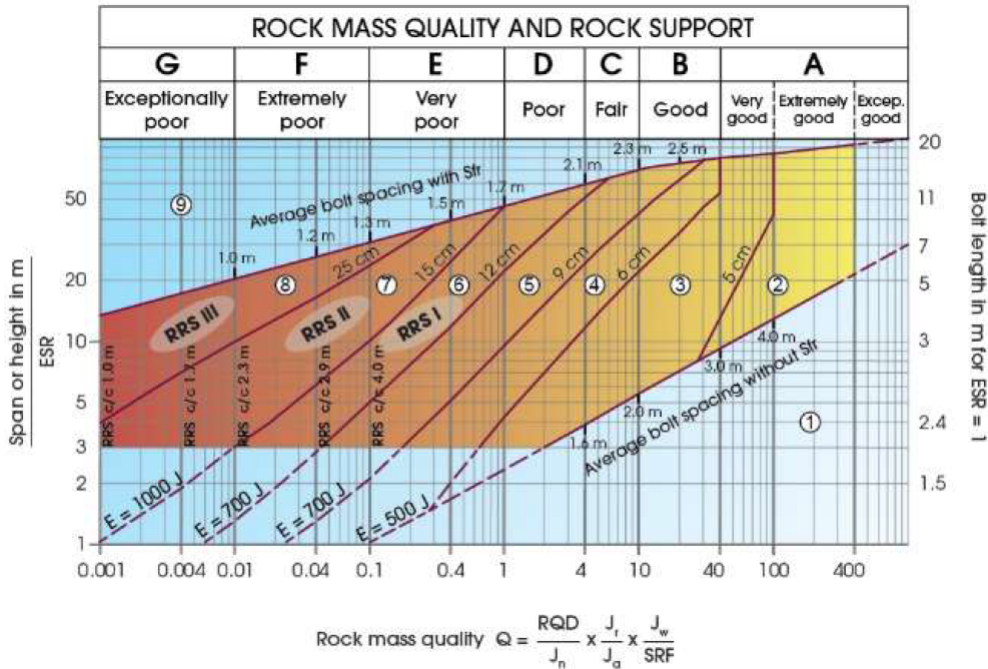


Figure 3.8: Permanent support recommendations based on Q-values and span/ESR (NGI, 2015)

Q-system can be used to design support. NGI (2015), provides the modification of chart by (Barton et al., 1974) as shown in Figure 3.8 along with the equivalent dimension along the vertical axis on the left-hand side. The support chart indicates what type of support is used in terms of the center to center spacing for rock bolts and the thickness of sprayed concrete. It is important to note that the support recommended by the chart is general and an adjustment is required according to the cases. And for difficult cases such as tunnelling in the weak rock mass, an increase in the amount of type of support may be relevant.

3.5.2 Geological Strength Index (GSI)

GSI was introduced as a means to estimate strength and deformation modulus of jointed rock masses for Hoek- Brown failure criteria (Hoek and Brown, 1997). The classification is based on joint surface quality and structure interlocking of rock pieces. The value ranges from 0 to 100. In Appendix A.2, the GSI system table has been attached which classifies the jointed rock mass as per Hoek and Marinos (2000). In Appendix A.3, the GSI system table for heterogeneous rock mass such as flysch has been attached as per Marinos and Hoek (2001).

3.6 Rock mass strength

The rock mass strength (σ_{cm}) is the ability of rock mass to withstand stress and deformation (Panthi, 2006). This ability is however influenced by discontinuities, foliation and their orientation in which the strength is assessed. The rock mass strength varies from the strength of intact rock. The determination of rock mass strength from the field, laboratory testing is difficult. Hence to estimate the strength, various researchers have provided different empirical and analytical relations which relate the intact rock strength (σ_{ci}) with rock mass strength (σ_{cm}) as shown in Table 3.6.

Table 3.6: Different relations for the determination of rock mass strength

Author(s)	Rock Mass Strength
Bieniawski (1989)	$\sigma_{cm} = \sigma_{ci} \times e^{\left(\frac{RMR-100}{18.75}\right)}$
Hoek et al. (2002)	$\sigma_{cm} = \sigma_{ci} \left(\frac{(m_b+4s-a(m_b-8s))(m_b/4+s)^{a-1}}{2(1+a)(2+a)} \right)$
Barton (2002)	$\sigma_{cm} = 5\gamma * Q_c^{\frac{1}{3}} = 5\gamma \left[\frac{\sigma_{ci}}{100} * Q \right]^{\frac{1}{3}} = 5\gamma \left(\frac{\sigma_{ci}}{100} * 10^{\frac{RMR-50}{15}} \right)^{1/3}$
Panthi (2006)	$\sigma_{cm} = \frac{\sigma_{ci}^{1.5}}{60}$ for highly schistose and deformed rock
Panthi (2017)	$\sigma_{cm} = \frac{\sigma_{ci}^{1.6}}{60}$ for strong and brittle rock mass

Where γ is the density of rock, Q_c is normalized rock mass quality rating, Q is the rock mass quality, RMR is the Bieniawski's rock mass rating computed as Equation 3.11, m_b is the reduced value of material constant m_i , s and a are the material constant related to Hoek-Brown failure criteria.

$$RMR = 15 \log Q + 50 \quad (3.11)$$

$$GSI = RMR - 5 \quad (3.12)$$

Bieniawski and Bernede (1979), Barton (2002) and Hoek et al. (2002) are based on rock mass classification methods. These methods relate rock mass strength with RMR , and it was found that there is a reduction in strength of discontinuous rock twice for weak, fractured, and schistose rocks. The reduction is first done for laboratory strength of intact rock (σ_{ci}) and again while determining the rock mass rating (RMR , Q or GSI) (Hoek and Marinos, 2000). However, the relations from Panthi (2006) and Panthi (2017) only depends on the intact rock strength (σ_{ci}). According to Panthi (2006), the correlation can be used for highly schistose, foliated, thinly bedded, and anisotropic rocks of metamorphic and sedimentary origin with low compressive strength.

3.7 Rock mass deformability

Rock mass deformability (E_m) is defined as the ratio of stress corresponding strain during loading of rock mass (Panthi, 2006). And includes both elastic and plastic behavior in the field. Unlike rock mass strength, deformation modulus can be measured directly in the field. Three types of in situ tests are mostly used: Plate Jacking tests (PJT), Plate

loading tests (PLT), and Radial jacking tests (Goodman jack test). Besides Flat jack tests, Cable jacking tests, Radial jack tests, Dilatometer tests, and Pressure chamber can be used for field measurement (Palmström and Singh, 2001). The results obtained from different methods were considerably different (Nilsen and Palmstrom, 2000). On the other hand, field measurement is time-consuming. Hence like rock mass strength, various researchers over time have provided various relations for the determination of rock mass deformability or modulus deformation (E_m) as shown in Table 3.7.

Table 3.7: Different relations for the determination of rock mass deformability

Author(s)	Rock mass deformation modulus
Bieniawski (1989)	$E_m = 2RMR - 100$
Serafim (1983)	$E_m = 10^{\frac{RMR-100}{40}}$
Palmstrom (1995)	$E_m = 5.6 * Rmi^{0.375}$
Hoek and Brown (1997)	$E_m = \sqrt{\frac{\sigma_{ci}}{100}} * 10^{\frac{GSI-10}{40}}$
Barton (2002)	$E_m = 10 * Q_c^{\frac{1}{3}} = 10 * \left(\frac{Q * \sigma_{ci}}{100}\right)^{\frac{1}{3}}$
Hoek and Diederichs (2006)	$E_m = E_{ci} * \left[0.02 + \frac{1 - \frac{D}{2}}{1 + e^{\left(\frac{60 + 15D - GSI}{11}\right)}}\right]$
Panthi (2006)	$E_m = E_{ci} \left(\frac{\sigma_{cm}}{\sigma_{ci}}\right)$

3.8 Rock Stresses

Rock stress induced on the rock mass is the force per unit area by the influence of the forces acting on the rock mass. A non-zero in situ stress condition prevails in an undisturbed rock mass due to overburden, confinement, and ancient stress (Basnet, 2013). The stress conditions in the rock mass get affected when an underground opening is excavated. Rock stresses acting on the rock mass get redistributed around the excavated opening. The stresses around these underground openings are defined by the stress situation beforehand excavation i.e. virgin stress and the geometry of the opening (Nilsen and Thidemann, 1993).

The virgin stress represents the resultant of: Gravitational stress, Topographical stress, Tectonic stress and Residual stress. Gravitational stress is induced due to gravity alone and when has two components: vertical and horizontal. For the horizontal surface the vertical gravitational stress (σ_z) at depth z is represented by Equation 3.13 (Nilsen and Thidemann, 1993).

$$\sigma_z = \gamma \cdot z \tag{3.13}$$

Where, γ = specific weight of rock,

In elastic rock with Poisson's ratio ν , the horizontal component of the topographical stress (σ_h) can be represented as Equation 3.14 (Nilsen and Thidemann, 1993).

$$\sigma_h = \frac{\nu}{1 - \nu} \cdot \sigma_z \tag{3.14}$$

In case of surface not being horizontal, topography will affect the rock stress. In high valley sides, the stress situation is dominated by the topographic effects (Nilsen and Thidemann, 1993).

The rock mass constitutes of faults and folds. The main cause for faulting and folding and tectonic stress is due to the plate tectonic action (Nilsen and Thidemann, 1993). The horizontal stress is much higher than the gravitational stress alone due to tectonic stress (σ_{tec}). The horizontal stress after tectonic stress effect can be represented as Equation 3.15 (Panthi, 2012).

$$\sigma_h = \frac{\nu}{1 - \nu} \times \sigma_z + \sigma_{tec} \tag{3.15}$$

$$\frac{100}{z} + 0.3 < k < \frac{1500}{z} + 1.5 \tag{3.16}$$

In Figure 3.9(a), the variation of vertical stress with the depth below the surface measured over the different parts of the world justifies Equation 3.13. For the shallow depth, the measurements are very close to accuracy as suggested by the stress value from Equation 3.13. Also, the high vertical stress values are observed which may be a result of some unusual geological or topographic feature present in the rock mass which has a greater influence on the rock stress field (Brown and Hoek, 1980).

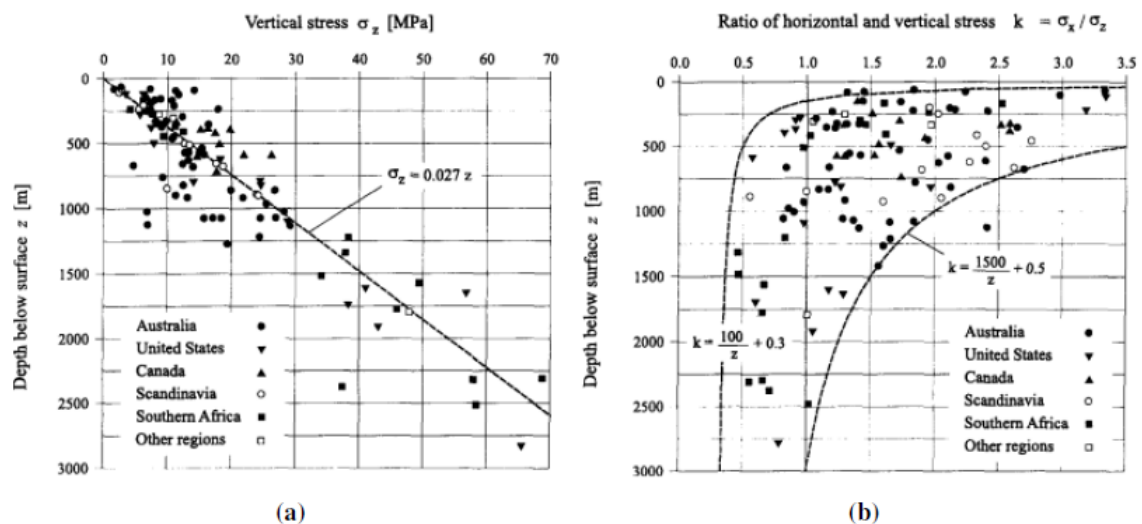


Figure 3.9: (a) Vertical stress against depth below the surface (left) and (b) Variation of ratio of horizontal stress to vertical stress(right) [extracted from Brown and Hoek (1980)]

Figure 3.9(b), shows the variation of the ratio of average horizontal stress to vertical stress, which summarizes the result of stress measurement in different part of the world.

For the depth z , the value of k falls under the limit shown in Equation 3.16 (Nilsen and Thidemann, 1993). The stress factor (k) values vary significantly as the it is influenced by topography and tectonic movements.

3.9 Stress distribution around tunnel

Excavation of underground structure in a rock mass causes the disturbance of in-situ stresses conditions. According to Nilsen and Palmström (2000), there will be a redistribution of in-situ stress around the opening after excavation. The load initially carried by the excavated rock needs to be transferred to the remaining rock mass, this results in the redistribution of stress around the opening. The stress induced by the excavation depends on the geometry of the opening and the magnitude and direction of the principal stresses (Nilsen and Palmström, 2000). In Figure 3.10 (left), stress distribution around the circular underground opening with elastic material and in isostatic state ($\sigma_h = \sigma_v = \sigma$) has been shown. As shown by Figure 3.10 (right), the tangential stress (σ_θ) at wall of tunnel is twice of principal stress (σ) whereas the radial stress (σ_r) is equal to zero. The radial stress and tangential stress will follow the function of the distance R from the center of the circle, as moving away from the opening (Nilsen and Thidemann, 1993). The calculation of the tangential stress (σ_θ) and the radial stress (σ_r) for circular tunnel of radius r can be done using Equation 3.17 and Equation 3.18 respectively.

$$\sigma_\theta = \sigma \left(1 + \frac{r^2}{R^2} \right) \quad (3.17)$$

$$\sigma_r = \sigma \left(1 - \frac{r^2}{R^2} \right) \quad (3.18)$$

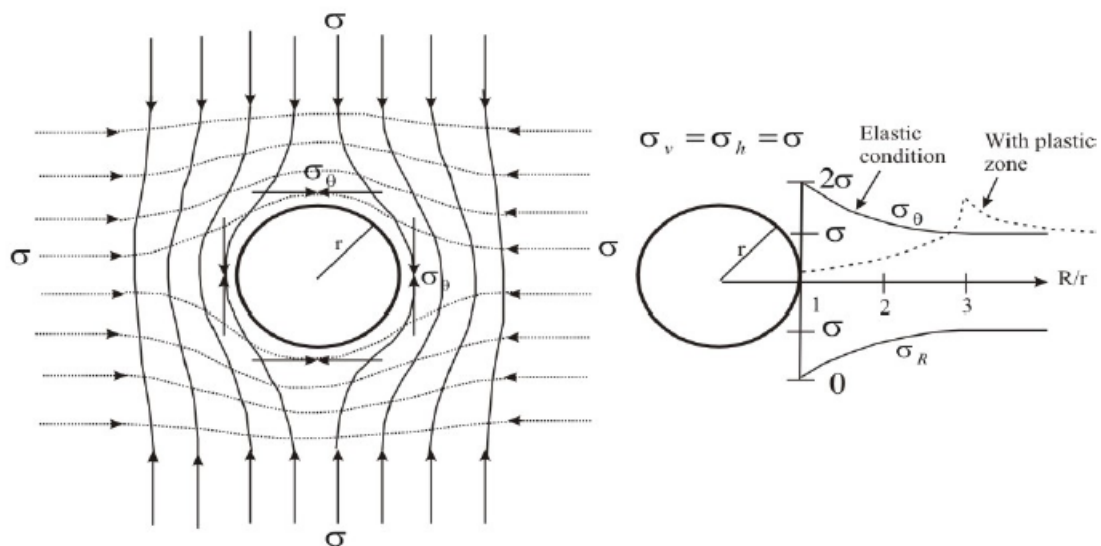


Figure 3.10: Circular underground opening and stress trajectories around the opening after excavation (left) and Tangential and radial stresses surrounding in a circular opening in an isostatic stress field(right) (Panthi, 2006)

The stress condition is often highly anisotropic, therefore according to Kirsch, in circular opening the maximum tangential stress ($\sigma_{\theta(max)}$) will reach where major principal stress (σ_1) is tangential to the contour. Similarly, the the minimum tangential stress ($\sigma_{\theta(min)}$) will reach where minor principal stress (σ_3) is tangential to the contour (Nilsen and Thidemann, 1993). The the maximum tangential stress ($\sigma_{\theta(max)}$) and the minimum tangential stress ($\sigma_{\theta(min)}$) can be calculated using Equation 3.19 and Equation 3.20 respectively also known as Kirsch's equations.

$$\sigma_{\theta(max)} = 3\sigma_1 - \sigma_3 \quad (3.19)$$

$$\sigma_{\theta(min)} = 3\sigma_3 - \sigma_1 \quad (3.20)$$

The validity of Kirsch solution is limited for a homogeneous, isotropic, and elastic rock mass with widely spaced and tight joints (Panthi, 2006). For weak rock mass, the plastic zone can be seen around the opening as represented by the dotted line in Figure 3.9 (right), as a result of a reduction in rock mass strength caused due to destruction and cracking of the material by the tangential stress (Shrestha, 2006). The extent of the plastic zone moved further from the opening until the elastic zone is reached (Panthi, 2006).

According to Nilsen and Thidemann (1993), non-symmetrical geometry and sharp corners in the underground opening will strongly affect the magnitude of tangential stress. The tangential stress will increase with a reduction in radius of curvature, and if there is a sharper corner between wall and roof the stress concentration is high in this corner. According to Chaudhary (2020), the magnitude of tangential stress depends on the shape of excavation rather than size while the zone of influence increases when the size increases. The stress distribution is more when the excavated masses from the rock mass is more (Myrvang, 2001).

4 Stability Assessment Methods

4.1 Weak Rock Mass

The rock masses with low strength, highly fractured decomposed, and tectonically disturbed rocks possessing the intermediate properties from brittle rocks to ductile soils are known as weak rock masses (Zhai et al., 2017). The intermediate stage between ductile (cohesive) soil and brittle (hard) rock are linked by geological processes, and the border between these three stages are variable as shown in Figure 4.1 (Nickmann et al., 2006).

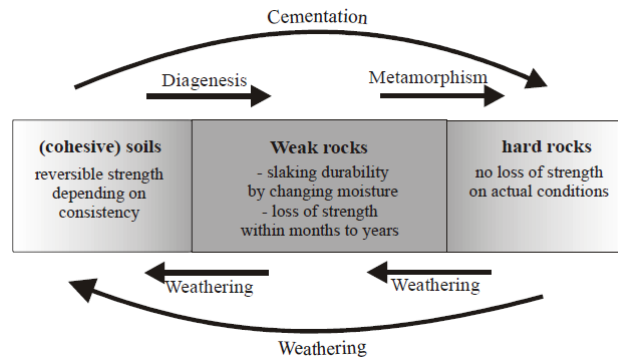


Figure 4.1: Weak rock position in between cohesive soils and hard rock (extracted from (Nickmann et al., 2006))

As shown in Figure 4.1, weathering is the reason for the transformation of hard rock into weak rocks and then to the soils. Physical and chemical weathering alters the mechanical properties of the rock material. During the physical weathering, the opening of the discontinuities occurs by rock fractures, and meanwhile, with the progression of the weathering the rock material breaks down and ultimately changes to soil-like material in the advanced stage of weathering (Arikan and Aydin, 2012). The rock found in nature is a composition of minerals and there exist some rocks like marbles and quartzites which contains only one mineral (Nilsen and Thidemann, 1993). In the case of chemical weathering, the weakening and alternation of rock occur due to the chemical changes in the minerals during the weathering process (Arikan and Aydin, 2012).

Table 4.1: Classification of engineering soft rock [extracted from (Manchao and Xiaoming, 2020)]

Category	Condition	Dominant plastic deformation
Swelling soft rock (low strength)	Shale content > 25%	Slipping along clay mineral of silicate; significant expansion under high water contents.
High strength soft rock	UCS \geq 25 MPa	Slipping along flaky clay minerals.
Jointed Soft rock	UCS < 25 MPa	Dilational slipping along the jointed surface.
Combined soft rock	Shale content \leq 25%	Combination of above characteristics

Engineering soft (weak) rocks are divided into four categories based on the geological characteristics and deformations behaviors namely: swelling soft rock (also called low

strength soft rock), high strength soft rock, jointed soft rock, and combined soft rock as shown in Table 4.1 (Manchao and Xiaoming, 2020).

4.2 Problems Associated with Weak Rock

The study of this thesis focuses on the weak rock mass. Therefore, the stability problems in the weak rock mass have been studied in depth.

4.2.1 Squeezing or plastic deformation

Squeezing can be defined as the stress-induced deformation in weak rock mass where the inward movement of the periphery of underground opening occurs. The weak and soft rock mass are plastic in nature and react in a way different than stronger and isotropic rock mass when tangential stresses are induced on them (Panthi, 2006). In weak rock high degree of schistosity, especially the extent of thin foliation is dominating (Chauhan, 2020). Micro cracks are formed along the schistosity or foliation plane, when induced maximum tangential stresses in tunnel is higher than strength of rock mass and this leads to the formation of visco-plastic zone as shown in Figure 4.2. This plastic zones formation results in the inward movement of the tunnel (Panthi, 2006). Squeezing is a time-dependent phenomenon causing the inward movement of tunnel perimeter caused due to shearing of the ground (Einstein, 1996). The plastic deformation in tunnel occurs in tunnel periphery immediately after excavation and continues even after rock support is installed (Chaudhary, 2020). Plastic deformation in tunnel is the summation of instantaneous deformation or time independent and time dependent deformation (Shrestha and Panthi, 2014).

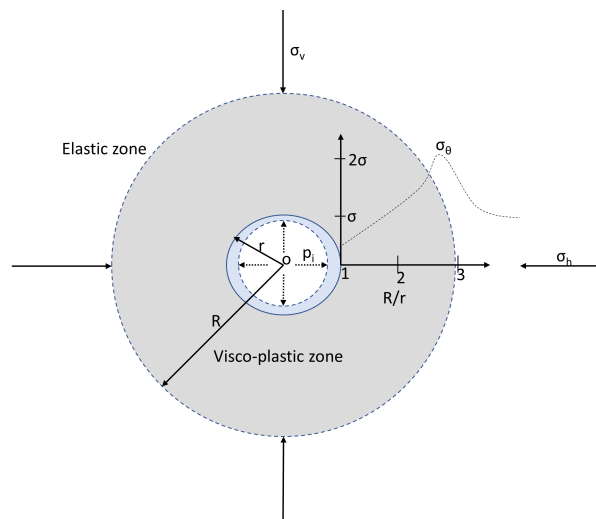


Figure 4.2: Illustration of plastic deformation in tunnel [extracted and redrawn after (Panthi, 2006)]

4.2.1.1 Instantaneous deformation

Instantaneous or time-independent deformation occurs during and after tunnel excavation. According to Shrestha and Panthi (2014), tunnel face after acts as a column giving

fictional support, and the time-independent deformation increases as the tunnel face advances. The redistribution of in-situ stress around the opening occurs after excavation. The new stresses are set up in the form of tangential and radial stresses. The yielding of the rock mass occurs as these induced stresses exceed the rock mass strength. This results in the inward displacement of the tunnel known as Instantaneous deformation (Chaudhary, 2020). As per Carranza-Torres and Fairhurst (2000), the maximum value of time-independent deformation reaches when the tunnel face has advanced by more than four times tunnel diameter.

4.2.1.2 Time-dependent deformation

Time-dependent deformation is also known as creep is the long-term deformation caused by constant loading (Shrestha and Panthi, 2014). According to Shrestha (2006), creep occurs by exceeding limiting shear stress. The materials showing no deformation after excavation may fail due to increasing deformation during constant stress induced on it over a long time. Goodman (1989) categorizes creep as primary creep, secondary creep, and tertiary creep. As shown in Figure 4.3, during primary creep the deformation occurs rapidly initially which lowers with time causing elastic strain. During secondary creep, the deformation continues at an almost constant rate. But during the tertiary stage, the deformation rate accelerates, and uncontrolled crack propagation continues leading to failure.

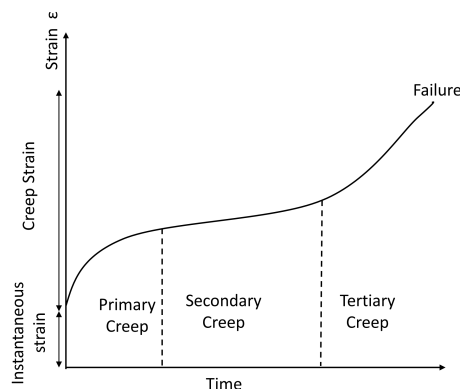


Figure 4.3: Illustration of different categories of creep [extracted and redrawn after (Goodman, 1989)]

4.2.2 Swelling

Swelling is the time-dependent increase in the volume of the ground, that leads to the inward movement of the tunnel perimeter (Einstein, 1996). It is a physiochemical mechanism of stress relief which occurs as rock interact with water (Einstein, 1996). Therefore, swelling occurs when the ground is deformed because of the water absorption (Nilsen and Palmstrom, 2000). Squeezing too is a time-dependent phenomenon causing the inward movement of tunnel perimeter, but is caused due to shearing of the ground (Einstein, 1996). The swelling problem may be encountered in weakness zone or faults and altered rocks which contain smectite/montmorillonite and also anhydrite and gypsum (Palmstrom and Broch, 2006).

Faults contains the filling materials known as gouge materials and the presence of minerals with swelling capacity in gouge material cause the stability problem in underground structure (Skrede, 2017). According to Skrede (2017), the most usual materials that can be found in the weakness zone are listed below:

- Inactive minerals (kaolinite, illite, limonite, zeolite etc)
- Minerals with low friction (chlorite, talc, graphite etc.)
- Solvable minerals such as carbonates
- Minerals with swelling properties, such as smectite

According to Bell and Haskins (1997), zeolites have swelling properties as smectites, however, in the above list, it has been listed as inactive minerals. Laumontite is the most commonly found naturally occurring zeolites and has the potential to change volume upon a change in moisture content (Bell and Haskins, 1997). Nilsen and Palmström (2000) listed three minerals as the main cause for swelling of the rock mass. The three minerals are namely, Smectite clay minerals, Anhydrite and Pyrrhotite.

According to Selmer-Olsen (1988), the alternation of silicate materials forms clay minerals. The structural composition of clay minerals are alumina octahedral (O layer) and silica tetrahedral layers (T layer) sheets and they belong to the family of phyllosilicate or sheet silicate family minerals (Frengen, 2020). According to Theng (2012), in kaolinite a non-swelling clay, T and O layer is condensed to sheet, and a 1:1 layer structure is formed as shown in Figure 4.4 (left). This structure does not absorb water as the structure remains unchanged as the oxygen tips of the T layer replace two-thirds of the hydroxyl ions (Frengen, 2020). Whereas smectites have a 2:1 layer structure as shown in Figure 4.4 (right), water is absorbed between sheets as the water molecule are polar and are attracted to clay structure (Frengen, 2020).

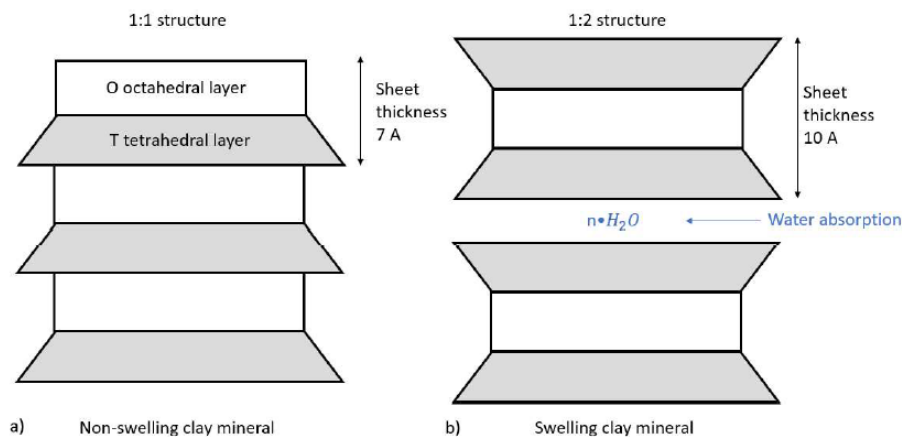


Figure 4.4: Structural difference between non swelling clay (left) and swelling clay (right) [Extracted from (Frengen, 2020) originally based on (Selmer and Palmstrom, 1989)]

As per Skrede (2017), the swelling process is divided into two stadiums, hydration, and osmotic swelling. The hydration can lead up to a 100% volume increase of dry minerals

due to surface adsorption of water between the Si-layers. The higher concentration of ions between the Si-layers in minerals than that of interstitial water outside causes an osmotic effect (Skrede, 2017). These are the two main causes for the swelling of clay minerals which then exerts swelling pressure on rock mass.

X-ray diffraction (XRD), differential thermal analysis (DTA), and color testing are the laboratory methods used to perform mineralogical analysis. X-ray diffraction (XRD) test has been used by Runa Berstad Frengen to perform mineralogical analysis of the Moglice headrace tunnel rock sample which results have been used for this thesis.

The free swelling test is the most common test for determining the swelling potential of a powder and it measures the free swell index of a powder (Vegvesen, 2014). NTNU swelling test and KiT swelling test can be used to find the swelling pressure of minerals. A study by Selen (2017), compare the methodology of the NTNU and KiT laboratory tests and concluded that Kit showed levels of swelling 2-4 times higher than that at NTNU. According to Skrede (2017), free swelling test and laboratory tests for determination of swelling pressure measures directly the swelling properties of the material. The swelling behaviour can be classified based on free swelling index and swelling pressure as shown in Table 4.2. Free swelling tests and NTNU swelling tests have been performed by Runa Berstad Frengen on the Moglice headrace tunnel rock sample which results have been used for this thesis.

Table 4.2: Classification of swelling and free swelling pressures (Nilsen and Palmström, 2000)

Classification	Free swelling index [%]	Swelling Pressure [MPa]
Very high	>200	>0.75
High	140 - 200	0.30 - 0.75
Moderate	100 - 140	0.1 - 0.3
Low	<100	<0.10

4.2.2.1 Assessment of In-situ Swelling Pressure

There is no direct method to assign in situ swelling pressure based on the laboratory test. Hence swelling pressure is assessed based on laboratory results for swelling pressure and observed in situ swelling pressure from some tunnel cases from Steiner (1993). Table 4.3 shows the laboratory and in situ swelling pressure measured for different tunnels. The swelling pressure observed for in situ conditions is less than the laboratory tested values for all cases. To find how laboratory test results value correlates with in situ swelling pressure, the ratio between maximum in situ swelling pressure and maximum laboratory swelling pressure is calculated. The maximum values of pressure are chosen to assess the worst-case scenario.

Table 4.3: Laboratory and In situ swelling pressure for different tunnel cases (summarized from Steiner (1993))

Case, Country	Geology overburden (m)	Laboratory Swelling Pressure (MPa)	In situ Swelling pressure (Mpa)
Belchen Tunnel, N2 motorway	Opalinus shale (Jurassic) 50-300 m	0.8 - 2.0	0.17 (Mean) 0.3 (Max)
Taubenbloch TS, Canton of Beru,E, Switzerland	Effinger shale (Jurassic) 100-250 m	0-0.8 (Mean 0.4)	0.06
Chamoise Tunnel, A40 Genve-Micon, France	Effinger shale, Oxfordien (Jurassic) 400 m	3-8	2.5
Hauenstein Base Tmnel, BaseI-Olte Railway, Switzerland,	H = 400-500m	1.7-4.7	1.4-2.5 (Mean 1.8±0.3)
Wagenburg Tunnel, Stuttgart, Germany	H = 40-60m	1-16.0	<4.0 (Mean 3.0)
Freudenstein Tunnel High Speed railway, Stuttgart-Manheim, Germany	H = 40-100m	>7	2.4
Heslasch tunnel road tunnel, Stuttgart, Germany	H = 40-60	>7	3.3

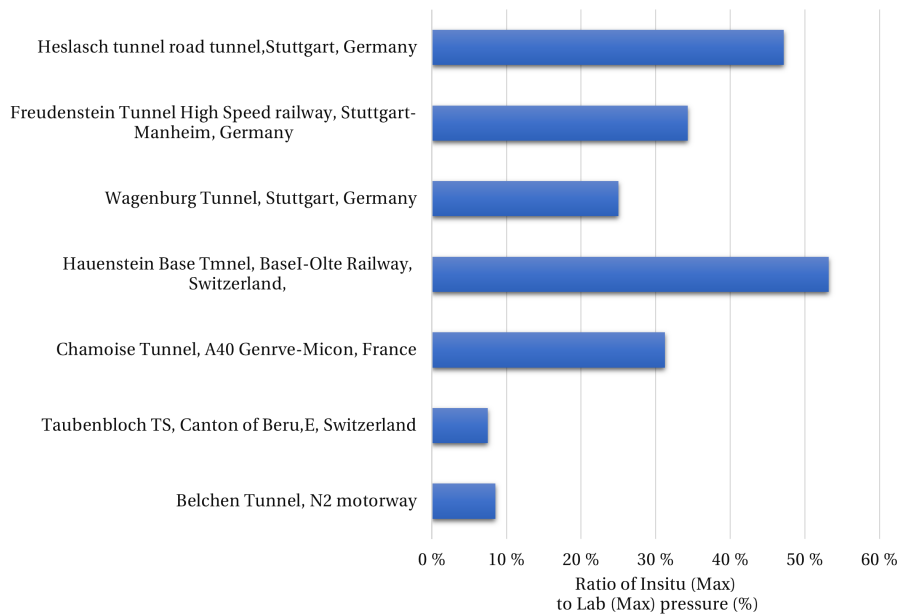


Figure 4.5: Ratio of maximum in situ swelling pressure to maximum swelling laboratory swelling pressure for different tunnel

As it can be seen from Figure 4.5, the ratio of in situ swelling pressure to laboratory swelling pressure varies from 8% to 53%. The ratio varies for each tunnel case which

suggests the in-situ swelling pressure may vary within a wide range depending on the geological conditions. Therefore, the uncertainty in the assessment of exact swelling demands performing sensitivity analysis for performing stability analysis of the hydropower tunnel in swelling rock mass by varying in-situ swelling pressure from 5% to 55% of the maximum swelling pressure measured in the laboratory.

4.2.3 Slaking

The deterioration and breakdown of rocks response to changes in humidity and temperature is known as slaking and the process is dependent on the cycles of drying and wetting (Goodman, 1993). The cycle of drying and wetting intensifies the process of slaking as the process induces micro-fissures in the rock (Dick et al., 1994; Erguler and Shakoor, 2009). Thus this may lead to failure to the construction work in such rock. Shales, mudstones, clayey friable sandstone, and conglomerates are the rocks known to have slaking behavior (Skrede, 2017). Slaking is most common with the rocks having swelling minerals. However, slaking also takes place in non-expansive shales and mudstones due to more complex mechanisms (Skrede, 2017). The swelling and slaking have been witnessed together in several cases around the world (Brattli and Broch, 1995). According to Franklin and Chandra (1972) three factors control slake durability:

1. Permeability and porosity
2. Reactions between the rock and fluids
3. Rock capacity to resist the disruptive forces

High permeability and porosity of rock increase the vulnerability of fluid entering the rock and increase the fluids mobility within rock (Franklin and Chandra, 1972). According to Franklin and Chandra (1972), the slaking is the mechanism of exchange of ion exchange as rock interacts with fluids with capillary action releasing the stress. This causes the breaking of bonds in the rock mass. The water invades the narrow capillaries which then induces pore water suctions leading to tensile failure of weak crystalline bonds (Taylor, 1988). According to Skrede (2017), the stress relief in rock may occur as the rock containing clay may store elastic strain due to over-consolidation and weakening of the intergranular bonds of rock.

To determine the effect of slaking, slake durability can be measure. Slake durability of rock is defined as the resistance of rock towards the disintegration when subjected to repeated cycles of drying and wetting (Franklin and Chandra, 1972). In Figure 4.6, the effect of repeated cycling on different rock samples have been presented from Franklin and Chandra (1972). Different materials show a variable degree of degradation after multiple rounds of wetting and drying. Table 4.4 shows the classification of slake durability based on the percentage retained after two cycles. The results of slake durability index (SDI) test on the Moglice headrace tunnel rock sample performed by Lena Selen have been considered for further study of this thesis.

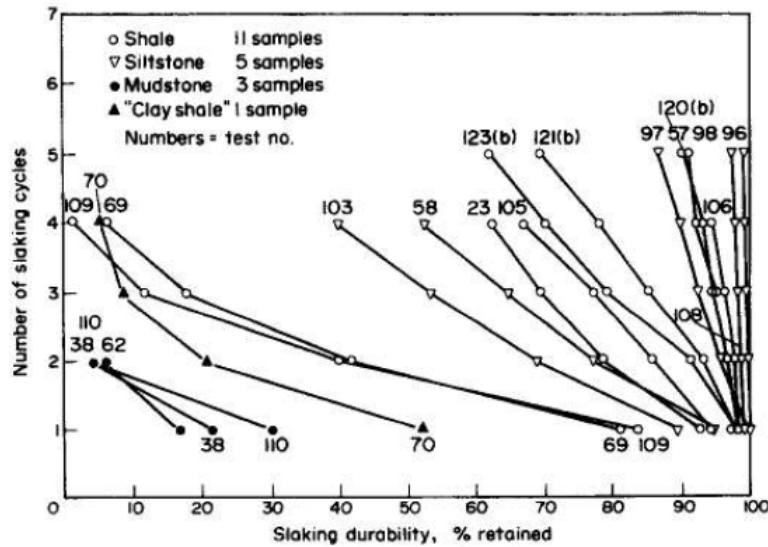


Figure 4.6: Effect of repeated slaking cycles on various rock materials (ISRM, 1979a)

Table 4.4: Classification for slaking after two slaking cycles (ISRM, 1979a)

Classification	Slake durability index (I_{d2}) [%]
Very High	98-100
High	95-98
Medium High	85-95
Medium	60-65
Low	30-60
Very Low	0-30

According to Selen et al. (2020), slaking and disintegration of rock is threat to the stability of hydropower tunnels passing through weak and heterogeneous rock mass. The surrounding rock mass of hydropower tunnel are exposed to dry condition during excavation and then filled with water during operation of hydropower plant. The periodic draining of hydropower tunnel for inspection and maintenance cause cyclic effect of drying and wetting of rock mass (Selen et al., 2020).

4.3 Review of stability assessment methods

The tunnel constructed in a weak rock mass can have instabilities problems like squeezing (plastic deformation), swelling, and slaking as discussed in section 4.2. Many methods for the evaluation of plastic deformations are available. The methods include empirical method such as Singh et al. (1992), Q-system (Grimstad, 1993) and Wood (1972) methods. Hoek and Marinos (2000) is semi-empirical methods and methods like Convergence Confinement Method (CCM) (Carranza-Torres and Fairhurst, 2000) and Panthi and Shrestha (2018) methods are the analytical methods for analyzing plastic deformation. Apart from these methods, numerical methods with finite element software like Rocscience can be used to analyze and evaluate the plastic deformation in underground structures.

The swelling analyses for this thesis have been performed using similar methods as plastic deformation analyses. The equations that will be discussed further in this section for the plastic deformation analyses for different methods have been modified for the evaluation of swelling. The selected analysis methods based on empirical, semi-empirical, and analytical methods have been modified. Apart from this numerical method using Rocscience software has been used for swelling analysis.

4.3.1 Empirical methods

The study carried by various researchers over time has developed several empirical relationships for estimating plastic deformation of underground structures based on experience and comparison cases of several underground structures. Based on the indicators used by different methods to represent the plastic deformation, the approaches can be classified into three categories as Strength-stress approach, Strain estimation approach, and Rock mass classification approach. For carrying out the study of this thesis, empirical methods have not been used. However, few empirical methods have been reviewed as this methods can be useful for similar plastic deformation analysis in the future study of other projects.

Q-system

Initially developed at Norwegian Geotechnical Institute (NGI) by Barton et al. (1974), the Q system is later updated by Grimstad (1993) by studying 100 more cases. The assessment is based on the Q system as reviewed in section 3.5.1. The Q value is calculated using Equation 3.10 which is based on the six rock mass parameters. The term J_w/SRF in Equation 3.10 is known as active stress and it incorporates the effect of the effect of water, faulting, strength /stress ratio, squeezing or swelling (Barton, 2002).

Table 4.5: Prediction of Squeezing condition according to Q-system (Barton, 2002)

Squeezing rock: plastic flow of incompetent rock under the influence of high rock pressure	$\frac{\sigma_{\theta}}{\sigma_{cm}}$	SRF
Mild squeezing rock pressure	1-5	5-10
Heavy squeezing rock pressure	>5	10-20

The squeezing prediction is based on the ratio of tangential stress and rock mass strength ($\sigma_{\theta}/\sigma_{cm}$). The tangential stress (σ_{θ}) can be computed using Equation 3.17 and the rock mass strength (σ_{cm}) can be computed as $\sigma_{cm} = 0.7\gamma Q^{1/3}$ where γ is the density of rock mass in kN/m^3 . As shown in Table 4.5, squeezing condition is used to assign the value of SRF. But to estimate the Q value SRF needs to be known. Hence, according to Shrestha (2006), this method leads to loop dependency. Thus, other empirical methods independent of Q value can be used to estimate rock mass strength as presented in Table 3.6.

4.3.2 Semi-empirical method

Several semi-empirical methods for plastic deformation analysis such as Hoek and Marinos (2000), Kovári (1998), Aydan et al. (1993), Jethwa et al. (1984) are available. The

thesis is focused on the flysch section of the Moglice headrace tunnel, where deformation has been measured. The study focused on the prediction of deformation rather than estimating the squeezing condition. Hence, Hoek and Marinos (2000) method has been reviewed and used to predict the deformation. Also, the method has been modified to predict the extent of deformation due to swelling pressure.

4.3.2.1 Hoek and Marinos (2000) method

Hoek and Marinos (2000) method is the most common semi-empirical method used for analyzing plastic deformation. Hoek and Marinos (2000) method describe the competency factor for a circular tunnel as ratio of rock mass strength and in-situ stress. The relationship between percentage strain (ϵ) and the competence factor (σ_{cm}/p_o) is established based on Sakurai (1984) approach. The results from numerical modeling by FAMA (1993) and analytical solution by Carranza-Torres and Fairhurst (2000) on a circular tunnel in a hydrostatic stress field has been used to establish this approach. Hoek and Marinos (2000) applies Monte Carlo simulation for several tunnel conditions. The in-situ stress is varied from 2 to 20 MPa, tunnel diameter of 4 to 16 m, UCS of 1 to 30 MPa, GSI of 10 to 35, dilation angle of 0° to 10° and Hoek and Brown constant (m_i) of 5 to 12 have been used to perform the simulation. Figure 4.7 (left) represents the result from the simulation.

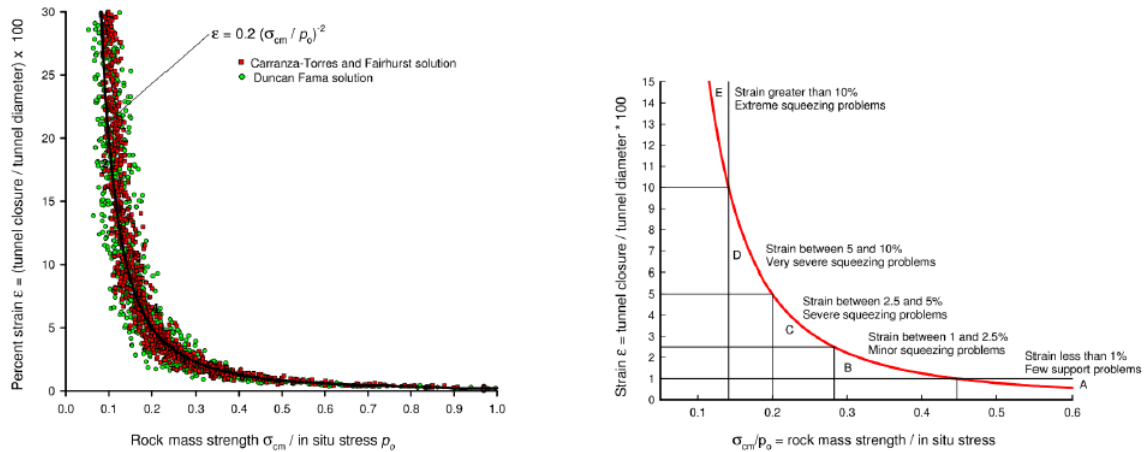


Figure 4.7: Monte Carlo simulation result by Hoek and Marinos (2000) showing tunnel convergence against the ratio of rock mass strength to in-situ stress (left) and Relationship between tunnel strain and degree of severity of squeezing problems in case of unsupported tunnel proposed by Hoek and Marinos (2000) (right)

The simulation is carried out for unsupported condition meaning without internal pressure (p_i) for which strain value can be computed using Equation 4.1. Further, internal pressure (p_i) is introduced by Hoek and Marinos (2000) to simulate the effect of support. Hoek and Marinos (2000) has proposed Equation 4.2 and Equation 4.3 to evaluate the size of plastic zone and to estimate the deformation of circular tunnel respectively.

$$\epsilon = 0.2 \left(\frac{\sigma_{cm}}{p_o} \right)^2 \quad (4.1)$$

$$\frac{d_p}{d_o} = \left(1.25 - 0.625 \frac{P_i}{P_o} \right) \frac{\sigma_{cm}^{\frac{P_i}{P_o} - 0.57}}{P_o} \quad (4.2)$$

$$\varepsilon = \left(0.002 - 0.0025 \frac{P_i}{P_o} \right) \frac{\sigma_{cm} \left(2.4 \frac{P_i}{P_o} - 2 \right)}{P_o} \quad (4.3)$$

Hoek and Marinos (2000) classifies the squeezing severity based on the strain percentage of tunnel as shown in Figure 4.7 (right) into five categories. The severity varies from "Few support system" for strain less than 1% to "Extreme squeezing problems" for strain greater than 10%. The simulation is performed for the tunnel with a circular cross-section in an isostatic stress field condition. However, the real field problem may not account for these conditions. The tunnel shape and in-situ stress condition vary about the assumption made by the Hoek and Marinos (2000) method. Hence, Hoek and Marinos (2000) recommend using numerical analysis based on real condition in case of significant squeezing problem predicted by this method.

4.3.2.2 Modified Hoek and Marinos (2000) method for swelling pressure

To evaluate the effect of swelling pressure on long-term deformation, the modification is made to Equation 4.3. The swelling pressure (P_s) is introduced. The assumption is made that along with the in-situ pressure (p_o), swelling pressure (P_s) acts on the tunnel. The modified relation for computing strain for swelling pressure is shown in Equation 4.4.

$$\varepsilon = \left(0.002 - 0.0025 \frac{P_i}{P_o + P_s} \right) \frac{\sigma_{cm} \left(2.4 \frac{P_i}{P_o + P_s} - 2 \right)}{P_o + P_s} \quad (4.4)$$

4.3.3 Analytical Method

Tunneling in a rock mass can be defined as a four-dimensional problem where stress distribution around tunnel occurring in three dimensions and each of these stresses is influenced by time-dependent straining (Shrestha, 2020). According to Carranza-Torres and Fairhurst (2000), Labasse (1949) describe the procedure of how standardization of support to minimize disturbance in underground constriction works in two ways. First, the limitation of support to one or two so that support will not disrupt the material supply in underground construction. Second, Labasse (1949) describe no detail or accurate calculation is required for immediate support behind the face. However, for precise solutions, each cross-section in each face required separate study and mathematical analysis. This task is time-consuming with which the excavation will certainly collapse by this time. Convergence Confinement Method (CCM) by Carranza-Torres and Fairhurst (2000) takes this constrains into account. This method studies the interaction of ground with the installed support, which accounts for the effect of change in rock mass properties on support loads.

According to Panthi and Shrestha (2018), both time-independent and dependent deformations result in the total deformation of a tunnel. Moreover, Panthi and Shrestha (2018) method is independent of tunnel shape and size, which in the case of Hoek and Marinos (2000) and CCM is limited to the circular cross-section. Therefore, CCM (Carranza-Torres and Fairhurst, 2000) and Panthi and Shrestha (2018) methods have been reviewed

for analytical solution of plastic deformation which similar to Hoek and Marinos (2000) method as in section 4.3.2.2, have been modified for long term deformation analysis due to swelling pressure.

4.3.3.1 Convergence Confinement Method (CCM)

Convergence Confinement Method (CCM) is a procedure to estimate the load imposed on the support behind the face of a tunnel (Carranza-Torres and Fairhurst, 2000). According to Carranza-Torres and Fairhurst (2000), because of the face effect, the section support installed in the vicinity of the tunnel face does not carry the full load as the tunnel face itself carried the part of the redistributed load. And with the advancement of tunnel face with the excavation, the face effect decreases, and installed supports have to carry more load which earlier has been carried out by face.

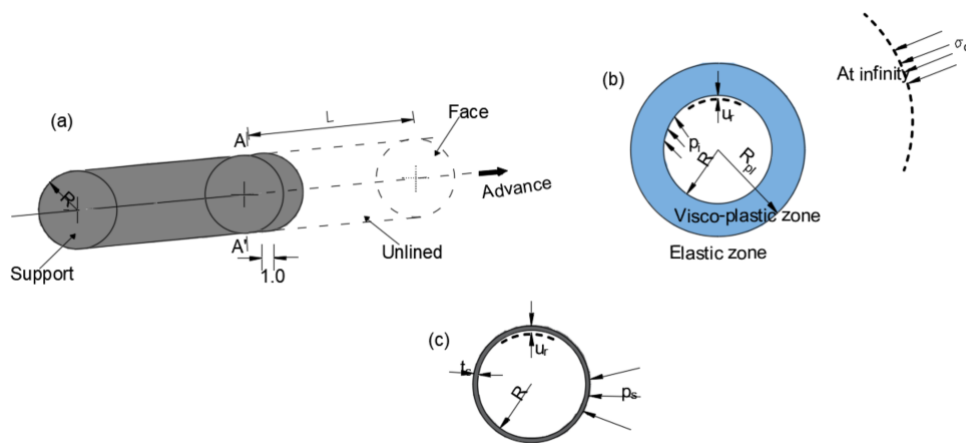


Figure 4.8: a) Cylindrical tunnel of circular Cross section of radius R b) Cross-section of circular tunnel section $A-A'$ c) Cross-section of the circular support system applied at section $A-A'$ [Redrawn after (Carranza-Torres and Fairhurst, 2000) for better readability]

Figure 10.1, illustrates the problem as per Carranza-Torres and Fairhurst (2000) where a cylindrical tunnel of radius R is constructed in a rock mass which is subjected to hydrostatic stress field (σ_o) in the beginning. Circular support is installed at section $A-A'$ at distance " L " behind the face of unit length. The purpose of the analysis is to determine the load that has been transferred to support from rock mass at section $A-A'$ from the time of support installation to the time until the face has moved ahead far enough that the face effect has disappeared (Carranza-Torres and Fairhurst, 2000). In Figure 10.1 (b) and (c), cross-section of circular rock mass showing plastic zone of unsupported tunnel and circular cross-section of support has been shown respectively where u_r, p_i, p_s and R_{pl} represents the radial displacement, internal pressure, external pressure (load transmitted from rock mass) and plastic radius respectively. The support of thickness t_c has been installed in the circular tunnel of radius R .

Figure 10.2, represents the sequence of convergence confinement method. Figure 10.2 (a) represents the time t_0 when support is installed at $A-A'$, and here it is assumed no

load is transferred by rock mass to support i.e. $p_s^0 = 0$, and the amount of ground that converged radially is u_r^0 . Figure 10.2 (b) represents the time t , when face has advance and the distance of face is now L_t from support at section A-A', now the ground convergence $u_r^t > u_r^0$ and rock mass transmit pressure p_s^t . Figure 10.2 (c) represents the time t_D , face has move sufficiently far so that face effect disappears. At this instance, support carries the design load p_s^D and ground has converged altogether by u_r^D . CCM (Carranza-Torres and Fairhurst, 2000) has three basic components, the Longitudinal Deformation Profile (LDP), the Ground Reaction Curve (GCC) and the Support Characteristics Curve (SCC).

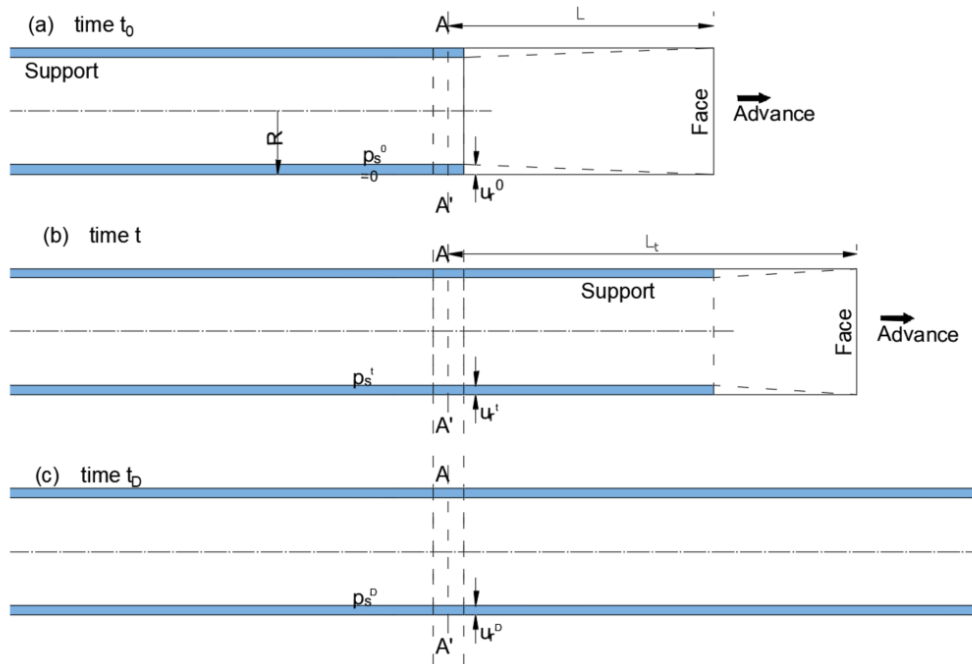


Figure 4.9: Loading of the support at section A-A' due to progressive advance of the tunnel face [Redrawn after (Carranza-Torres and Fairhurst, 2000) for better readability]

Longitudinal Deformation Profile (LDP)

The graphical representation of radial displacement occurring along the unsupported tunnel excavation, for sections located ahead and behind the face is known as LDP (Carranza-Torres and Fairhurst, 2000). Figure 4.10 (on top) shows the typical LDP showing behind the face at some distance maximum convergence u_r^m has been occurred. To calculate the radial displacement u_r at distance x behind the face of a circular tunnel of radius R , Carranza-Torres and Fairhurst (2000) has suggested to use Panet (1995) relation as represented by Equation 4.5.

$$\frac{u_r}{u_r^m} = \frac{1}{4} + \frac{3}{4} \left[\left(1 - \frac{3}{3 + 4x/R} \right)^2 \right] \quad (4.5)$$

Chern et al. (1998) measured convergence in the vicinity of the face for a tunnel in the Mingtam Power Cavern project, which was plotted by Carranza-Torres and Fairhurst (2000) and as per Carranza-Torres and Fairhurst (2000), Hoek suggests the best fit to measured value is represented by relation represented by Equation 4.6.

$$\frac{u_r}{u_r^m} = 1 + \exp \left[\left(\frac{-x/R}{1.1} \right)^{-1.7} \right] \quad (4.6)$$

Vlachopoulos and Diederichs (2009) proposed the improved method for LDP for convergence confinement analysis. According to Vlachopoulos and Diederichs (2009), the relations are given in Equation 4.7, Equation 4.8 and Equation 4.9 can be used to locate the position of displacement accurately in the tunnel to accurately sequence the support installation in n in staged 2D plane strain analyses. The co-relation between maximum normalized plastic zone ($R^* = R_p/R$) with normalized tunnel closure (u_o/u_m) is represented by Equation 4.7.

$$u_o^* = \frac{u_o}{u_{max}} = \frac{1}{3} e^{-0.15R^*} \quad (4.7)$$

Equation 4.8 and Equation 4.9 give the tunnel deformation on rock mass for $X^* \leq 0$ and $X^* \geq 0$ respectively.

$$u^* = \frac{u}{u_{max}} = u_o^* \cdot e^{X^*} \quad (4.8)$$

$$u^* = 1 - (1 - u_o^*) \cdot e^{-\frac{3X^*}{2R^*}} \quad (4.9)$$

Ground Reaction Curve (GRC) The relationship between the increase in radial displacement (u_r) of the wall and the decrease of internal pressure (p_i) is represented GRC. The representation of internal pressure does not reflect the true condition rather substitutes the effect of gradual reduction of radial displacement initially provided by the tunnel core (Vlachopoulos and Diederichs, 2009). Figure 4.10, shows the GRC where OE represents the elastic deformation and E represents the transition from elastic to the plastic regime. At O, the far-field stress (σ_o) is equal to internal pressure (p_i). Before E, internal pressure (p_i) \geq critical internal pressure (p_i^{cr}). With further decrease in internal pressure (p_i) $<$ (p_i^{cr}), plastic deformation of the rock mass occurs and plastic zone of radius (R_p) is formed. The uniform internal pressure (p_i), and far-field stress (σ_o) can be scaled using Equation 4.10 and Equation 4.11 to give scaled internal pressure (P_i), and far-field stress (S_o) respectively (Carranza-Torres and Fairhurst, 2000).

$$P_i = \frac{p_i}{m_b \sigma_{ci}} + \frac{s}{m_b^2} \quad (4.10)$$

$$S_o = \frac{\sigma_o}{m_b \sigma_{ci}} + \frac{s}{m_b^2} \quad (4.11)$$

The scaled critical (internal) pressure (P_i^{cr}) for which the elastic limit is defined by Equation 4.12 and non scaled critical internal pressure (P_i^{cr}) is found using Equation 4.13.

$$P_i^{cr} = \frac{1}{16} \left[1 - \sqrt{1 + 16S_o} \right]^2 \quad (4.12)$$

$$p_i^{cr} = \left[P_i^{cr} - \frac{s}{m_b^2} \right] m_b \sigma_{ci} \quad (4.13)$$

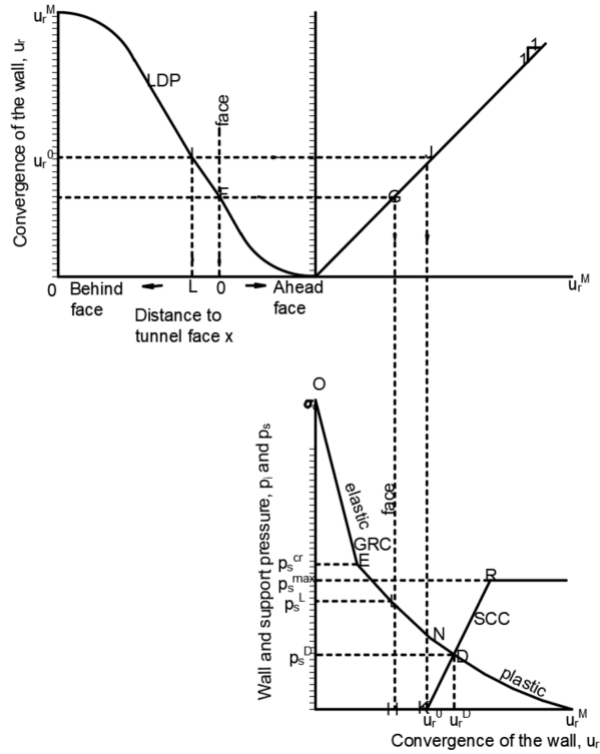


Figure 4.10: Schematic Representation of GRC, SCC and LDP of a circular tunnel [Redrawn after (Carranza-Torres and Fairhurst, 2000) for better readability]

The radial displacements (u_r^{el}) and internal pressure (p_i) in the elastic part of the GRC is given by Equation 4.14. G_{rm} is the shear modulus of the rock-mass.

$$u_r^{el} = \frac{\sigma_o - p_i}{2G_{rm}} \tag{4.14}$$

For values of internal pressure $p_i < p_i^{cr}$, the extent of the plastic region R_{pl} is calculated using Equation 4.15 .

$$R_{pl} = R \times \exp \left[2\sqrt{P_i^{cr} - \sqrt{P_i}} \right] \tag{4.15}$$

To define the plastic part of GRC, the flow rule of material is used (Carranza-Torres and Fairhurst, 2000). The relation between the strains that produce distortion and those that produce volumetric changes, as plastic deformation occurs in the material is defined by flow rule (Carranza-Torres and Fairhurst, 2000). The dilation constant (K_ψ) is defined for flow rule as Equation 4.16 .

$$K_\psi = \frac{1 + \sin \psi}{1 - \sin \psi} \tag{4.16}$$

The plastic part of GCC is represented by Eq. 4.17 and Eq. 4.18 for dilation angle $\psi > 0$ and $\psi = 0$ respectively.

$$\begin{aligned} \frac{u_r^{pl}}{R} \frac{2G_{rm}}{\sigma_o - p_i^{cr}} &= \frac{K_\psi - 1}{K_\psi + 1} + \frac{2}{K_\psi + 1} \left(\frac{R_{pl}}{R} \right)^{K_\psi + 1} + \frac{1 - 2\nu}{4(S_o - P_i^{cr})} \left[\ln \left(\frac{R_{pl}}{R} \right) \right]^2 \\ &\quad - \left[\frac{1 - 2\nu}{K_\psi + 1} \frac{\sqrt{P_i^{cr}}}{S_o - P_i^{cr}} + \frac{1 - \nu}{2} \frac{K_\psi - 1}{(K_\psi + 1)^2} \frac{1}{S_o - P_i^{cr}} \right] \\ &\quad \times \left[(K_\psi + 1) \ln \left(\frac{R_{pl}}{R} \right) - \left(\frac{R_{pl}}{R} \right)^{K_\psi + 1} + 1 \right] \end{aligned} \quad (4.17)$$

$$\begin{aligned} \frac{u_r^{pl}}{R} \frac{2G_{rm}}{\sigma_o - p_i^{cr}} &= \left[\frac{1 - 2\nu}{2} \frac{\sqrt{P_i^{cr}}}{S_o - P_i^{cr}} \right] \left(\frac{R_{pl}}{R} \right)^2 + \frac{1 - 2\nu}{4(S_o - P_i^{cr})} \left[\ln \left(\frac{R_{pl}}{R} \right) \right]^2 \\ &\quad - \frac{1 - 2\nu}{2} \frac{\sqrt{P_i^{cr}}}{S_o - P_i^{cr}} \left[2 \ln \left(\frac{R_{pl}}{R} \right) + 1 \right] \end{aligned} \quad (4.18)$$

Support Characteristic Curve (SCC)

Figure 4.10 shows the SCC, which can be constructed using the elastic relationship between the applied stress p_s and the resulting closure u_r by using Equation 4.19 for a section of the support of unit length in the direction of the tunnel (Carranza-Torres and Fairhurst, 2000).

$$p_s = K_s u_r \quad (4.19)$$

4.3.3.2 Modified of CCM for swelling pressure

The swelling pressure (P_s) is added in addition to the far field-induced stress (σ_o). The addition of additional swelling pressure to field stress will then make changes accordingly in LDP, GRC, and SCC as σ_o will be replaced by $(\sigma_o + P_s)$. A similar approach has been used for CCM analysis of long-term deformation due to swelling pressure swelling as described in section 4.3.3.1. The equations describes will be changed wherever σ_o has been defined which will be replaced by $(\sigma_o + P_s)$. To illustrate change in GRC upon addition of swelling pressure, the modification in elastic part is represented by Equation 4.20 and for plastic part is represented by Equation 4.21 and Equation 4.22 for dilation angle $\psi > 0$ and $\psi = 0$ respectively.

$$u_r^{el} = \frac{(\sigma_o + P_s) - p_i}{2G_{rm}} \quad (4.20)$$

$$\begin{aligned} \frac{u_r^{pl}}{R} \frac{2G_{rm}}{\sigma_o + P_s - p_i^{cr}} &= \frac{K_\psi - 1}{K_\psi + 1} + \frac{2}{K_\psi + 1} \left(\frac{R_{pl}}{R} \right)^{K_\psi + 1} + \frac{1 - 2\nu}{4(S_o - P_i^{cr})} \left[\ln \left(\frac{R_{pl}}{R} \right) \right]^2 - \\ &\quad \left[\frac{1 - 2\nu}{K_\psi + 1} \frac{\sqrt{P_i^{cr}}}{S_o - P_i^{cr}} + \frac{1 - \nu}{2} \frac{K_\psi - 1}{(K_\psi + 1)^2} \frac{1}{S_o - P_i^{cr}} \right] \\ &\quad \times \left[(K_\psi + 1) \ln \left(\frac{R_{pl}}{R} \right) - \left(\frac{R_{pl}}{R} \right)^{K_\psi + 1} + 1 \right] \end{aligned} \quad (4.21)$$

$$\frac{u_r^{pl}}{R} \frac{2G_{rm}}{(\sigma_o + P_s) - p_i^{cr}} = \left[\frac{1 - 2\nu}{2} \frac{\sqrt{P_i^{cr}}}{S_o - P_i^{cr}} \right] \left(\frac{R_{pl}}{R} \right)^2 + \frac{1 - 2\nu}{4(S_o - P_i^{cr})} \left[\ln \left(\frac{R_{pl}}{R} \right) \right]^2 - \frac{1 - 2\nu}{2} \frac{\sqrt{P_i^{cr}}}{S_o - P_i^{cr}} \left[2 \ln \left(\frac{R_{pl}}{R} \right) + 1 \right] \quad (4.22)$$

4.3.3.3 Panthi and Shrestha (2018) method

In tunnels passing through weak and schistose rock mass, the total plastic deformation is constituted by both time-independent and time-dependent deformation (Panthi and Shrestha, 2018). Rock mass deformability properties and in situ stress prevailing in the area greatly influence the extent of total deformation and if in situ stress is not isotropic, the deformation magnitude along the longitudinal alignment and within the periphery of the tunnel will be different (Panthi and Shrestha, 2018). Panthi and Shrestha (2018) has studied three headrace tunnel cases from Nepal, which have undergone plastic deformation during construction. Carranza-Torres and Fairhurst (2000) and Hoek and Marinos (2000) methods assume the isostatic in-situ stress condition for a circular tunnel. However, according to Panthi and Shrestha (2018), the in-situ condition is seldom isostatic. Hence, to represent the effect of anisotropy, horizontal vertical stress ratio (k) has been used to establish the relation of both time-independent and time-dependent tunnel strain. Instantaneous closure (ϵ_{IC}) and final closure (ϵ_{FC}) have been linked with vertical gravitational stress (σ_v), support pressure (p_i) and rock mass deformability expressed by shear modulus (G) as shown in Equation 4.23 and Equation 4.24 respectively based on the correlation plot shown in Figure 4.11 (left) .

$$\epsilon_{IC} = 3065 \left(\frac{\sigma_v + (1+k)/2}{2G(1+p_i)} \right)^{2.13} \quad (4.23)$$

$$\epsilon_{FC} = 4509 \left(\frac{\sigma_v + (1+k)/2}{2G(1+p_i)} \right)^{2.09} \quad (4.24)$$

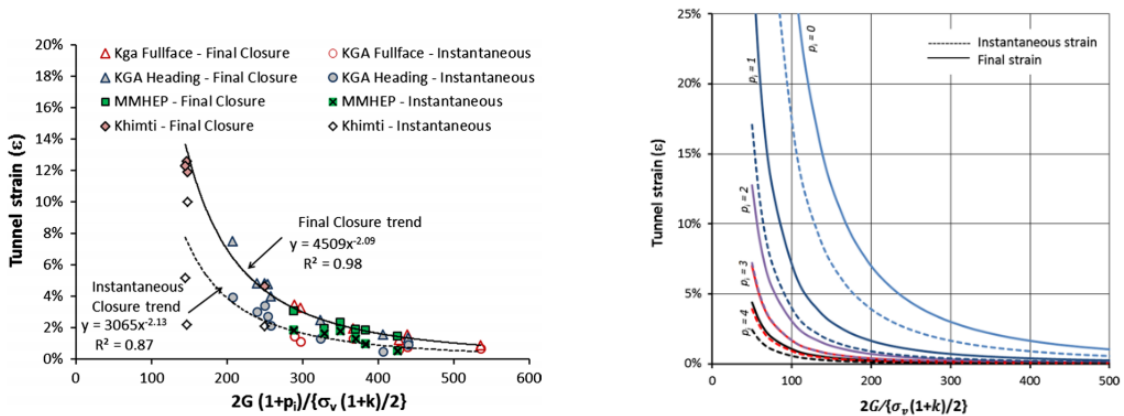


Figure 4.11: Correlation of instantaneous and final closure with rock mass property, support pressure and in situ stress (left) (Shrestha, 2014) and Tunnel strain versus rock mass shear modulus, in situ stresses for different support pressure magnitude (right) (Shrestha, 2014)

Panthi and Shrestha (2018) further using Equation 4.23 and Equation 4.24, developed a chart as shown in Figure 4.11 (right) that incorporates rock mass shear modulus and in situ condition for different support pressure and this chart can be used to estimate required support pressure (p_i) if shear modulus (G), horizontal vertical stress ratio (k) and vertical gravitational stress (σ_v) are known.

The rock mass shear modulus (G) is linked with rock mass deformation modulus (E_{rm}) as shown in Equation 4.25 (Carranza-Torres and Fairhurst, 2000). The rock mass deformation modulus (E_{rm}) is linked with the rock mass strength (σ_{cm}), deformation modulus for the intact rock (E_{ci}) and intact rock strength (σ_{ci}) by Equation 4.26 (Panthi, 2006) and Hoek and Brown (1997) linked the rock mass strength (σ_{cm}) with with cohesion (c) and angle of international friction (ϕ) as shown in Equation 4.27.

$$G_{rm} = \frac{E_{rm}}{2(1 + \nu)} \quad (4.25)$$

$$E_{rm} = E_{ci} \times \frac{\sigma_{cm}}{\sigma_{ci}} \quad (4.26)$$

$$\sigma_{cm} = \frac{2c \times \cos\phi}{1 - \sin\phi} \quad (4.27)$$

4.3.3.4 Modified Panthi and Shrestha (2018) method for swelling pressure

CCM and Hoek and Marinos (2000) methods analyze plastic deformation in isostatic in-situ stress condition. Hence, the modified CCM as explained in section 4.3.3.2 and modified Hoek and Marinos (2000) method explained in section 4.3.2.2 for swelling pressure also analyze the deformation in similar isostatic in-situ stress condition. To overcome this in Panthi and Shrestha (2018) method, swelling pressure is also added to horizontal stress. This is done by calculating the value of k (ratio of horizontal to vertical stress) as shown in Equation 4.28. Therefore, unlike in CCM and Hoek and Marinos (2000), swelling pressure has been added to both horizontal and vertical stress. Equation 4.29 represent the modified Panthi and Shrestha (2018) equations for computing final closure as there will be no change in instantaneous closure. The instantaneous closure takes place during the construction of the tunnel and the rock mass gets dried during that time and hence no swelling pressure will be exerted by a rock mass.

$$k = \frac{\sigma_h + P_s}{\sigma_v + P_s} \quad (4.28)$$

$$\varepsilon_{FC} = 4509 \left(\frac{(\sigma_v + P_s)(1 + k)/2}{2G(1 + p_i)} \right)^{2.09} \quad (4.29)$$

4.3.4 Numerical Modeling

The discretization of the rock mass into a large number of individual elements is known as numerical modeling where models are prepared to analyze the rock stress and deformation due to stress in underground structure (Nilsen and Palmström, 2000). In comparison

to empirical, semi-empirical, and analytical methods discussed earlier in this chapter, numerical modeling has several advantages in analyzing the stress-related problem in the rock mass. The empirical and analytical methods are limited to shape, size such as in CCM and Hoek and Marinos (2000) are developed based on the circular tunnel, and treat rock as homogeneous in isostatic stress conditions. Panthi and Shrestha (2018), however, consider the anisotropy and can be used any shape, still lacks the representation of real field scenario which is possible to analyze with numerical modeling. Therefore, the use of numerical analysis provides unlimited possibilities to represent real field conditions. The rock mass properties as described in Chapter , depends on a large number of variables such as rock mass classification, intact rock properties, and presence of weakness zones. The different combinations of these variables result in different rock mass properties which are unique (Neupane, 2010). Numerical modeling is best for analyzing rock stress problems but while using numerical modeling software one must be careful with input parameters. The users should be careful regarding " Garbage in- Garbage out" which means feeding wrong meaningless input results in wrong output (Udpa et al., 1989).

Various numerical models are available that can be used to analyze rock stress problem which are built based on different methods. Nilsen and Palmström (2000) categories the numerical models into two main categories: Continuous Models and Discontinuous models as shown in Figure 4.12.

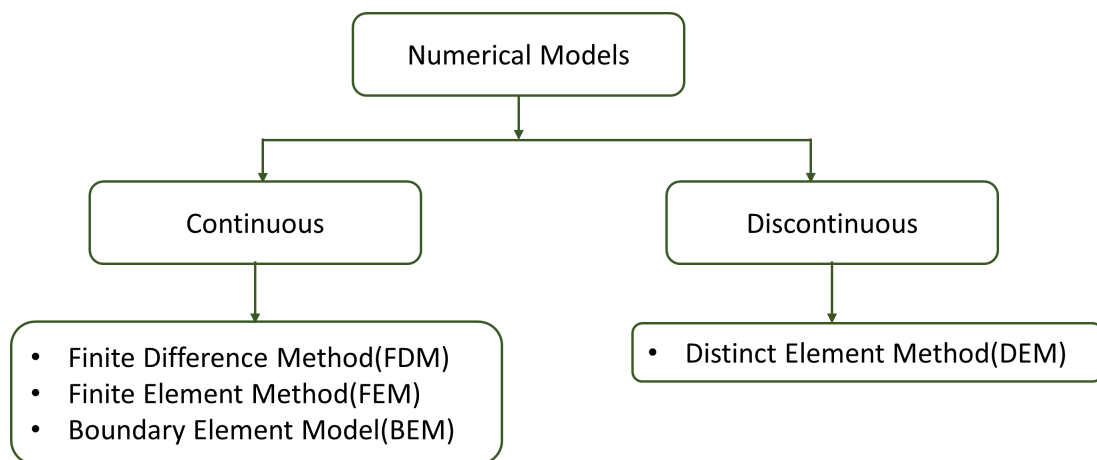


Figure 4.12: Different types of numerical methods (based on (Nilsen and Palmström, 2000))

4.3.4.1 Selection of Model

For this thesis, the RS2 model has been chosen for analyzing the stability against plastic deformation and swelling pressure. The software is based on the finite element method. RS2 is 2D software for analyzing stress-related problems and computing displacement in underground or surface excavation (Rocscience, 2007). RS2 comes with 3-standalone programs which include: MODEL, COMPUTE, and INTERPRET. RS2 provides numerous features to define the rock stress model. The model setup for analyzing the problem related to this thesis has been defined in the subsequent section as follows.

4.3.4.2 RS2 Model setup for analyzing Plastic deformation and Swelling pressure

Model setup

For numerical modeling using RS2, both elastic and plastic model setup is done as defined in Table 4.6. Plane strain analysis is chosen for modeling. The plane strain assumes that the length is infinite and excavation is normal to the plane section of analysis of excavation(s) (Rocscience, 2007). The plane strain analysis computes the major and minor in-plane principal stresses (Sigma 1 and Sigma 3), the out-of-plane principal stress (Sigma Z), in-plane displacements, and strains. As per definition in plain strain, the out-of-plane displacement (strain) is zero (Rocscience, 2007). The constant field stress is used to define stress situations whose value is computed by performing modeling on the topography also termed as valley modeling. The details of valley modeling are provided in the following chapter while assessing the in situ stress condition. Generalized Hoek and Brown failure criterion as described in section 3.3.1. The mesh setup and discretization are done using 3 noded triangles with gradation factor and number of nodes as 0.1 and 110 respectively. According to Frengen (2020), a low gradation value allows the higher density of nodes to be formed around the excavation, this helps to compute faster in the area like excavation where stress gradient is higher.

Table 4.6: Model setup for RS2 modeling

Model Setup Parameters	Description in RS2
Analysis Type	Plain Strain
Solver Type	Gaussian Elimination
Convergence Type	Absolute Force and Energy
Field Stress Type	Constant
Failure Criterion	Generalized Hoek and Brown
	3 Noded Graded
Mesh Type	Gradation Factor:0.1
	No. of nodes on Excavation: 110

External Model Boundary and Boundary conditions

The distance from the excavation to the model boundary should be at least 4 to 5 times the underground opening (Frengen, 2020). By setting this distance between excavation and external boundary, the possible boundary effects near the excavation can be avoided. Thus, the expansion factor 5 has been chosen to create an external boundary. However, in some sections of the Moglice headrace tunnel consisting of very weak rock mass with this expansion factor, the model does not converge. Hence, in such cases, the expansion factor has been increased to 10. After creating the external boundary, boundary conditions have been defined. The model has been restrained in both the X and the Y directions on all four sides as shown in Figure 4.13.

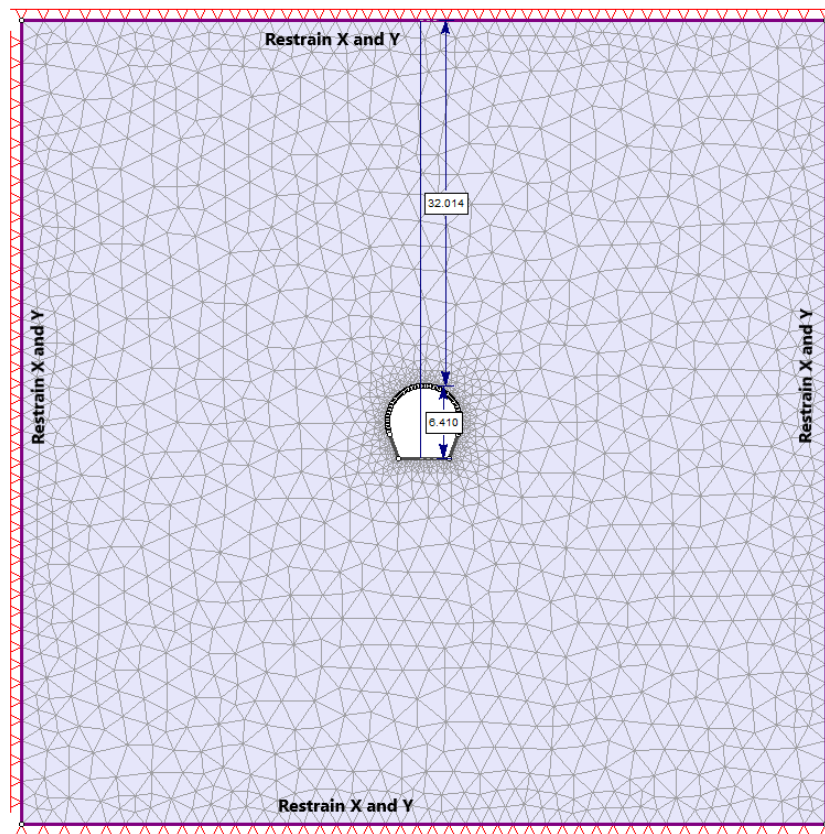


Figure 4.13: RS2 model showing excavation and external boundary with defined external boundary conditions

Stages

The stages are defined to closely resemble the construction and post-construction stages. Figure 4.14 shows the four stages define for the modeling namely: Pre-Excavation, Excavation, Support Installation, and Swelling. The first three stages define the construction stages and during this plastic deformation takes place. Therefore, these stages will be used to perform plastic deformation analysis using RS2. The final stage swelling represents the operation phase when the tunnel is filled with water and due to which surrounding rock mass gets saturated resulting in deformation of rock mass due to swelling phenomenon.

The excavation of the tunnel is carried out in a single stage as represented by stage 2 in Figure 4.14. However, the support is installed in the following stage. This is done as rock support installation always lags excavation. Using two separate stages for excavation and support installation allows some deformation to takes place before support is installed in the excavation stage.

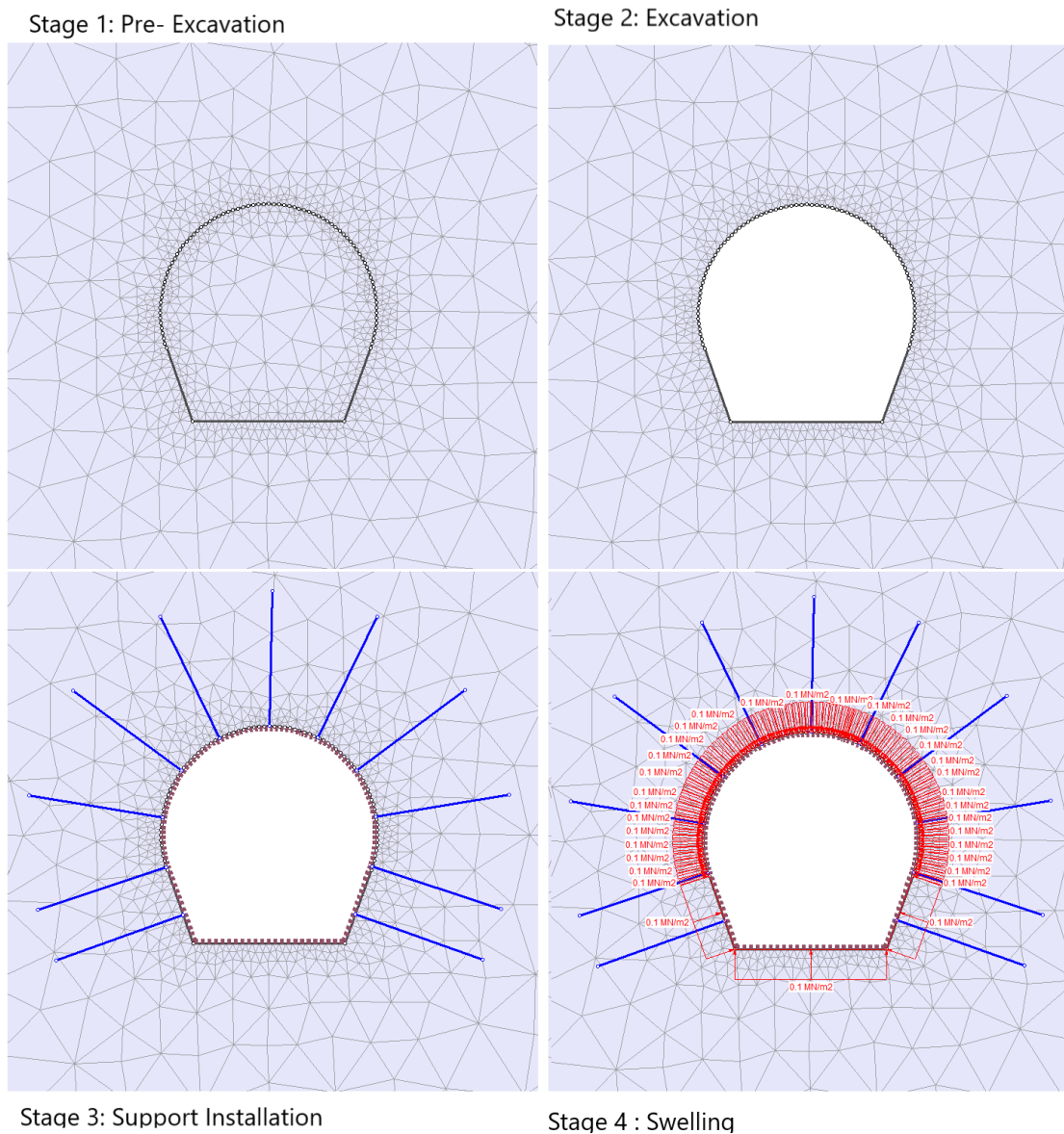


Figure 4.14: Different model stages used to define construction and swelling process in tunnel

Load Split

RS2 allows load splitting, which helps to split the induced load into different stages. As described, the excavation stage and support installation stage are defined in two separate stages, this allows some deformation to take place before support installation. When load split is not used and the model is run allowing all stress to act in the excavation stage will result in unrealistic deformation. It represents the situation when the tunnel is excavated and left unsupported. To avoid this support can be installed in the same stage as excavation. However, this situation also creates an unrealistic situation where support takes a higher load than the actual case. Therefore, load splitting has been implemented.

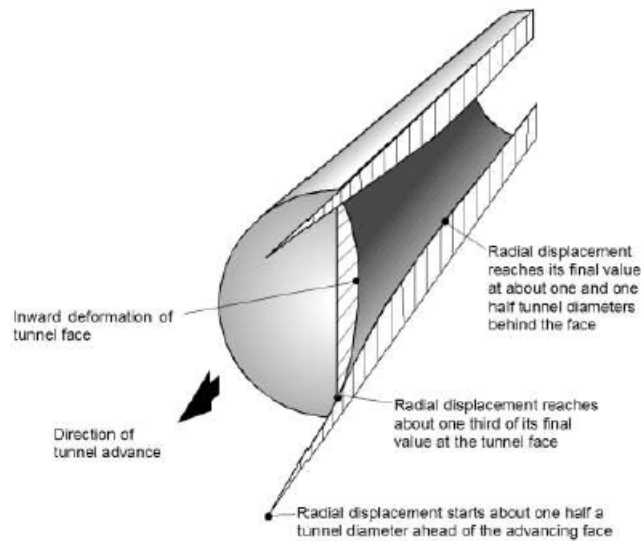


Figure 4.15: Deformation pattern in the rock mass surrounding of an advancing tunnel (Hoek, 2000)

The radial displacement during the excavation of the tunnel starts roughly half of the tunnel diameter in front of the advancing face and reached one-third of the final value at the face as shown in Figure 4.15 (Hoek, 2000). According to Carranza-Torres and Fairhurst (2000), because of face effect as shown in Figure 10.2 and explained in section 4.3.3.1, initially face acts as column as bear the distributed load. This suggests that only a few stress is released by rock mass after excavation at the section of support installation which keeps on increasing as the face advance and finally full load is induced on support. On this basis, it is assumed that 30% stress is induced during excavation before rock support has been installed. Therefore the load split factor is considered as 0.3 and 0.7 for the excavation stage and support installation stage respectively which sum ups to value 1 representing total induced load.

5 Cases of failure with Tunnels in a weak rock mass

The stability problems that are likely to occur while constructing the tunnel in a weak rock mass are reviewed in Chapter 4.2 which are squeezing, swelling, and slaking. In the past, many cases of failure in the tunnel have been recorded due to these problems. Therefore, this chapter will try to review some of the failure cases of the tunnel around the world to understand the problem. The cases reviewed in the chapter are Laodongshan Tunnel (China), and Chacabuquito Hydropower Plant Project (Chile).

5.1 Laodongshan Tunnel

5.1.1 Project description

The Laodongshan Tunnel is located in western Yunnan-Guizhou Plateau, China. It is a part of the Guangtong-Kunming railway. The length of the Laodongshan Tunnel tunnel is 7.6 km and the maximum overburden of the tunnel is 370 m (Cao et al., 2018). The Laodongshan Tunnel is a double-track railway tunnel with the height and the width of the tunnel are 12.37 m and 14.76 m which accounts for a cross-sectional area of about 138 m^2 (Cao et al., 2018). The construction of the tunnel takes more than 4 years as the construction was completed in September 2012 which began in January 2008.

5.1.2 Project Geology

The Laodongshan Tunnel passes through the Late Cretaceous aged, Early Cretaceous aged, and Late Jurassic aged formation geological units (Cao et al., 2018). According to Cao et al. (2018), the rock types found in the Laodongshan Tunnel are mudstone, sandstone, marl, or alternate appearance of them in combination form. In Figure 5.1, the geological cross-section of the Laodongshan Tunnel is shown describing lithology as ① to ⑦ respectively as silty clay; gravel soil; mudstone interbedded with sandstone; sandstone interbedded with mudstone; sandstone interbedded with marl; sandstone interbedded with mudstone; mudstone interbedded with sandstone and marl; and W2, W3, and W4 represent moderately-weathered, highly-weathered and completely-weathered rock, respectively. The tunnel passes through three fault zones (fault zone I, II, III). The rock mass is classified according to RMR system Bieniawski (1989) to quantify rock mass quality. The classification shows the rock mass present in tunnel alignment are of grades III, IV, and V suggesting fair, poor, and very poor rock mass.

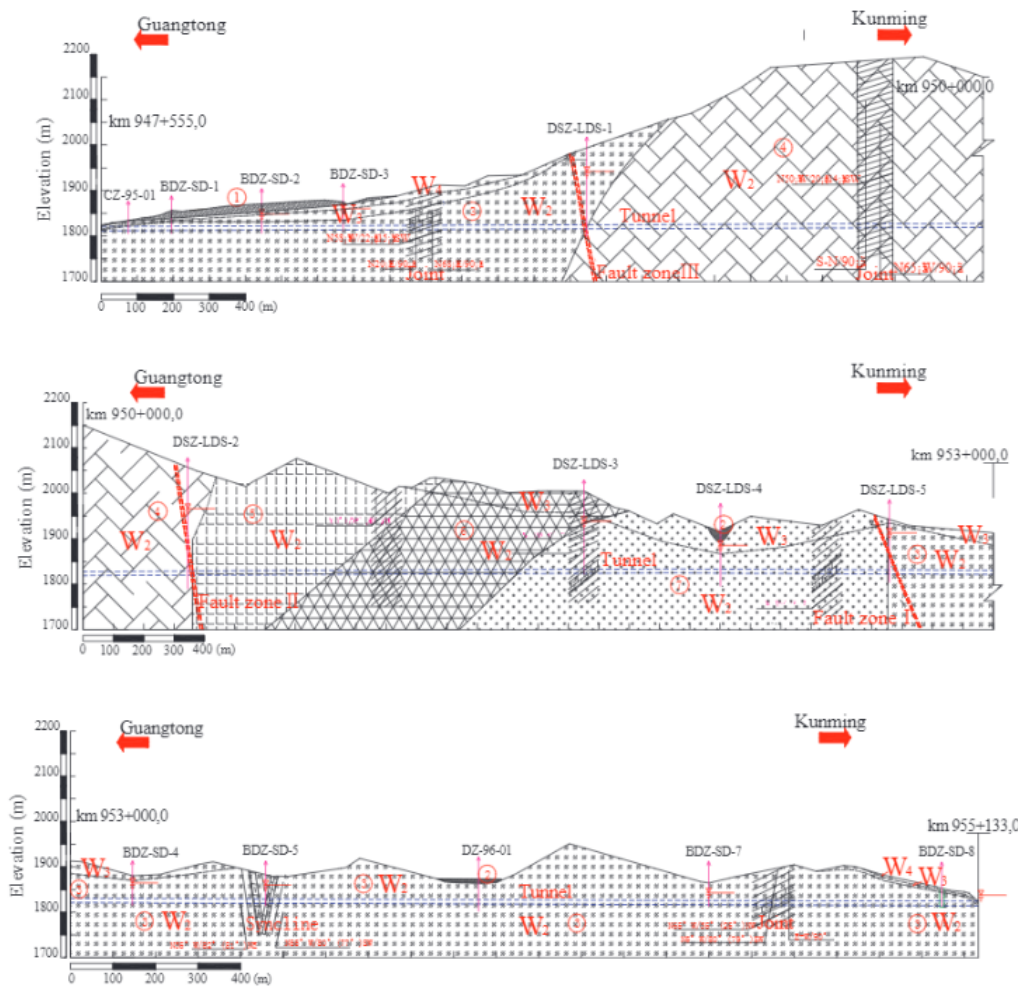


Figure 5.1: Geological cross section of the Laodongshan Tunnel (Cao et al., 2018)

5.1.3 Failure due to long term deformation

The Laodongshan tunnel is excavated in seven stages using the Three-bench-seven-step excavation method. The deformation has been measured at chainage 950+680 (Cao et al., 2018). According to the results of real-time measurement, the at first crown settlement and horizontal convergences rapidly increased during the excavation of the top heading. The crown settlement and horizontal convergence of arch feet measured after finishing the excavation of top heading are found to be 71 mm and 122 mm, respectively at the rate of 35 mm/d and 61 mm/d, respectively. During the excavation of the middle bench crown settlement and horizontal convergence of the arch feet increased further and reached 170 mm and 249 mm, respectively. The horizontal convergence value of wall waists also reached 40 mm. The rate of crown settlement rate and horizontal convergence decrease after installing primary support of the top heading. However, the convergence value of wall waists increased again during the excavation of the lower bench of the tunnel and the rate convergence rate of wall waists reached up to 68 mm/d. During the excavation of core soil and bottom part of the tunnel, the rise in the horizontal convergence of the tunnel continues and reached 60 mm/d. The maximum crown settlement and horizontal

convergence after 168 days have reached 275 mm and 402 mm, respectively (Cao et al., 2018). The long-term deformation was reached out of control causing failure during construction demanding many control measures to be taken to ensure the stability of the tunnel. Figure 5.2 shows the failure in the tunnel due to uncontrolled long-term deformation.

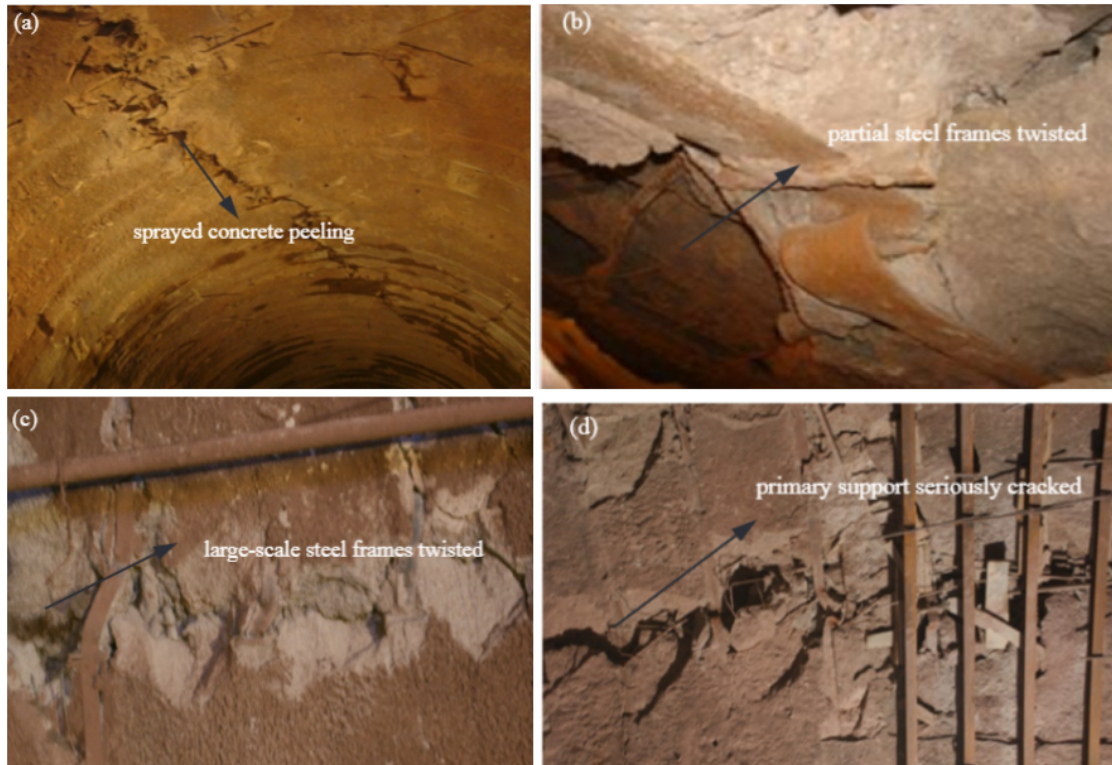


Figure 5.2: Tunnel failure in Laodongshan tunnel. (a) Peeling of sprayed concrete ; (b) Twisted partial steel frames; (c) Twisted large-scale steel frames; (d) Serious crack on primary support (Cao et al., 2018)

5.2 Chacabuquito Hydropower Plant Project

5.2.1 Project description

The Chacabuquito Hydropower Plant Project 25 MW, is situated in the valley of the Aconcagua River, 65 km north-northeast of Santiago, Chile. The water conveyance system of the hydropower consists of an open channel and two horseshoe tunnels of dimension 4.20 m * 4.35 m. The length of the Los Quilos tunnel is 788 m and the length of the Chacabuquito tunnel is 2,171 m.

5.2.2 Project Geology

The Chacabuquito tunnel passes through the Los Pelambres Formation, formerly known as the Abanico Formation, of the Cretaceous age. The formation is built up of stratified porphyric and aphanitic andesite, aphanitic basaltic andesite and basalt, volcanic breccia, and local thin layers of fine-grained sandstone and/or andesitic tuff and limolites Castro et al. (2003).

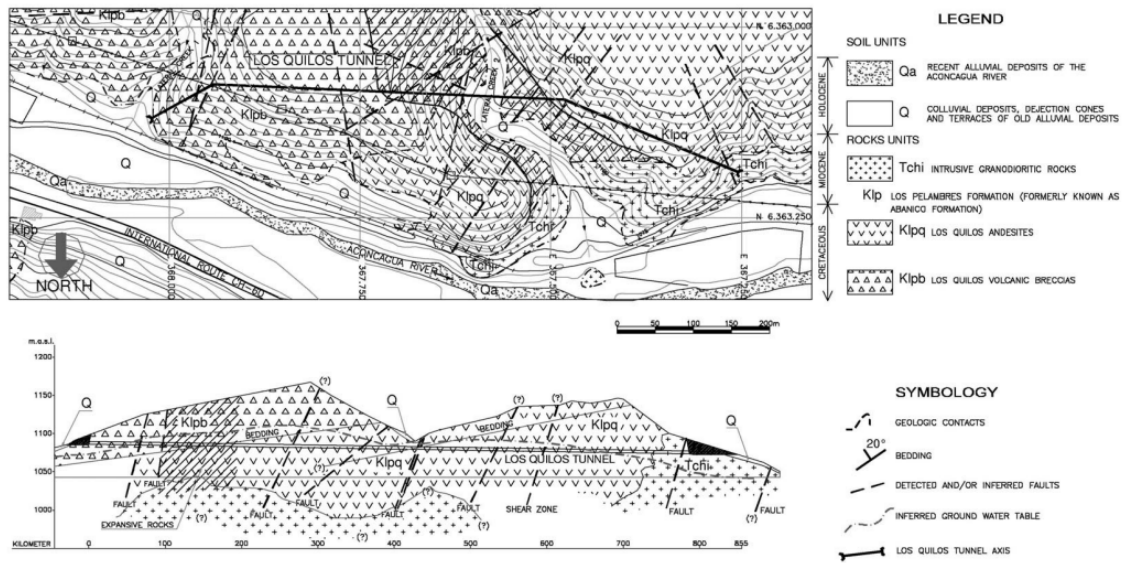


Figure 5.3: Geological map and tunnel profile of the Los Quilos Tunnel (Castro et al., 2003)

In Figure 5.3 and Figure 5.4, the geological maps and profiles along the tunnel for the Los Quilos tunnel and the Chacabuquito tunnel have been shown respectively. The project location consists of fractured and oxidized soft rock mass with grayish stronger rock. The rock mass is of poor geotechnical quality and the tunnel crosses some fault zones. The rock consists of clay were detected and such rocks tend to disintegrate when react with the water.

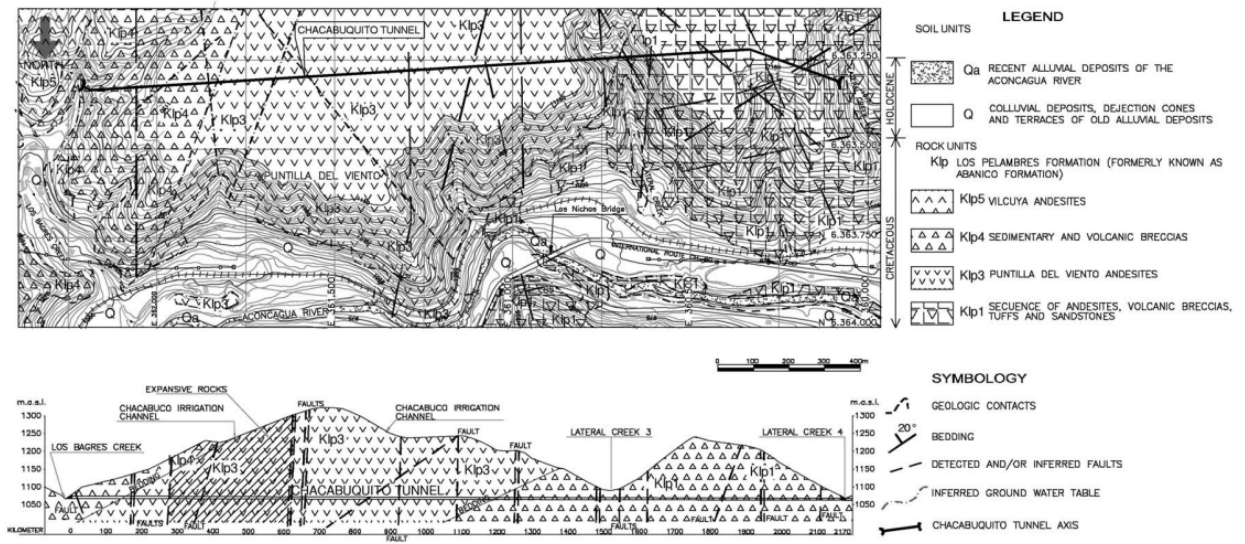


Figure 5.4: Geological map and tunnel profile of the Chacabuquito Tunnel (Castro et al., 2003)

5.2.3 Failure due to swelling

During the construction of tunnels, serious problems related to rocks exhibiting an expansive behavior were encountered. This problem encounters while crossing important

north-south trending faults, where the rock is strongly fractured and associated with the three geological features Castro et al. (2003):

- Presence of clayey, with thick montmorillonitic and caolinitic soft fracture fillings in both tunnels
- The zones with thin veins of ceolites and additionally a few calcite and clay minerals (montmorillonite, caolinite, and illite) (Encounter only in in the Chacabuquito tunnel eastern front)
- Also withinside the Chacabuquito tunnel eastern front, Hydrothermal alteration of the host andesitic rock mass because of the contact with an intrusive monzogranodioritic stock hence permitting the presence of clay minerals.

At the following chainage of the Eastern Front of the Chacabuquito Tunnel expansive rock zones were found Castro et al. (2003):

- At the chainage PK 0+287 to PK 0+550, a large deformation due to huge expansion rock has occurred. The rock mass at this section contains the fractured rock of robust to poor quality. The infilling materials present in joint plane are iron oxides, clay minerals (sericite, illite, caolinite and minor montmorillonite), and in particular ceolites (predominantly laumontite, and secondarily chabazite and stilbite) and calcite
- The most critical situation was encountered at chainage PK 0+340 to 0+347, PK 0+440 to 0+447, and PK 0+535 to 550. The rock mass at this chainage was soft, decomposed, with hematite and argillized (predominantly montmorillonite). The tested expansion pressure was numerous from much less than 0.3kg/cm^2 to 1.40kg/cm^2 .

In the case of the eastern front of Los Quilos tunnel, the large deformation due to the expansion of rocks extend from chainage PK 0+230 to PK 0+420. The hydrothermal alteration was noticed with the presence of pyrite, sericite, montmorillonite, and minor caolinite-illite. The rock mass contained the rock of strong quality with intense fractured and crossing some fault zones. The rocks were plastic and expansive where the tunnel crosses fault zones. The swelling pressure measured at this zone is 0.3kg/cm^2 to 3.3kg/cm^2 . A maximum of 0.7m shrinkage of the floor was observed during construction which may occur due to the combined effect of heavy traffic and saturation.

Laboratory tests were carried on the rock samples collected during the construction to measure swelling pressure. Based on the test results geomechanical analysis was carried out and the rock support is then designed based on the results from this analysis. A load factor of 1.4 was applied for both, the expansion pressure and the vertical load during the design of rock support. This assumption of load factor means rock support can accept more minor designs without collapsing (Castro et al., 2003).

6 Assessment of La Higuera Tunnel Collapse

6.1 Project Description

La Higuera hydropower plant is located within the Tinguirrica valley approximately 170 km south of Santiago, Chile as shown in Figure 6.1. It is run-of-river scheme hydropower with an installed capacity of 156 MW. The headrace tunnel is of length 17.5 km. The design discharge of the project is $50\text{m}^3/\text{s}$ and the design gross head is 400 m. The water is conveyed to the surface powerhouse from the head pond through a shotcrete lined headrace tunnel and surface steel penstock pipe of 4 m diameter. The surface powerhouse consists of two Francis turbines each with a capacity of 78 MW. The annual average energy generation is 811 GWh. The project is constructed under the engineering, procurement, and construction (EPC) contract with Consortia Queiroz Galvão as Contractor and Lahmeyer GmbH as Designer (Broch, 1984).

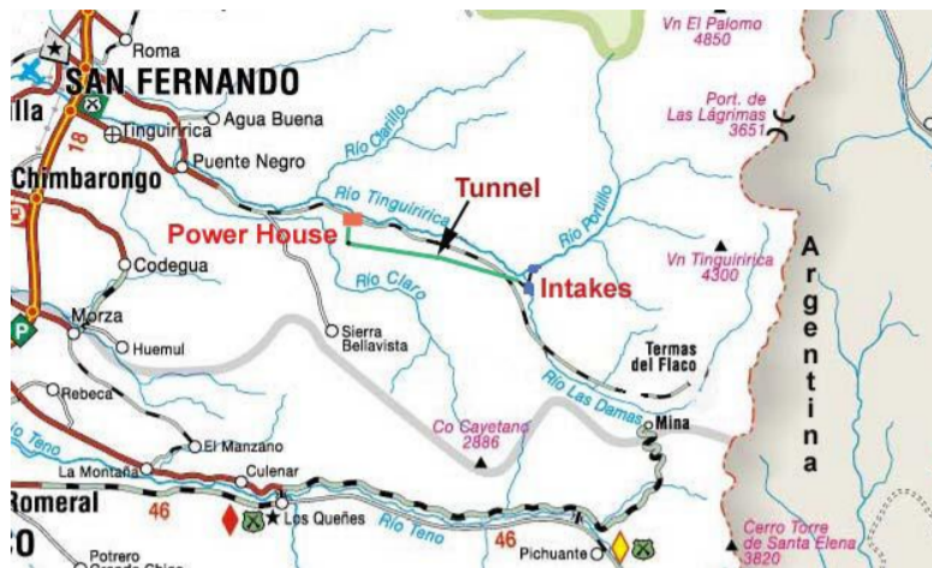


Figure 6.1: Map showing location of La Higuera hydropower project [extracted from UNFCC (2004)]

6.2 Project Layout

The intake of the project is located at the Los Helados River which discharges water into the Azufre river. Azufre Intake at an elevation 1140 masl diverts the flows through canal and tunnel to Tinguirrica intake. The water from these three intakes at Tinguirrica river, Los Helados River, and Azufre Intake are diverted via weir constructed at 1100 masl at Tinguirrica intake to desanding basins on the north bank of the Tinguirrica river. The water is then transferred to an off-channel headpond through 18 km long tunnel of diameter 5.8 m. The water is then conveyed to the powerhouse from headpond through steel penstock of 600 m length. The surface powerhouse is located on the south bank of Tinguirrica at around 715 masl. The tailrace returns the water to the Tinguirrica river approximately 100 m downstream of the powerhouse. The generated energy is evacuated from the switchyard near the powerhouse to the substation near the town of San Fernando by 38 km 154 kV high tension transmission line, where it joins the SIC grid (UNFCC, 2004).

6.3 Engineering Geology condition of failure zone

The Tinguiririca River rises in the Andes Mountains about 120 km south of Santiago and flows westward to the Pacific Ocean (UNFCC, 2004). The Andes mountain range is the youngest in the world and considers to have the most complex geological conditions (Carlos Lang and Salazar, 2017). The tunnel passes through volcanic layers in Tinguiririca valley as shown in Figure 6.2.

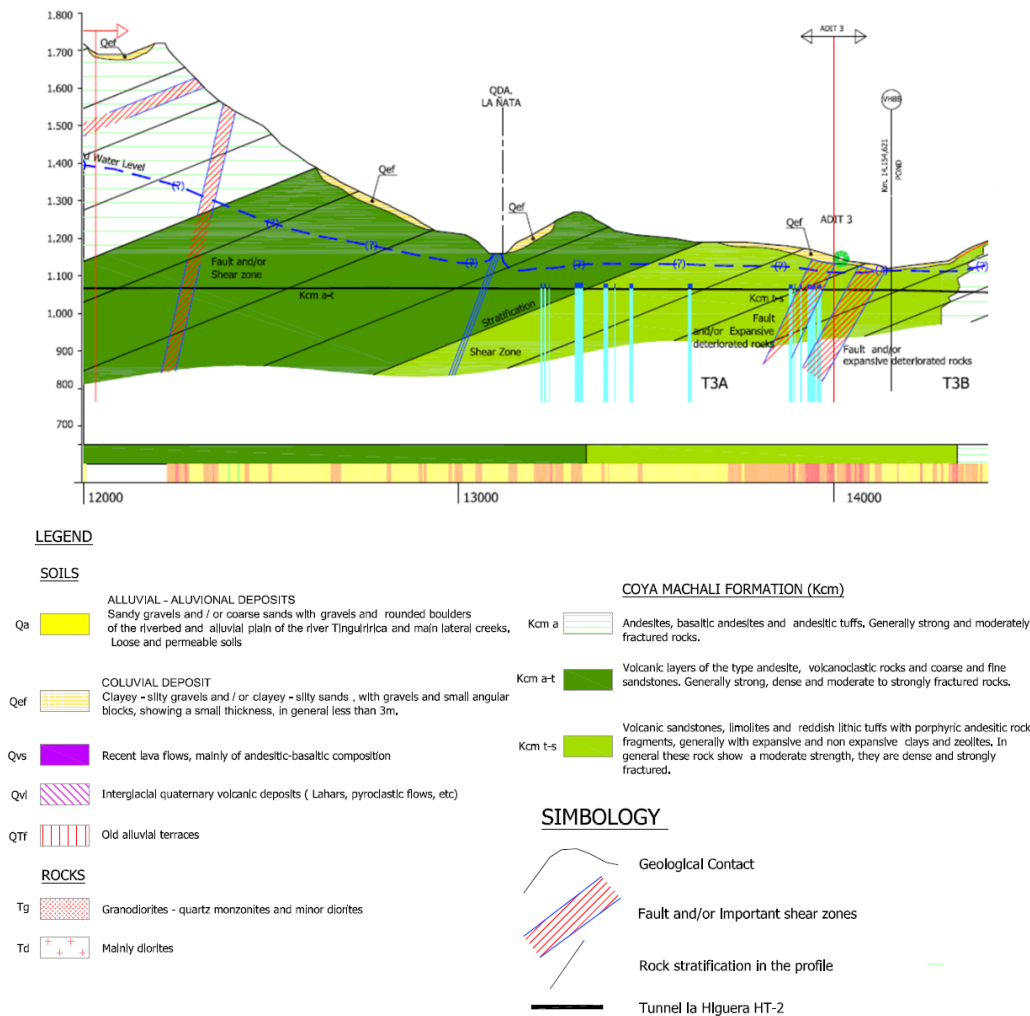


Figure 6.2: Geological Map of La Higuera headrace tunnel (SNPower, 2012)

In 2011, after almost 9 months of operation, the headrace tunnel collapse. During the operation, headloss was observed few months after the production has commissioned. The tunnel was dewatered and inspection was carried out and it was found the collapse has occurred with a volume of 12,000 m³ debris extending 500 m downstream from the location of failure (Broch, 1984) as shown in Figure 6.3. The collapse of the tunnel occurs between chainage 12+300 to 12+500. It was found that a prominent geological fault was intersected at this region (Brox, 2019). After drill and blast excavation of the tunnel, shotcrete has been applied immediately by the contractor. This restricts engineering geologists to study the rock mass behavior over time. The remedy applied in the project for

the collapse was the construction of 238 m long bypass tunnel (Broch, 1984).



Figure 6.3: Weathered rock associated with the geological fault at the collapse location of La Higuera headrace tunnel (Brox, 2019)

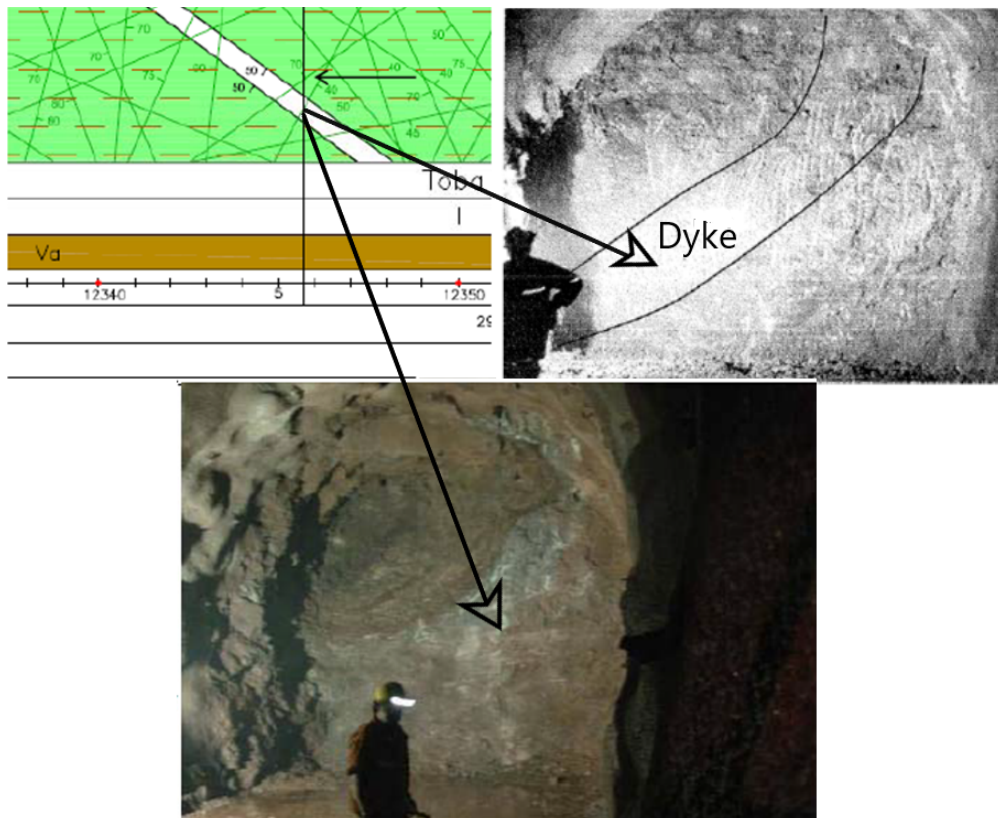


Figure 6.4: Geological Map (Top left) of the La Higuera and Tunnel face at chainage 12+347 showing dyke (fault zone) (top left and bottom) as per as built records (SNPower, 2012)

Figure 6.4 shows the tunnel face at chainage 12+347 where dyke is visualized on the tunnel face. This is the structural fault zone where the transition between the rock types occurred. Figure 6.2 shows the tunnel passes through scarification of volcanic layers of andesitic rock and sandstone rock and at chainage 12+347 the tunnel encounters such stratification. The preliminary conclusion from the investigation of failure found that the reasons for the failure were the presence of fault zone i.e. dyke along with swelling minerals which was associated with zeolite veins, and underestimated support for the transient water pressure and rock stress.

Table 6.1: Q-value measured during face mapping during excavation of headrace tunnel

Chainage	Q	GSI
12+337.30	3.8	54
12+339.70	3.3	53
12+342.00	3.7	54
12+344.10	3.0	52
12+348.20	0.4	39
12+350.90	3.8	54
12+347.00	1.3	47
12+357.10	1.7	48
12+360.60	2.2	50

During the excavation of the headrace tunnel, tunnel mapping was carried out. The Q-values at different chainages were calculated after excavation at the tunnel face. As shown in Table 6.1 shows the Q-value noted at different chainages during face mapping ranges from 0.4 to 3.8. According to Q-chart shown in Figure 3.8, the rock mass present in these sections can be classified as very poor to poor. Further using the relation shown in Equation 3.11 and Equation 3.12, GSI values have been computed as shown in Table 6.1. The GSI values range from 39 to 54 suggesting the presence of fair to good quality of weathered rock mass with multiple joints.

6.4 Tunnel cross section and installed Rock support

The La-Higuera headrace tunnel is of horse-shoe shaped as shown in Figure 6.5. The cross-sectional area of the tunnel is 28.98 m². The rock support consist of fibre reinforce sprayed concrete of 70 mm thickness and systematic rock bolting of length 2.5 mm and diameter of 22 mm. The details of material properties of fibre reinforce sprayed concrete and rock bolt have been presented in Table 6.2.

Table 6.2: Material properties of fibre reinforce sprayed concrete and rock bolt

Bolts		Fibre reinforced sprayed concrete	
Parameters	Value	Parameters	Value
Bolt diameter (mm)	22	Thickness (mm)	70
Bolt length (m)	2.5	Young's Modulus (Mpa)	25000
Bolt Modulus, E (Mpa)	200000	Possion's ratio	0.18
Tensile Capacity (MN)	0.15	Compressive strength (Mpa)	40
Residual Tensile Capacity (MN)	0.016	Tensile Strength	5
Outplane -Spacing (m)	1		

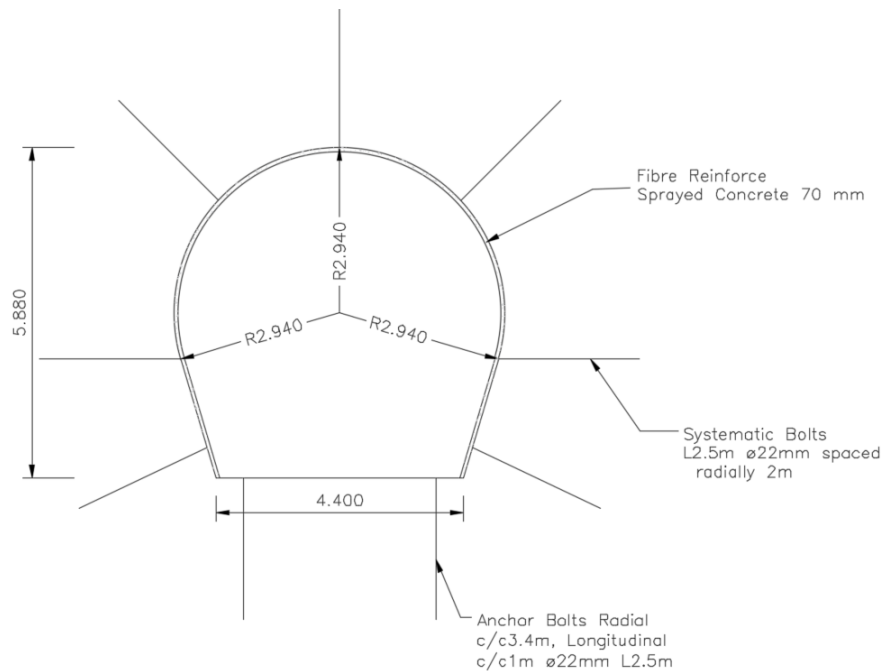


Figure 6.5: La-Higuera tunnel cross section showing installed support

6.5 Mineral Content of La Higuera Rock sample

The rock samples were collected from all along the longitudinal section at different chainages of the La Higuera tunnel and were tested by different laboratories. The results are collected only for the area of interest i.e. the area where the collapse occurs. The results of the rock samples within the chainage 12+000 to 13+000 are collected. Table 6.3 shows the results obtained from the laboratory testing for mineral content at different chainages of the headrace tunnel. It can be seen the samples contain a rich amount of Laumontite ranging from 8.6% to 42.1%. Laumontite falls under the zeolite group which have similar swelling potential as smectites and are very sensitive to the change in moisture content (Bell and Haskins, 1997).

Table 6.3: Mineral content at different chainages at La Higuera headrace tunnel

Chainage	12+305	12+325	12+327	12+330	12+343
Quartz	9.6	27.1	10.3	9.4	32.0
Plagioclass	24.3	19.5	21.9	22.8	3.0
Laumontite	11.7	31.1	42.1	35.5	26.0
Hematite	4.7	1.6	4.5	8.9	7.0
Clinochlore	7.4	10.5	9.8	8.2	3.0
K-feldspar	6.2	3.5	7.0	6.0	3.0
Diopside	3.9	1.5	2.9	3.2	1.0

6.6 Mechanical Properties of Intact rock sample

The Uniaxial Compression Strength (UCS) test and Point load tests were carried out on intact rock samples to determine the Uniaxial Compression Strength. For the area of

interest, only one UCS test result is found at chainage 12 +180 which is insufficient to represent the rock mass with dyke. From the point load test, the point load strength (I_{50}) is found in the range of 1.81 to 3.63 which per Table 3.2 suggested that the compressive strength will vary from 25 -100 MPa. Using this range compressive strength and based on classification shown in Table 3.1, the rocks can be classified from medium strong to strong. The rock types in the rock mass is represented as strong sandstone of compressive strength >50 MPa and dyke (volcanic andesites rock) of medium strength with UCS <50 MPa. For the computation of UCS from the point load test the values of K_{50} for strong and medium-strong rock are taken as 16 and 14 respectively as suggested in Table 3.2. The mechanical properties of the La-Higuera headrace tunnel rock sample have been summarized in Table 6.4.

Table 6.4: Mechanical Properties of La-Higuera headrace tunnel intact rock sample

Description	Strong Sandstone	Dyke	Remarks
Compressive strength, σ_{ci} (MPa)	55	-	Form UCS Test
E-modulus, E_i (GPa)	41	17	Form PLT
Density, γ (gm/cm^3)	2.7	2.7	Form UCS Test
Poisson's ratio ν	0.18	0.25	

6.7 Rock Mass Properties

The rock mass properties like rock mass strength (σ_{cm}) and rock mass deformability (E_{rm}) has been computed based on the chapter 3.6 and chapter 3.7 . The input parameters for the calculation of rock mass strength (σ_{cm}) and rock mass deformability (E_{rm}) based on the relations provided in Table 3.6 and Table 3.7 respectively are taken from Table 6.4. The Hoek and Brown Constant (m_i) is taken as 17 according to Appendix and the value of disturbance factor (D) is taken as 0.2 from Appendix considering that the tunnel is carefully excavated using drill and blast method.

Table 6.5: Rock mass strength (MPa) calculation using different relations

Chainage	Bieniawski (1989)	Hoek et al. (2002)	Barton (2002)	Panthi (2006)
12+337.30	5.5	11.0	16.7	5.9
12+339.70	5.3	10.8	16.0	5.9
12+342.00	5.5	11.0	16.6	5.9
12+344.10	5.1	10.7	15.5	5.9
12+347.20	2.5	7.9	7.9	5.9
12+350.90	5.5	11.0	16.7	5.9
12+347.00	3.8	9.4	11.7	5.9
12+357.10	4.2	9.8	12.8	5.9
12+360.60	4.6	10.2	13.9	5.9

The rock mass strength estimated using different relations is shown in Table 6.5 which shows varying values of rock mass strength. Each method depends on varying input parameters which leads to the variation in the estimation of rock mass strength. The methods like Hoek et al. (2002) and Barton (2002) estimates the high rock mass strength.

Bieniawski (1989) method estimates the minimum value of rock strength but the value is almost similar to the estimation from Panthi (2006).

Table 6.6: Rock mass deformation modulus (GPa) calculation using different relations

Chainage	Hoek & Brown [1997]	Barton[2002]	Panthi [2006]	Hoek & Diederichs [2006]
12+337.30	8.75	12.39	4.83	11.90
12+339.70	8.30	11.82	4.83	11.27
12+342.00	8.66	12.28	4.83	11.78
12+344.10	8.01	11.45	4.83	10.85
12+347.20	3.76	5.85	4.83	4.57
12+350.90	8.75	12.39	4.83	11.90
12+347.00	5.85	8.66	4.83	7.66
12+357.10	6.47	9.47	4.83	8.59
12+360.60	7.13	10.32	4.83	9.56

The rock mass deformability estimated has been presented in Table 6.6. Barton (2002) and Hoek and Diederichs (2006) estimate the higher value of rock mass deformability whereas the estimate from Hoek and Brown (1997) method is of average value. The estimate from Panthi (2006) method is the smallest in comparison to other methods except for chainage 12+348.2 since at this chainage the Q value is smallest. The smallest Q value is estimated by Hoek and Brown (1997) method at chainage 12+348.2.

6.8 Laboratory results of Swelling Test

La-Higuera headrace tunnel is constructed in the rock mass containing swelling minerals as discussed in chapter 6.5. The presence of Laumontite minerals of the zeolite group in the rock sample makes the tunnel vulnerable to the swelling phenomenon. The test has been performed on rock samples to measure swelling pressure and free swelling. The result from the laboratory test has been presented in Table 6.7. The swelling pressure ranges from 0.4 MPa to 2.7 MPa and the free swelling index varies from 110% to 155%. The swelling can therefore be classified as ranging from high to very high swelling based on the classification shown in Table 4.2.

Table 6.7: Laboratory test results of Swelling

Description	Max	Min	Average	Standad deviation
Swelling Pressure (Mpa)	2.7	0.4	1.3	±0.7
Free Swelling %	155	88	110	±17.7

6.9 In situ stress Assessment

It is important to establish the insitu stress condition in the rock mass while analyzing the rock mass problem. The stress condition at any location is represented by the three principal stresses. Hence, it is important to determine the magnitude and direction of these stresses. In the case of La-Higuera in absence of results of in situ stresses measurements

from any of the field methods like hydraulic fracturing and 3D overcoring, numerical analysis has been carried out.

The project layout of the La- Higuera hydropower project is shown in Figure 6.6, where the green line represents the tunnel alignment. The valley modeling at chainage 12+347 is carried for two sections one longitudinal section along the tunnel axis and another cross-section which is perpendicular to the tunnel axis (represented by the red line in Figure 6.6) as shown in Figure 6.7 and Figure 6.8. The factors affecting the in situ stresses are irregular surface topography, tectonic stress, and the presence of the weakness zone. From the world stress map, it has been found that the tectonic stress acting near the project area is found to be of magnitude 5.2 MPa and oriented N98°E. The tunnel is oriented N112°E. A major weakness zone is found in the study area where the failure has occurred. The weakness zone has a strike of N143°E and a dip of 63°SE. The details of modeling type and field stress have been presented in Table 6.8 The input parameters for material a have been taken from Table 6.4.

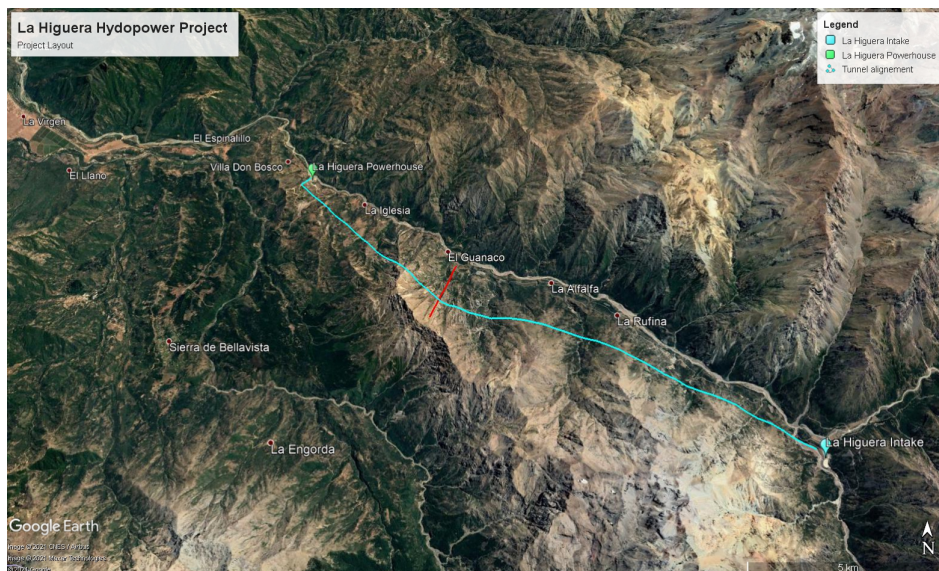


Figure 6.6: La-Higuera Hydropower project layout

Table 6.8: Valley modeling type and details at chainage 12+347 of La Higuera headrace tunnel

	Descriptions	Value	
Longitudinal section valley model	Type of Analysis	Elastic	
	Field stress Type	Gravity	
	In -plane stress ratio	1	
	Out-plane Stress ratio	1	
	In plane Locked in horizontal stress(MPa)	5.05	
	Out-plane Locked in horizontal stress(MPa)	1.26	
	Cross section	In-plane Locked in horizontal stress(MPa)	1.26
	Valley Model	Out-plane Locked in horizontal stress(MPa)	5.05

The boundary conditions for the modeling as shown in Figure 6.7 and Figure 6.8 is defined as the top boundary of the model is freed, right, and left boundaries are restrained

on x to prevent displacement horizontal displacement. And the bottom boundary is restrained on Y to allow only horizontal displacement.

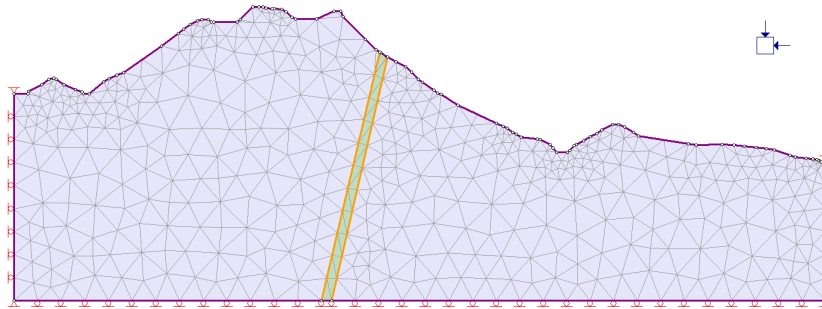


Figure 6.7: RS2 longitudinal valley section of La-Higuera headrace tunnel

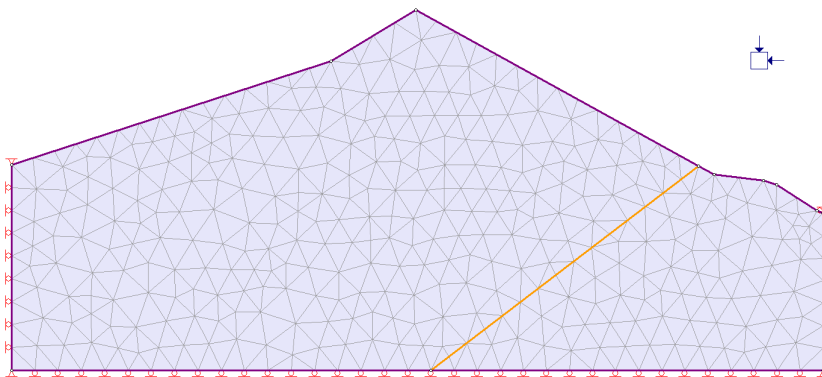


Figure 6.8: RS2 cross section of valley of La-Higuera headrace tunnel

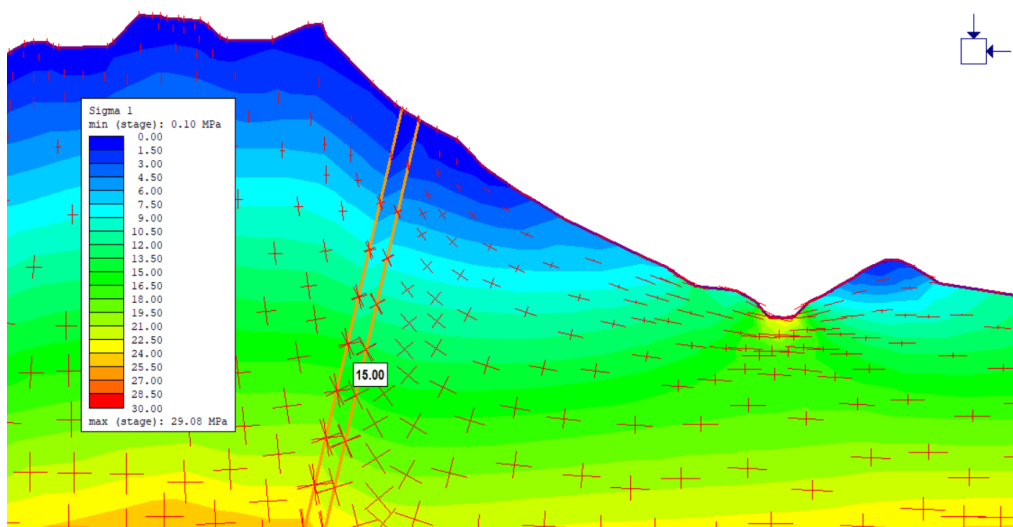


Figure 6.9: RS2 analysis result showing sigma 1 of longitudinal valley section of La-Higuera headrace tunnel

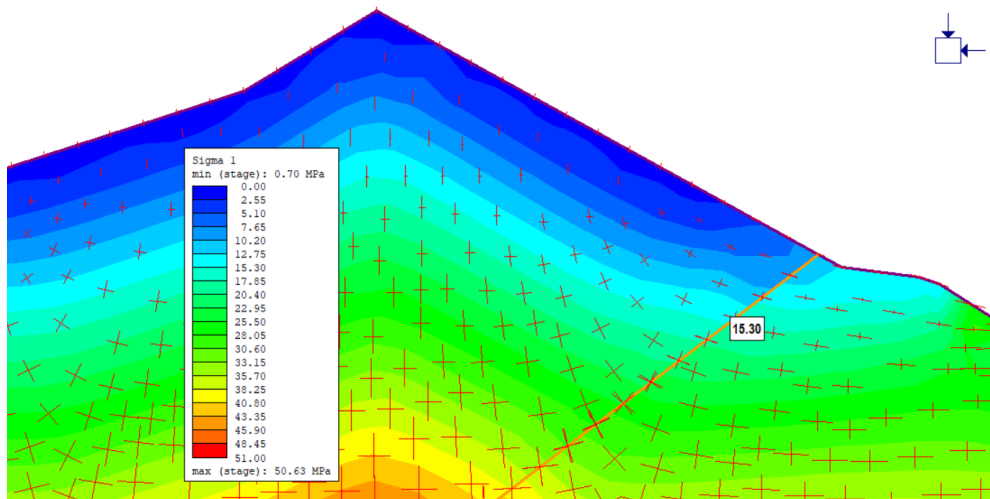


Figure 6.10: RS2 analysis result showing sigma 1 of cross section of valley of La-Higuera headrace tunnel

Figure 6.9 and Figure 6.10 show the result of elastic analyses of longitudinal and cross-sectional valley model respectively of La-Higuera headrace tunnel. The principal stresses computed from modeling has been summarized in Table 6.9. The results of stresses from the cross-section valley modeling is consider for the numerical modeling.

Table 6.9: In-situ stresses at La-Higuera headrace tunnel

Valley Model	σ_1 (MPa)	σ_3 (Mpa)	σ_z (Mpa)	σ_1 angle from horizontal ($^\circ$)
Longitudinal Section	15.00	9.60	13.50	127
Cross section	15.30	7.25	14.25	161

6.10 Assessment of La-Higuera Tunnel Collapse due to Swelling Pressure

The assessment of failure is carried out on section 12+347 of the La-Higuera headrace tunnel. As shown in Figure 6.4, the tunnel passes through the weakness zone, and also rock mass present in this section is very poor with the Q value of 0.3 as shown in Table 6.1. The assessment of swelling pressure is carried out using semi-empirical, analytical, and numerical modeling as reviewed in chapter 4.3. The maximum swelling pressure measured at the lab as shown in Table 6.7 is assumed to prevail in this section to assess the possible worst-case scenario. The in-situ swelling pressure will not be the same as measured at the laboratory, hence the sensitivity analysis of swelling pressure is carried out based on chapter 4.2.2.1. The in situ swelling pressure will therefore varied from 5% to 55% of maximum laboratory-measured swelling pressure.

6.10.1 Semi-empirical and Analytical method

The modified Hoek and Marinos (2000), CCM (Carranza-Torres and Fairhurst, 2000) and Panthi and Shrestha (2018) methods as reviewed in chapter 4.3.2.2, chapter 4.3.3.2 and chapter 4.3.3.4 respectively have been used. The modification done is based on

the addition of swelling pressure to the in situ stress. The maximum swelling pressure measured from the laboratory is 2.7 MPa, and to carry out the swelling analysis it is varied from 5% to 55% to represent the in situ swelling pressure. The input parameters required for the analyses have been taken from Table 6.4, Table 6.5 and Table 6.6.

6.10.1.1 CCM (Carranza-Torres and Fairhurst, 2000)

CCM is developed for a circular tunnel, therefore for the La-Higuera headrace tunnel, an equivalent circular radius has been computed as 3.03 m. The other required parameters for CCM have been taken from Table 6.4. The extent of deformation (u) estimated by CCM at distance (L) 1 m behind the face is 36 mm as presented in Table 6.10.

Table 6.10: Estimation of deformation at chainage 12+347 of La-Higuera headrace tunnel by CCM

Chainage	Vertical Stress (P_0) (MPa)	E_{rm} (MPa)	G_{rm} (MPa)	Support Pressure P_i (MPa)	L(m)	u (mm)
12+347	14.1	3140	1207	0.9	1	36

For analyzing the long-term deformation due to swelling pressure, varying swelling pressures have been added to the vertical stress (P_0). The long-term deformation estimated for different swelling pressure is presented in Table 6.11. The deformation increases gradually from 42 mm with swelling pressure of 0.14 MPa to a maximum of 134 mm with maximum swelling pressure of 1.49 MPa.

Table 6.11: Long-term deformation due to swelling pressure estimated by modified CCM

Swelling Pressure P_s (Mpa)	$P_0 + P_s$ (MPa)	Deformation (u) [mm]
0.14	14.24	42
0.27	14.37	48
0.41	14.51	55
0.54	14.64	63
0.68	14.78	71
0.81	14.91	80
0.95	15.05	89
1.08	15.18	100
1.22	15.32	110
1.35	15.45	122
1.49	15.59	134

6.10.1.2 Hoek and Marinos (2000) method

Hoek and Marinos (2000) method estimates deformation of the circular cross-sectional tunnel similar to CCM. Therefore, the equivalent circular diameter of 3.03 m is used for the La-Higuera headrace tunnel. The extent of plastic deformation and long term deformations to swelling pressure have been estimated using Equation 4.3 and Equation 4.4 respectively and the required input parameters are taken from Table 6.4. The tunnel

strain without support ($\epsilon(\%)(P_i = 0)$) and with support ($\epsilon(\%)(P_i > 0)$) have been calculated. The extent of deformation $u_{max}(P_i = 0)$ and $u_{max}(P_i > 0)$ without and with support respectively have been computed and presented in the Table 6.12. Based on the tunnel strain without support, the extent of squeezing can be classified from few support problems for strain less than 1% to extreme squeezing problems for strain greater than 10% as shown in Figure 4.7 and as shown in remarks in Table 6.12, the extent of squeezing at chainage 12+357 at La- Higuera headrace tunnel is associated with a minor squeezing problem.

Table 6.12: Estimation of deformation at chainage 12+347 of La-Higuera headrace tunnel by Hoek and Marinos (2000) method

Chainage	Support Pressure P_i (Mpa)	$\epsilon(\%)(P_i = 0)$	$u_{max}(P_i = 0)$ (mm)	$\epsilon(\%)(P_i > 0)$	$u_{max}(P_i > 0)$ (mm)	Remarks
12+347	0.90	2.29	69	1.75	53	Minor Squeezing

The long-term deformation due to swelling pressure is estimated by varying swelling pressures and added to the vertical stress (P_0). The extent of long-term deformations due to varying swelling pressures estimated using Hoek and Marinos (2000) method are presented in Table 6.13. Similar to CCM there are gradual increases in deformation as the minimum estimated value is 54 mm with swelling pressure of 0.14 MPa and a maximum value is 134 mm for maximum swelling pressure of 1.49 MPa.

Table 6.13: Long-term deformation due to swelling pressure estimated by modified Hoek and Marinos (2000) method

Swelling Pressure P_s (MPa)	$P_0 + P_s$ (MPa)	Deformation (u) [mm]
0.14	14.24	54
0.27	14.37	55
0.41	14.51	56
0.54	14.64	57
0.68	14.78	59
0.81	14.91	60
0.95	15.05	61
1.08	15.18	62
1.22	15.32	63
1.35	15.45	64
1.49	15.59	66

6.10.1.3 Panthi and Shrestha (2018) method

Unlike CCM and Hoek and Marinos (2000) method, Panthi and Shrestha (2018) method can be used to tunnel with any shape and size. Panthi and Shrestha (2018) considers the field in situ stress as anisotropic which the other two methods fail to do by relating the tunnel strain with k which is the ratio of horizontal to vertical stress. The value of k has been computed from ins situ stress assessment in chapter 6.9 and found to be 0.56. The

time-independent and dependent deformation can be computed using this method. The instantaneous closure (u_{ic}) which occurs immediately after excavation and final closure (u_{fc}) that occurs after long time have been computed using Equation 4.23 and Equation 4.24 respectively. During construction, it is difficult to measure the instantaneous deformation and the deformation measured is usually after the support is installed. Therefore, the value of measured deformation (u) will be the difference between the final closure and the instantaneous closure. According to Panthi and Shrestha (2018), in addition to in situ stress condition and support pressure, rock mass shear modulus (G_{rm}) should be linked with tunnel strain calculation. Therefore, Equation 4.26 by Carranza-Torres and Fairhurst (2000) is used to relate rock mass shear modulus (G_{rm}) and rock mass deformation modulus (E_{rm}). In addition to this, Hoek and Marinos (2000) linked rock mass deformation modulus (E_{rm}) with rock mass deformation modulus of intact rock (E), rock mass strength (σ_{cm}) and intact rock strength (σ_{ci}) as shown in Equation 4.26. And Hoek and Brown (1997) relates rock mass strength (σ_{cm}) with the cohesion (c) and friction angle (ϕ) as shown in Equation 4.27. To find the value of cohesion (c) and friction angle (ϕ), RocData has been used and the input parameters are taken from Table 6.4. The extent of deformation estimated using Panthi and Shrestha (2018) method at chainage 12+357 of the La-Higuera headrace tunnel is presented in Table 6.14.

Table 6.14: Estimation of deformation at chainage 12+347 of La-Higuera headrace tunnel by Panthi and Shrestha (2018) method

Chainage	c (MPa)	ϕ	σ_{cm}	E_{rm} (MPa)	G_{rm} (MPa)	u_{ic} (mm)	u_{fc} (mm)	u (mm)
12+347	1.41	35.56	4.43	1961	654	93	153	60

In CCM and Hoek and Marinos (2000) method, swelling pressure is only added to the vertical gravitational stress. However, in Panthi and Shrestha (2018) method swelling pressure is added to both horizontal and vertical gravitational stress. The new value of k is computed using Equation 4.28. The final closure is due to swelling pressure has been computed using Equation 4.29. The instantaneous deformation remains the same as during construction the surrounding rock mass of the tunnel becomes unsaturated and hence no swelling pressure will be excreted. But during operation, the surrounding rock mass gets saturated and the tunnel experience the swelling pressure increasing the value of final closure. In Table 6.15, the results for the long-term deformation due to varying swelling pressures estimated using Panthi and Shrestha (2018) method have been presented. The maximum deformation is computed to be 106 mm for maximum swelling pressure of 1.49 MPa.

Table 6.15: Long-term deformation due to swelling pressure estimated by modified Panthi and Shrestha (2018) method

Swelling Pressure P_s (Mpa)	$P_0 + P_s$ (MPa)	u_{ic} (mm)	u_{fc} (mm)	u (mm)
0.14	14.44	92	156	64
0.27	14.57	92	160	68
0.41	14.71	92	164	72
0.54	14.84	92	168	76
0.68	14.98	92	172	80
0.81	15.11	92	176	84
0.95	15.25	92	181	106
1.08	15.38	92	185	93
1.22	15.52	92	189	97
1.35	15.65	92	193	101
1.49	15.79	92	198	106

6.10.2 Numerical Modeling

For the numerical modeling using RS2, the model is setup accordingly as described in chapter 4.3.4.2. The La-Higuera headrace tunnel at chainage 12+357 passes through the weakness zone having dip of 50° SE and strike of $N143^{\circ}$ E. Hence the representation of dyke in cross-section is done by creating material boundaries as shown in Figure 6.11.

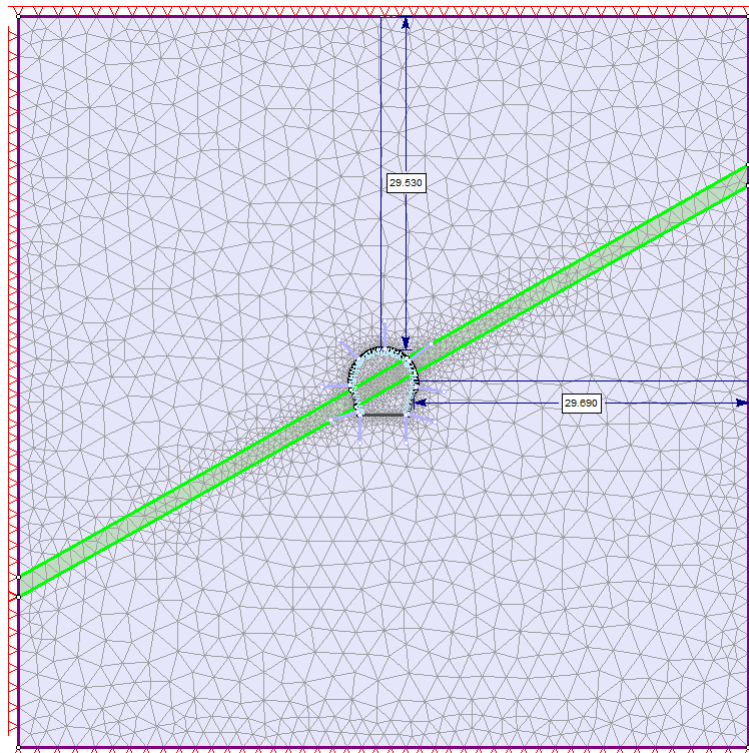


Figure 6.11: RS2 model setup of La-Higuera headrace tunnel

For successful numerical modeling, the good quality of input parameters must be fed. The input parameters for numerical modeling of the La-Higuera headrace tunnel are

therefore taken from the laboratory test results, rock mass classification of the face during excavation, and in situ stresses from numerical modeling. The residual values are taken as 25% of the peak value as mentioned in chapter 4.3.4.2. The details of input parameters are presented in Table 6.16. The details regarding the input parameters for the support have been presented in Table 6.2.

Table 6.16: Input parameters for RS2 modeling of the La-Higuera headrace tunnel at chainage 12+347

Description	Strong Sandstone		Dyke	
	Peak	Residual	Peak	Residual
Compressive Strength σ_{ci} (MPa)	55		35	
Rock mass Modulus E_{rm} (MPa)	37600	640	37600	640
GSI	39	10	39	10
Rock mass constant m_i	17	4	17	4
Disturbance factor D	0.2	0.2	0.2	0.2
Institu stress				
Loading Type	σ_1 (MPa)	σ_3 (MPa)	σ_z (MPa)	σ_1 angle with horizontal
Constant	15.3	7.25	14.3	161

6.10.3 Elastic analysis

The objective of carrying out the elastic analysis of the tunnel cross-section is to evaluate the strength factor and distribution of stress around the tunnel opening. The strength factor is the ratio of rock strength based on the failure and the induced stress at a given point. The input parameters are taken from Table 6.16 and since the materials are defined as elastic, residual values are not needed for elastic analysis.

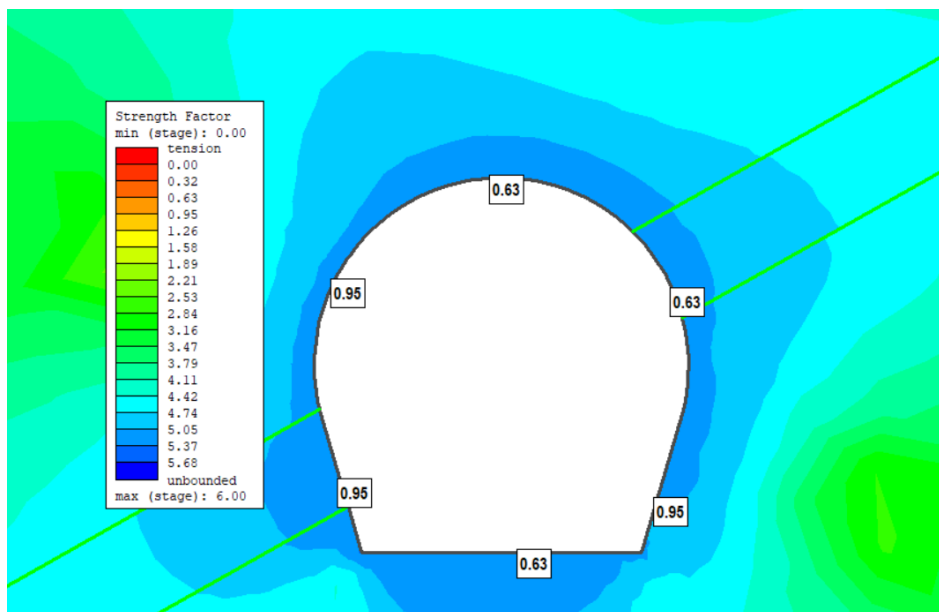


Figure 6.12: Strength factor for Elastic model of La-Higuera headrace tunnel in RS2

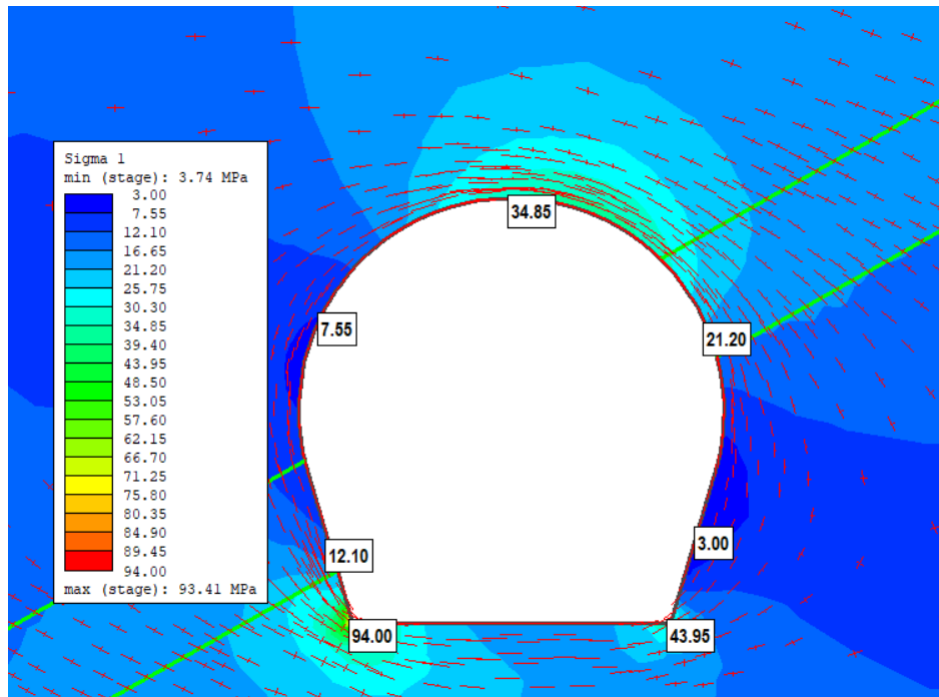


Figure 6.13: Major principal stress with trajectories in elastic model of La-Higuera headrace tunnel in RS2

The results for the elastic analysis of the model shown in Figure 6.12, show that the strength factor around the cross-section of the tunnel is less than unity suggesting the rock mass material in the elastic model will yield. Since the material is defined as elastic, the model will not show the yielding of material. But as the result of the strength factor suggest the material will yield, therefore plastic analysis of the model is required to be carried for further analysis. In Figure 6.13, it can be seen that the stress concentration is mainly at the crown and the corners of the invert due to redistribution of stress after tunnel excavation. The value strength factor at these places where stress concentration occurs is minimum than other areas which causes due to overstressing in the rock mass.

6.10.4 Plastic analysis

The main objective of the plastic analysis is to determine the in situ swelling pressure and to simulate the collapse of the tunnel due to swelling pressure. The analyses are therefore carried out in four different stages as explained in chapter 4.3.4.2. The first three stages represent the situation before the tunnel is filled with water for power production. During the last stage, the tunnel is filled with water, and this causes saturation of surrounding rock mass which then will exert swelling pressure on the tunnel support. The tunnel collapse occurs as the installed rock support cannot withstand the swelling pressure exerted by the rock mass. So, to determine the swelling pressure which causes the tunnel support to yield, the liner in RS2 is defined as elastic and failure is defined based on support capacity plot. Shotcrete applied in the tunnel is represented as reinforced concrete in RS2, so that support capacity plots can be generated. Then the failure of support is defined as the situation when the plots are outside the support capacity plot for the factor of safety one.

The input parameters for rock mass materials and rock support have been taken from Table 6.16 and Table 6.2 respectively.

Before performing swelling analysis on the model, the model is run for the plastic deformation analysis. In stage 2 and stage 3, load splitting has been done as 30% and 70% respectively suggesting that only 30% load is exerted in stage 2 and the remaining 70% is added during stage 3. In Figure 6.14, the stress distribution in stage 2 and stage 3 has been shown. In the plastic analysis in contrast to the elastic model, as shown in Figure 6.13 where overstressing occurs, the rock mass here undergoes distressing. The distressing of stresses in the rock mass helps to increase the strength factor suggesting that the rock mass strength will be able to withstand the induced pressure. The stress concentration in stage 2 and stage 3 is higher at the corners of the invert.

The plastic deformation contains both time-independent and time-dependent deformation. The representation of these deformations in the model is done in stage 2 and stage 3. Stage 2 deformation is the time-independent instantaneous deformation and the deformation in stage 4 represents the long-term deformation due to creep. As shown in Figure 6.15, the maximum deformation occurs at invert. But during construction, the deformation of few centimeters in the invert is usually removed and no support is provided to the invert. In the La-Higuera headrace tunnel, the support is not provided at invert. Hence, the deformation of the crown and wall (spring line) are of interest. The maximum deformation, therefore, can be seen occurring at the wall of 0.156 m at stage 3 which in stage 2 was 0.016 m. The final closure predicted by Panthi and Shrestha (2018) method in chapter 6.10.1.3 was 0.153 m which is close to the value obtained from numerical modeling. Since in absence of value of measured deformation, the final closure from Panthi and Shrestha (2018) method is used as a reference to verify the results. The support capacity plot showing the moment capacity plot and shear capacity plot for installed shotcrete is presented in Figure 6.16. As it can be seen the plots fall inside the factor of safety one, therefore the support is assumed to be stable.

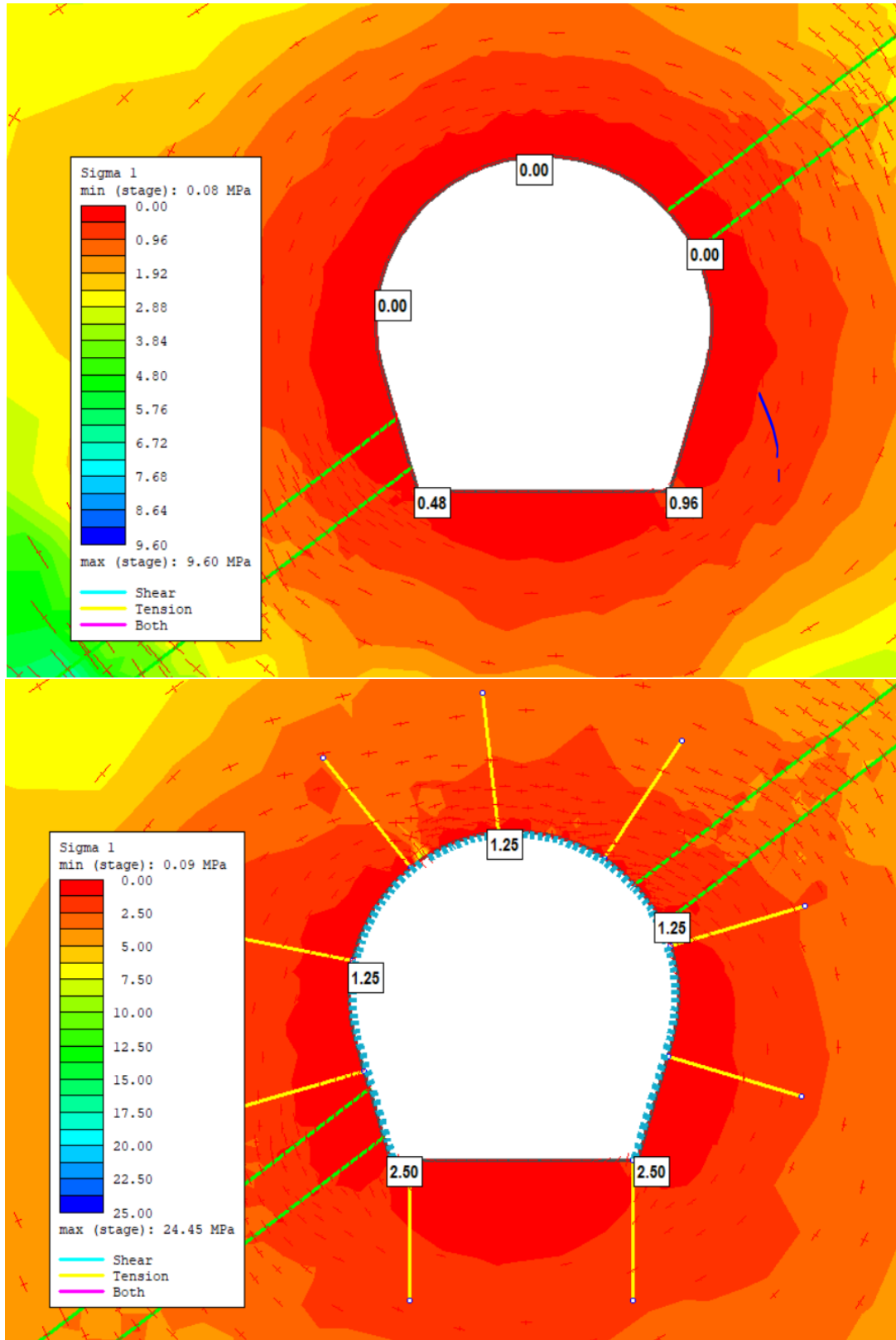


Figure 6.14: Major principal stress with trajectories in plastic of La-Higuera headrace tunnel in RS2 in Stage 2 (top) and Stage 3 (bottom)

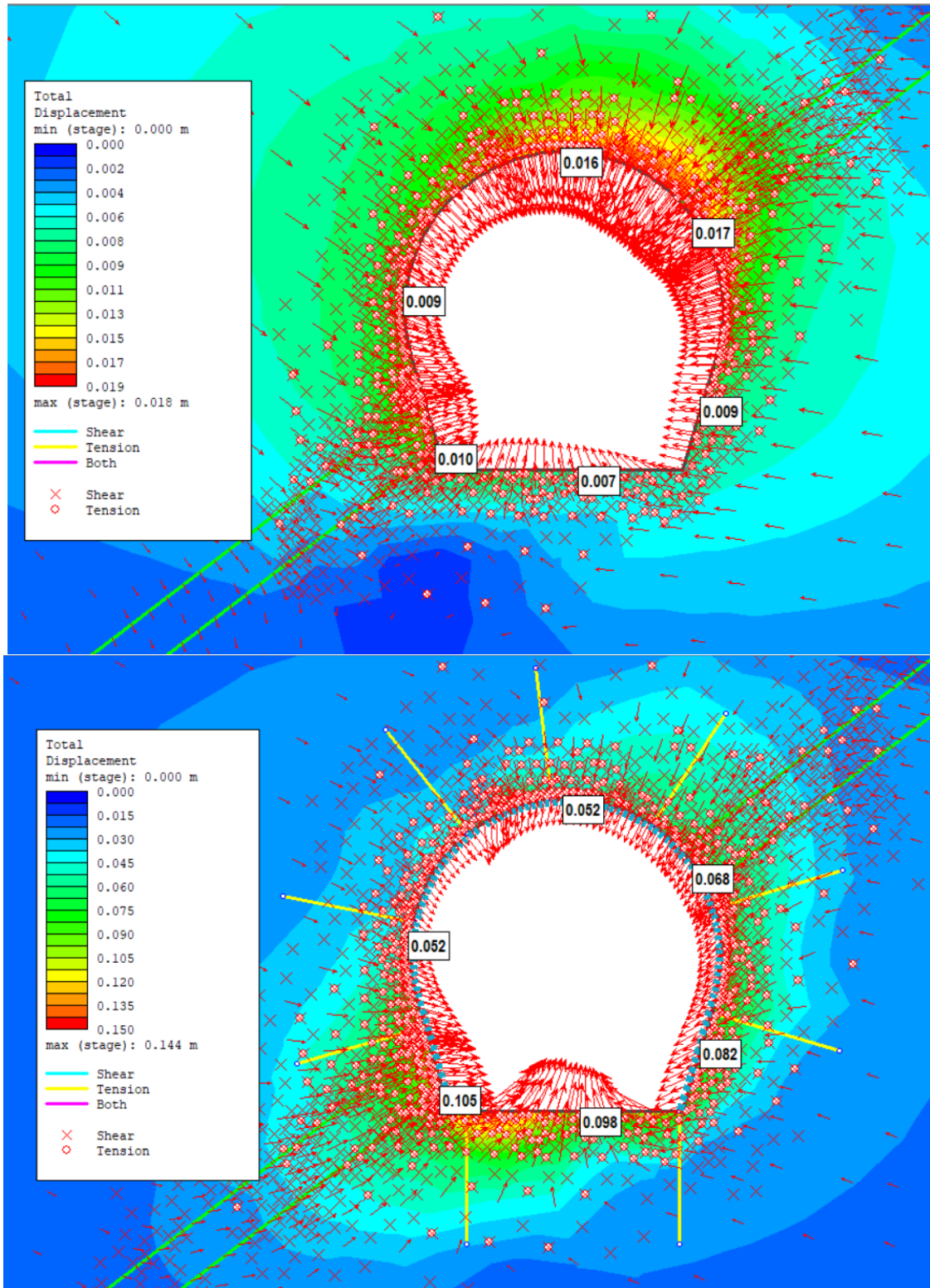


Figure 6.15: Deformation for plastic analysis of stage 2(top) and stage 3(bottom)

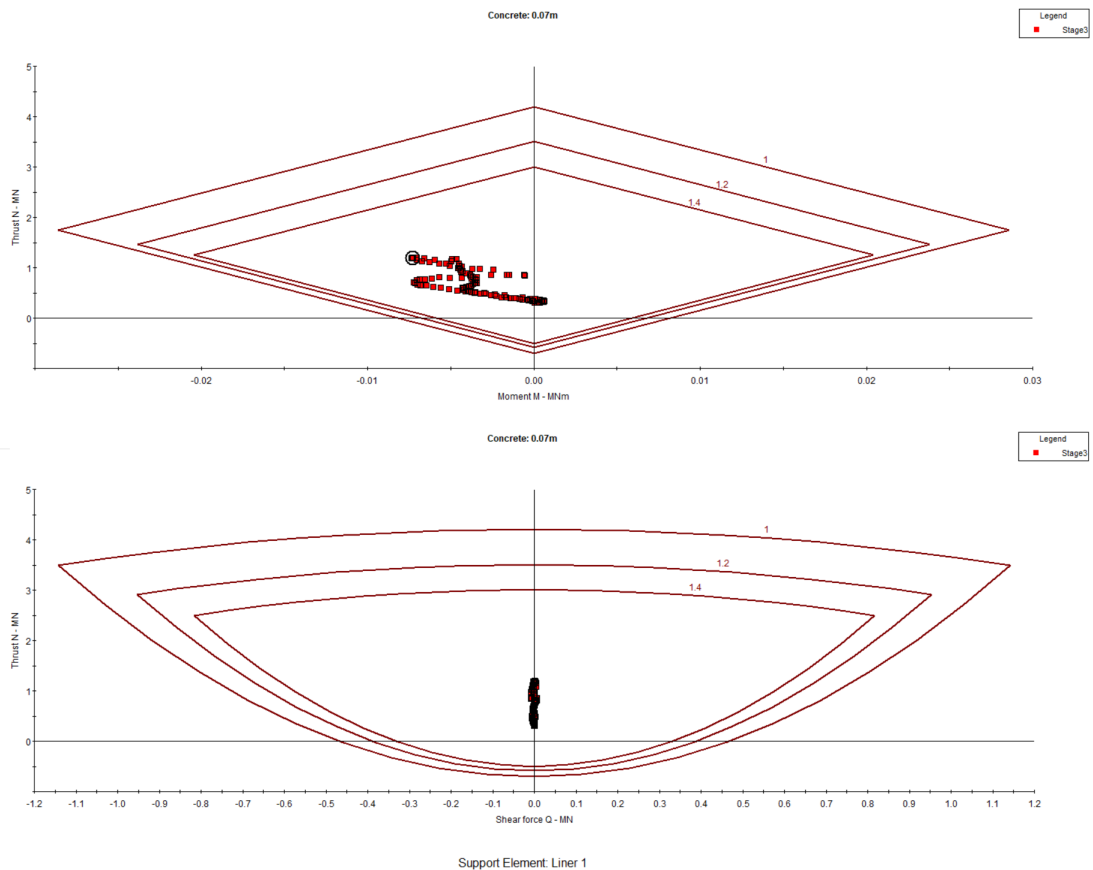


Figure 6.16: Support capacity plot for shotcrete in La-Higuera headrace tunnel at chainage 12+347

Due to uncertainty in the in situ swelling pressure, similar to empirical and analytical methods, varying swelling pressures are applied to the model. Uniformly distributed load of varying magnitudes are applied all around the tunnel cross-section. The loading is RS2 is done by adding 11 stages after stage 3. In each stage, swelling pressure is applied to vary from 5% to 55% of maximum swelling pressure measured in the laboratory at an interval of 5%. The support capacity plots are then generated to see at which swelling pressure the support fails. In Figure 6.17, the support capacity plots generated for various stages are shown and failure is witnessed at stage 12 where the magnitude of swelling pressure acting on the tunnel is 1.22 MPa which is 45% of maximum swelling pressure measured at the laboratory. The flexural failure has caused the collapse of the shotcrete as suggested by the moment capacity plot as the plots lie away from the factor of safety one. In Figure 6.18, deformation in tunnel cross-section due to various swelling pressure has been shown. The values of deformation increase in comparison to values shown in Figure 6.15 as the magnitude of swelling pressure increases. At swelling pressure of 1.22 MPa which causes collapse of the tunnel the deformation at the wall has increased up to 0.956 m which was initially 0.156 m. The maximum deformation of 0.956m is more than 15% of tunnel width. Similarly, the deformation all around the tunnel has increased ranging from 5% to 15% of tunnel width.

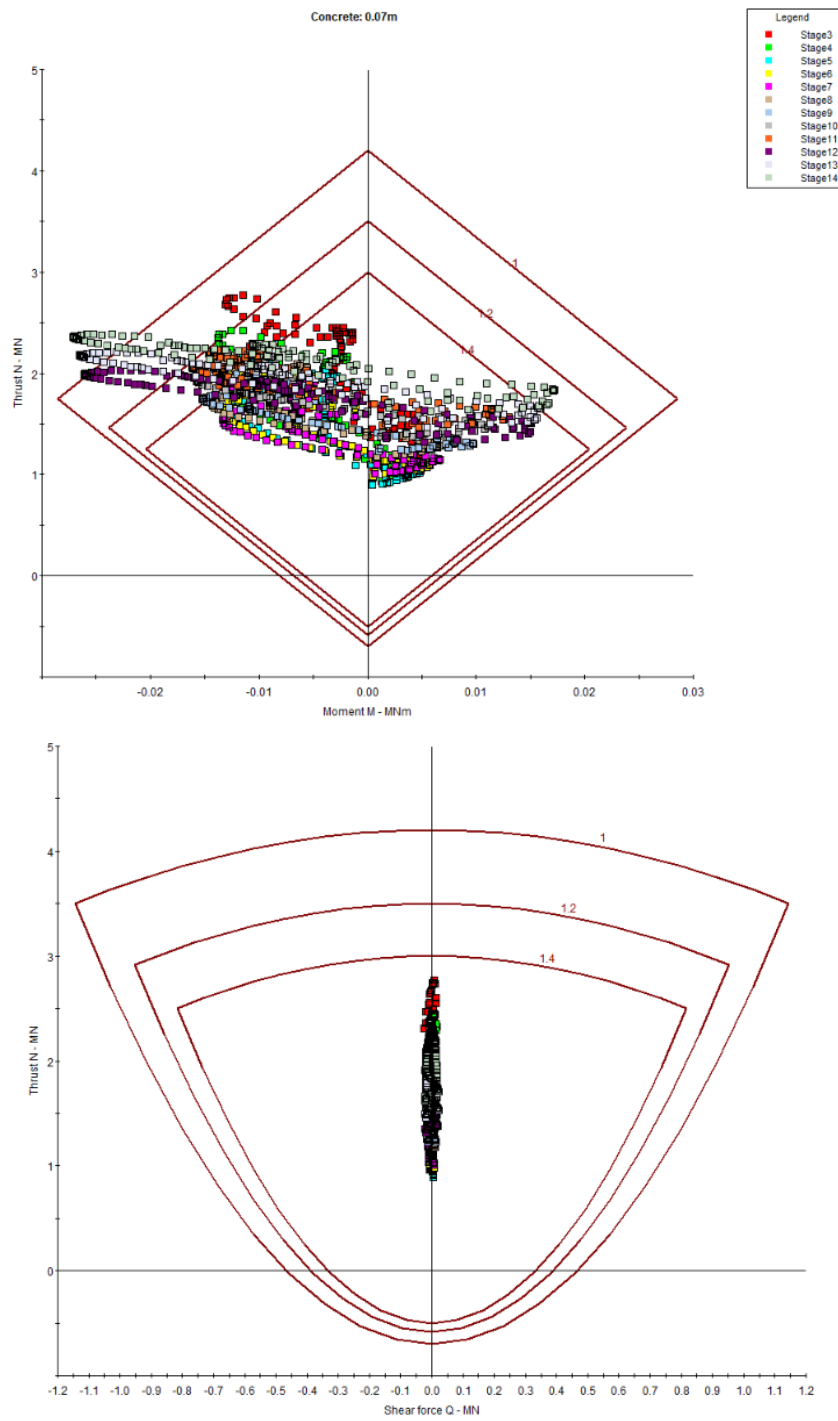


Figure 6.17: Comparison of Support capacity plot for shotcrete for different swelling pressure in La-Higuera headrace tunnel at chainage 12+347

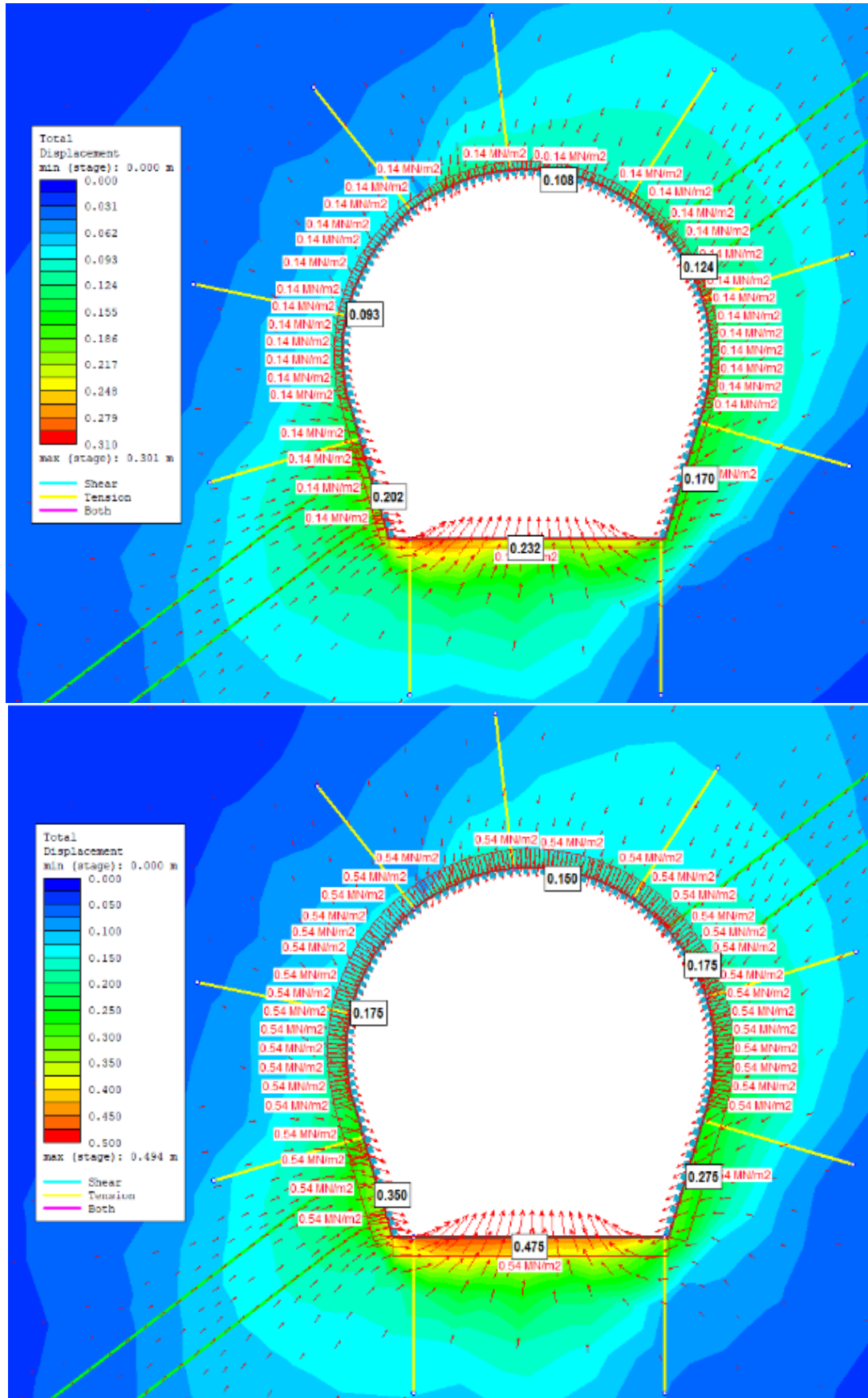


Figure 6.18: Comparison of deformation due to different swelling pressure in La-Higuera headrace tunnel at chainage 12+347 with elastic support

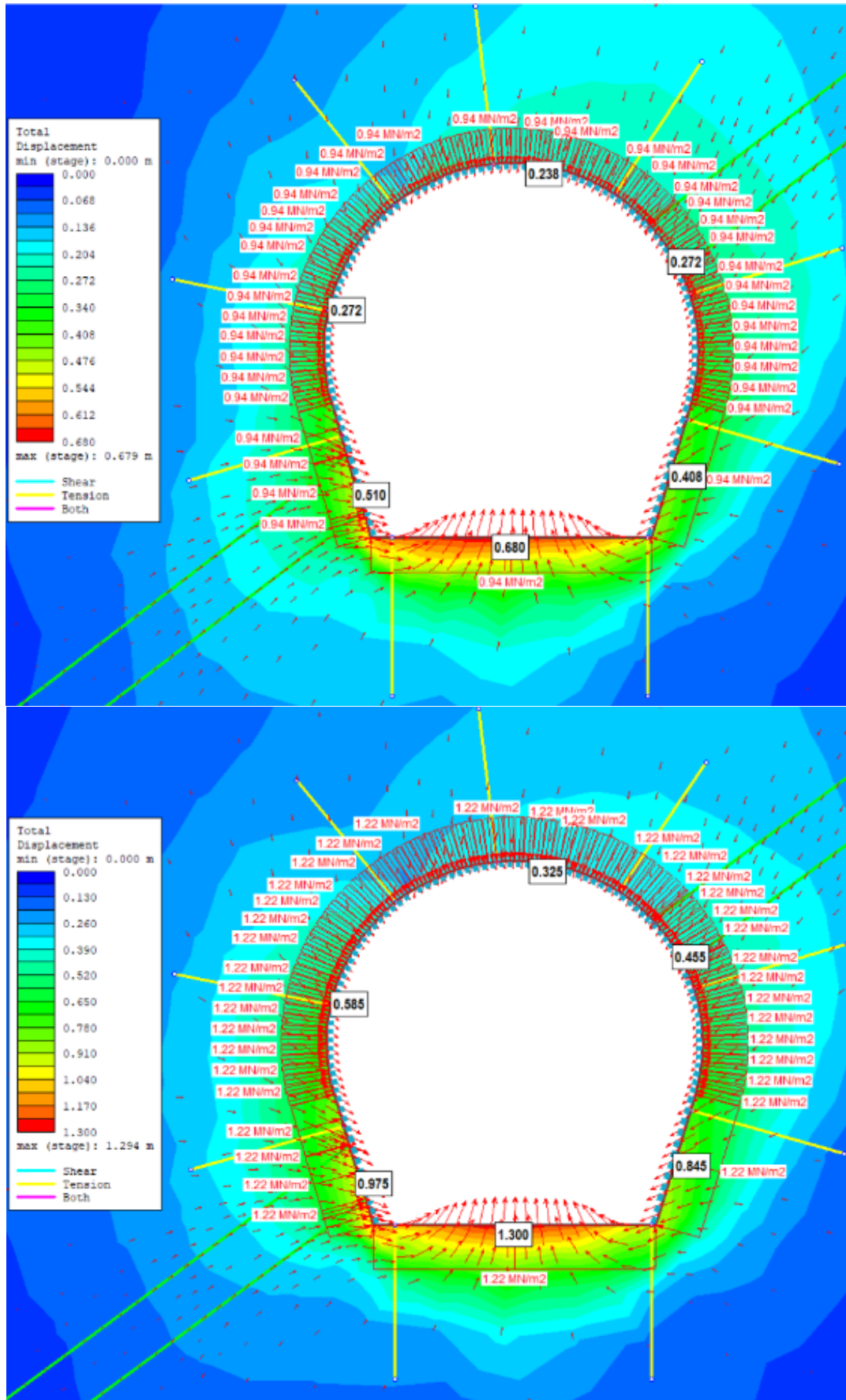


Figure 6.19: Comparison of deformation due to different swelling pressure in La-Higuera headrace tunnel at chainage 12+347 with elastic support

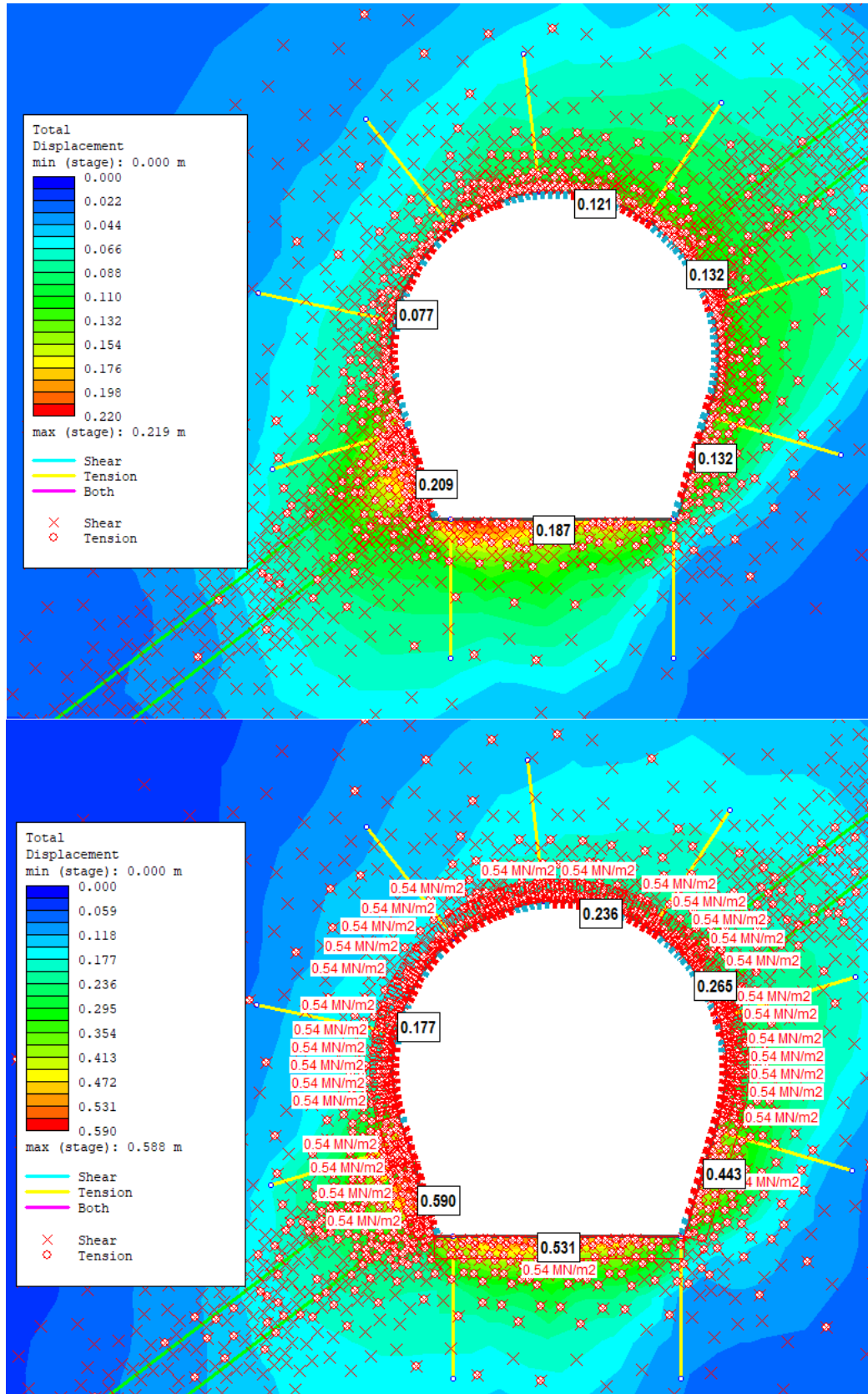


Figure 6.20: Comparison of deformation with and without swelling pressure in La-Higuera headrace tunnel at chainage 12+347 for plastic liner

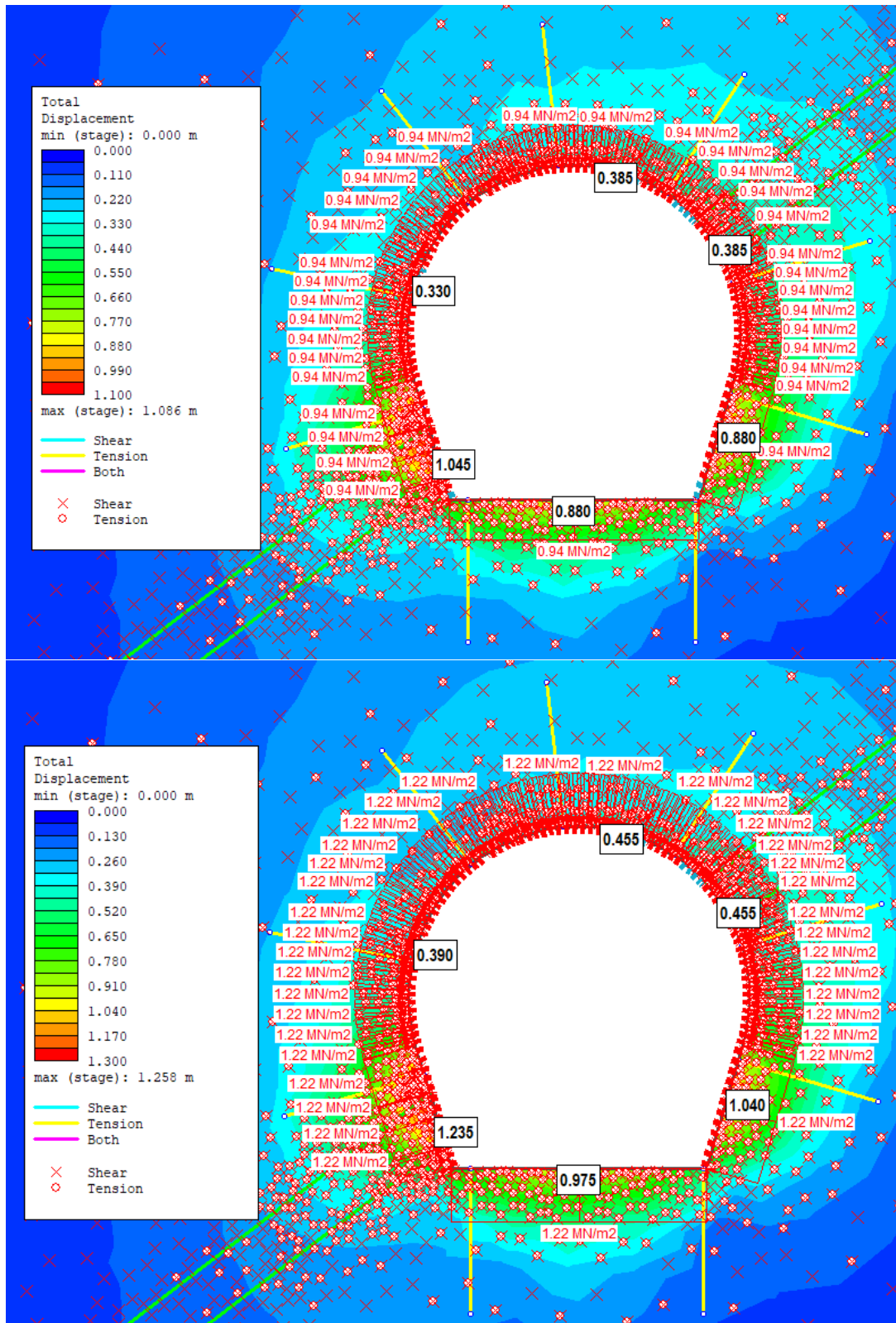


Figure 6.21: Comparison of deformation due to different swelling pressure in La-Higuera headrace tunnel at chainage 12+347 for plastic liner

The installed support, in reality, is not elastic and to define the failure in RS2 with the

support capacity plots the liner is assumed to be elastic. Therefore the analysis is performed assuming the liner as plastic to see how the results varied in comparison to results for elastic liner. The deformation of the tunnel increases as the liner is assumed as plastic. In comparison to the deformation of the tunnel in stage 3 from Figure 6.15 when the liner is elastic with the deformation tunnel when the liner is as shown in Figure 6.20, the maximum deformation of the wall has increased from 0.156 m to 0.209m which is just 3% of tunnel width. In stage 3 with no swelling pressure, 1795 finite elements yield along with the yielding of all 9 bolts and 56 liner elements. When 1.22 MPa swelling pressure is exerted on the tunnel the deformation increases up to 1.235 m at the wall from 0.209 m as shown in Figure 6.20 which is 20% of the tunnel width. The number of yielded finite elements increases to 3092 and the number of liner elements yielded is 103. The results show that the installed support is unable to withstand the swelling pressure and yield causing the deformation of 20% of tunnel width. Therefore, there is a possibility the liner fails at lower swelling pressure than 1.22 MPa at which the elastic liner was found to be safe. In Table 6.17, displacements of tunnel at different swelling pressure are presented. The extent of deformation increases as the magnitude of swelling pressure increases along with the increase in a number of yielded liner elements. For the swelling pressure up to 0.27 MPa tunnel strain is up to 5% of tunnel width and from 0.38 MPa the tunnel strain exceeds 10% of tunnel width.

Table 6.17: Displacements after application of swelling pressure in La-Higuera tunnel

Description	Displacements in (m) after application of swelling pressure (Mpa)								
	0	0.14	0.27	0.41	0.54	0.68	0.81	0.94	1.22
Left wall	0.209	0.257	0.351	0.485	0.590	0.730	0.780	1.045	1.235
Left wall	0.077	0.095	0.130	0.153	0.177	0.219	0.234	0.330	0.390
Roof	0.121	0.149	0.185	0.230	0.236	0.292	0.312	0.385	0.445
Right wall	0.132	0.149	0.203	0.230	0.265	0.292	0.312	0.385	0.455
Right wall	0.132	0.176	0.259	0.383	0.443	0.584	0.624	0.880	1.040
Invert	0.187	0.230	0.315	0.459	0.531	0.620	0.663	0.880	0.975
No. Yielded Liner elements	56	56	64	70	75	85	90	96	103

The extent of deformation increases as the magnitude of swelling pressure increases causing the increase in the number of yielding elements of plastic liner and an increase in the number of yielded bolts. The in situ swelling pressure of just 10% of maximum laboratory pressure causes a significant increase in deformation which shows the installed rock support is of not enough capacity to restrained the deformation caused by a small amount of swelling pressure which eventually leads to the tunnel collapse.

7 Moglice Hydropower Project

The study is carried on the Moglice Hydropower project for this thesis which is located in the eastern part of Albania. In Devoll river, the Devoll Hydropower project of installed capacity 278 MW has been developed and this project is the first large-scale Public-Private Partnership (PPP) project of Albania (PowerTechnology, 2021). The project consists of three hydropower stations namely, Banje, Moglice, and Kokel. Moglice hydropower project is the biggest among two completed projects with an installed capacity of 197 MW own and developed by Statkraft, Norway on Devoll river. The projects are built, own and operate in cascade along the Devoll River as per the concession agreement between Statkraft and the Government of Albania (Statkraft, 2021).

7.1 Project description

The Moglice hydropower project is located in Korce and Elbasan districts, Albania. The installed capacity of the project is 197 MW and generates annual average energy of 450 GWh (Statkraft, 2021). The Moglice hydropower project is the uppermost plant developed in the Devoll River. The asphalt core dam of height 167 m as shown in Figure 7.1 has been constructed, which is one of the highest asphalt dam constructed around the world (Statkraft, 2021). The Moglice reservoir has a storage capacity of approximately 380 million cubic meters and surface area of 7.21 square kilometers (Statkraft, 2021).



Figure 7.1: Moglice Hydropower Dam [Photo taken by Runa B. Frengen 27.03.2019 (Frenge, 2020)]

The gross head of the Moglice Hydropower plant is 300 m after utilizing the head between 650 m to 350 m above mean sea level. The water is conveyed to the power station through a 10.7 km long tunnel from the Moglice reservoir. The power station consists of

two large Francis turbines. The power generated is evacuated from the Moglice switch-yard to Elbasan II substation via 48 km 220 kV Transmission line which is connected with the Albanian national electricity grid (Statkraft, 2021).

7.2 Project Layout

The headworks of the Moglice hydropower project consist of an asphalt core dam that forms a reservoir behind it. The intake is located on the right bank of the Devoll river then transfer water to the powerhouse through the headrace tunnel. The layout of the project along with the longitudinal profile showing the headrace tunnel is shown in Figure 7.2. The layout is adapted after design according to findings of the ground investigations along with consideration of project-specific minimum requirements (Aasen et al., 2013).

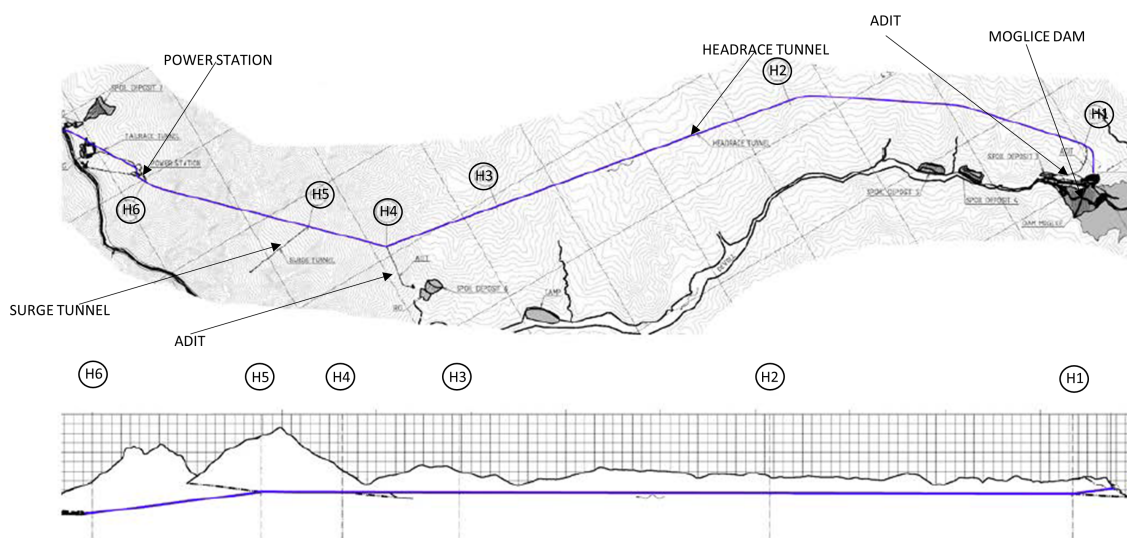


Figure 7.2: Project layout and longitudinal section showing the headrace tunnel of Moglice hydropower project [extracted and slightly modified for better readability from Aasen et al. (2013)]

For the design of the tunnel, from the early stage of the planning, a Norwegian unlined design was considered. The geological and topographical conditions of the project locations are favorable for the unlined design. The tunnel passes through various rock formations as described in the following subsection. Depending on the rock conditions, a various method for excavation has been considered which is summarized in Table 7.1.

Table 7.1: Excavation method for different tunnel section adopted for Moglice headrace tunnel (Aasen et al., 2013)

Headrace tunnel section	Rock formation	Tunnel Design concept	Excavation method
Intake to H1	Flysch	Unlined/sprayed concrete	Drill and Blast
H1-H3	Flysch	Segmental lining	TBM
H3-H4	Melange	Concrete lining	Drill and Blast
H4-H6	Ophiolite	Unlined/sprayed concrete	Drill and Blast

7.3 Regional Geology

The Albanides represent the geological structure of Albania along with Dinarides and Hellenides from north to the south from the southern branch of the Mediterranean Alpine Belt (Frashëri, 2005). The Internal Albanides present in eastern and External Albanides present in the western part of Albania are two major palaeogeographical domains. The External Albanides are characterized by regular overthrust structural belts affected from later palaeotectonic stages. The Moglice hydropower project lies in the Internal Albanides, which according to Frashëri (2005) is characterized by the presence of an immense and intensively tectonized ophiolitic belt, which is detached from east to west as an overthrust nappe (Frasher et al., 1996). The project area which lies in Korca- Kolonja region in the ophiolite belt has a complicated geological structure (Shallo and Vranaj, 1994).

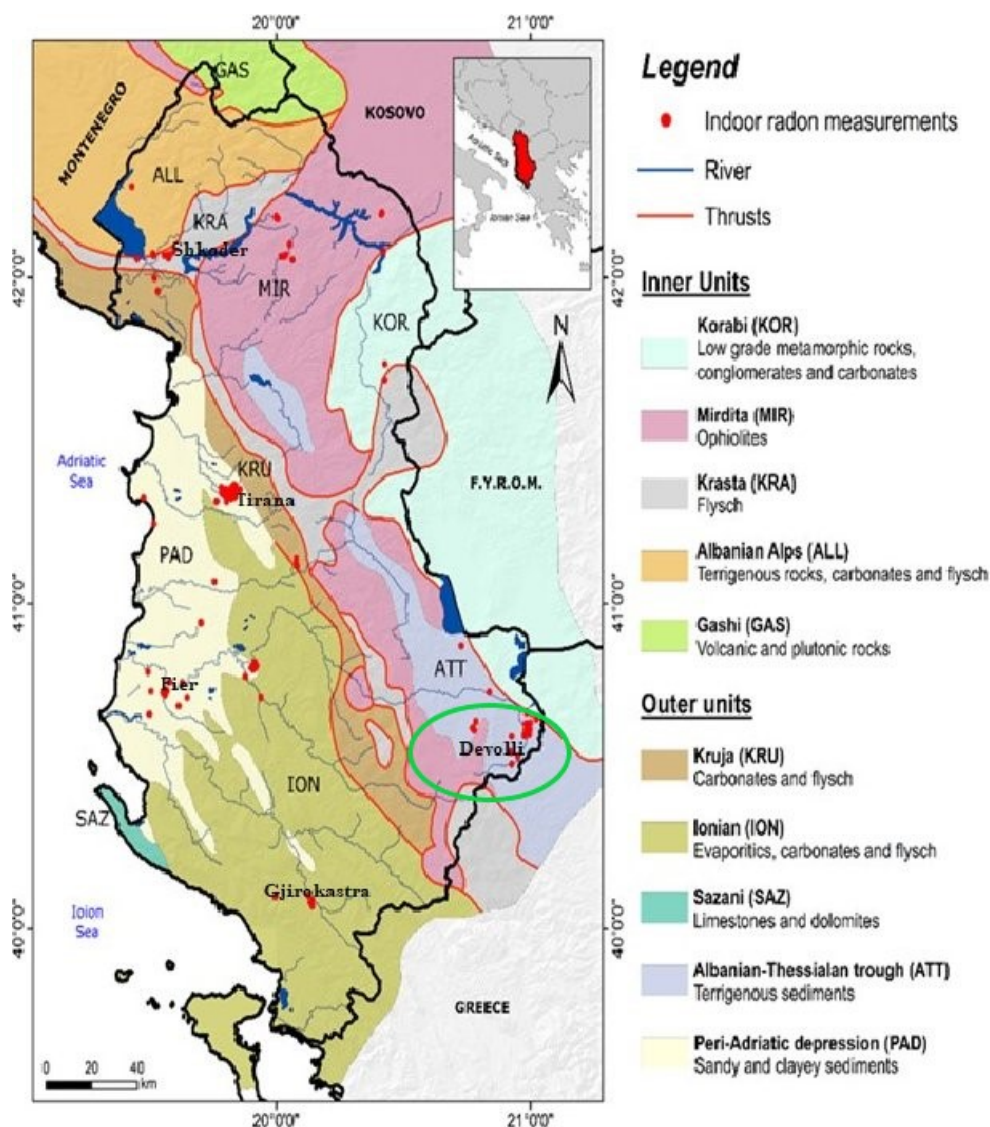


Figure 7.3: Regional geological map of Albania; Green circle is marked to show the project location of Moglice hydropower project [Figure taken from Dilek et al. (2008)]

In Figure 7.3, the regional geological map of Albania has been shown where the project

location is marked with a green circle. The outer units shown in the figure represent the External Albanides and the inner units represent Internal Albanides. As it can be seen from the figure the project area lies in inner ophiolite units as discussed above part of inner units. The project geology has been briefly described in the following subsection.

7.3.1 Project Geology

The geological condition of the project area is dominated by two main lithological units: the ophiolitic rocks, mainly variants of preiodite, and the sedimentary rocks (Aasen et al., 2013). In the geological map of the project area as shown in Figure 7.4, the representation of ophiolitic rocks is done by green and the sedimentary rocks by pink. The border of these rocks is of very poor quality being tectonic nature (Aasen et al., 2013).

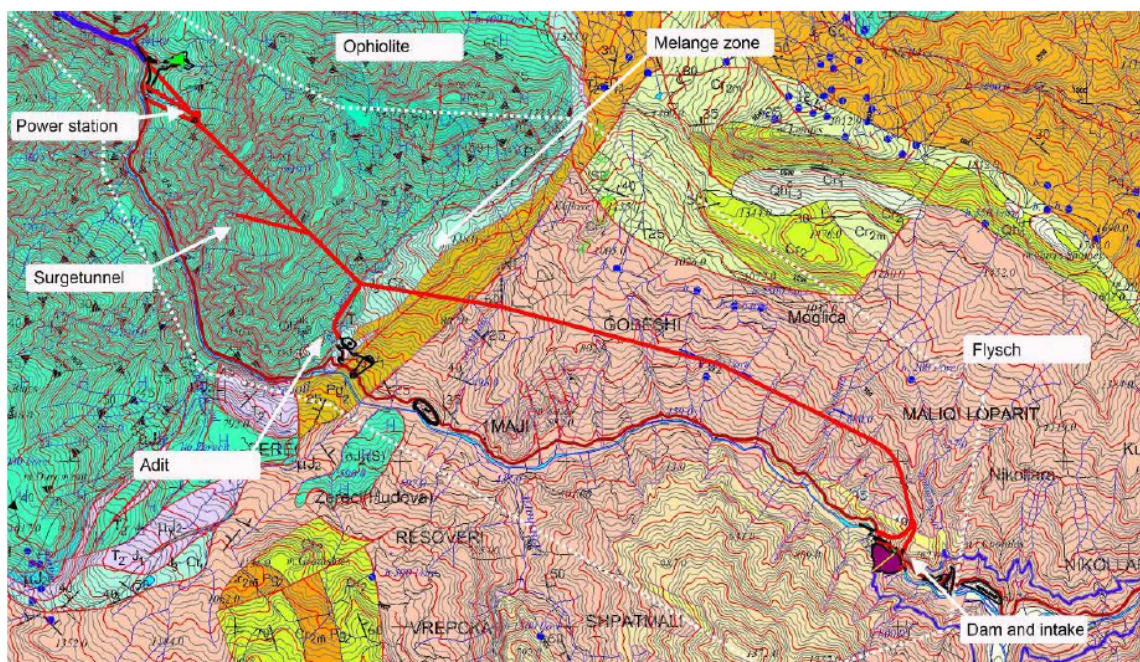


Figure 7.4: Project geological map of Moglice Hydropower project taken from Aasen et al. (2013). The red line shows the tunnel alignment

The headworks of the project lie in the flysch formation. The tunnel alignment passes through a different rock formation. The upstream part of the tunnel passes through flysch typically consists of alternating layers of claystone, siltstone, sandstone, and rare conglomerates (Aasen et al., 2013). This portion of this area is considered for the study of this thesis. The tunnel passes through melange, to sound quality of ophiolitic rock mass in downstream section. The longitudinal profile of tunnel alignment passing through different rock formation is shown in Figure 7.5. According to Aasen et al. (2013), the ophiolite rocks are homogeneous and sound, however flysch are heterogeneous, and of very poor rock mass quality.

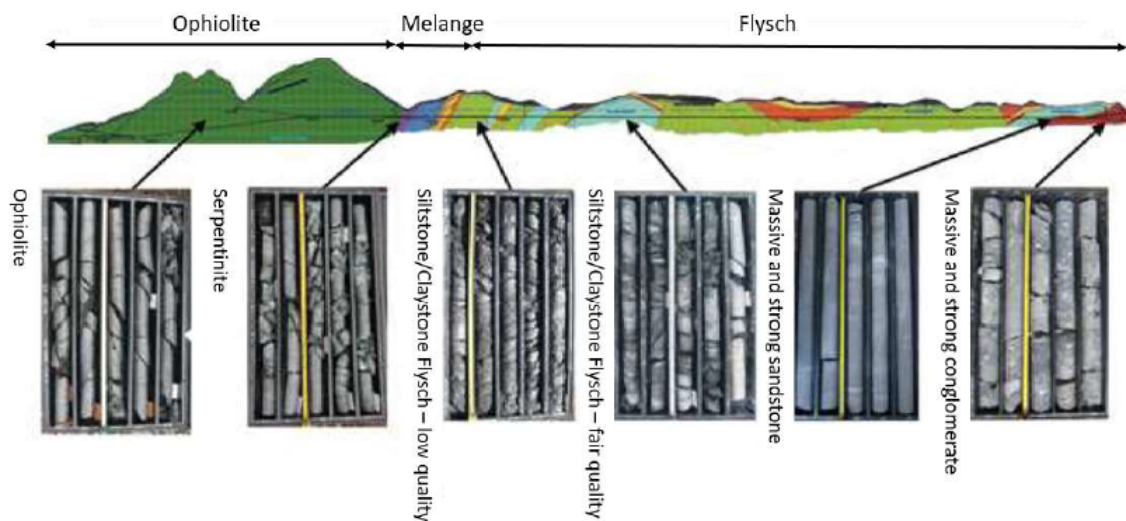


Figure 7.5: Longitudinal profile of Moglice headrace tunnel passing through different rock formation [extracted from Frengen (2020) originally based on Aasen et al. (2013)]

7.4 Instrumentation carried out in the tunnel

The headrace tunnel at chainage 0+430 to 7+581 passes through weak rock masses composed of sheared and deformed flysch. This section consists of rock mass containing a variable proportion of clayey and hard material Almenara (2021). The headrace passes through the relatively poor rock mass in the section containing flysch and to determine the behavior of relatively poor rock mass, flat jack instrumentation has been installed in these sections over the first period of operation. The purpose of the installation of flat-jack is to measure the deformation of headrace tunnel that passes through the relatively poor rock mass in the section containing flysch. To determine the behavior of relatively poor rock mass, flat jack instrumentation has been installed in these sections over the first period of operation (NGI, 2019). The location of the installation of flatjack in the headrace tunnel is shown in Figure 7.6 (left) and the location lies in the area with weak rock and swelling properties. The procedure for the installation and measurement is based on ASTM D4729-08 "Standard Test Method for In-situ Stress and Modulus for In Situ Stress and Modulus of Deformation Using Flatjack Method" Last amended 2008-07-01 (NGI, 2019). The information of compressive strength and rock mass deformation has been collected from the laboratory test of rock samples obtained from the core derived from the slots as described in section 8.2.1. According to NGI (2019), the standard length requires for the flatjack in minimum is 600 mm but due to close spacing of the reinforced in shotcrete arches, the square flatjacks of dimension 400 mm × 400 mm has been used as shown in Figure 7.6 (right). Table 7.2 shows the results obtained from the flat jack instrumentation. The minimum stress noted in flat jack mounted in rock is 0.8 MPa and the maximum is 5 MPa. The minimum stress noted in flat jack mounted in rock is 0.8 MPa and the maximum is 5 MPa. Deformation measurement has also been carried out in along this section and the measured values are shown in Table 7.3.

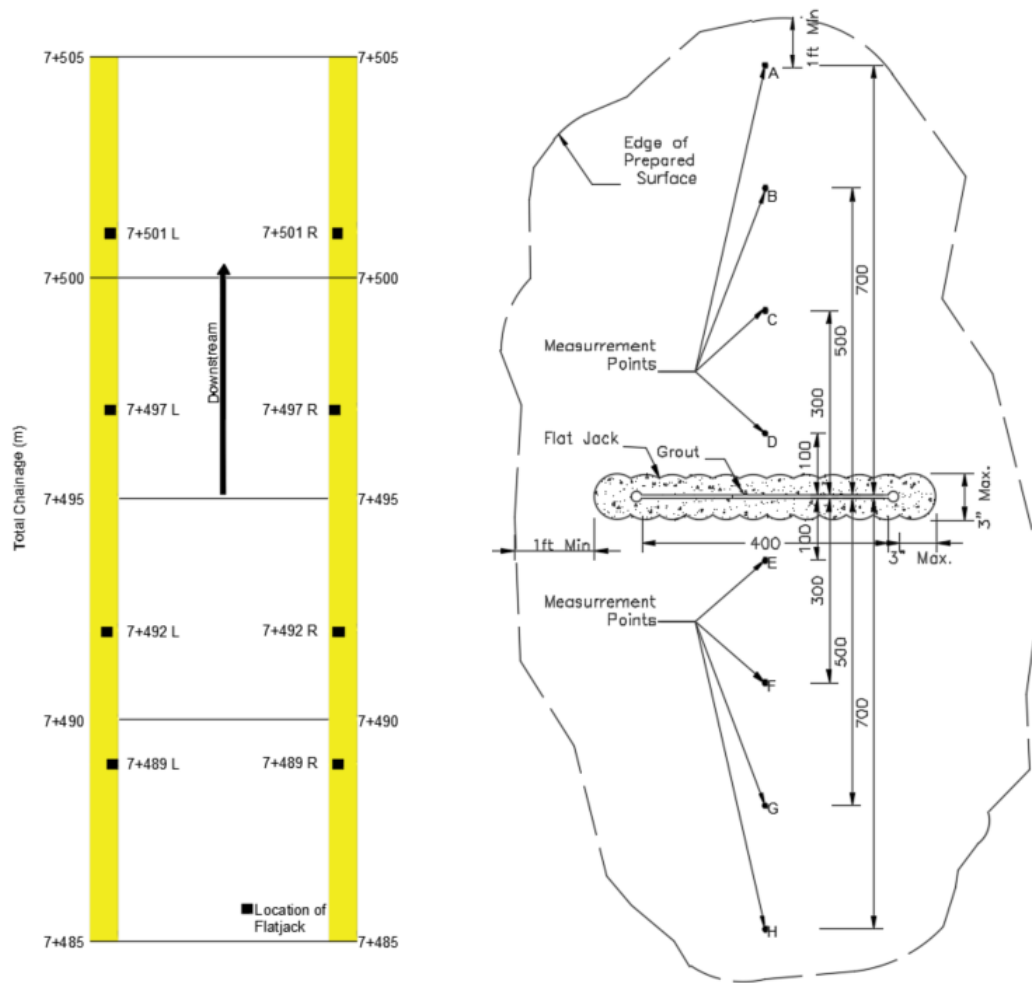


Figure 7.6: Location of flatjacks in the head race tunnel , L is for left and R is fro Right of tunnel looking downstream (left) and Flatjack measurement array, surface prepared in field, dimensions in mm (right)

Table 7.2: Flat jack test results performed between chainage 7+492 to 7+501

Chainage	L/R	Installation Description	σ_h (MPa)
7 +492	L	Flat Jack on Shotcrete, fully grouted pins	1.0
7+492	R	Flat jack in rock, 40 cm outer part of pins free	5.0
7+489	L	Flat jack in rock, 40 cm outer part of pins free	0.5
7+489	R	Flat jack in rock, fully grouted pins free	0.8
7+497	L	Flat jack in rock, 40 cm outer part of pins free	1.0
7+497	R	Flat jack in shotcrete, fully grouted pins free	4.5
7+501	L	Flat jack in rock, 40 cm outer part of pins free	5.0
7+501	R	Flat jack in rock, 40 cm outer part of pins free	5.0

Table 7.3: Measured deformation along the Moglice headrace tunnel

Chainage	Over-burden (m)	Measured Final Closure (mm)
7+029	226	34
7+064	238	32
7+092	250	30
7+136	271	20
7+168	280	32
7+194	281	18
7+218	279	24
7+266	277	12
7+291	275	18
7+316	271	16
7+342	279	16
7+423	284	6
7+455	285	8
7+531	250	46

7.4.1 Geological condition of the location of Flatjacks installation

The area selected for the study lies within the chainage 7+000 to 7+581. As it can be seen in Figure 7.7, the area lies in a zone containing clayey shale and siltstone. The degree of faulting and folding varies in great proportion within this region. The rock mass is composed of a deformed and alternating section of weak rocks (<25MPa) like claystone, siltstones, and clay shales with embedded layers of stronger rock (24-55MPa) (Devoll, 2015). The proportion of weak rock and strong rock in the rock mass is variable, although the dominant content is found to be weak rock. The strong rock content has always been less than 50%. Therefore, the behavior of rock mass is highly controlled by the weaker part (Devoll, 2015). The Q-value mapped during the construction ranges from 0.05 to 2 in these sections, suggesting presence of extremely poor rock mass (Almenara, 2021).

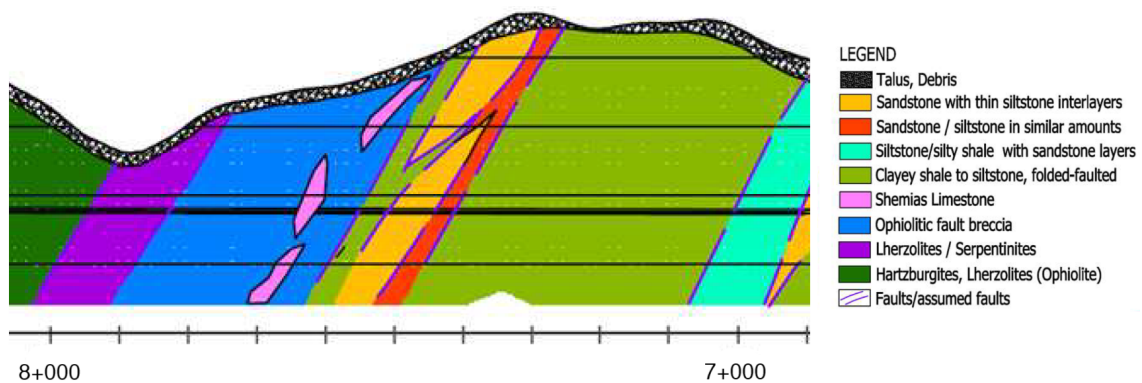


Figure 7.7: Longitudinal profile of Moglice headrace tunnel passing through different rock formation at study area (Almenara, 2021)

As the section contains weak rock mass there may be a stability problem. Deformation measurement has been carried out in various sections. The maximum convergence was measured at chainage 7+531 of 46 mm. The convergence is evident that the deformation takes place in the tunnel. Another stability problem in this section is because of the

swelling rock. The stability problem in the flysch rock is because of swelling and slaking. The XRD test shows variable contents of the expandable minerals (Devoll, 2015). During the design of the factored in situ swelling pressure of 0.15 MPa has been considered and the design will be capable to cope with the swelling values above 0.15 MPa to 0.2 MPa (Devoll, 2015).

7.5 Rock Support

The support installation usually took place in several stages. In the case of Moglice, the sequence of installation of support was carried out as first placing sprayed shotcrete followed by installation of reinforced ribs of sprayed concrete (RRS) and bolts in the crown and wall. Finally, the invert is placed. But, for modeling the equivalent homogeneous support has been considered. The installed support installed is sprayed shotcrete of thickness 150 to 200mm and reinforced ribs on sprayed concrete of thickness 300mm as shown in Figure 7.8. Also, the invert is designed with a thickness of 400 mm reinforced concrete. The invert design is carried out because of the presence of swelling claystone in these sections. During the sample collection in the field of the installed support, at most of the section, it was found that the thickness of the support is 650mm. Hence, for the modeling, the homogenous sprayed concrete thickness of 650 mm is considered. The details of the support and bolts used for the modeling are shown in Table 7.4 and Table 7.5 respectively.

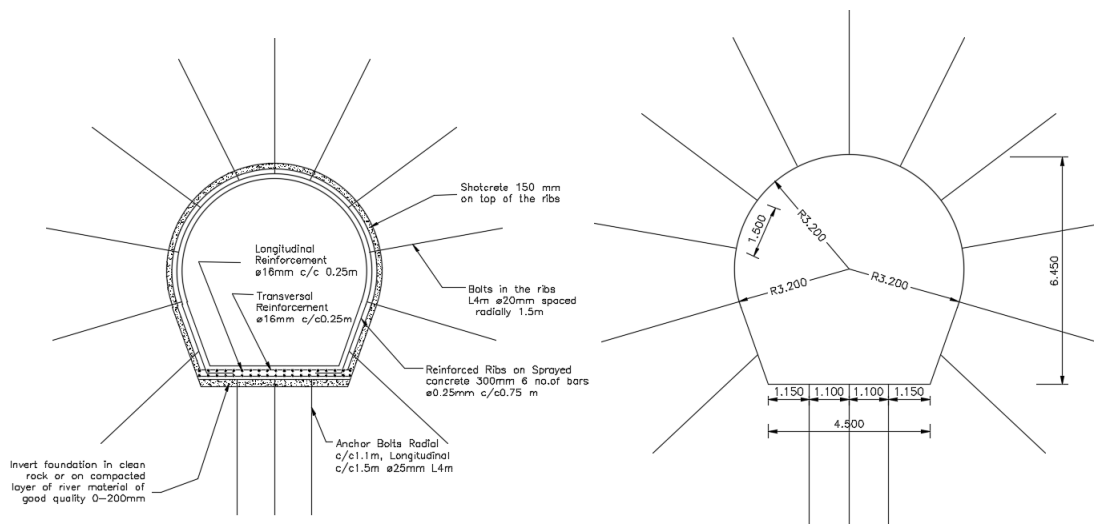


Figure 7.8: Installed Support at Moglice head race tunnel at the section containing flysch rock (left) and Tunnel cross section used for the modeling (Right)

Table 7.4: Actual liner installed and equivalent liner described for modeling

Parameter	Actual Support	Equivalent Support
Support	Shotcrete + RRS +Invert	Sprayed Reinforced Concrete
Thickness (mm)	S(150-200)+RRS300 & Invert400	650
Young's Modulus (Mpa)	25000	25000
Possion's ratio	0.2	0.2
Compressive Strength (Mpa)	30	30
Tensile Strength (Mpa)	5	5
Reinforcement	RRS 6no.s ϕ 16mm c/c 0.75m & Invert ϕ 16 mm c/c 0.25	ϕ 16mm c/c 0.25m

Table 7.5: Bolt parameters used for modeling

Parameter	Crown and Wall	Invert
Bolt diameter (mm)	20	25
Bolt length (m)	4	4
Bolt Modulus E (MPa)	200000	200000
Tensile Capacity (MN)	0.15	0.15
Residual Tensile Strength (MN)	0.015	0.015
Out of Plane Spacing	1.5	1.5
In Plane Spacing	1.5	1.1

7.6 Assessment of Norwegian design Principle

The inclined part of the Moglice headrace tunnel from section H5 to H6 as shown in Figure 7.2, has been constructed as an unlined tunnel based on the Norwegian design principle reviewed in Chapter 2. The design is carried out as during planning it was found that both topographical and geological conditions were suitable for construction of unlined tunnel (Aasen et al., 2013). In this section, the assessment has been carried out to check the stability of the unlined tunnel based on the Norwegian design principle. As it can be seen in Figure 7.5, the inclined part of the headrace tunnel contains ophiolitic rocks which in general are homogeneous and sound.

7.6.1 Analysis of Norwegian Confinement criteria

In section 2.2.1, Norwegian confinement criteria have been reviewed. The factor of safety using Equation 2.3 and Equation 2.5 has been computed as shown in Table 7.6. In Figure 7.9, the longitudinal profile of the headrace tunnel has been shown which is developed based on the Figure 2.2 to show the values of different parameters used for calculating factor of safety. Different sections of the tunnel are chosen for the assessment such that chainages represent different possible situations such as minimum and maximum overburden, and minimum and maximum water pressure. The topographic correction has been done with the assumption that contribution from the undulated ground surface to confinement is negligible.

Table 7.6: Analysis of Moglice headrace tunnel using Norwegian Confinement Criteria

Chainage	Overburden (h) [m]	Shortest Length (L) [m]	Static water head (H) [m]	FoS ₁	FoS ₂
8+900	418.9	348.9	59.3	18.8	12.9
9+100	325.0	270.4	90.3	9.6	6.6
9+500	482.1	344.1	158.2	8.1	4.1
9+900	458.8	427.1	224.0	5.5	4.8
10+300	367.6	343.8	290.3	3.4	3.0

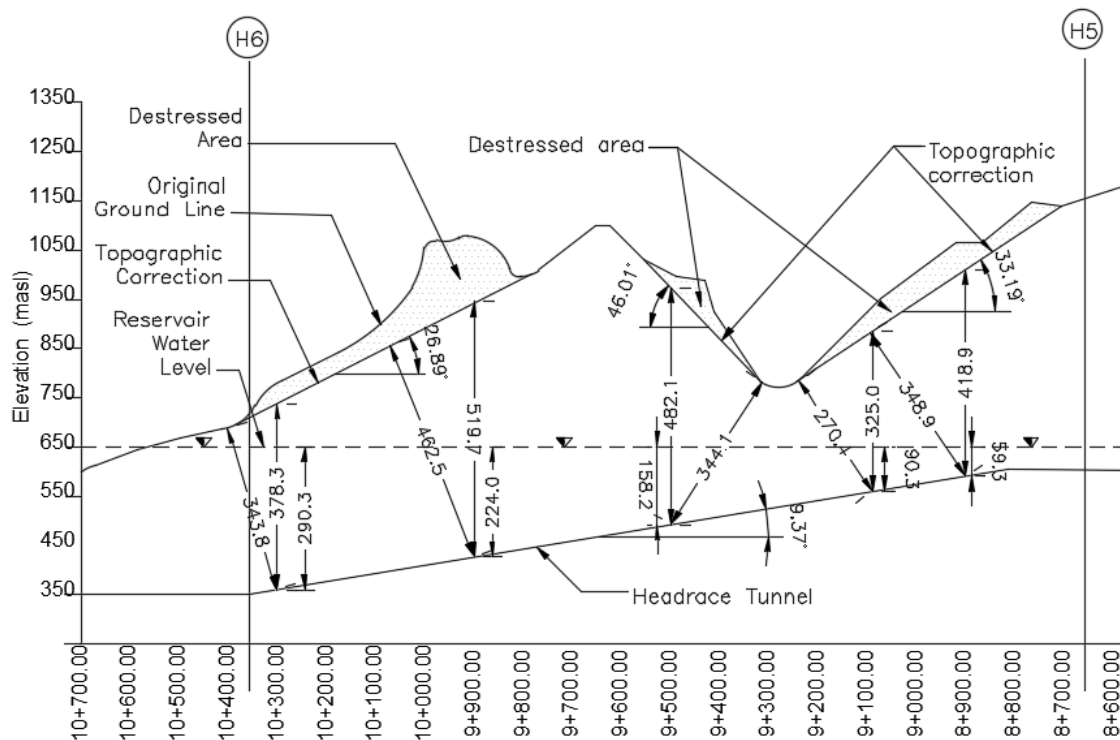


Figure 7.9: Longitudinal profile of Moglice inclined headrace tunnel, showing the value of parameters used in different design criteria for unlined shaft/tunnel

The results in Table 7.6 suggested that for all chainages the FoS_1 and FoS_2 computed using Equation 2.3 and Equation 2.5 is greater than 1.5 which is recommended. The maximum FoS_1 and FoS_2 computed are 18.8 and 12.9 respectively for the chainage 8+900, where the static water head is minimum. As the static water head increases the factor of safety decreases. The tunnel meets the Norwegian confinement criteria to avoid hydraulic jacking.

7.6.2 Analysis of Minimum principle stress criteria

As described in section 2.2.2, Norwegian confinement criteria do not account for the prevailing in situ stress in the tunnel location. Therefore, minimum principle stress criteria have been developed. The in situ stress field measurement has not been carried out in

these sections of the headrace tunnel. Hence to assess the in situ stress, numerical modeling using RS2 has been done. At each section of the tunnel which has been analyzed using Norwegian confinement criteria in section 7.6.1, the in situ stress has been computed from numerical modeling. For numerical modeling, the cross-section of each chainage has been analyzed using elastic analysis. The input parameters are taken from Table 7.7.

Table 7.7: Input parameters for Numerical Modelling at locations with Ophiolitic rocks

Material	UCS (Mpa)	GSI	m_i	E_{ci} (Gpa)	ν	Source
Ophiolitic Clasts	100-250	10-25	25±5	133	-	Rusi (2016)
Ophiolite (Powerhouse Cavern)	84	45	-	111.8	0.18	Flåten (2015)

The Moglice headrace tunnel orientation at this section is N136⁰E. The tectonic stress of the area has been assessed in section 9.5. The tectonic stress prevailing in the project location is 4.5 MPa oriented at N127⁰E. The tectonic stress is therefore resolved to compute locked in stress. For cross sectional valley model of the tunnel locked in in-plane and out-plane stresses are computed to as 0.7 MPa and 4.44 MPa. The boundary conditions for the model have been set as four corners of the models are restrained in both the x-direction and the y-direction to prevent any sort of vertical or horizontal displacements as shown in Figure 7.10 for chainage 10+300. The top boundary of the model is freed. Right, and left boundaries are restrained on x to prevent displacement horizontal displacement. And the bottom boundary is restrained on Y to allow only horizontal displacement.

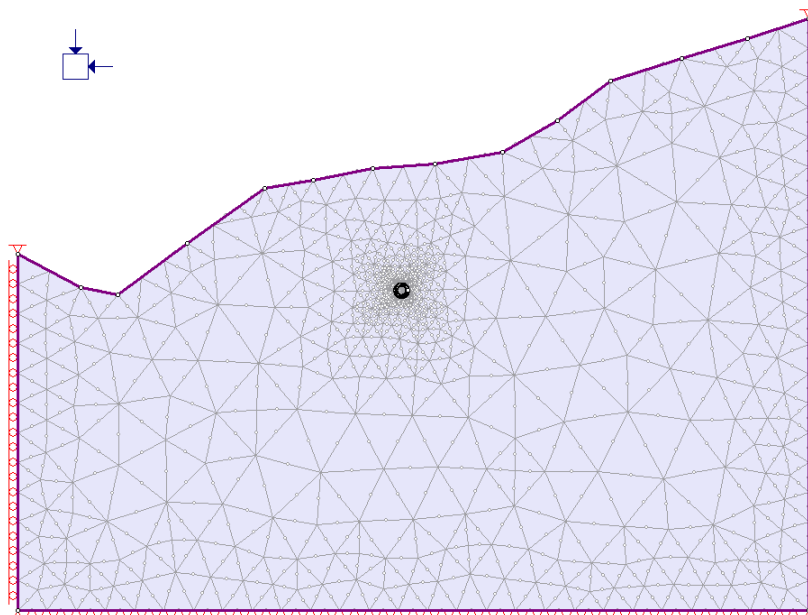


Figure 7.10: RS2 Topographical model for chainage 10+300 for in situ stress assessment

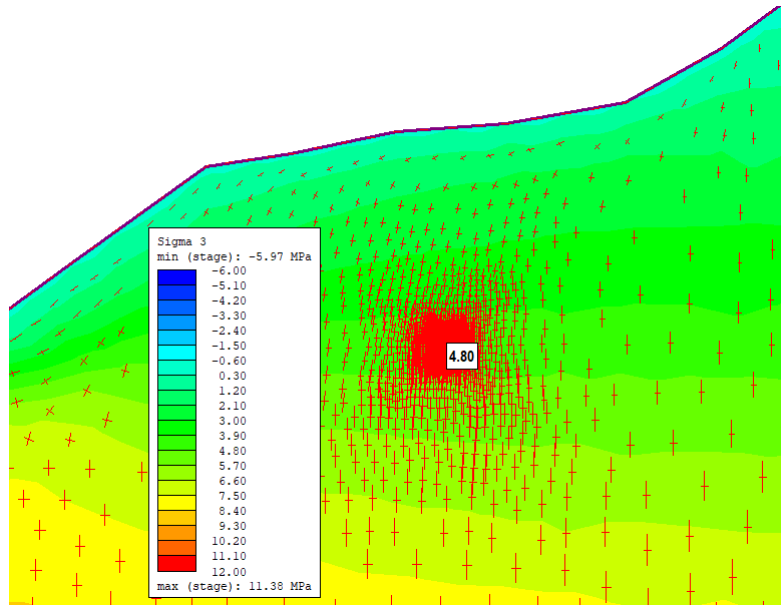


Figure 7.11: Minimum principal in-situ stress at chainage 10+300 m for in situ stress assessment

The minimum principal criteria have been reviewed in section 2.2.2. The criteria for safety against the hydraulic jacking is set as the minimum principal stress of surrounding rock mass should be greater than the maximum static water pressure inside the tunnel. The factor of safety is computed using Equation 2.6. The minimum principal stress is computed by numerical modeling and the result for chainage 10+300 has been shown in Figure 7.11. The minimum principal stress is found to 4.8 MPa for all chainages. The result for the factor of safety has been presented in Table 7.8, which shows the minimum factor of safety computed is 1.6 which is greater than the recommended value of 1.5. With the recommended value of FoS_3 , it can be concluded that the studied sections are safe against hydraulic jacking and possible leakages. of The computed minimum principal stress is significantly higher than static water pressure which varies from 0.6 MPa to 2.9 MPa. Similar to FoS_1 and FoS_2 , here FoS_3 too varies with the static water head.

Table 7.8: Analysis of Moglice headrace tunnel using Minimum Principal stress Criteria

Chainage	Static water head (H) [m]	Static Water pressure [MPa]	σ_3 [MPa]	FoS_3
8+900	59.3	0.6	4.8	8.0
9+100	90.3	0.9	4.8	5.3
9+500	158.2	1.6	4.8	3.0
9+900	224.0	2.2	4.8	4.2
10+300	290.3	2.9	4.8	1.6

8 Input parameter assessment for Moglice headrace tunnel

8.1 Engineering geological properties

The study area of headrace tunnel passes through layers containing weak rock masses containing claystone and siltstone which has low strength for intact rock <25 MPa and variable proportion of hard rock which intact rock strength >25 MPa. In the studied chainage from 7 +029 to 7 + 531, continuous face mapping was carried out during excavation. Q and GSI values were used for the mapping. Table 8.1 shows the description of the mapped section with the estimated weak rock proportion present in the respective chainage according to Almenara (2021).

Table 8.1: Summary of mapped rock mass conditions at the studied convergence sections between 7+029 and 7+531 [from Almenara (2021)]

Chainage	Q-value	GSI	% of weak rock content	Rock mass Description
7+029	0.1	25	90	Siltstone dominated rock mass with a high degree of shearing and disturbance. Embedded parts of sheared
7+064	0.11	25	80	The sheared and disturbing sequence of thin laminated siltstones, clayshales and broken sandstones
7+092	0.29	25	60	Tectonically disturbed and sheared rock mass composed of broken and partly chaotic blocks inside a weak matrix of strained dark siltstones
7+136	0.5	35	60	Stratified and partially disturbed, folded rock mass composed by alternates of persistent siltstone and carbonatic layers
7+168	0.38	27	60	Deformed and partially sheared rock mass composed of weak and strained siltstones and micritic siltstones.
7+194	0.25	25	70	Laminated and strongly disturbed rock mass composed of sheared, clayey siltstones, and embedded broken parts of harder, carbonatic rocks.
7+218	0.2	25	50	Disturbed, partly chaotic rock mass with nearly disappeared structure, a significant amount of harder and embedded blocks inside a weak matrix, that reminds to a typical block-in-matrix (bimrock) mass
7+266	0.2	35	50	Sheared and deformed rock mass composed by broken fragments of weathered and disturbed reddish sandstones embedded in a weak and dark matrix of clayey siltstones
7+291	0.16	30	90	Thinly laminated rock mass composed of weak and dark-clayey siltstones with thin carbonatic layers
7+316	0.5	30	60	Disturbed folded and siltstone dominant rock mass with intercalations of sandstones and limestones

Table 8.1: Summary of mapped rock mass conditions at the studied convergence sections between 7+029 and 7+531 [from Almenara (2021)]

Chainage	Q-value	GSI	% of weak rock content	Rock mass Description
7+342	0.1	32	70	Thinly laminated and partially disturbed rock mass composed of sheared and clayey siltstones, and embedded thin laminations of carbonation rocks
7+423	0.11	35	30	Sheared rock mass composed by an alternate of disturbed and partly tectonized big sandstone blocks embedded in weak clayey siltstone material
7+455	0.2	33	50	Highly disturbed, partly chaotic rock mass with nearly disappeared structure, a significant amount of harder and embedded blocks in the rock mass, like a typical block-in-matrix (bimrock) mass
7+531	0.15	25	80	Thinly laminated and strongly disturbed rock mass composed of sheared and folded siltstones, and embedded broken parts of harder, carbonatic rocks

The Q values mapped in during the construction ranges from 0.1 to 0.5 which according to rock mass classification using Q-system shown in Figure 3.8 suggests the rock mass present is of very poor quality. The GSI value ranges from 25 to 35, which according to the classification of Flysch according to GSI system about Table shown in Appendix shows that the rock mass is poorly to fairly weathered and contains a variable amount of sandstone and siltstone. The Q-value and GSI values shown in Table 8.1 do not relate to each other according Equation 3.11 and 3.12 which relates Q and GSI. Therefore, as rock mass classification is an important parameter to define to perform stability analysis, back-calculation is carried in Chapter 9.2 out using measured deformation shown in Table 7.3 to assess the real field rock mass classification.

8.2 Mechanical properties of intact rock

8.2.1 Laboratory Tests Results of Moglice Rock Sample

Different tests were performed on the rock samples collected from the headrace tunnel of the Moglice hydropower project. The tests were performed by Runa Berstad Frengen for her specialization project in 2019 and her Master's thesis in 2020. Lena Selen had performed the slake durability Index (SDI) test. The results were collected and used for further analyses.

The tested samples used by Runa were collected from the flysch section at Moglice headrace tunnel through the sprayed concrete lining. Samples were extracted during the flat jack installation in the tunnel at the chainage 7+492 to 7+501. Three additional flysch cores from the unknown chainage were also tested provided by Lena Selen. Figure 8.1 shows the rock samples extracted from the Moglice headrace tunnel.



Figure 8.1: Rock samples extracted from Moglice headrace tunnel from chainage 7+492 to 7+501 (Photo by Runa B. Frengen (Frenge, 2020))



Figure 8.2: Additional Rock samples used by Runa B. Frengen during laboratory testing (Frenge, 2020)

The descriptions of the rock samples with the location and rock content in the sample are shown in Table 8.2. During testing of rock samples, Runa has given an ID number to the samples to relate rock material to a core. The 13 cores used for testing are numbered according to the chainage from where those cores were extracted. According to Frengen (2020), the rock samples to be tested were limited so she has used the remaining cores left from preliminary projects done on the rock sample of the Moglice headrace tunnel. In Figure 8.2, additional 3 rock samples flysch 6, flysch 7, and flysch 10 used by Runa for testing are shown. Two of these samples with an ID number F6 and F7 were sandstone flysch and the remaining one F10 was claystone. Therefore, F6 and F7 samples can be used to prepare a test specimen that can be used to perform a uniaxial compression test, while since claystone reacts with water only a point load test is performed on it.

Table 8.2: Description of rock samples collected at different chainage along the headrace tunnel

Chainage	L/R	ID	Rock Content	Comment
7+501	L	10	Clay/sandstone Flysch	
7+501	L	11	Clay Flysch	
7+489	R	2	Clay Flysch	Non-cylindrical sprayed concrete
7+501	R	8	Clay Flysch	
7+497	L	7	Clay Flysch	
7+792	L	3	Conglomerate	
7+498	R	1	Clay Flysch	
7+492	L	5	Clay Flysch	Non-cylindrical sprayed concrete
7+501	L	9	Sandstone Flysch	
7+497	R	6	N/A	Only sprayed concrete
7+492	L	4	Conglomerate	
		12	Clay Flysch	Unknown chainage, rock only
		13	Clay Flysch	Unknown chainage
		F6	Sandstone Flysch	Material from Preliminary project
		F7	Sandstone Flysch	Material from Preliminary project
		F10	Clay Flysch	Material from Preliminary project

8.3 Determination of Mineral content by use of XRD

The presence of expansive clay minerals in the rock mass of the water tunnel can have a serious threat to the stability of the tunnel due to their swelling behavior when absorbing water (Zhang et al., 2017). Therefore, it is important to identify the presence of such expansive clay minerals beforehand. It has been established that the Moglice headrace tunnel passing through flysch contains the rock mass containing swelling minerals in them. Hence to find the mineral composition in the rock sample and to check the presence of swelling clay, an X-ray diffraction (XRD) test is conducted on the rock samples. The test results obtained by Runa after the test are shown in Table 8.3.

The results of the XRD test shows that the mineralogical contents in the rock samples are consistent. The composition of minerals shows that samples are composed of quartz which is the dominant minerals with content varying from 22% to 48%, feldspars (plagioclase and k-feldspar), sheet silicates (muscovite and chlorite) calcites, and pyrite. According to Frengen (2020), the results show the amorph content in the sample is up to 47.9%, and this indicates some level of weathering or mineral alteration. Runa found four out of six samples contain the swelling clay.

Table 8.3: Mineral content results from XRD test of the rock sample from Moglice headrace tunnel (Fren-gen, 2020)

	Flysch nr.	6	7	8	9	10	11	Average
Mineral Content (%)	Quartz	48.0	43.3	22.7	25.4	24.1	22.0	30.9±10.6
	Plagioclase	17.2	17.1	5.8	10.7	10.7	12.1	12.3±4
	Muscovite	4.6	6.4	6.9	14.4	14.4	19.4	11±5.4
	Chlorite	8.1	11.6	23.4	27.2	32.0	29.8	22±9.1
	Calcite	18.6	18.7	40.0	20.6	17.2	15.1	21.7±8.4
	K-Feldspar	3.5	2.5	1.0	1.5	1.4	1.4	1.9±0.8
	Pyrite	0.1	0.4	0.1	0.2	0.2	0.2	0.2±0.1
Crystalline content (%)	77.1	72.4	62.9	60.3	56.7	52.1	63.6±8.7	
Amorph Content (%)	22.9	27.6	37.1	39.7	43.3	47.9	36.4±8.7	
Swelling Clay	Yes	Yes	Yes	No	Yes	No		

8.4 Mechanical Properties Laboratory Testing

To determine the mechanical properties of the rock samples collected from the Moglice headrace tunnel, the tests such as Uniaxial Compression Strength (UCS), point load test, and Brazil test were performed. The mechanical properties determined included compressive strength, tensile strength, Poisson's ratio, and density. The tests were performed in both rock samples and sprayed concrete samples. According to Fren-gen (2020), the initial plan was to perform all tests on these samples, however, due to few issues with the rock samples, some of the tests were not carried out on all rock samples. The flysch rocks react with water and slakes, which cause difficulty in preparing specimens for UCS and Brazil tests using water. For, sand and conglomerate flysch samples, during the preparations of specimens some sections of samples broke and fall into pieces. Therefore, Brazil tests were not conducted on this sample which means only sprayed concrete samples were tested. The test results from each tests are explained in the following respective subsections.

8.4.1 Uniaxial Compression Strength Test and Deformability

Only sandstone and conglomerate flysch were tested for uniaxial compression strength as discussed above. Runa tested five specimens of the rock core material, eleven specimens of sprayed concrete, and four specimens of sample from F-series in accordance to ISRM (1979b). The results obtained from the UCS test are presented in Table 8.4. The tests were also performed on wet samples to determine the UCS in wet conditions to see the effect of water. The samples used for wet condition F6W and F7W were submerged in water for a respective one week and two weeks duration. The result for the UCS test for dry and wet conditions is shown in Table 8.5.

The test result for dry specimen shows the results of compressive strength ranging from 74.2 MPa to 158 MPa suggesting the presence of high strength rock according to classification based on UCS value as shown in Table 3.1. The average compressive strength is found to be 132.3 ± 22 MPa. The test specimen's diameter varies from 44.16 to 50.13 mm. Hence, the UCS needs to be corrected for 50 mm diameter. Also, the UCS varied out on the wet samples shows a reduction in strength in comparison to the dry sample. For saturated condition, the results obtained from lab test shows the strength reduction

of 10% and 18% for F6 and F7 respectively. Therefore, after correcting the UCS for 50 mm diameter the strength due to the effect of water is computed using Equation 3.1. The corrected UCS values for 50 mm diameter and considering the effect of water are found to be a minimum of 55 MPa, maximum of 117 MPa, and mean value of 98 MPa. According to Devoll (2015), the rock mass in the studied section i.e. between 6+984 to 7+581, a stronger rock of strength 25-55 MPa is present. Therefore, the UCS values obtained from mean and maximum UCS from the laboratory overestimate the strength.

Table 8.4: Results of Uniaxial Compressive Strength Test

Material	UCS (MPa)			Young's Modulus (GPa)			Poisson's Ratio		
	Max	Min	Avg	Max	Min	Avg	Max	Min	Avg
Flysch Rock	158.0	74.2	132.3±22	75.2	27.6	55.8±17.1	0.38	0.26	0.29±0.02
Sprayed Concrete	60.5	25.1	39.9±11.7	23.8	9.8	18.2±5.3	0.26	0.13	0.18±0.05

Table 8.5: Results of Uniaxial Compressive Strength reduction due to water

Test condition	Uniaxial compressive strength (MPa)	
	F6	F7
Laboratory condition (D)	117.3	90.3
Submersion in Water (W)	105	74.2
Strength reduction	10 %	18 %

The sprayed concrete used in the tunnel is of high strength. Hence, as for sprayed strength is concerned the average value obtained from the test which is 39.9 MPa can be used as its representative compressive strength.

Density of the rock samples and sprayed concrete samples were computed from the rock samples. Seismic velocity was computed to find the quality of rock mass. According to Nilsen and Palmström (2000), good quality rock mass has typically seismic velocity over 5000 m/s, while weakness zones have velocities lower than 4000 m/s. Table 8.6 shows the results for density and velocity.

Table 8.6: Density and velocity results

Material Type	Velocity (m/s)	Density (g/cm^3)
Sand/Conglomerate flysch	5601±134	2.67±0.03
Sprayed Concrete	4514±121	2.21±0.1

8.4.2 Point Load Test

The I_{S50} values for the samples were obtained as shown in Table 8.7 from point load test and then it is required to determine the k value to compute UCS. From Table 3.2, the k value can be estimated for sandstone flysch and sprayed concrete. But for claystone flysch, the table does not provide the k value as the strength is expected to be less than

25 MPa. Authors like Singh et al. (2012), Vallejo et al. (1989) and Smith (1997) have used the value of k as 12.6 for Shale which may be the closest weak rock for which the correlation has been found. Hence, taking this as a reference and consulting with Professor Panthi, the k value has been fixed for claystone as shown in Table 8.8.

Table 8.7: Results from Point Load Test

Material type	I_{s50} Mpa		
	Max	Min	Average
Claystone Flysch	1.01	0.35	0.72±0.28
Sandstone Flysch	5.43	3.67	4.87±0.57
Sprayed Concrete	4.89	2.35	3.42±0.6

Table 8.8: Estimated Uniaxial Compressive Strength from Point Load Test

Material type	Classification	K value	Estimated UCS MPa		
			Max	Min	Average
Claystone Flysch	Very low strength	11	11.11	3.85	8.00
Sandstone Flysch	High strength	24	130.32	88.08	116.88
Sprayed Concrete	Medium Strength	12	28.2	66.27	41.04

Similar to the UCS test, the estimated UCS for sandstone from flysch suggests the presence of high-strength rock in the rock mass. The estimated strength from the point load test is similar to the UCS test. After the diameter correction and consideration of water effect similar to UCS test results in the compressive strength of the minimum value of 65 MPa, the maximum value of 96 MPa, and an average of 86 MPa. The strength values computed are overestimated as the strength exceeds 55 MPa.

The estimated UCS for claystone flysch indicates that the rock is of low strength as per classification shown in Table 3.1. As per Devoll (2015), the weak rock present in studied chainages are of strength less than 25 MPa. The lab results verify this statement. The estimated UCS values are in the range of 3.85-11.11 MPa. According to Almenara (2021), the range compressive strength values of the weak rock in studied chainages are in the range of 10-25 MPa. Therefore, with this comparison, the author chooses maximum UCS estimated of value 11 MPa as the compressive strength of the claystone flysch at study chainages.

The UCS estimated for the sprayed concrete from the point load test is similar to the test results obtained from the UCS test. Hence, as discussed in section 8.4.1, the average value of 41.04 can be used to represent the compressive strength of the sprayed concrete.

8.4.3 Brazil Test

The test is limited to testing only sprayed concrete. The reason for not performing the test on the rock sample was the unavailability of suitable rock material to prepare the test specimen. The test result is shown in Table 8.9.

Table 8.9: Results from Brazil test

Material Type	Tensile Strength, σ_t (MPa)
Sprayed Concrete	4.9±0.8

8.4.4 Swelling Test and Slake Durability Index (SDI)

Tunnels constructed through sedimentary rocks containing clay, clayshales, or anhydritic shales experience swelling phenomena (Steiner, 1993). According to Steiner (1993), clay shales with low to moderate swelling pressures results mostly in invert heave, and the anhydritic shales with high swelling pressure cause extreme heave and the crushing of strong inverts. Hence, the swelling tests need to be performed on rock samples to estimate the swelling pressure likely to occur. However, the swelling pressure obtained from the crushed sample does not represent the exact in situ swelling condition. But the results can be used to estimate the in situ swelling pressure.

Runa Berstad Frengen performed the swelling test during her specialization project in 2019 at NTNU. Lena Selen had performed the Slake Durability Index (SDI) test on the rock sample from the headrace tunnel. Table 8.10 shows the results from the test.

Table 8.10: Results from swelling test and swelling durability index

Flysh nr.	6	7	8	9	10	11	Average
Swelling Pressure Mpa	0.17	0.07	0.25	0.16	0.16	0.24	0.17±0.06
Free Swelling %	111	133	158	135	147	120	134±17.15
SDI %	97.6	93.4	70.8	48.9	64.9	43.3	70±20

According to Table 4.2, the samples can be classified from moderate to high swelling capability. The results do not show a clear correlation among the three measured parameters. The reason for the absence of correlation is may be due to insufficient samples being tested.

As discussed, the high swelling pressure can cause extreme heave and the crushing of strong inverts. Hence as the laboratory swelling pressure is classified from moderate to high, the Moglice headrace tunnel needs to consider the swelling pressure while designing the support. Hence, to study the stability of the installed support at the Moglice headrace tunnel, maximum swelling pressure obtained from the laboratory is considered as intact swelling pressure. therefore, the swelling pressure of 0.25 MPa is considered for further analysis in this thesis.

8.5 Conclusion on Laboratory results

The laboratory test results, provide the range of values for different mechanical properties of a rock sample. Table 8.11, summarizes the test results obtained from laboratory testing. These test results are to be used for estimating rock mass properties. To use the results, one should understand the real field geological condition and use the suitable results accordingly. In Chapter 8.1, engineering geological conditions of the Moglice hydropower project area have been assessed. Based on the geological information and laboratory test results, the values for mechanical properties and swelling pressure to be

used for further analyses have been decided. In Table 8.11, the adopted values for different mechanical properties of the intact rock are shown. The basis for the adoption of values is made based on reports and literature reviews. The compressive strength of rock samples is adopted based on the information provided by Devoll (2015) and Almenara (2021). According to Devoll (2015) UCS for claystone is less than 25 MPa and Almenara (2021) used the UCS for claystone ranging from 10-25 MPa. Similarly for sandstone according to Devoll (2015), UCS ranges from 25-55 MPa and Almenara (2021) used the UCS ranging from 40-50 MPa.

Table 8.11: Mechanical properties of intact rock and sprayed concrete obtained from laboratory testing

Description		σ_{ci} (MPa)	σ_t (MPa)	E_{ci} (GPa)	γ (gm/cm^3)	ν	Test Method
Sandstone	Mean	98	-	55.8	2.67	0.29	UCS
	Range	55-117	-	27-55	2.66-2.7	0.29-0.38	
Flysch	Mean	86	-	-	-	-	PLT
	Range	65-96	-	-	-	-	
	Adopted	55	-	55.8	2.67	0.29	
Claystone	Mean	8	-	-	-	-	PLT
	Range	4-11	-	-	-	-	
Flysch	Adopted	11	-	-	-	-	
	Mean	40	4.9	18.2	2.21	0.18	UCS & Brazil
Sprayed Concrete	Range	25-60	3-6	10-25	1.99-2.25	0.13-0.26	
	Mean	41	-	-	-	-	PLT
Range	28-66	-	-	-	-		
	Adopted	40	4.9	25	2.21	0.18	

8.6 Mechanical Properties of clay stone

The laboratory tests performed on claystone samples fail to assessed many rock mechanical properties. The missing information regarding these properties is important for further study. According to Devoll (2015), the properties of rock mass mainly depend on the content of weak rock present in the rock mass. Therefore, it is important to gather the missing value for mechanical properties of claystone and is gathered from the study carried out by Malaj et al. (2017). The study is based on the characterization of Flysch Rock in Albania and for this field and laboratory testing methods have been used. The required missing information extracted form Malaj et al. (2017) is summarized in Table 8.12.

Table 8.12: Mechanical properties for claystone flysch at Moglice headrace tunnel (Malaj et al. (2017))

Properties	Range of Values for clystone flysch
Tensile strength, σ_t (Mpa)	1.60-2.40
E-modulus, E_i (GPa)	5.00-10.00
Density, γ (gm/cm^3)	2.34-2.82
Possion's ratio, ν	0.31-0.37

9 Estimation of rock mass parameters for Moglice headrace tunnel

9.1 Input data

The methods for estimating rock mass properties such as strength and deformability have been reviewed in Chapter 3.6. The methods described demand the input which is related to the properties of intact rock. The laboratory results provide some of this information regarding the properties of intact rock. The missing inputs are hence collected from various sources. The sources of these data are Moglice project reports, literature published on Moglice hydropower project, literature related to similar rock type and rock mass condition, and discussion with the supervisor.

After collecting the information on the mechanical properties of intact rock, the input parameters for the determination of rock mass properties are described as shown in Table 9.1. The average values for missing mechanical properties are considered for the claystone flysch from the range of values shown in Table 8.12.

Table 9.1: Input parameters for rock mass properties estimation

Parameters	Sandstone flysch	Claystone flysch	Remarks
Compressive strength, σ_{ci} (MPa)	55	11	From Table 8.11
E-modulus, E_i (GPa)	55.8	7.5	From Table 8.11 and Table 8.12
Density, γ (gm/cm^3)	2.67	2.58	From Table 8.11 and Table 8.12
Possion's ratio, ν	0.29	0.34	From Table 8.11 and Table 8.12
Hoek and Brown Constant, m_i	17	6	From Appendix
Disturbance factor, D	0.2	0.2	Carefully excavated D& B tunnel

Table 9.2: Weighted Input parameters for rock mass properties estimation

Chainage	Compressive strength, σ_{ci} (MPa)	E-modulus, E_i (GPa)	Hoek and Brown Constant, m_i	Possion's ratio, ν	Density, γ (gm/cm^3)
7+029	15.40	12.25	7.10	0.34	2.59
7+064	19.80	17.00	8.20	0.33	2.60
7+092	28.60	26.50	10.40	0.32	2.62
7+136	28.60	26.50	10.40	0.32	2.62
7+168	28.60	26.50	10.40	0.32	2.62
7+194	24.20	21.75	9.30	0.33	2.61
7+218	33.00	31.25	11.50	0.32	2.63
7+266	33.00	31.25	11.50	0.32	2.63
7+291	15.40	12.25	7.10	0.34	2.59
7+316	28.60	26.50	10.40	0.32	2.62
7+342	24.20	21.75	9.30	0.33	2.61
7+423	44.00	43.13	14.25	0.30	2.65
7+455	33.00	31.25	11.50	0.32	2.63
7+531	19.80	17.00	8.20	0.33	2.60

The input parameters for each chainage of the headrace tunnel of Moglice hydropower will be different depending on the content of weak rock in the rock mass. The weak rock content varies from chainages to chainages as shown in Table 8.1. The rock mass properties is governed by weak rock as the content percentage of the weak rock is more than 50%. Therefore, to determine the rock mass properties at each chainages, the weighted parameters are used depending on the weak rock content percentage. The weighted parameters computed for each chainages are presented in Table 9.2.

9.2 Back calculation

For the determination of rock mass properties, another input needed is the rock mass condition. The Q-value has been measured in the field. However, through the report and literature, two different values of rock mass conditions Q system and GSI system are found as shown in Table 8.1. To assess the real ground conditions at each chainage back-calculation of intact rock strength has been carried out based on measured deformation which is presented in Table 7.3. By using Hoek and Marinos (2000) method, for known deformation and applied rock support, approximate back-calculation of intact rock strength is possible (Shrestha and Panthi, 2014). Henceforth, for two different rock mass conditions, it is attempted to back-calculate the intact rock mass strength. The objective of back-calculation is to see which classification systems back-calculated strength is similar to the weighted rock strength given in Table 9.2. The input for back-calculation is taken from 8.1 for rock mass conditions and other parameters are taken from Table 9.2. Equation 4.3 has been used to relate the measured deformation with rock mass strength. The support pressure is used as 2.14 MPa computed from CCM method in Chapter 4.3.3.2. The calculated rock mass strength is then used to find intact rock strength using Equation 9.1 suggested by Hoek and Marinos (2000).

$$\sigma_{cm} = (0.0034m_i^{0.85})\sigma_{ci} \left\{ 1.029 + 0.025e^{(-0.1m_i)} \right\}^{GSI} \tag{9.1}$$

Table 9.3: Rock mass conditions at the studied convergence sections between 7+029 and 7+531 after back calculation

Chainage	Q	GSI
7+029	0.05	25
7+064	0.05	25
7+092	0.05	25
7+136	0.22	35
7+168	0.06	27
7+194	0.25	36
7+218	0.05	25
7+266	0.22	35
7+291	0.10	30
7+316	0.10	30
7+342	0.10	30
7+423	0.22	35
7+455	0.16	33
7+531	0.15	33

The back-calculated intact rock strength result using GSI value is close to weighted compressive strength for most of the chainages except three chainages 7+194, 7+342, and 7+531. For these three chainages, the Q value gives the back-calculated intact rock strength close to weighted compressive strength. Hence, based on the results of the back-calculation the rock mass condition at the Moglice headrace tunnel passing through flysch rock is as presented in Table 9.3. These values are, therefore, further used to determine the rock mass properties.

9.3 Rock mass strength

Rock mass strength is calculated based on the empirical and analytical relations provided by various researchers which are reviewed in Chapter 3.6. The equations used for computing rock mass strength based on these relations have been presented in Table 3.6. For the calculation of rock mass strength, the GSI value has been taken from Table 9.3. The other respective input parameters for calculating rock mass strength are taken from Table 9.1 and Table 9.2.

Table 9.4: Rock mass strength (MPa) calculation using different relations

Chainage	(Bieniawski, 1989)	(Hoek et al., 2002)	(Nick Barton, 2002)	(Panthi, 2006)
7+029	0.37	1.04	5.26	1.00
7+064	0.47	1.44	5.72	1.46
7+092	0.68	2.36	6.46	2.53
7+136	1.16	3.15	7.53	2.53
7+168	0.76	2.52	6.66	2.53
7+194	0.58	1.89	6.11	1.97
7+218	0.79	2.87	6.77	3.14
7+266	1.34	3.83	7.90	3.14
7+291	0.48	1.22	5.68	1.00
7+316	0.89	2.75	6.98	2.53
7+342	0.84	2.32	6.80	1.97
7+423	1.69	5.29	8.55	4.47
7+455	1.20	3.63	7.66	3.14
7+531	0.47	1.44	5.72	1.46

Table 9.4 shows the rock mass strength calculated using different methods. The results vary for each method as each method depends on different input parameters. Barton (2002) estimated rock strength in comparison to other methods are high which are unlikely for the weak flysch rock mass present in Moglice headrace tunnel. The estimation of rock mass by Bieniawski (1989) method is on the lower side. However, as it can be seen the results obtained by the Hoek et al. (2002) method and Panthi (2006) method are almost similar. Despite having different approaches for calculation for these two methods, the results are similar and the estimated rock mass strength values lie between the values estimated by Bieniawski (1989) and Barton (2002). The estimated rock mass strength by Panthi (2006) has been used as this method is developed for schistose, foliated, and anisotropic rocks of sedimentary origin with low compressive strength (Panthi (2006)). Also, the Hoek et al. (2002) estimated values have been used for the analysis of plastic deformation using Hoek and Diederichs (2006) method.

9.4 Rock mass deformation modulus

Similar to rock mass strength, rock mass deformation modulus is calculated based on the empirical and analytical relations provided by various researchers which are reviewed in Chapter 3.7. Rock mass deformation modulus calculation is done using the relations shown in Table 3.7. The results of estimated rock mass deformation modulus using different methods have been shown in Table 9.5. Barton (2002) method estimates higher rock mass deformation modulus in comparison to other methods. The estimated values by Hoek and Brown (1997) and Panthi (2006) are almost similar. However, among these two values the deformation modulus predicted by Panthi (2006) being smaller, it has been used in numerical modeling.

Table 9.5: Rock mass deformation modulus (GPa) calculation using different relations

Chainage	Hoek and Brown (1997)	Barton (2002)	Panthi (2006)
7+029	0.931	1.926	0.801
7+064	1.055	2.095	1.261
7+092	1.268	2.368	2.362
7+136	2.255	3.950	2.362
7+168	1.423	2.623	2.362
7+194	1.167	2.240	1.783
7+218	1.362	2.483	2.992
7+266	2.422	4.143	2.992
7+291	1.241	2.488	0.801
7+316	1.691	3.058	2.362
7+342	1.745	3.204	1.783
7+423	2.797	4.560	4.768
7+455	2.159	3.740	2.992
7+531	1.055	2.095	1.261

9.5 Tectonic Stress

The determination of in situ situations is important to analyze the stress-induced problems likely to occur in underground structures. At Moglice hydropower plant hydraulic fracturing test and 3D overcoring test has been performed at different locations to assess in situ stress. However, none of these tests were performed in the sections where the study of this thesis has been carried out. Since no tests have been performed in the flysch section of the headrace tunnel, it is important to carry out other methods to assess the in situ stress. For assessment of in situ stress valley numerical modeling has been carried out. As per Panthi (2014), there is a considerable contribution of tectonic stress in total horizontal stress. So to carry out in situ stress assessment it is important to know the tectonic stress value for the rock mass of the project area.

Albania lies in the Dinaric-Hellenic belt which is originated from the Mesozoic-Tertiary convergence and subsequent continental collision related to the closure of the eastern branch of the Tethyan oceanic basin (Marroni et al., 2009). And as per Marroni et al. (2009), this belt is divided into different tectonostratigraphic zones and each zone consists of an assemblage of variably deformed and metamorphosed tectonic units of oceanic and/or continental origin. Therefore, the total horizontal stress of the project area is af-

ected by tectonic activity and the orientation and magnitude of tectonic stress prevailing in that area. The magnitude and orientation of the tectonic stress close to the project location are accessed from the world stress map as shown in Figure 9.1. The figure shows the main direction for the maximum horizontal stress (S_H) in Albania. From the world stress map database by Heidbach et al. (2016b), the magnitude of the main direction for the maximum principal horizontal stresses close to the project location is 4.5 MPa and is oriented N156°E. The quality of the stress lies in the D scheme which means S_H orientation is questionable to the range of ($\pm 25-40^\circ$) Heidbach et al. (2016a). Since there is uncertainty with the orientation of the tectonic stress, the assessment of the tectonic stress is carried out based on the misfit criteria with the available data of measured in situ stress at different locations of the project area.

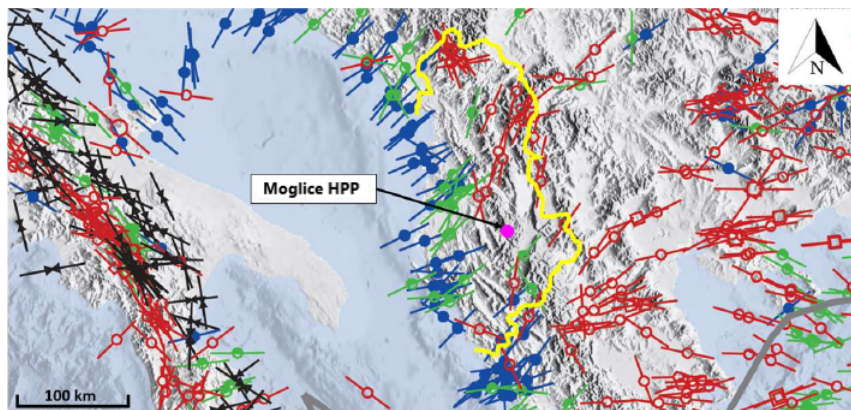


Figure 9.1: World stress map showing direction for maximum principal stress horizontal stresses for Albania 2016 by Heidbach et al. (2016a) [extracted from Almenara (2021)]

Hydraulic fracturing test has been performed at chainage 7+884 and powerhouse cavern and for chainage 10+827 3D overcoring test has been performed. able 9.6 shows the results from the field measurements. To assess the tectonic stress, the results from the measurement will be used. The misfit criteria have been defined as described in the following subsection. For the defined criteria, the calculated stress is required. Therefore, for the calculation of stress RS2 software has been used to perform numerical modeling of the location where the test has been performed. For calculating misfit, a standard deviation of measured values is needed, and only for the test performed at chainage 7+884, the standard deviation is known. Hence, the modeling is carried out only for this section.

Table 9.6: Test results of stress measurement at various location at Moglice Hydropower

Location	Method	Depth (m)	σ_v (Mpa)	σ_{Hmax} (Mpa)	σ_{Hmin} (Mpa)	θ_{SH}	Source
7+884	Hydraulic fracturing	120	3.8±0.3	13.9±1.8	7.0±0.5	N134E	Devoll (2015)
Powerhouse Cavern	Hydraulic fracturing	263	8.3	18.5	9.3	N49E	Almenara (2021)
10+827	CSIRO 3D Overcoring	320	6.9	14.6	5.4	N71E	Almenara (2021)

9.5.1 Model setup and Input parameters

In absence of the detailed results for powerhouse cavern and chainage 10+827, only the results from the chainage 7+884 have been used. The numerical modeling is carried for chainage 7+884. Since, RS2 is two-dimensional software, to analyze the 3D solution to the problem two sections have been analyzed. The longitudinal section and cross-section of the terrain are analyzed. The longitudinal section is drawn along the tunnel alignment as represented by the green line in Figure 9.2, and the cross-section is drawn perpendicular to the tunnel alignment along the red line shown in the same figure.

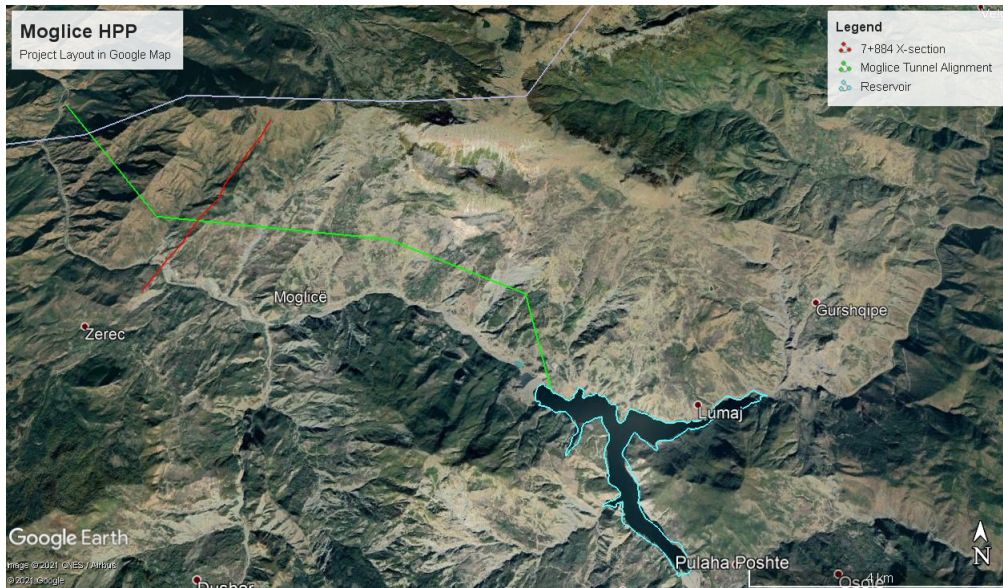


Figure 9.2: Project layout of Moglice hydropower project showing tunnel alignment (in green) and cross section alignment for chainage 7+884(in red) (from Google Earth)

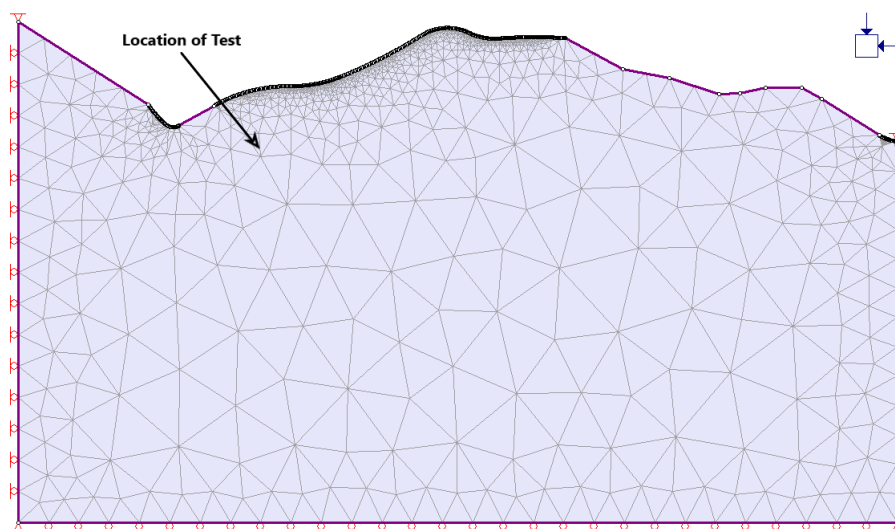


Figure 9.3: RS2 Model of Longitudinal section of Terrain at chainage 7+884

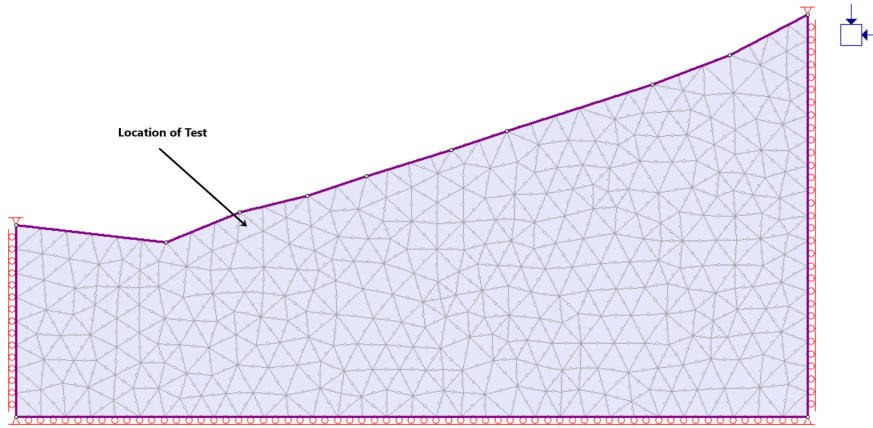


Figure 9.4: RS2 Model of cross section of Terrain at chainage 7+884

The four corners of the models are restrained in both the x-direction and the y-direction to prevent any sort of vertical or horizontal displacements as shown in Figure 9.3 and Figure 9.4 for longitudinal section and cross section respectively. The top boundary of the model is freed. Right, and left boundaries are restrained on x to prevent displacement horizontal displacement. And the bottom boundary is restrained on Y to allow only horizontal displacement.

The chainage 7+884 lies in ophiolitic fault breccia and powerhouse cavern and chainage 10+827 lies in ophiolites. The input parameters are collected from various literature. Table 7.7 shows the input parameters consider for the modeling.

9.5.2 Definition of misfit

The l_1 -norm misfit function has been defined for both hydraulic fracturing and overcoring methods. The misfit functions are defined as Eq. 9.2 and Eq. 9.3 for hydraulic fracturing and overcoring respectively (Basnet and Panthi, 2019):

$$\psi^{HF} = \sum_{m=1}^M \frac{|\sigma_{mes1}^m - \sigma_{cal1}^m|}{\sigma_m^d} \quad (9.2)$$

From the modeling, principal stresses are computed from which vertical and maximum and minimum horizontal stresses are computed. Eq.9.2 has been used to compute the misfit. The tectonic stress magnitude and orientation used for modeling along with the results for misfit has been shown in Table 9.7.

Where, σ_{mes1} and σ_{cal1} are measured and calculated (from numerical modeling) principal stresses respectively and, σ_d is the standard deviation in the measurement which is represented by standard deviation and M is the total number of measurement.

$$\psi^{OC} = \sum_{n=1}^N \frac{|\sigma_{mes2}^n - \sigma_{cal2}^n|}{\sigma_n^d} \quad (9.3)$$

Where, σ_{mes2} and σ_{cal2} are measured and calculated (from numerical modeling) principal stresses respectively and, σ_d is the standard deviation in the measurement which is represented by standard deviation and N is the total number of measurement.

Basnet and Panthi (2019) define the global misfit function for both hydraulic fracturing and overcoring. The application of the global misfit function is defined as the two methods are of different natures. This function is applicable to find the stress when the methods are applied at similar regions to estimate the principal stress. In such a case, the application of global misfit is sensible. But since the measurements of principal stresses by hydraulic fracturing and 3D overcoring are carried out at differed project locations, only the misfit criteria defined in Eq. 9.2 and Eq. 9.3 are used for this study purpose.

9.5.3 Existence of tectonic stresses

The horizontal stress is influenced by tectonic stress as shown in Eq. 3.15. If σ_{tecmin} and σ_{tecmax} are the minimum and maximum tectonic stress respectively then, σ_{Hmin} and σ_{Hmax} are represent by Eq. 9.4 and Eq. 9.5 respectively (Basnet and Panthi (2019)).

$$\sigma_{Hmin} = \frac{\nu}{1 - \nu} \cdot \sigma_z + \sigma_{tecmin} \tag{9.4}$$

$$\sigma_{Hmax} = \frac{\nu}{1 - \nu} \cdot \sigma_z + \sigma_{tecmax} \tag{9.5}$$

If θ be the angle made by σ_{Hmax} with the north the normal stresses as shown in Figure 9.5, σ_{xx} and σ_{yy} and the shear stress σ_{xy} initialized in a zone are given by the equations Eq. 9.6, Eq. 9.7 and Eq. 9.8 respectively.

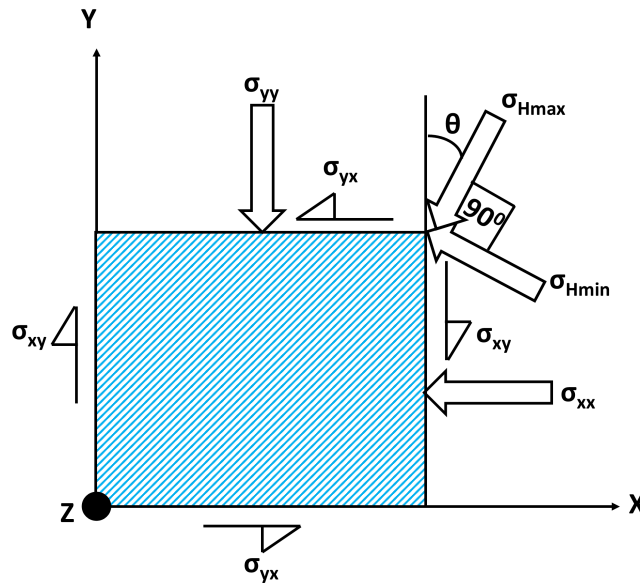


Figure 9.5: Resolving horizontal stresses in X and Y directions [extracted and modified from Basnet (2013)]

$$\sigma_{yy} = \sigma_{Hmax} \cos^2 \theta + \sigma_{Hmin} \sin^2 \theta \tag{9.6}$$

$$\sigma_{xx} = \sigma_{Hmax} \sin^2 \theta + \sigma_{Hmin} \cos^2 \theta \tag{9.7}$$

$$\sigma_{xy} = \sigma_{yx} = \frac{\sigma_{Hmax} - \sigma_{Hmin}}{2} \sin 2\theta \tag{9.8}$$

To know whether the horizontal stresses are contributed by tectonic stress along with the gravitational and topographical- led horizontal stresses in the Moglice project area, the model is run with different tectonic stress combination. The model is first run with zero tectonic stress and various combination of tectonic stresses are used.

The intact rock strength is considered to be 100 MPa, Young’s modulus to be 133 GPa, GSI of 25, Poisson’s ratio of 0.18, and m_i to be 25 as initial input parameters. For this combination of input parameters, the gravity-induced stress elastic model is run. The tectonic stresses are feed to the model in different combinations as shown in Table 9.7. The in-plane and out plane tectonic stress provided in the table is for the longitudinal model and will be vice versa for the cross-sectional model.

Table 9.7: Minimization of Hydraulic fracturing misfit for different combinations of tectonic stress magnitude and orientation

Trails	$\sigma_{inplane}$ (MPa)	$\sigma_{outplane}$ (MPa)	Hydraulic Fracturing			L-section model		X-section Model		ψ^{HF}	
			σ_v (MPa)	σ_H (MPa)	σ_h (MPa)	σ_v (MPa)	σ_h (MPa)	σ_H (MPa)	σ_h (MPa)		
1	0.0	0.0	3.8	13.9	7	3.4	4.2	2.9	3.2	3.4	6.3
2	2.1	4.0	3.8	13.9	7	3.4	6.2	4.8	7.2	6.2	2.9
3	4.2	1.7	3.8	13.9	7	3.4	8.1	4.3	4.3	8.2	4.0
4	4.0	2.0	3.8	13.9	7	3.4	8.1	4.3	5.2	7.9	3.6
5	3.8	2.4	3.8	13.9	7	3.4	8.1	4.3	5.3	7.9	3.6
6	3.6	2.7	3.8	13.9	7	3.4	7.1	4.2	6.1	7.9	2.7
7	3.3	3.0	3.8	13.9	7	3.4	7.2	4.8	6.1	7.9	2.6
8	3.1	3.3	3.8	13.9	7	3.4	7.2	4.8	6.3	7.9	2.5
9	2.8	3.5	3.8	13.9	7	3.4	7.2	4.8	7.1	7.6	2.3
10	2.5	3.8	3.8	13.9	7	3.4	6.2	4.8	7.1	6.2	2.8
11	1.8	4.1	3.8	13.9	7	3.4	5.2	4.8	7.2	5.9	3.4
12	1.4	4.3	3.8	13.9	7	3.4	5.1	0.8	7.2	5.9	4.0
13	1.0	4.4	3.8	13.9	7	3.4	5.1	0.8	8.1	4.6	4.6
14	0.6	4.5	3.8	13.9	7	3.4	4.1	0.7	8.1	4.6	5.1
15	0.2	4.5	3.8	13.9	7	3.4	4.1	0.7	4.2	4.6	5.9

The results as shown in Table 9.7 suggested that the misfit is minimized when the orientation of tectonic stress is in the range 127^0 to 132^0 . The modeling is further carried after changing the input parameters. The intact rock strength is changed to 84 MPa, Young’s

modulus as 100 GPa, and Poisson’s ratio as 0.25. The reduction in the values of input parameters is done to see if the initial model is too optimistic.

Table 9.8: Minimization of Hydraulic fracturing misfit for change in input parameters

Trails	σ_{tec} in plane (Mpa)	σ_{tec} out plane (MPa)	$\theta_{tec}(degree)$	ψ^{HF}
1	0.00	0.00	0	2.38
2	2.11	3.97	157	2.05
3	4.17	1.69	117	1.96
4	4.01	2.04	122	1.82
5	3.82	2.38	127	1.52
6	3.59	2.71	132	1.54
7	3.34	3.01	137	2.04
8	3.07	3.29	142	2.04
9	2.77	3.55	147	1.90
10	2.45	3.77	152	2.05
11	1.76	4.14	162	2.18
12	1.39	4.28	167	3.44
13	1.01	4.38	172	3.82
14	0.63	4.46	177	3.82
15	0.24	4.49	182	3.82

The results of modeling after changing the input parameters presented in Table 9.8 shows a similar result in comparison to the initial model. The minimum misfit is found for the tectonic stress having an orientation of 127^0 . Figure 9.6 and Figure 9.6 shows the result for RS2 modeling showing sigma 1 for longitudinal and cross-section respectively model for second input parameters.

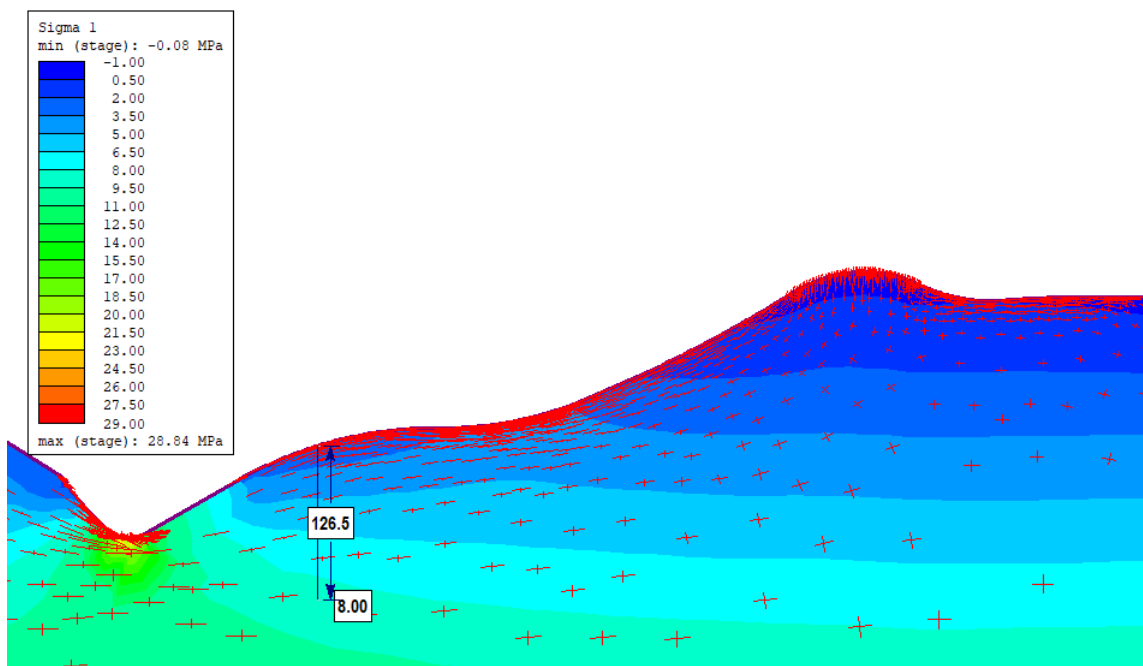


Figure 9.6: RS2 Model result showing sigma 1 for Longitudinal section of Terrain at chainage 7+884 for combination of tectonic stresses for orientation of 127^0

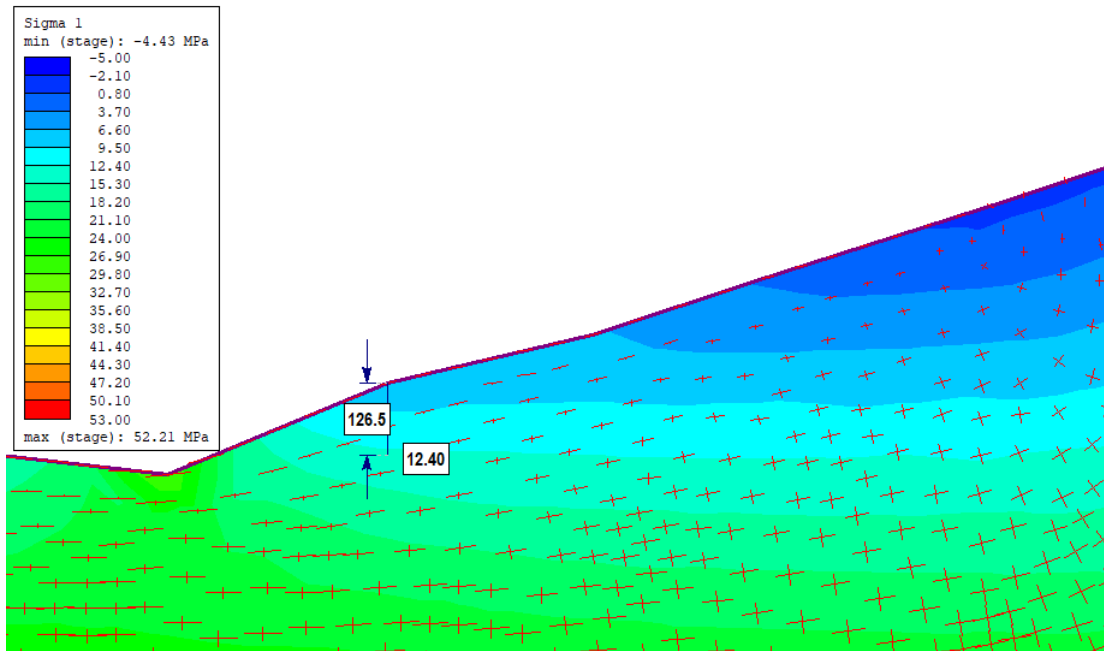


Figure 9.7: RS2 Model result showing sigma 1 for cross section of Terrain at chainage 7+884 for combination of tectonic stresses for orientation of 127°

Table 9.8 indicates the hydraulic fracturing misfits for the combination of tectonic stresses for orientation in the range 127° to 132° is very close to each other. With a small margin, the hydraulic fracturing misfit for tectonic stress orientation with azimuth 127° is minimum. Therefore, the author assumes the tectonic stress of magnitude 4.5 MPa with an azimuth of 127° is acting at the project area.

9.6 Estimation of In situ stress condition

In the headrace tunnel section passing through flysch, no field tests were carried out for stress measurement. Hence to estimate the in situ stress condition, valley modeling is carried at each chainage where deformation measurements have been carried out. The input parameters for the modeling have been taken from Table 9.2, Table 9.3, and Table 9.5 for intact rock mass properties, rock mass condition and rock mass deformation modulus respectively. The procedure for analysis of estimation of in situ stress carried out for the chainage 7+063 has been explained below.

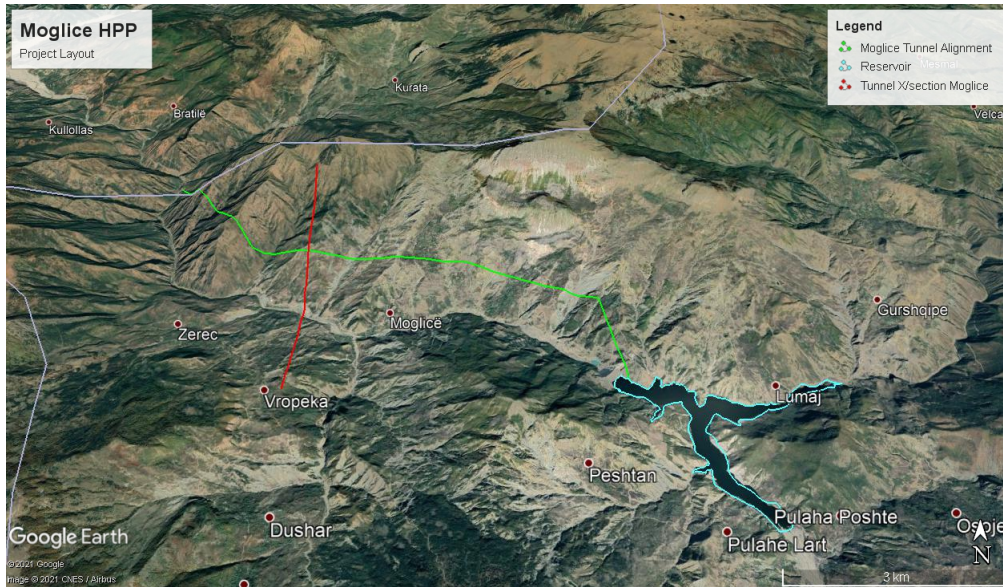


Figure 9.8: Project layout of Moglice hydropower project showing tunnel alignment (in green) and cross section alignment for chainage 7+063(in red) (from Google Earth)

9.6.1 Model Setup

The model is setup similar as setup for chainage 7+884 in Chapter 9.5.1 . Two cross sections, one parallel and normal to the tunnel alignment has been set up as represented by green line and red line respectively in Figure 9.8. Figure 9.9 and 9.10 shows the longitudinal and cross-sectional RS2 model setup respectively for in situ stress assessment at chainage 7+063.

The boundary conditions are defined as all four corners of the models are restrained in both the x-direction and the y-direction to prevent any sort of vertical or horizontal displacements as shown in Figure 9.9 and Figure 9.10 for longitudinal section and a cross-section respectively. The top boundary of the model is freed. Right, and left boundaries are restrained on x to prevent displacement horizontal displacement. And the bottom boundary is restrained on Y to allow only horizontal displacement. The details of modeling type and field stress for the model are defined as shown in Table 9.9.

Table 9.9: Valley modeling type and details at chainage 7+063 of Moglice headrace tunnel

	Description	Value
	Type of Analysis	Elastic
	Field stress Type	Gravity
	In -plane stress ratio	0.87
	Out-plane Stress ratio	0.87
Longitudinal section	In plane Locked in horizontal stress (MPa)	3.85
	valley model Out-plane Locked in horizontal stress (MPa)	2.31
Cross section	In plane Locked in horizontal stress (MPa)	2.31
	Valley model Out-plane Locked in horizontal stress (MPa)	3.85

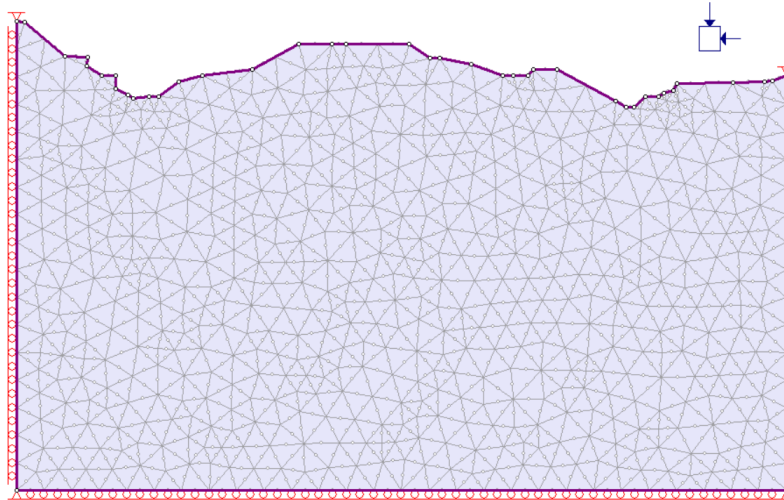


Figure 9.9: RS2 Model of Longitudinal section of Terrain of Moglice headrace tunnel

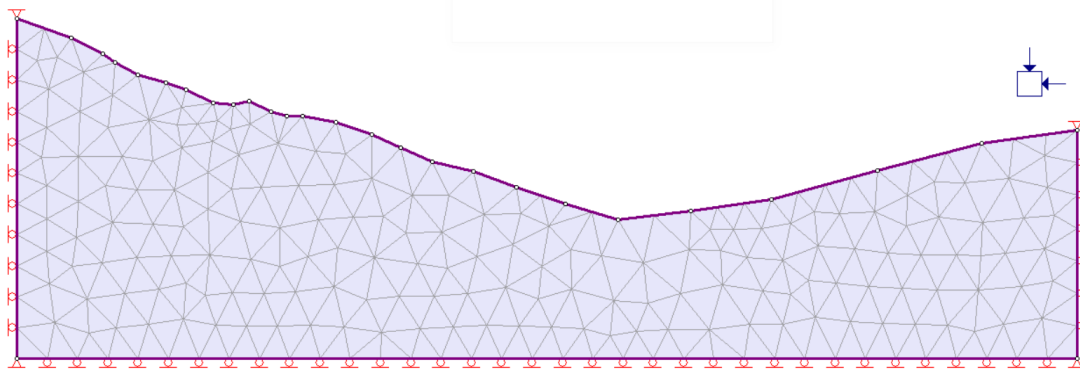


Figure 9.10: RS2 Model of cross section of Terrain at chainage 7+063

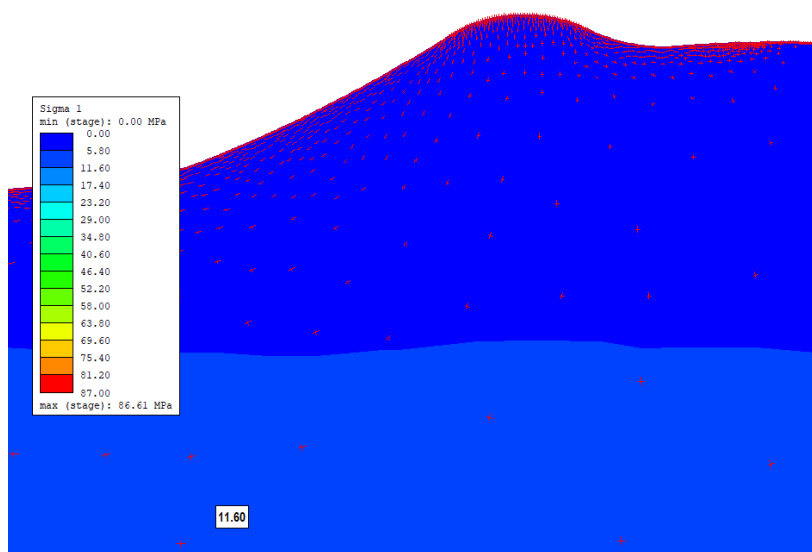


Figure 9.11: RS2 analysis result showing sigma 1 of cross section of valley of MOgllice headrace tunnel at chainage 7+063

Figure 9.11 shows the result of elastic analysis for cross-sectional valley model of Moglice headrace tunnel. The results from the cross-sectional valley model are used further to define the in-situ stress conditions at each chainage. The details of in-situ stress result from valley model have been presented in Table 9.10.

Table 9.10: In-situ stresses at Moglice headrace tunnel

Chainage	σ_1 (MPa)	σ_3 (MPa)	σ_z (MPa)	σ_1 angle with horizontal ($^\circ$)
7+029 to 7+064	11.60	6.75	11.25	164
7+092 to 7+531	13.25	6.75	11.25	164

10 Plastic Deformation Analysis of Moglice headrace tunnel

Moglice headrace tunnel passes through rock formation consisting of ophiolite, serpentinite, and flysch. The quality of rock mass varies greatly depending upon the rock formation and degree of weathering. The flysch rock is deformed, thinly layered, laminated, and folded, and is relatively weak. The Q-value in this rock mass varies between 0.05 to 0.22. The rock mass of flysch formation has undergone plastic deformation of different magnitude at different chainages. Rock mass deformation may cause stability problems in underground excavation. Hence, a dependable prediction of the deformation in advance is necessary to reduce the stability problems. Hence reliable prediction of the deformation in advance is necessary to reduce the stability problems. During headrace tunnel construction, systematic deformation measurement was carried out at different chain ages as shown in Table 7.3. As it can be seen the values of deformations vary from chainages to chainages. This is because several factors influence the deformation (squeezing) condition in the rock mass to various extent. Shrestha (2006) summarized the factors that affect the degree of squeezing as stress conditions, strength and deformability of rock mass, rock type, the orientation of the geological structures, water pressure, and porosity of the rock mass, and construction procedure, and support systems.

The existing rock mass conditions at different chainages are described in Chapter 8.1. There is variation in rock mass quality as suggested by different Q-values recorded in each section. Also, the strength and deformability of rock mass vary depending on the section. Due to such variations in rock mass condition and strength, the measured deformation varies from chainages to chainages.

As explained in Chapter 4.3, many researchers have developed various methods over time to estimate the extent of tunnel deformation. In this chapter, an attempt has been made to analyze plastic deformation using three analytical methods and numerical modeling and the achieved results are compared with the measured deformations. The methods that has been used are Convergence confinement method (CCM) (Carranza-Torres and Fairhurst (2000)), Hoek and Marinos (2000), Panthi and Shrestha (2018) and Numerical modeling.

10.1 Convergence confinement method (CCM)

Convergence confinement method (CCM) (Carranza-Torres and Fairhurst (2000)) is a procedure that estimates the load imposed on the installed support behind the face at distance L and analyzes the deformation in a weak rock mass. The approach is based on the interaction of Load deformation profile (LDP), Ground reaction curve (GRC), and Support confining curve (SCC). To generate this curves the equations provided by Carranza-Torres and Fairhurst (2000) as reviewed in Chapter 4.3.3.1 are used. The equations are developed to define the response of circular underground openings. Hence, the equivalent circular tunnel radius is computed and found to be 3.10 m.

The input data required for CCM analysis are taken from Table 7.3, Table 9.2, and Table 9.3 for overburden, intact rock properties and rock mass classification respectively. The support installed consists mainly of a shotcrete liner embedded with reinforced ribs of sprayed concrete (RRS) of thickness 450 mm and ribs are spaced c/c 1.5 m, systematic bolting of 20 mm diameter, 4 m long bolts with in-plane spacing of 1.5 m having tensile

capacity of 0.15 MN. An invert of the headrace tunnel is lined with concrete of 450 mm (original 400 mm). In Figure 10.1 and Figure 10.2, the results of analysis on LDP, GRC, and SCC at each different chainages are shown, which varies accordingly to the rock mass conditions at these chainages.

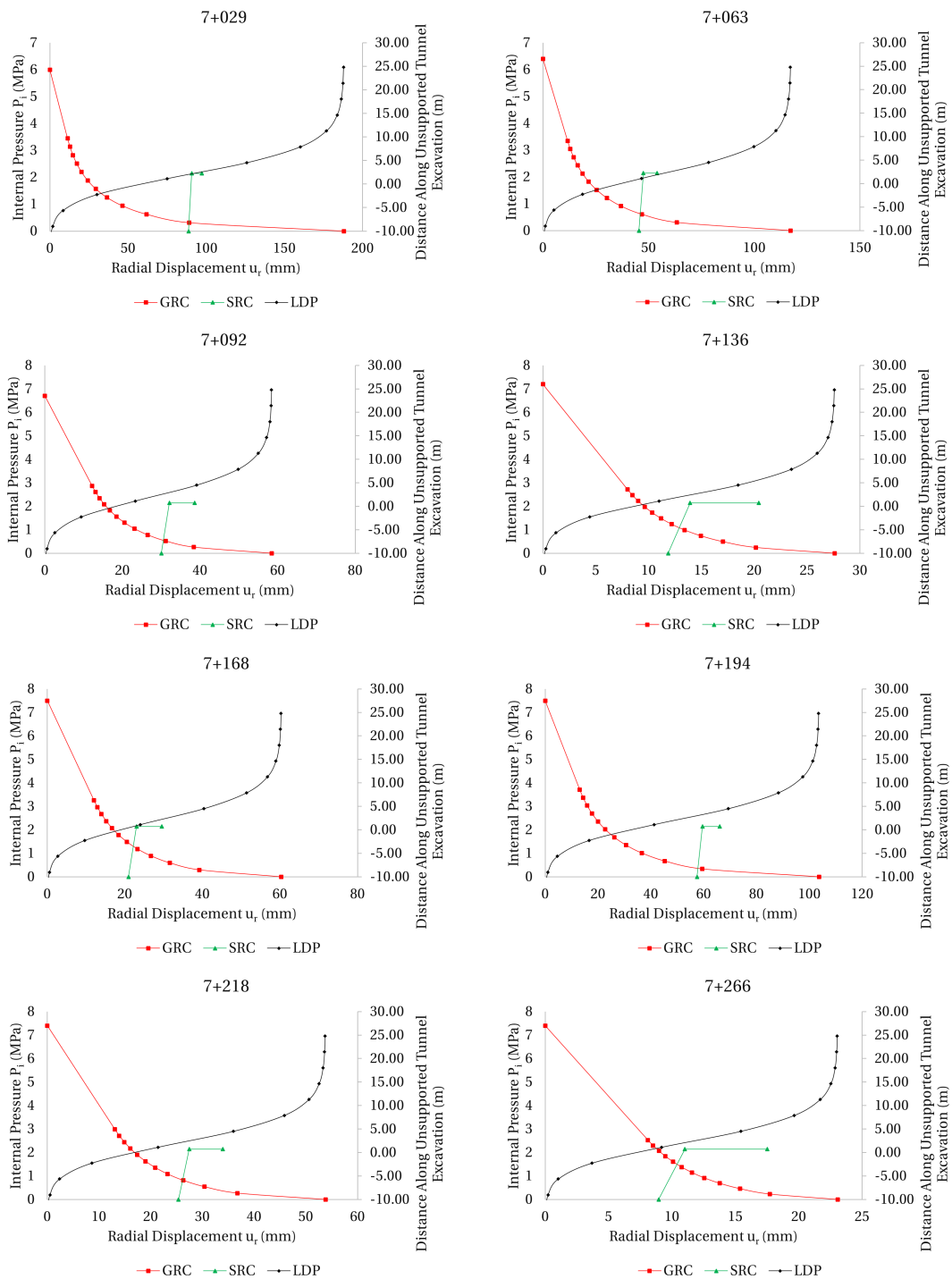


Figure 10.1: Convergence Confinement Method predicting squeezing for chainages 7+029 to 7+266 of Moglice headrace tunnel

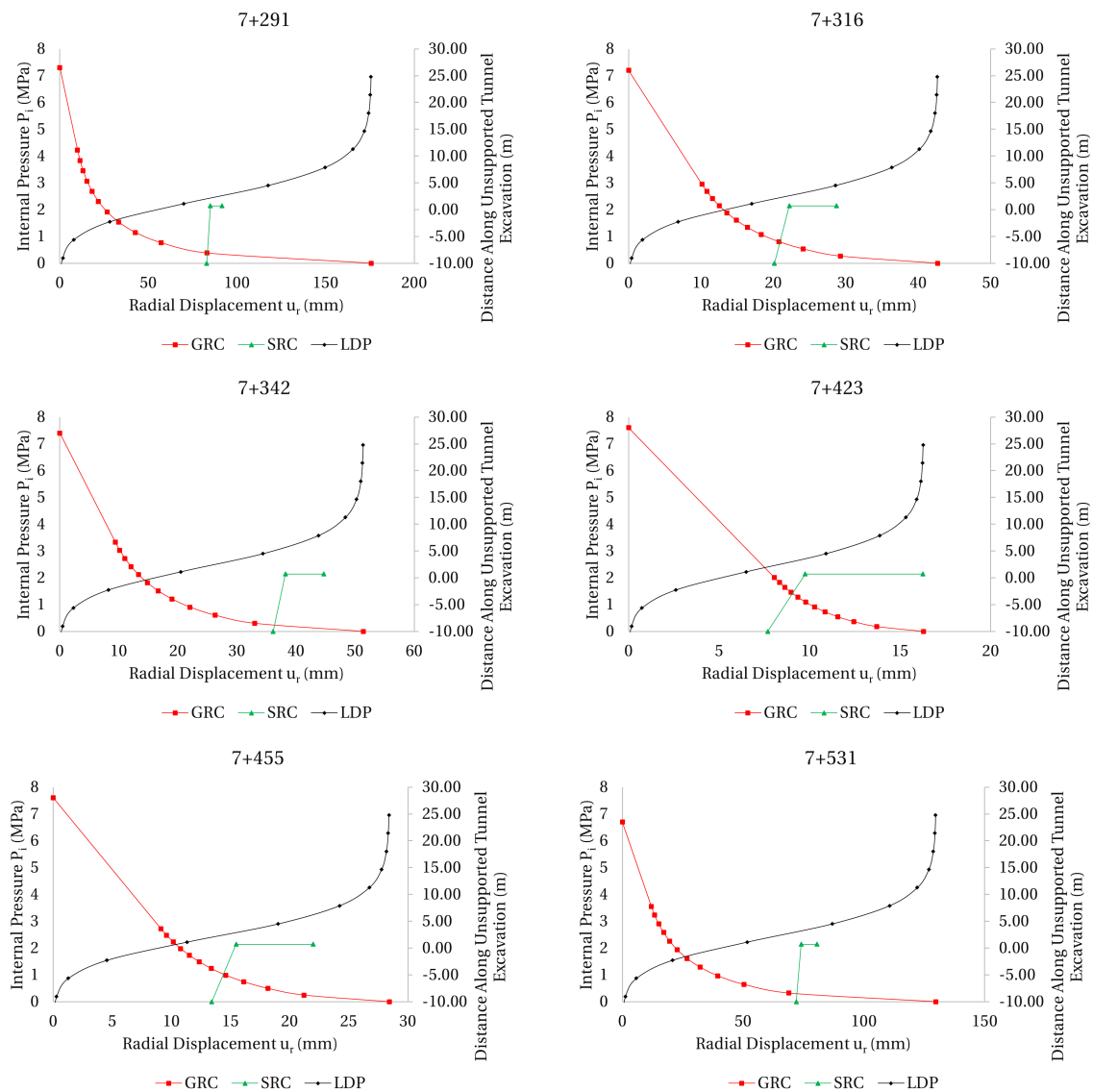


Figure 10.2: Convergence Confinement Method predicting squeezing for chainages 7+029 to 7+266 of Moglice headrace tunnel

The extent of deformation (u) at the distance L behind the face estimated using CCM is presented in Table 10.1 along with the vertical stress due to overburden and deformation modulus of the rock mass. Since the radius and the support pressure is the same for all chainages, the extent of variation of deformations estimated can be related to the rock mass deformation modulus and in situ stress.

CCM is a useful tool for the prediction of the plastic deformation of weak rock mass with some drawbacks. The use of the method is restricted for a tunnel with circular cross-section and also the method assumes the in-situ stress condition as isostatic which is seldom a case. Therefore, the analysis has been carried using the equivalent circular radius for the horseshoe tunnel in isostatic in-situ stress conditions. The results thus obtained from the analysis are later compared with the measured deformation and the estimated deformation from other methods.

Table 10.1: Deformation estimation using CCM by Carranza-Torres and Fairhurst (2000)

Chainage	Vertical Stress (P_0) (MPa)	E_{rm} (MPa)	G_{rm} (MPa)	Support Pressure (P_i) (MPa)	L(m)	u (mm)
7+029	6.0	931	350	2.14	2.0	89
7+064	6.4	1055	406	2.14	1.0	46
7+092	6.7	1268	488	2.14	2.5	31
7+136	7.2	2255	867	2.14	1.5	14
7+168	7.5	1423	547	2.14	0.5	22
7+194	7.5	1167	449	2.14	3.0	59
7+218	7.4	1362	524	2.14	2.0	26
7+266	7.4	2422	932	2.14	1.0	11
7+291	7.3	1241	477	2.14	2.0	74
7+316	7.2	1691	650	2.14	2.0	21
7+342	7.4	1745	671	2.14	5.0	37
7+423	7.6	2797	1076	2.14	2.0	10
7+455	7.6	2159	830	2.14	2.0	15
7+531	6.7	1055	406	2.14	3.0	72

10.2 Hoek and Marinos (2000) method

Hoek and Marinos (2000) is a semi-analytical method that is used for estimating the extent of squeezing based on the tunnel strain percentage. The extent of squeezing varies from few support problems for strain less than 1% to extreme squeezing problems for strain greater than 10% as shown in Figure 4.7. The tunnel strain used for classification of the extent of squeezing is computed for zero support pressure using Equation 4.1. The input data required for Hoek and Marinos (2000) method are taken from Table 7.3, Table 9.2, and Table 9.3 for overburden, intact rock properties and rock mass classification respectively. For the Moglice headrace tunnel passing through the flysch rock mass, tunnel strain without support ($\epsilon(P_i = 0)$) has been computed as presented in Table 10.2. Based on computed tunnel strain, the squeezing severity has been estimated as shown in remarks in Table 10.2. The severity of the squeezing varies from minor squeezing to extreme squeezing as tunnel strain varies from 0.76% to 15.26%. Similar to CCM the extent of deformation variation can be related to rock mass condition and in situ stress.

Apart from estimating tunnel squeezing problems, the Hoek and Marinos (2000) method can also be used to estimate the deformation after installing support. The tunnel strain is the percentage of inward radial displacement of the tunnel radius. Hence, in the unsupported condition, the support pressure is zero and after knowing the installed support pressure (P_i) the estimation of the tunnel deformation strain with support ($\epsilon(P_i > 0)$) can be done using Equation 4.3. Thus, after computing tunnel strain with support, the deformation u_{max} ($P_i > 0$) can be estimated. This value is then compared with the measured deformation. The support pressure is considered the same as computed in the CCM method. Similar to the CCM method, the drawbacks of this method is the consideration of curricular tunnel which forces the use of equivalent circular tunnel radius for the analysis and consideration of isostatic in situ stress condition.

Table 10.2: Squeezing prediction and strain % estimation using Hoek and Morinos (2000) Hoek and Marinos (2000)

Chainage	Support Pressure P_i^* (MPa)	ε (%) ($P_i=0$)	u_{max} ($P_i=0$) (mm)	ε (%) ($P_i>0$)	u_{max} ($P_i>0$) (mm)	Remarks
7+029	2.14	15.26	458	1.34	40	Extreme Squeezing
7+064	2.14	8.65	259	1.09	33	Very Severe Squeezing
7+092	2.14	3.47	104	0.69	21	Severe Squeezing
7+136	2.14	1.94	58	0.55	16	Minor Squeezing
7+168	2.14	3.75	113	0.88	26	Severe Squeezing
7+194	2.14	6.97	209	1.33	40	Severe Squeezing
7+218	2.14	2.89	87	0.74	22	Severe Squeezing
7+266	2.14	1.38	41	0.45	14	Minor Squeezing
7+291	2.14	15.08	452	2.11	63	Extreme Squeezing
7+316	2.14	2.81	84	0.69	21	Minor Squeezing
7+342	2.14	4.03	121	0.92	28	Severe Squeezing
7+423	2.14	0.76	23	0.31	9	Minor Squeezing
7+455	2.14	1.69	51	0.53	16	Minor Squeezing
7+531	2.14	9.54	286	1.29	39	Very Severe Squeezing

10.3 Panthi and Shrestha (2018) method)

Panthi and Shrestha (2018) method enforces that the in situ condition that prevails in the field is seldom isostatic. Hoek and Marinos (2000) and Carranza-Torres and Fairhurst (2000), however consider a isostatic stress condition for the estimation of tunnel deformation of a circular tunnel. Therefore, Panthi and Shrestha (2018) method relates the tunnel strain, with k which is the ratio of horizontal to vertical stress. This incorporates the influence of stress anisotropy on deformation which overcomes the limitation of using only vertical gravitational stress in Hoek and Marinos (2000) and Carranza-Torres and Fairhurst (2000) methods. Another advantage of using this method that it does not limit its application to a particular tunnel shape. Irrespective of tunnel shape and size, this method can be implemented to calculate the instantaneous and final strain in a rock mass.

The input data required for Panthi and Shrestha (2018) method are taken from Table 7.3, Table 9.2, and Table 9.3 for overburden, intact rock properties and rock mass classification respectively. The value of k is found from the results of valley modeling of the different chainages carried out to assess in situ stress in Chapter 9.6. The value of k is found to be 1.5 for chainages 7+029 and 7+064 and 1.8 for other chainages. In addition to in situ stress condition and support pressure, rock mass shear modulus (G_{rm}) should be linked with tunnel strain calculation (Panthi and Shrestha, 2018). Carranza-Torres and Fairhurst (2000) shows the relation between rock mass shear modulus (G_{rm}) and rock mass deformation modulus (E_{rm}) as shown in Equation 4.25. Hoek and Marinos (2000) linked rock mass deformation modulus (E_{rm}) with rock mass deformation modulus of intact rock (E), rock mass strength (σ_{cm}) and intact rock strength (σ_{ci}) as shown in Equation 4.26. Hoek and Brown (1997) further relates rock mass strength (σ_{cm}) with the cohesion (c) and friction angle (ϕ) as shown in Equation 4.27. Therefore, RocData is used to find these values of cohesion and frictional angle at each chainages to compute

the rock mass strength as shown in Table 10.3.

Table 10.3: Rockmass Properties estimated using RocData

Chainage	c	ϕ	σ_{cm}
7+029	0.34	23.40	1.02
7+064	0.34	23.27	1.04
7+092	0.44	27.23	1.44
7+136	0.51	30.10	1.77
7+168	0.50	27.19	1.63
7+194	0.43	24.70	1.33
7+218	0.53	28.90	1.80
7+266	0.67	28.90	2.27
7+291	0.41	30.70	1.44
7+316	0.53	28.50	1.77
7+342	0.53	27.80	1.75
7+423	0.80	36.15	3.14
7+455	0.65	31.85	2.35
7+531	0.35	23.01	1.06

Table 10.4: Deformation estimation using Panthi and Shrestha method Panthi and Shrestha (2018)

Chainage	E_{rm} (MPa)	G_{rm} (MPa)	u_{ic} (mm)	u_{fc} (mm)	u (mm)
7+029	814	306	73	121	48
7+064	889	334	65	108	43
7+092	1336	502	33	55	22
7+136	1640	617	25	42	17
7+168	1512	568	41	69	28
7+194	1198	450	53	88	35
7+218	1707	642	23	38	15
7+266	2153	809	15	25	10
7+291	1149	432	52	87	35
7+316	1638	616	28	46	19
7+342	1570	590	33	56	23
7+423	3242	1219	8	14	6
7+455	2228	837	14	24	10
7+531	913	343	77	127	50

The instantaneous closure (u_{ic}) and final closure (u_{fc}) for the tunnel has been computed using Equation 4.23 and Equation 4.24 respectively and the results is presented in Table 10.4. The support pressure is used as estimated by the CCM method. It is usually difficult to measure the instantaneous deformation and the deformation measured that is measured is usually done after the support is installed. Therefore, the value of measured deformation (u) will be the difference between the final closure and the instantaneous closure.

10.4 Numerical Modeling

To perform numerical modeling the model has been set up as described in Chapter 4.3.4.2. For plastic deformation analysis first three stages 1.Pre Excavation, 2.Excavation and 3.Support Installation are analyzed. The model geometry is set as shown in the Figure 7.8 along with the details of the installed support.

The modeling has been carried out for all chainages. This chapter however presents the results for four chainages:- 7+029, 7+423, 7+455, and 7+531. The selection of chainages is based on the content of the weak rock. Chainages 7+029 and 7+531 contain most share of weak rock and chainages 7+423 and 7+455 contain least percentage of weak rock relatively strong among the studied cross-sections. The results for the remaining chainages are presented in Appendix B.

During the numerical analysis, it is important to have a quality assessment of the input parameters. The objective of the setting model is to create a prevailing field rock mass condition. Therefore to replicate the real ground condition, one must feed quality input to the model. Numerical modeling does provide good results if the input is valid.

The failure criterion used to define material properties is Generalized Hoek and Brown. The input parameters are taken from Table 9.2, and Table 9.3 for intact rock properties and rock mass classification respectively. The input parameters for the model of each section are shown in Table 10.5. The residual values are considered as 25% of peak values. Young's modulus of rock mass estimated by Panthi method is used as the estimated value is smallest in comparison to other methods.

Table 10.5: Input parameters for RS2 modeling

Chainage	Intact Rock UCS (MPa)	GSI		Intact Rock Constant m_i		Rock mass Modulus (MPa)	
		Peak	Residual	Peak	Residual	Peak	Residual
7+029	15	25	6	7	2	801	200
7+064	20	25	6	8	2	1260	315
7+092	29	25	6	10	3	2361	590
7+136	29	35	9	10	3	2361	590
7+168	29	27	7	11	3	2361	590
7+194	24	25	6	9	2	1783	445
7+218	33	25	6	12	3	2991	747
7+266	33	35	9	12	3	2991	747
7+291	15	30	8	7	2	801	200
7+316	29	30	8	10	3	2361	590
7+342	24	32	8	9	2	1783	445
7+423	44	35	9	14	4	4767	1191
7+455	33	33	8	12	3	2991	747
7+531	20	25	6	8	2	1260	315

10.4.1 Elastic Analysis

Initially, the elastic analysis is carried out by defining the material as elastic. The objective of the elastic analysis is to evaluate the strength factor and distribution of stress

around the tunnel opening.

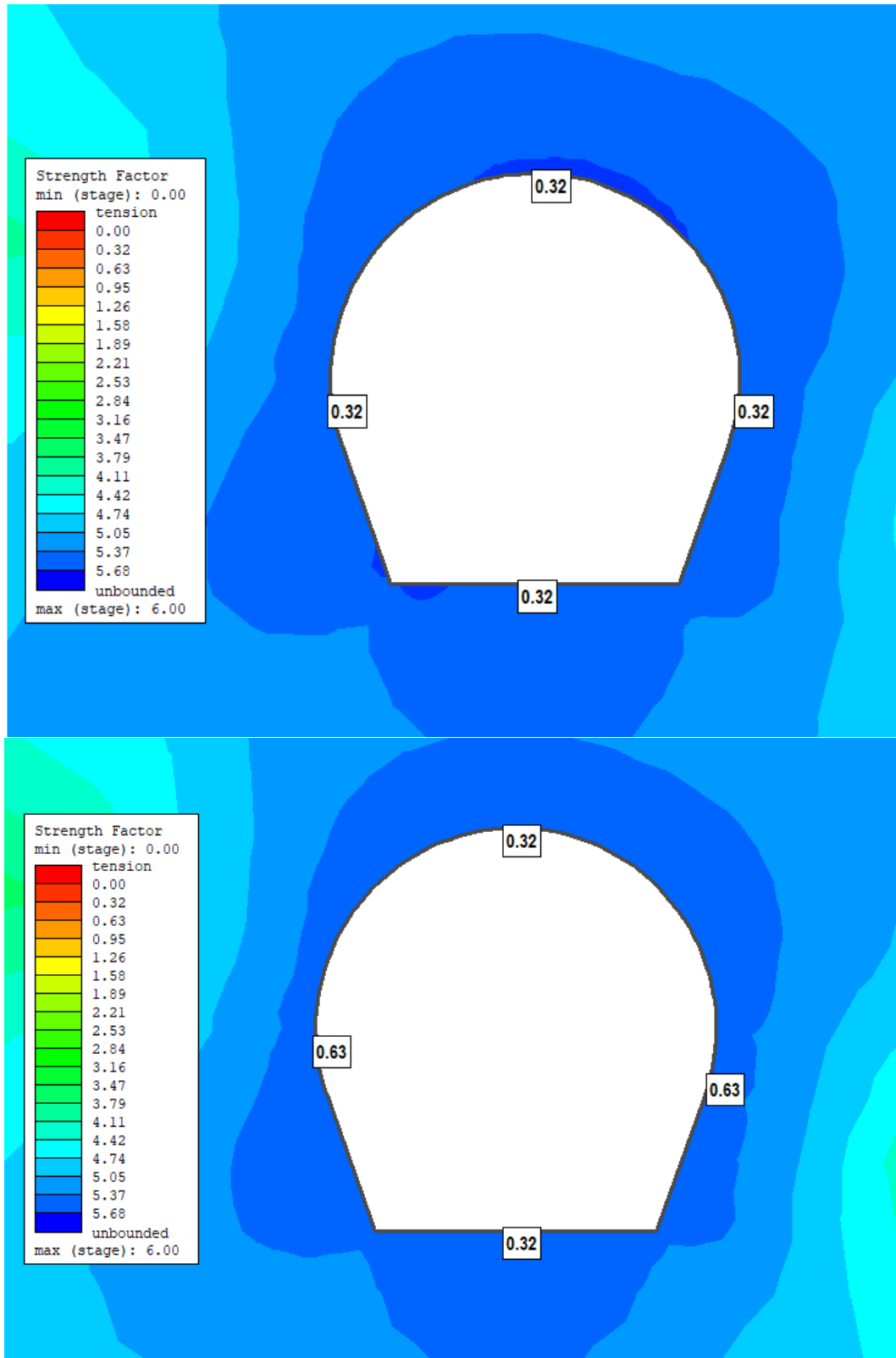


Figure 10.3: Strength factor for weak rock at chainages 7+029 (top) and 7+531 (bottom)

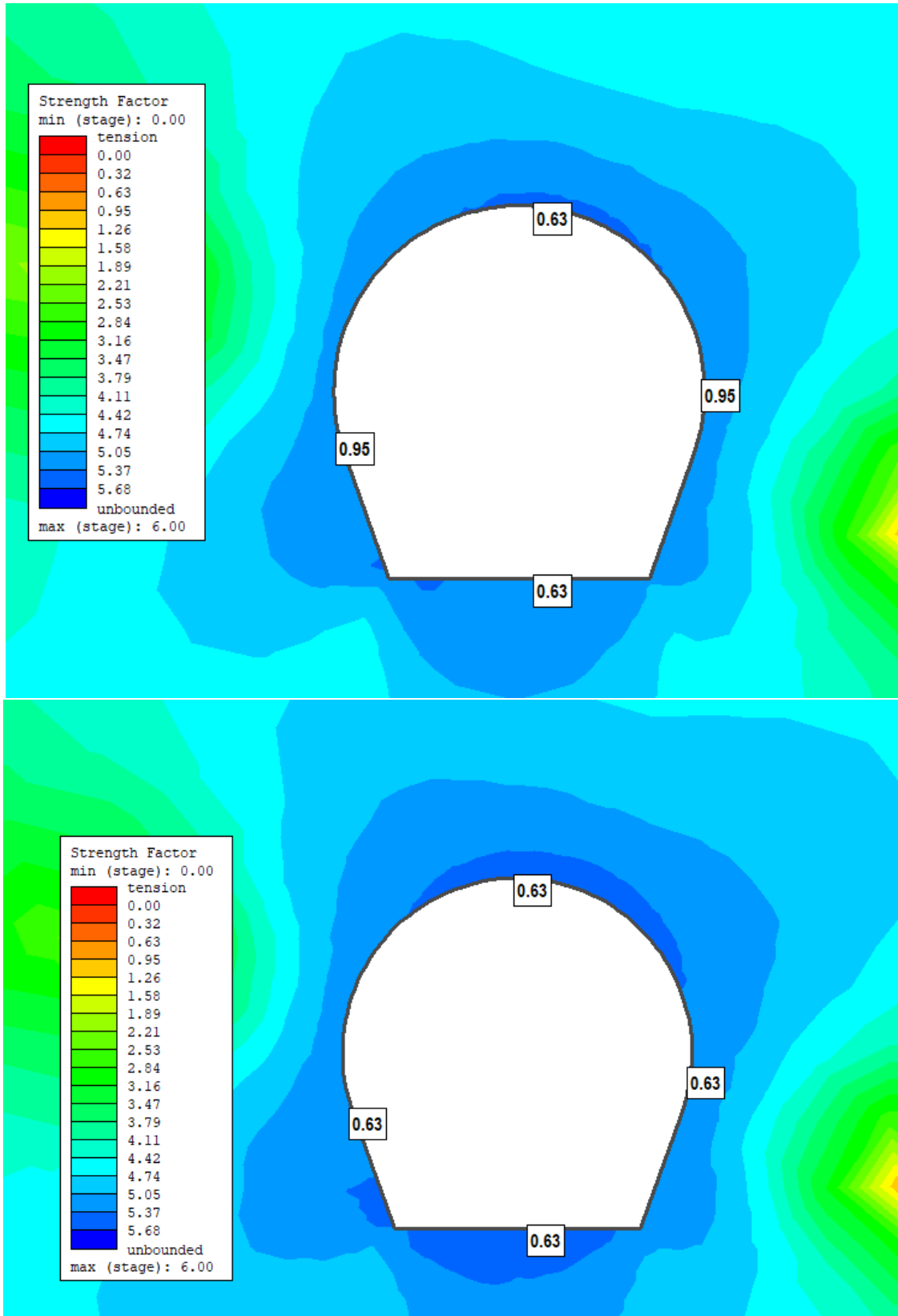


Figure 10.4: Strength factor for strong rock at chainages 7+423 (top) and 7+455 (bottom)

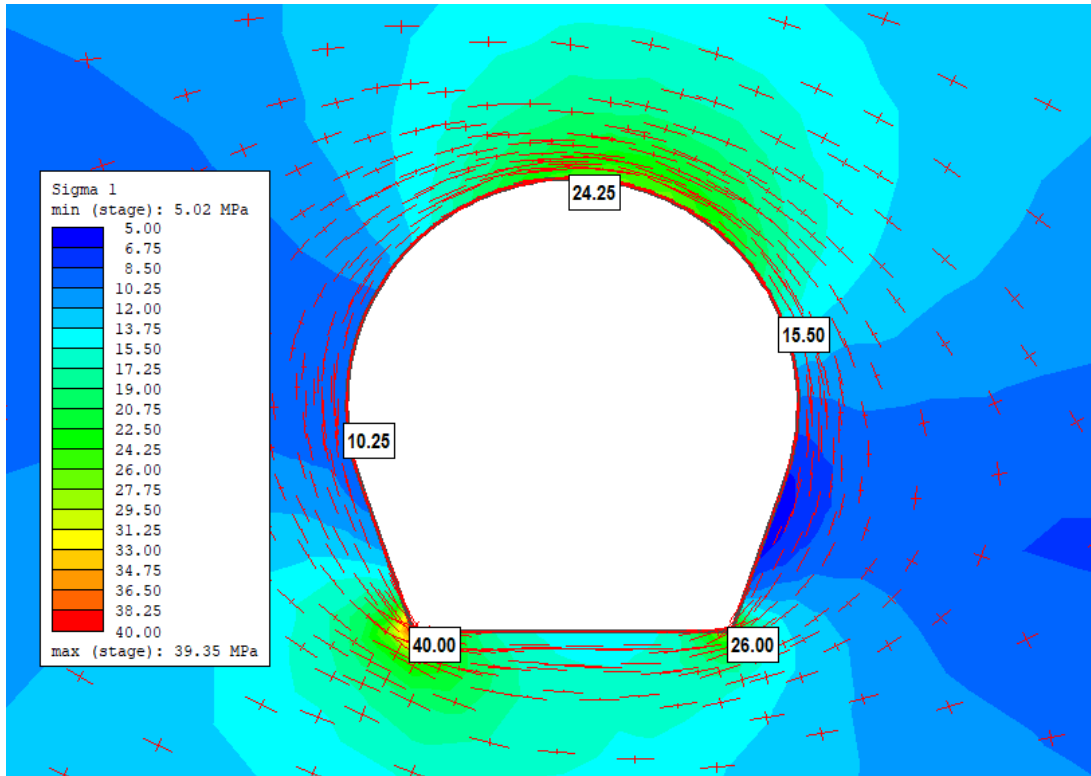


Figure 10.5: Major principal stress with trajectories in elastic model for weak rock at chainages 7+029

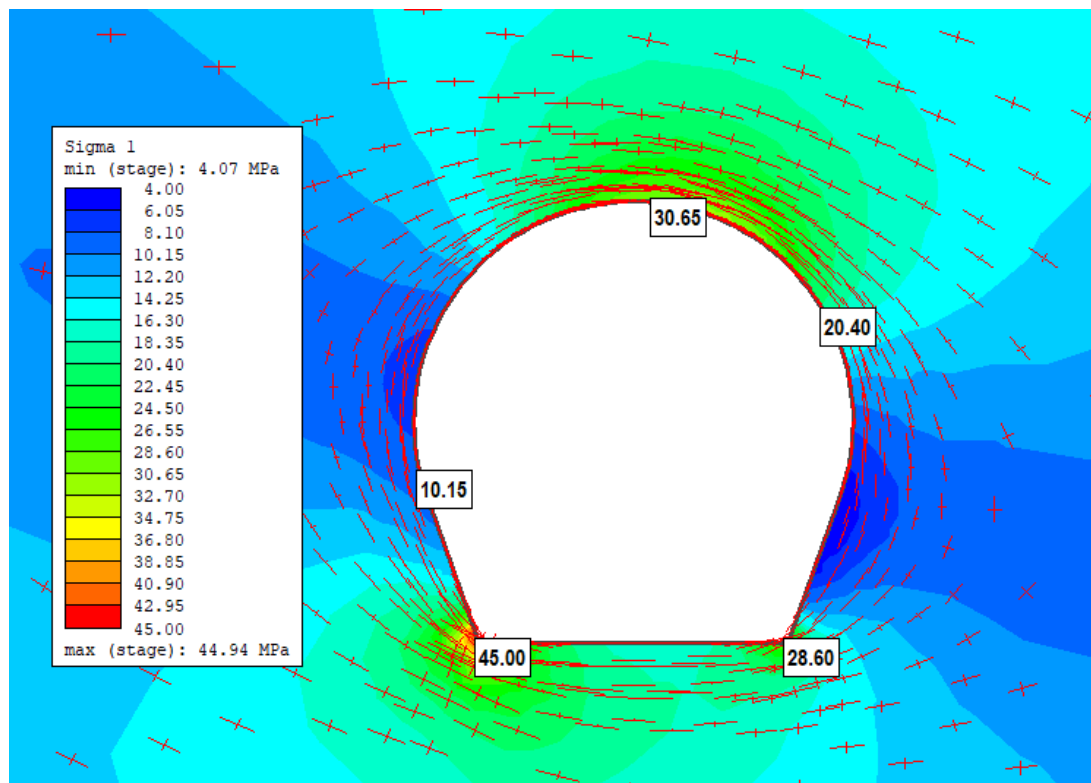


Figure 10.6: Major principal stress with trajectories in elastic model for relatively strong chainage 7+423

In Figure 10.3 and Figure 10.4, results for the strength factor after elastic analysis for weak rock mass (at chainages 7+029 and 7+531) and relatively strong rock mass (at chainages 7+423 and 7+455) respectively are presented. The strength factor all around the tunnel cross-section for all four chainages is less than one. The result suggests that the elastic model will yield, which means plastic analysis is required. In Figure 10.5 and Figure 10.6, the stress distribution after tunnel construction has been presented. The stress concentration is mainly at the crown and the corners of the invert after redistribution of stress after tunnel excavation. The strength factor is the ratio of rock strength based on the failure and the induced stress at a given point, so for chainages 7+029 and 7+531, since the rock strength is smaller so the lowest strength factor is as low as 0.32. Whereas chainages 7+423 and 7+455 having relatively high rock strength in comparison to chainages 7+029 and 7+531, the lowest strength factor is 0.63. The elastic analysis results suggest that the model will yield and since in the elastic model it is not possible to analyze the failure, it is necessary to carry out plastic analysis.

10.4.2 Plastic Analysis

Since the elastic model yields the plastic analysis is performed on the same model to assess the stress situation after excavation and to find out the amount of plastic deformation of the tunnel. The input parameters for material for plastic analysis have been taken from Table 10.5 and for support liner and bolt parameters are taken described in Table 7.4 and Table 7.5 respectively.

10.4.2.1 Stress distribution

In Figure 10.5 and Figure 10.6, the major principal stress distribution after tunnel construction in elastic model has shown. The major stress concentration is at crown and corners of invert due to overstressing. But as the material is defined as plastic the destressing of stress occurs around the tunnel cross-section. The destressing of stresses in the rock mass increase the strength factor. As described in Chapter 7.4, the flatjack has been installed to determine the behavior of relatively poor rock mass containing flysch. In Table 7.2, the results for the measurement of minimum principal stress from flatjack instrumentation have been shown. Hence the minimum principal stress distribution at various chainages in the plastic model has been assessed for the assessment of in-situ stress situation after excavation of the tunnel.

In Table 7.2, the flatjack installation details have been presented, according to which the flatjack are installed in rock and shotcrete. The measurement of minor principal stress in rock mass varies from 0.8 MPa to 5.0 MPa. For chainages 7+0629 and 7+531, the value of minor principal stress in the rock mass varies from 0.8 MPa to 2.6 MPa at the location of the installed flatjack and the major stress concentration is at the crown and in the corner of the invert as shown in Figure 10.7. Similarly, for the chainages 7+423 and 7+455, the value of minor principal stress varies from 1.4 MPa to 4.9 MPa, and the stress concentration is at crown and corners of invert as shown in Figure 10.8. In comparison to the results from measurement and numerical modeling, the conclusion can be drawn that the flatjack with a reading of minor principal stress 0.5 MPa to 1.0 MPa are either installed in the weak rock mass or very close to support in the relatively strong rock mass

and the flatjack with readings 4.5 to 5.0 MPa are installed in the section with relatively strong rock mass.

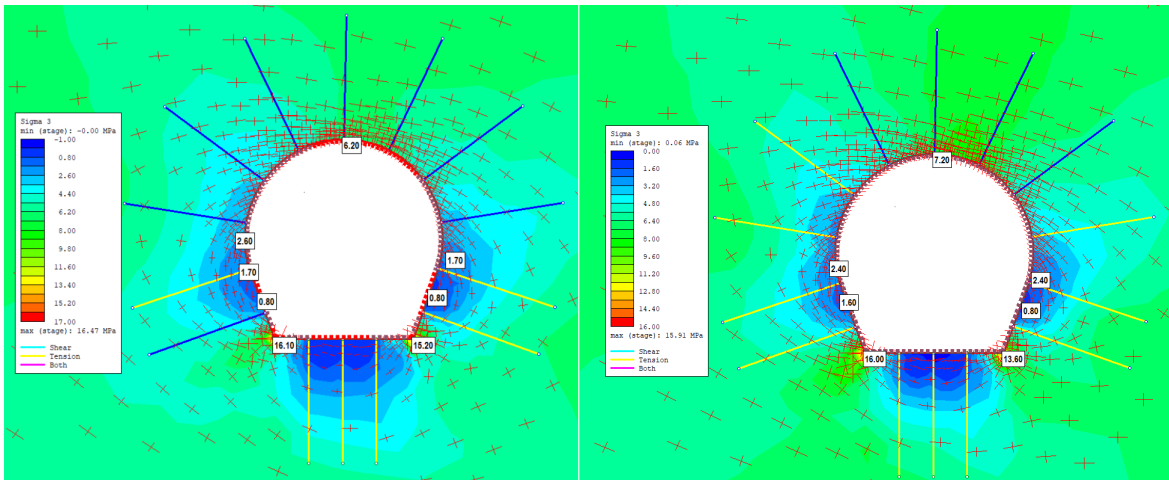


Figure 10.7: Minor principal stress with trajectories in plastic model for weak rock at chainages 7+029 (left) and 7+531 (right)

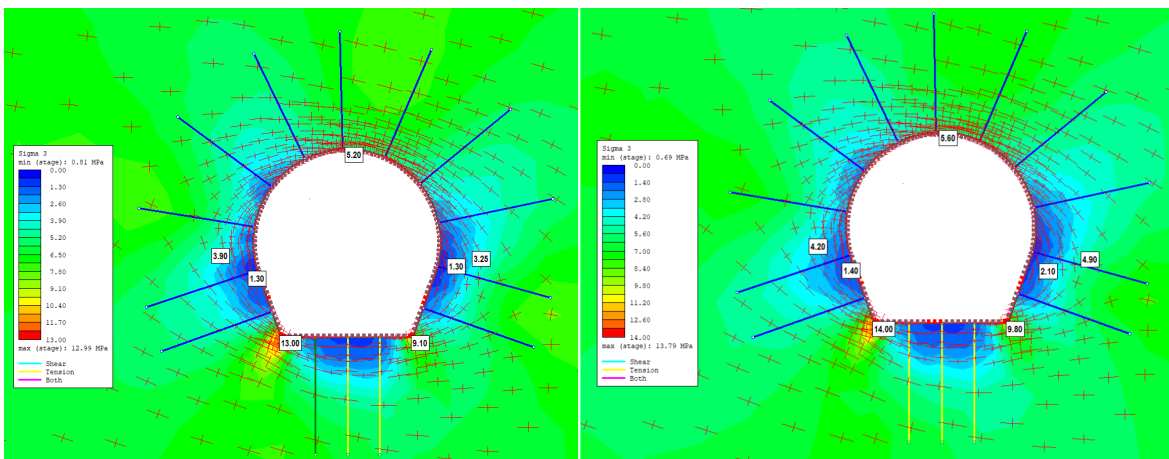


Figure 10.8: Minor principal stress with trajectories in plastic model for strong rock at chainages 7+423 (left) and 7+455 (right)

10.4.2.2 Plastic deformation

The systematic deformation was carried out at different chainages as shown in Table 7.3. The numerical modeling is therefore carried out to estimate the extent of deformation at these chainages. Along with this, the objective of numerical modeling in RS2 is to replicate the field situation with the help of measured deformation so that model represents the real ground condition. After the model is calibrated to represent the real ground condition, swelling analysis is carried out to assess the long-term stability of the Moglice headrace tunnel passing through the rock mass containing flysch. In stage 2: Excavation and stage : Support Installation, load splitting has been done as 30% and 70% respectively suggesting that only 30% load is exerted in stage 2 and the remaining

70% is added during stage 3. Therefore, the deformation occurs in both stages. The deformation at stage 2 is hard to measure as it occurs instantaneously after excavation and the deformation at stage 3 represents the final closure of the tunnel. Therefore the measured deformation (u) is the difference in deformations at stage 2 and stage 3.

Table 10.6: Results of numerical modeling for deformation at various chainages using RS2

Chainage	Stage 2: Excavation Deformation (mm)	Stage 3: Support Installation Deformation (mm)	Differential Deformation (u) (mm)
7+029	61	99	38
7+064	80	112	32
7+092	22	54	32
7+136	14	36	22
7+168	21	53	32
7+194	26	45	19
7+218	15	40	25
7+266	9	21	12
7+291	25	45	20
7+316	14	29	15
7+342	18	36	18
7+423	5	13	8
7+455	9	18	9
7+531	7	55	48

Table 10.7: Details on magnitude of deformation (in mm) measured along different location of tunnel cross-section along with the details of yielded finite elements of model, liner and bolt

Description	7+023		7+423		7+455		7+531	
	Stage 2	Stage 3	Stage 2	Stage 3	Stage 2	Stage 3	Stage 2	Stage 3
Left wall	63	99	5	13	9	18	7	55
Left wall	43	63	5	13	9	19	7	38
Roof	61	54	4	5	6	6	6	6
Right wall	54	72	5	9	8	15	7	38
Right wall	47	81	6	15	9	21	7	49
Invert	68	171	4	11	7	16	7	104
No. of Yielded Elements	1017	1093	491	511	617	634	722	803
No. of Yielded Liner	0	55	0	7	0	12	0	50
No. of Yielded Bolts	0	6	0	2	0	3	0	10

The result of plastic analysis for the total displacement at respective stages: excavation and support installation for the chainages 7+029, 7+423, 7+455 and 7+531 are presented in Figure 10.9, Figure 10.10, Figure 10.11 and Figure 10.12 respectively. The figures show the magnitude of tunnel deformation at different locations of tunnel cross-section along with the deformation vectors and yielded elements, liners, and bolts. The maximum deformation (u) is computed as the difference of the maximum tunnel deformation in tunnel wall and the magnitude of deformation computed for the chainages 7+029, 7+423,

7+455, and 7+531 are 38 mm, 8 mm, 9 mm, and 48 mm respectively and for remaining chainages the differential deformation (u) are presented in Table 10.6.

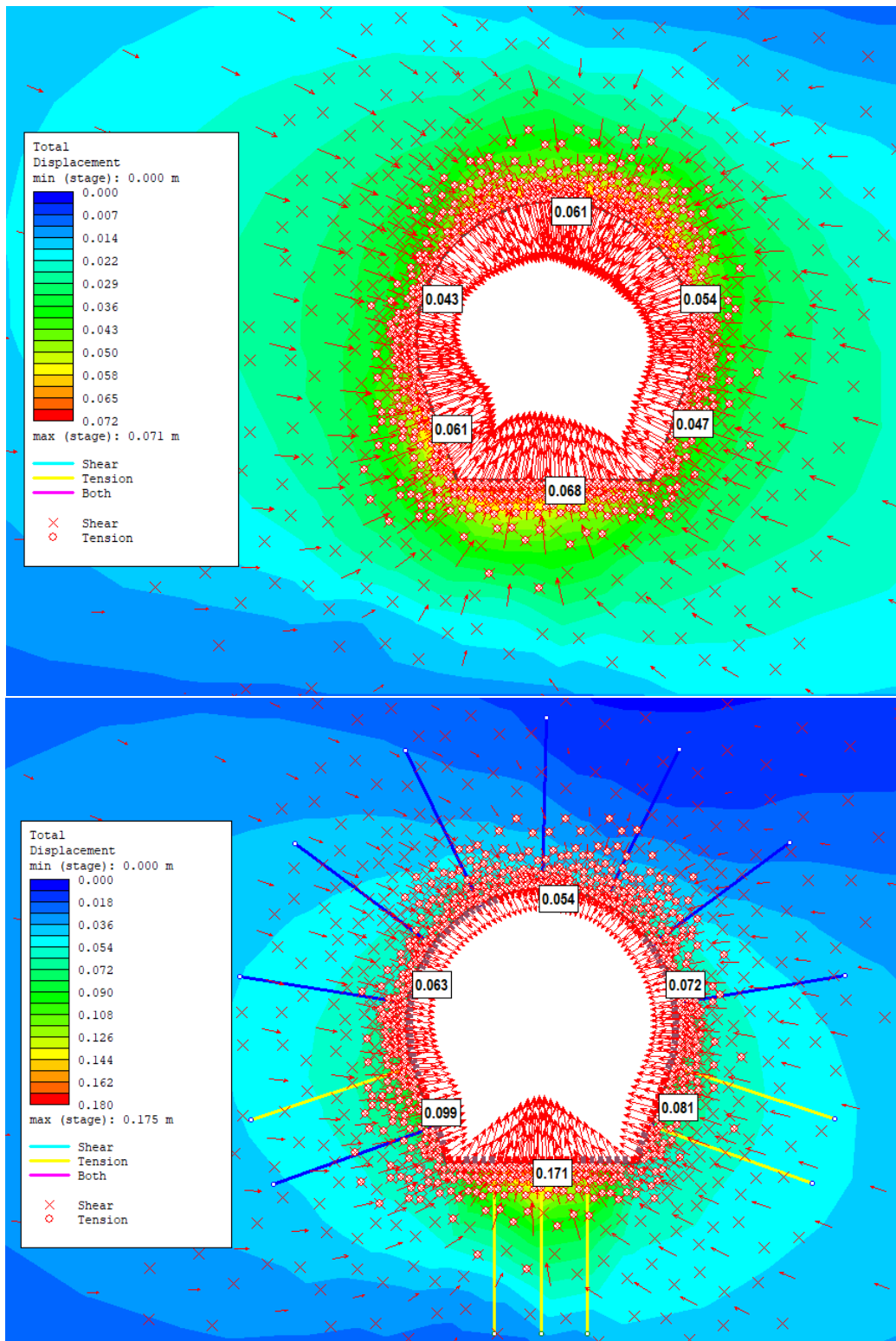


Figure 10.9: Results of plastic analysis at chainage 7+029 showing total displacement: Excavation stage(top) and Support Installation stage (bottom)

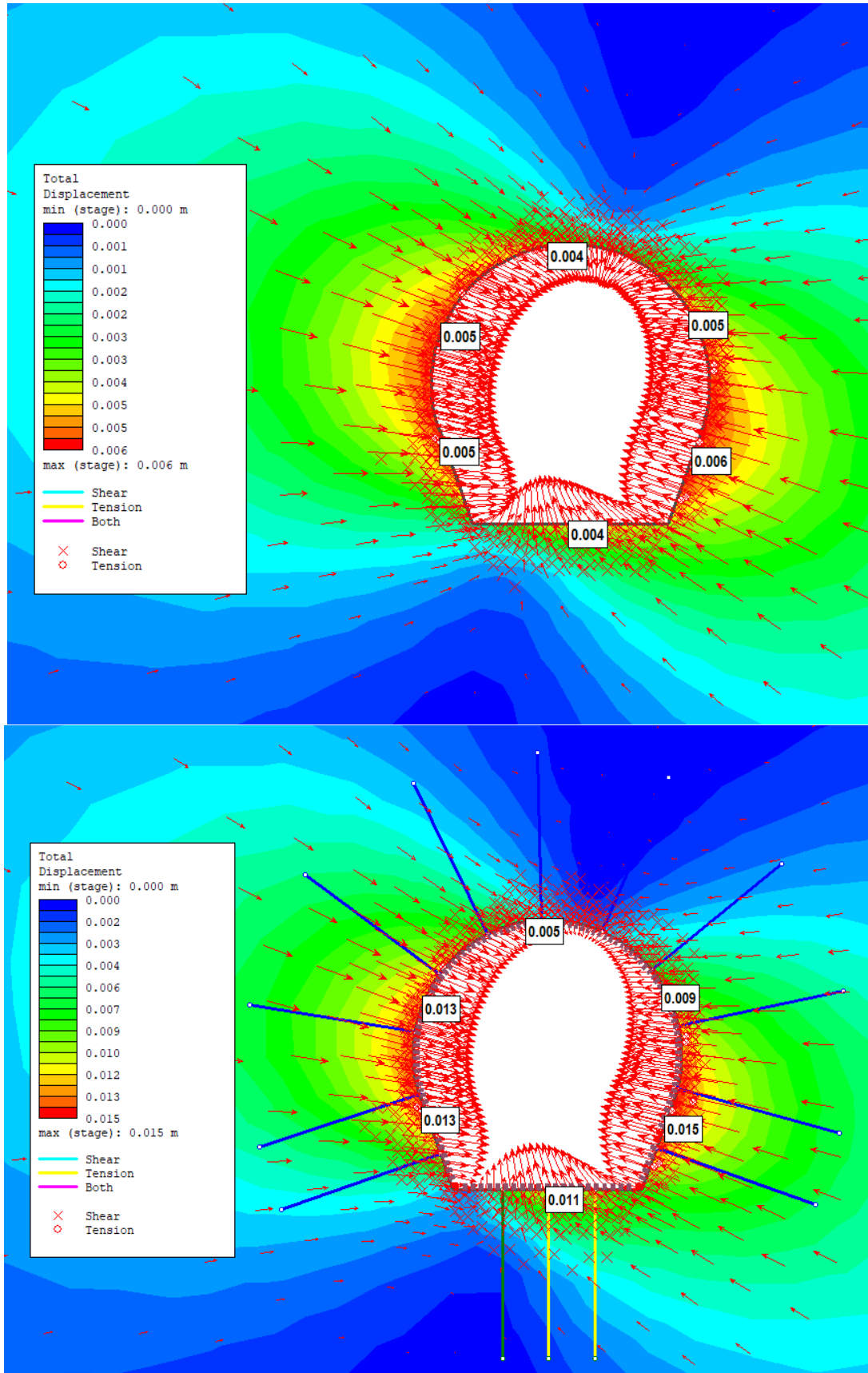


Figure 10.10: Results of plastic analysis at chainage 7+423 showing total displacement: Excavation stage(top) and Support Installation stage (bottom)

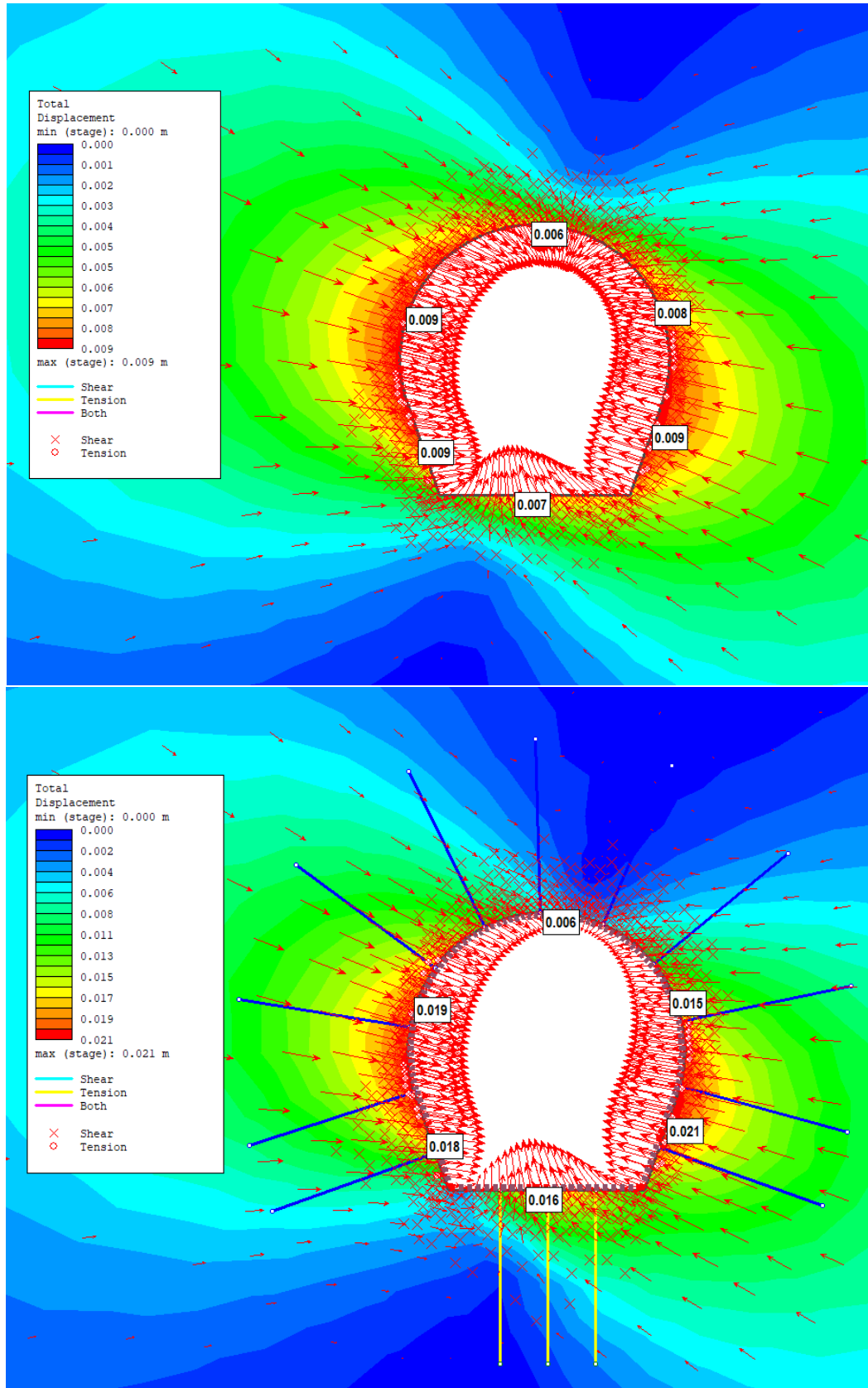


Figure 10.11: Results of plastic analysis at chainage 7+455 showing total displacement: Excavation stage(top) and Support Installation stage (bottom)

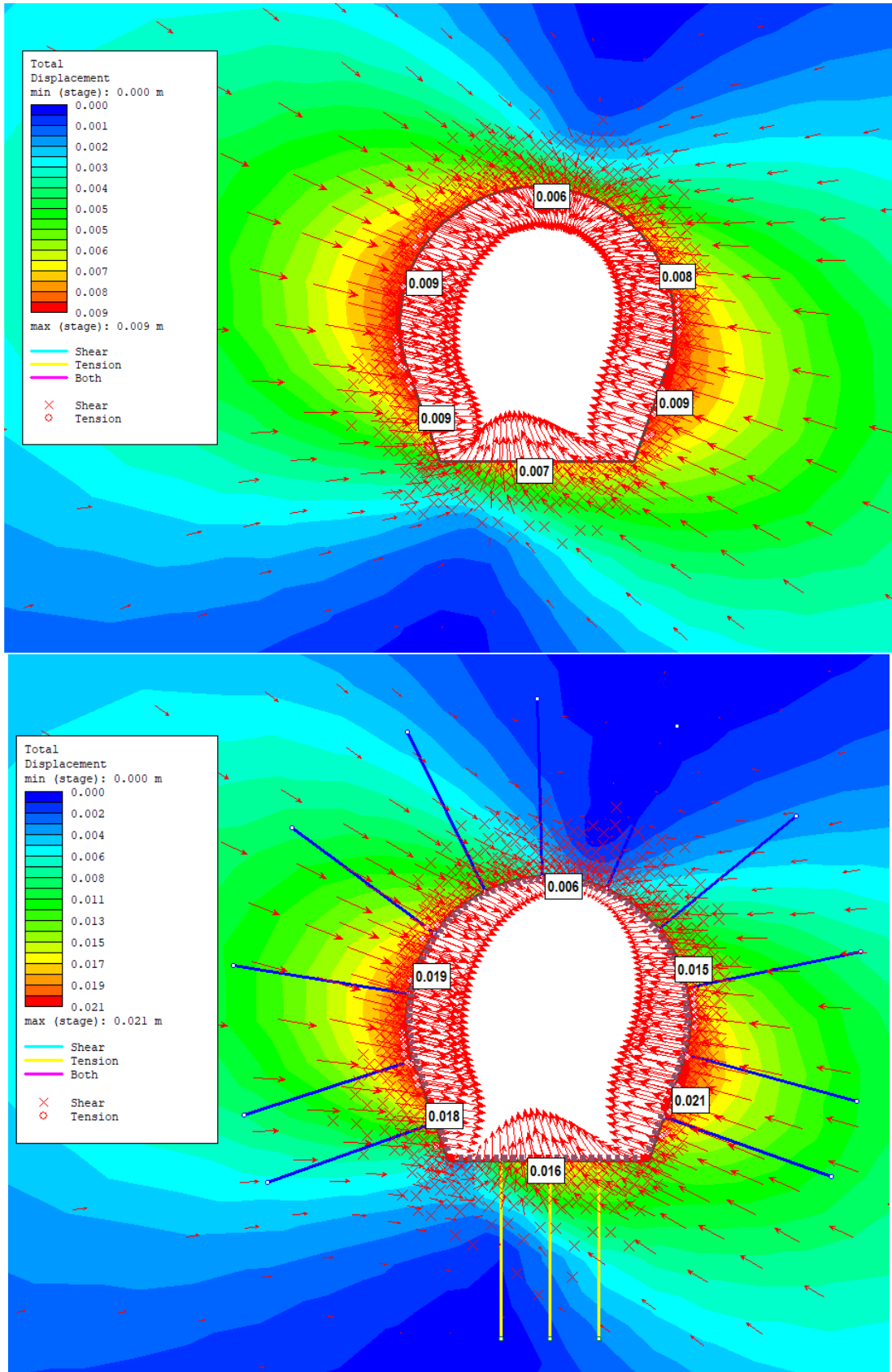


Figure 10.12: Results of plastic analysis at chainage 7+531 showing total displacement: Excavation stage(top) and Support Installation stage (bottom)

In Table 10.7, the details regarding the deformation occurring at different locations of tunnel cross-section during stage 2 and stage 3 at chainages 7+029, 7+423, 7+455, and 7+531 are presented. The material and support are defined as plastic for the analysis, therefore after excavation of the tunnel, the materials and liner yield. The number of elements, liner, and bolts that yield are presented in Table 10.7. As it can be seen at chainage 7+029 and chainage 7+531, a maximum number of elements yields, and also these are the chainages with maximum estimated and measured deformation. These sections contain relatively weak rock mass because of which the number of yielded elements and the deformation is maximum in comparison to other studied chainages. Similarly, the number of yielded liner and yielded bolt is maximum at these sections. As the rock mass is weak the support needs to bear more stress which causes the increase in the number of yielded supports. The chainage 7+423 and chainage 7+455 which are the section with the strong rock mass among the studied chainages, the number of yielded elements and support is minimum.

11 Stability Assessment of Moglice headrace tunnel due to Swelling Pressure

The laboratory test performed on intact rock sample from the Moglice headrace tunnel confirms the presence of swelling minerals as discussed in Chapter 8.3. The presence of swelling minerals possesses the stability problem to tunnel during construction and operation. The case study of the Chacabuquito hydropower plant failure in Chapter 5.2 which during construction faces serious problems as tunnel passes through rock mass exhibiting expansive behavior. Another assessment carried out on the collapse of the La-Higuera tunnel in Chapter 6 is an example of another failure due to swelling during the operation of the hydropower tunnel. The construction of the Moglice headrace tunnel has been completed and therefore the stability analysis is carried out to analyze the long-term stability of the headrace tunnel due to swelling during the long-run operational period of the hydropower plant. The stability assessment is performed using three analytical methods and numerical modeling. The analytical methods used are CCM (Carranza-Torres and Fairhurst, 2000), Hoek and Marinos (2000) method and Panthi and Shrestha (2018) methods which are modified to introduce swelling pressure as described in Chapter 4.3.3.2, Chapter 4.3.2.2 and Chapter 4.3.3.4 respectively. From the assessment of in-situ swelling pressure in Chapter 4.2.2.1, it was found that the in-situ swelling pressure varies from 5% to 55% of the laboratory swelling pressure. Hence, for the assessment of collapse of La-Higuera tunnel in Chapter 6, the swelling pressures were varied accordingly as the objective was to find the in-situ swelling pressure which causes the failure in the tunnel. However, for the Moglice headrace tunnel, the objective is to per from stability analysis, therefore the swelling pressure is varied from 25% to 55% of the maximum selling pressure measured in the laboratory.

11.1 Convergence Confinement Method (CCM)

CCM (Carranza-Torres and Fairhurst, 2000) estimates the tunnel deformation for a circular tunnel. The plastic deformation analysis for the Moglice headrace tunnel has been done in Chapter 10.1. A similar approach has been used for estimating the deformation due to swelling pressure. As discussed in Chapter 4.3.3.2, the swelling pressure (P_s) is added in addition to the ins situ vertical gravitational induced stress (σ_0). The change in stress condition will cause a change in Longitudinal Deformation Profile (LDP) and Ground reaction curve (GRC) and their interaction with the Support Capacity Curve (SCC). Equation 4.20, Equation 4.21, and Equation 4.22 describe the change in elastic part, plastic part for dilation angle $\psi > 0$ and $\psi = 0$ respectively in GRC due to additional of swelling pressure.

In Table 11.1, the results for the estimation of deformation using the CCM method for the various magnitude of swelling pressure at different chainages is presented. The no swelling pressure indicates the results for the plastic deformation and then the swelling pressure is gradually increased as 25%, 35%, 45%, and 55% of the maximum laboratory swelling pressure. At chainages 7+029, 7+064, 7+194, and 7+531, the increase in deformation due to maximum swelling pressure of 0.14 MPa is more than 2 mm. At chainages 7+029 and 7+531, where rock mass content maximum weak rock content and the measured deformation value is maximum, the increase in deformation due to swelling

pressure is also maximum being 4 mm and 6 mm respectively. For other chainages, the increase in deformation is less than or equal to 1 mm. The results from the CCM analysis show that the magnitude of deformation will not vary much even due to the maximum in-situ swelling pressure.

Table 11.1: Long-term deformation due to varying magnitude of swelling pressure estimated using CCM

Chainage	Displacement (mm)				
	No swelling pressure	0.06 MPa	0.09 MPa	0.11 MPa	0.14 MPa
7+029	89.1	90.9	91.7	92.4	93.1
7+064	46.8	47.5	47.8	48.1	48.4
7+092	31.1	31.5	31.7	31.9	32.0
7+136	13.8	14.0	14.2	14.2	14.3
7+168	22.9	23.2	23.2	23.3	23.7
7+194	59.4	60.3	60.6	61.0	61.3
7+218	26.3	26.6	26.7	26.8	26.9
7+266	11.0	11.0	11.0	11.0	11.0
7+291	83.0	84.4	85.0	85.6	86.1
7+316	20.8	21.0	21.1	21.2	21.3
7+342	37.3	37.8	38.0	38.2	38.4
7+423	9.7	9.8	9.8	9.8	9.9
7+455	14.6	14.7	14.8	14.8	14.9
7+531	71.5	72.7	73.2	73.7	77.3

11.2 Hoek and Marinos (2000) method

Hoek and Marinos (2000) method estimates the deformation of a circular tunnel in iso-static in situ stress condition. This analysis has been used to perform plastic deformation analysis of the Moglice headrace tunnel as shown in Chapter 10.2. The equation used for performing the plastic deformation analysis using Hoek and Marinos (2000) method has been modified to introduce swelling pressure (P_s) as discussed in Chapter 4.3.2.2. Equation 4.4 is the modified equation for estimating deformation where swelling pressure is added along with in-situ vertical gravitational in situ stress (p_0).

The results from the analysis using Hoek and Marinos (2000) method for estimating long-term deformation for varying magnitude of swelling pressure at different chainages of the Moglice headrace tunnel is presented in Table 11.2. Similar to CCM, no swelling pressure means the results for the plastic deformation and then the swelling pressure is gradually increased as 25%, 35%, 45%, and 55% of the maximum laboratory swelling pressure. The results show that similar to the CCM, at chainages 7+029, 7+064, 7+194, and 7+531, the increase in deformation due to maximum swelling pressure of 0.14 MPa is more than 2 mm and difference being maximum for chainages 7+063 and 7+531 of 4 mm and 3 mm respectively. For the remaining chainages, the deformation is less than or equal to 1 mm. The magnitude of increase in deformation at every chainage shows that no significant deformation will occur in the Moglice headrace tunnel due to swelling pressure that can cause any stability problems in the tunnel during operation.

Table 11.2: Long-term deformation due to varying magnitude of swelling pressure estimated using Hoek and Marinos (2000) method

Chainage	Displacement (mm)				
	No swelling pressure	0.06 MPa	0.09 MPa	0.11 MPa	0.14 MPa
7+029	40.3	41.9	42.5	43.2	43.9
7+064	32.8	33.9	34.4	34.8	35.3
7+092	20.8	21.4	21.6	21.9	22.1
7+136	16.4	16.8	16.9	17.1	17.2
7+168	26.4	27.1	27.3	27.6	27.8
7+194	39.9	40.9	41.4	41.8	42.2
7+218	22.1	22.7	22.9	23.1	23.3
7+266	13.5	13.8	13.9	14.0	14.2
7+291	63.4	65.3	66.0	66.8	67.5
7+316	20.8	21.3	21.5	21.7	21.9
7+342	27.5	28.2	28.5	28.7	29.0
7+423	9.4	9.6	9.6	9.7	9.8
7+455	16.0	16.3	16.5	16.6	16.7
7+531	38.8	40.0	40.5	41.0	41.5

11.3 Panthi and Shrestha (2018) method

Panthi and Shrestha (2018) method estimates the deformation considering anisotropic in situ stress condition and is not limited to the specific shape and size of the tunnel. Using this method plastic deformation analysis of the Moglice headrace tunnel has been carried out in Chapter 10.3. In CCM and Hoek and Marinos (2000) method, the swelling pressure (P_s) has been added only to vertical gravitational in-situ stress, whereas in Panthi and Shrestha (2018) method the swelling pressures has been added to both vertical and horizontal gravitational in situ stresses as shown in Equation 4.28 as discussed in Chapter 4.3.3.4. The instantaneous deformation remains the same as during construction the surrounding rock mass of the tunnel becomes unsaturated and hence no swelling pressure will be excreted and hence only final closure will vary as swelling pressure is excreted by the surrounding rock mass to tunnel during operation which is computed using Equation 4.29.

In Table 11.3, the results for estimating long-term deformation using Panthi and Shrestha (2018) for varying degree of magnitude of swelling pressure. The increase in maximum deformation from no loading condition to maximum swelling pressure of 0.14 MPa for every chainage is less than 2 mm. In contrast to CCM and Hoek and Marinos (2000) which have predicted the increase in deformation of more than 2 mm for chainages like 7+029, 7+064, 7+194, and 7+531, Panthi and Shrestha (2018) method estimates the deformation less than 2 mm. The results show the installed support can withstand the swelling pressure without any significant increase in deformation.

Table 11.3: Long-term deformation due to varying magnitude of swelling pressure estimated using Panthi and Shrestha (2018) method

Chainage	Displacement (mm)				
	No swelling pressure	0.06 MPa	0.09 MPa	0.11 MPa	0.14 MPa
7+029	48.2	49.0	49.4	49.7	50.0
7+064	43.8	44.5	44.8	45.1	45.3
7+092	26.5	26.8	27.0	27.1	27.3
7+136	20.2	20.5	20.6	20.7	20.8
7+168	25.9	26.2	26.3	26.5	26.6
7+194	41.5	42.0	42.3	42.5	42.7
7+218	19.7	19.9	20.0	20.1	20.2
7+266	12.3	12.4	12.5	12.6	12.6
7+291	42.8	43.4	43.6	43.8	44.0
7+316	20.2	20.5	20.6	20.7	20.8
7+342	23.3	23.6	23.7	23.9	24.0
7+423	5.6	5.7	5.7	5.8	5.8
7+455	12.1	12.3	12.3	12.4	12.4
7+531	57.3	58.1	58.4	58.7	59.0

11.4 Numerical Modeling

Swelling is introduced as the fourth stage in numerical modeling as described in model setup for RS2 in Chapter 4.3.4.2. Numerical modeling carried out for plastic deformation analysis has been presented in Chapter 10.4. In the same model, four more stages are added where swelling pressure of magnitude 0.06 MPa, 0.09 MPa, 0.11 MPa, and 0.14 MPa have been added. The maximum wall deformations at each stage after applying swelling pressure of all chainages are presented in Table 11.4. The results show no significant deformation after the application of swelling pressure. The maximum increase in deformation due to the application of swelling pressure of magnitude 0.14 MPa is 9 mm at chainage 7+029. For the remaining chainages, the increase in deformation due to maximum swelling pressure is less than 3 mm.

Table 11.4: Long-term deformation at different stages in RS2 model: From Stage 4 to Stage 7 varying magnitude of swelling pressure are applied in model

Chainage	Displacement (mm)					
	Stage 2 Excavation	Stage 3 Support Installtion	Stage 4 0.06 MPa	Stage 5 0.09 MPa	Stage 6 0.11 MPa	Stage 7 0.14 MPa
7+029	57.0	85.0	90.0	90.0	94.0	94.0
7+064	71.0	104.0	105.0	105.0	105.0	105.0
7+092	23.0	55.0	57.0	57.0	57.0	58.0
7+136	14.0	36.0	37.0	37.0	37.0	37.0
7+168	21.0	53.0	55.0	55.0	56.0	56.0
7+194	26.0	45.0	46.0	46.0	46.0	46.0
7+218	15.0	40.0	40.0	40.0	40.0	40.0
7+266	9.0	21.0	21.0	21.0	21.0	21.0
7+291	25.0	45.0	46.0	46.0	47.0	48.0
7+316	14.0	29.0	30.0	30.0	30.0	30.0

Table 11.4: Long-term deformation at different stages in RS2 model: From Stage 4 to Stage 7 varying magnitude of swelling pressure are applied in model

Chainage	Displacement (mm)					
	Stage 2 Excavation	Stage 3 Support Installtion	Stage 4 0.06 MPa	Stage 5 0.09 MPa	Stage 6 0.11 MPa	Stage 7 0.14 MPa
7+342	18.0	36.0	37.0	37.0	37.0	37.0
7+423	5.0	13.0	14.0	14.0	14.0	14.0
7+455	9.0	18.0	19.0	19.0	19.0	19.0
7+531	7.0	54.0	55.0	55.0	55.0	55.0

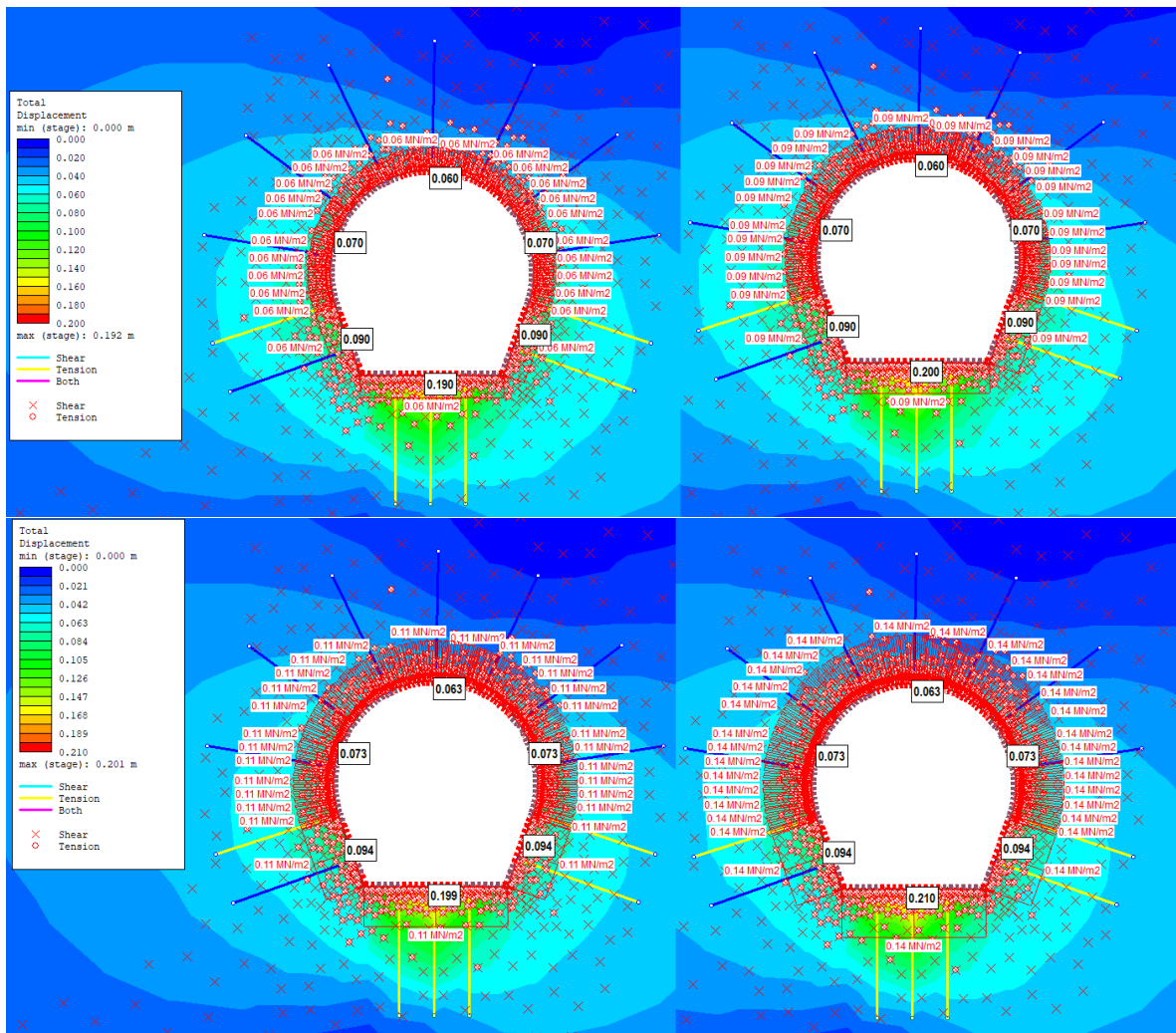


Figure 11.1: RS2 modeling result for Chainage 7+029 showing deformation and yielded elements and support for different swelling pressure

Table 11.5: Deformation in mm at various location of tunnel cross section at change 7+063 and details of yielded elements and supports

Description	Stage 4	Stage 5	Stage 6	Stage 7
	0.06 MPa	0.09 MPa	0.11 MPa	0.14 MPa
Left wall	90	90	94	94
Left wall	70	70	73	73
Roof	60	60	63	63
Right wall	70	70	73	73
Right wall	90	90	94	94
Invert	190	200	200	210
No. of Yielded Elements	1118	1123	1126	1126
No. of Yielded Liner	56	57	57	57
No.f Yielded Bolts	6	6	6	6

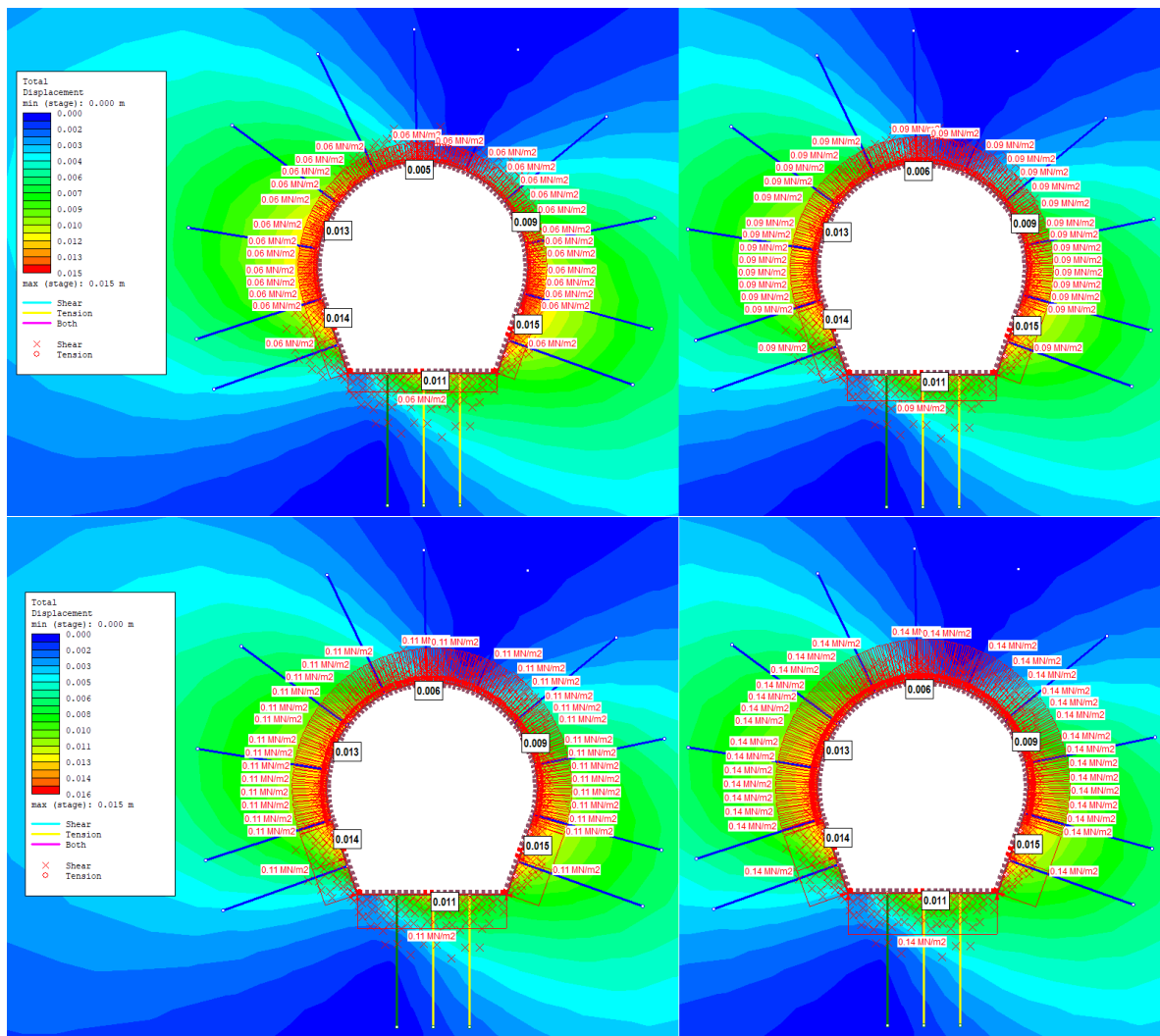


Figure 11.2: RS2 modeling result for Chainage 7+423 showing deformation and yielded elements and support for different swelling pressure

Table 11.6: Deformation in mm at various location of tunnel cross section at change 7+423 and details of yielded elements and supports

Description	Stage 4	Stage 5	Stage 6	Stage 7
	0.06 MPa	0.09 MPa	0.11 MPa	0.14 MPa
Left wall	14	14	14	14
Left wall	13	13	13	13
Roof	5	6	6	6
Right wall	9	9	9	9
Right wall	15	15	15	15
Invert	11	11	11	11
No. of Yielded Elements	538	538	538	538
No. of Yielded Liner	9	9	9	9
No.f Yielded Bolts	2	2	2	2

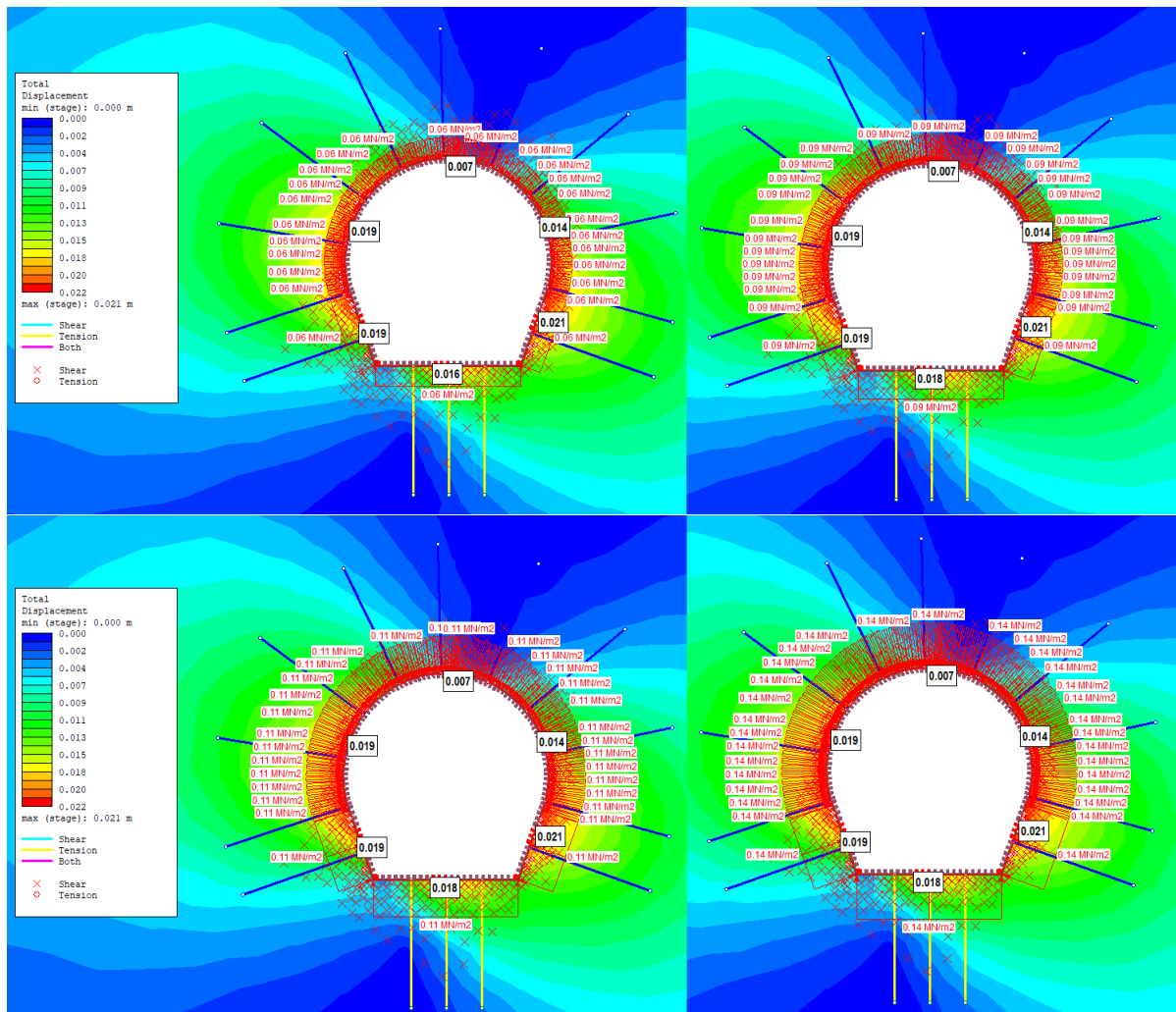


Figure 11.3: RS2 modeling result for Chainage 7+455 showing deformation and yielded elements and support for different swelling pressure

Table 11.7: Deformation in mm at various location of tunnel cross section at change 7+455 and details of yielded elements and supports

Description	Stage 4	Stage 5	Stage 6	Stage 7
	0.06 MPa	0.09 MPa	0.11 MPa	0.14 MPa
Left wall	19	19	19	19
Left wall	19	19	19	19
Roof	7	7	7	7
Right wall	14	14	14	14
Right wall	21	21	21	21
Invert	16	18	18	18
No. of Yielded Elements	650	650	650	650
No. of Yielded Liner	12	12	12	12
No. of Yielded Bolts	3	3	3	3

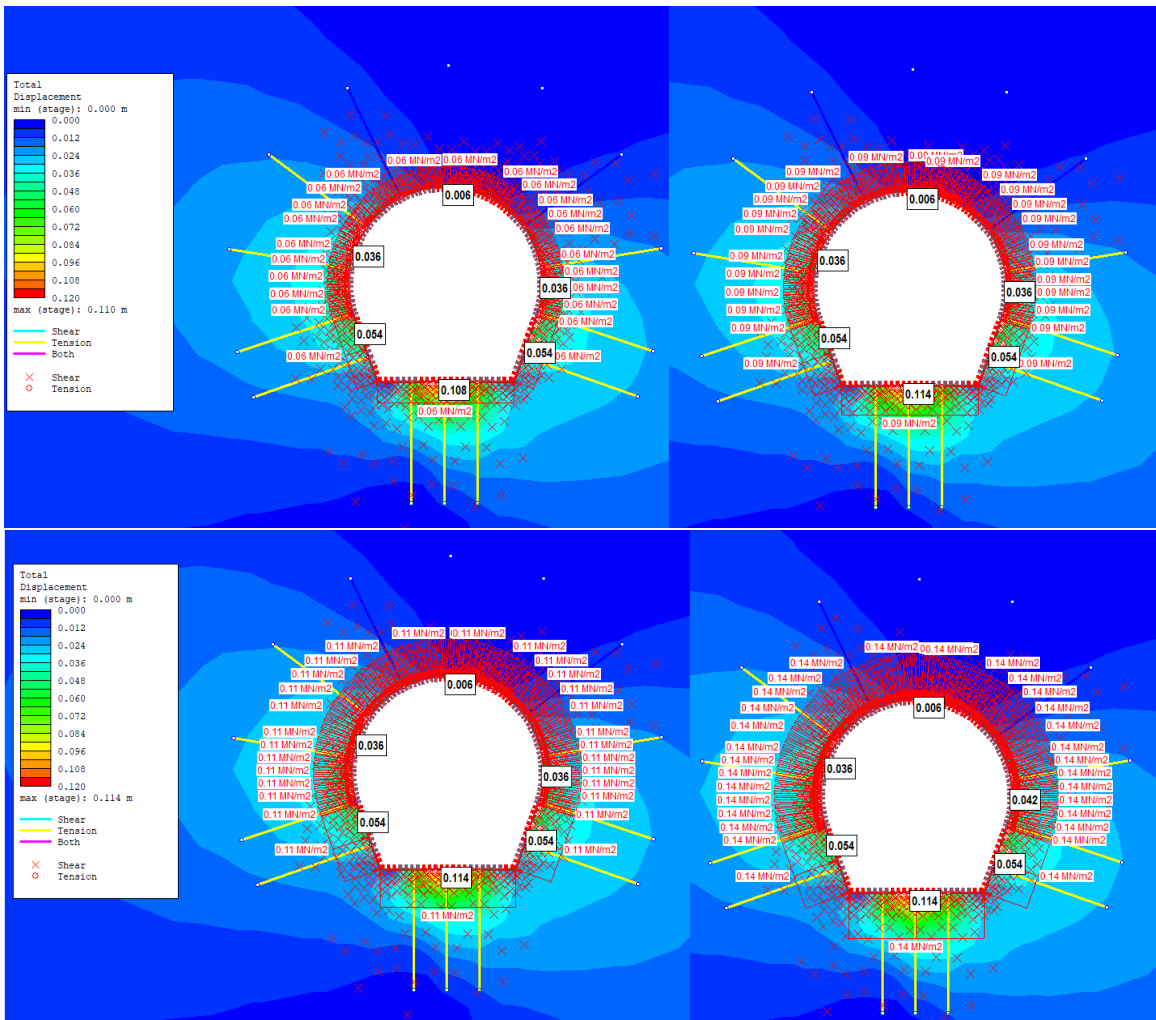


Figure 11.4: RS2 modeling result for Chainage 7+531 showing deformation and yielded elements and support for different swelling pressure

Table 11.8: Deformation in mm at various location of tunnel cross section at change 7+531 and details of yielded elements and supports

Description	Stage 4	Stage 5	Stage 6	Stage 7
	0.06 MPa	0.09 MPa	0.11 MPa	0.14 MPa
Left wall	55	55	55	55
Left wall	38	38	38	38
Roof	6	6	6	6
Right wall	38	38	38	38
Right wall	54	54	54	54
Invert	108	114	114	114
No. of Yielded Elements	840	840	843	847
No. of Yielded Liner	50	50	50	50
No.f Yielded Bolts	10	10	10	10

For four chainages 7+063, 7+423, 7+455, and 7+531 for which results of plastic deformation analysis are discussed in Chapter 10.4, the results for swelling analysis from the numerical model are discussed in this chapter. For the remaining chainages results from numerical modeling are presented in Appendix . The results from numerical modeling showing deformation and yielded elements and support due to application of varying magnitude of swelling pressure for chainages 7+029, 7+423, 7+455, and 7+531 are presented in Figure 11.1, Figure 11.2, Figure 11.3, and Figure 11.4 respectively. The details of results showing magnitude of deformation and number if yielded elements and supports from the numerical analysis done for swelling in four chainages 7+029, 7+423, 7+455, and 7+531 are presented in Table 11.5, Table 11.6, Table 11.7, and Table 11.8 respectively.

In comparison to the results from the plastic deformation analysis carried out at these chainages as shown in Table 10.7, the extent of deformation after the swelling pressure is applied on the model around the tunnel is none for chainages 7+423 and 7+455. The rock mass at these chainages is relatively strong than other studied chainages. The increase in the number of yielded elements and support is also less and no additional bolts are yielded. The bolts were failed in shear during plastic deformation analysis and the effect of application of swelling pressure on remaining non yielded bolts is seemed to be none. In the case of chainages 7+063 and 7+531 which are the weakest rock mass among the studied cross-sections of the Moglice headrace tunnel, there is an increase in the magnitude of deformation. The deformation at the wall and roof at these chainages are limited to a maximum value of 4 mm whereas in invert the increase in deformation due to application of maximum swelling pressure of 0.14 MPa is 20 mm at chainage 7+023. The maximum tunnel strain caused due to swelling at the invert is 0.3% of the tunnel width. The results show that there is an increase in the number of yielded elements at chainages 7+023 and 7+531 but the increase in number is not that significant whereas the number of yielded liners and support remains the same suggesting the applied support is enough capacity to withstand the swelling pressure.

12 Discussion

12.1 Discussion on Norwegian Design Principle

The inclined portion of the Moglice headrace tunnel is designed as an unlined tunnel based on the Norwegian design principle. The assessment carried out on the Norwegian design principle in Chapter 7.6, shows that the factors of safety for Norwegian confinement criteria are more than 3.0 and the factor of safety for minimum stress criteria is more than 1.6. According to Aasen et al. (2013), the factor of safety considerations for design is 1.5 for Norwegian confinement criteria and 1.3 for minimum principal stress. Therefore, the results of the assessment carried out at the different locations of the inclined portion of the Moglice headrace tunnel concur that the unlined tunnel design is safe as the value of factors of safety obtained are more than recommended during design.

12.2 Discussion on La-Higuera Failure Assessment

The La-Higuera headrace tunnel passes through the rock mass having swelling minerals as verified by the laboratory test done for assessment of the mineralogical composition of intact rock in Chapter 6.5. The samples contain a rich amount of Laumontite ranging from 8.6% to 42.1% which falls under the zeolite group which has similar swelling potential as smectites. In addition to this, the tunnel passes through the weakness zone dyke having a dip of 50° SE and strike of N143 $^{\circ}$ E.

The assessment carried out at chainage 12+347 of the La-Higuera headrace tunnel shows that the installed rock support yields as the displacement increases after the swelling pressure is exerted in the tunnel. The semi-empirical, analytical, and numerical analysis show that due to swelling pressure there is substantial deformation in the tunnel. The semi-empirical and analytical method only incorporates swelling pressure whereas in numerical analysis the weakness zone is also considered. Therefore, numerical analysis simulates the better ground condition and provides better results. As shown in Table 6.17, for swelling pressure greater than 0.27 MPa, the tunnel deformation increases more than 5% of the tunnel width along with the increase in the number yielded liner elements. Therefore, the collapse of the La-Higuera headrace tunnel occurs due to underestimated support to cope swelling pressure exerted by surrounding rock mass.

12.3 Discussion on Plastic deformation Analysis

Various methods can be used to estimate the plastic deformation of the tunnel based on the various rock mass properties as discussed in Chapter 4.3. These methods are used to estimate the tunnel deformation of two tunnels, the La-Higuera headrace tunnel, and the Moglice headrace tunnel. For the La-Higuera headrace tunnel, the deformation measurement during construction is not available which makes it hard to compare the accuracy of methods to estimate the deformation. However, in absence of measured deformation, the estimated results from various methods are compared with each other as shown in Figure 12.1. The results show that numerical modeling estimated the highest deformation among all. The reason for the higher estimation of deformation from numerical modeling is because in numerical modeling it is possible to consider the weakness zone, unlike other methods. The absence of measured deformation creates uncertainty to conclude the

numerical method results as accurate. However, the numerical model simulates the real ground condition in a better and detailed way so it can argue that the numerical method is most suitable for cases like La-Higuera to estimate deformation.

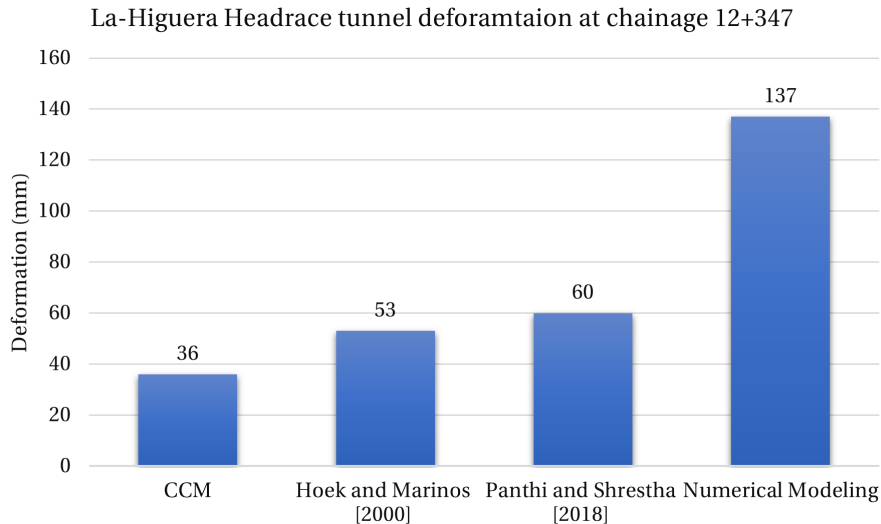


Figure 12.1: Comparison of estimated deformation at chainage 12+347 of the La-Higuera headrace tunnel

At the section of the Moglice headrace tunnel passing through weak flysch rock mass, systematic deformation measurement has been carried out during construction. Hence, it is possible to compare the estimated results from different methods with the measured data and thus, the comparison is shown in Figure 12.2. The magnitude of deformation is different at different chainages depending on the rock mass properties at each chainage.

In a comparison of estimated deformation using CCM with the measured deformation, for chainages 7+029, 7+194, 7+291, 7+342, and 7+531 where the rock mass has higher weak rock content ranging from 70% to 90%, the estimated deformation is higher. As discussed in Chapter 10.1, deformation CCM can be linked with rock mass deformation modulus which depends on rock mass properties and in situ stress. So based on these arguments and comparison of estimated results with the measured value, it can be said that for weak rock mass CCM tends to over-estimate deformation for the Moglice headrace tunnel. Another reason may be the use of equivalent radius since CCM consider a circular tunnel while the tunnel in actuality is of horseshoe shape and consideration of isostatic in-situ stress condition. The estimated deformation using Hoek and Marinos (2000) method is higher for most of the chainages in comparison to measured values. However, the estimated deformation for weak rock is not as high as estimated by CCM. The estimated values of deformation using Panthi and Shrestha (2018) method is also variable as the other two methods. However, for most chainages, the estimation is close to the measured value. For weak rock mass, the analytical methods have estimated the deformation higher than the measured value in comparison to relatively strong rock mass. The results from the numerical modeling are closest to the measured deformation.

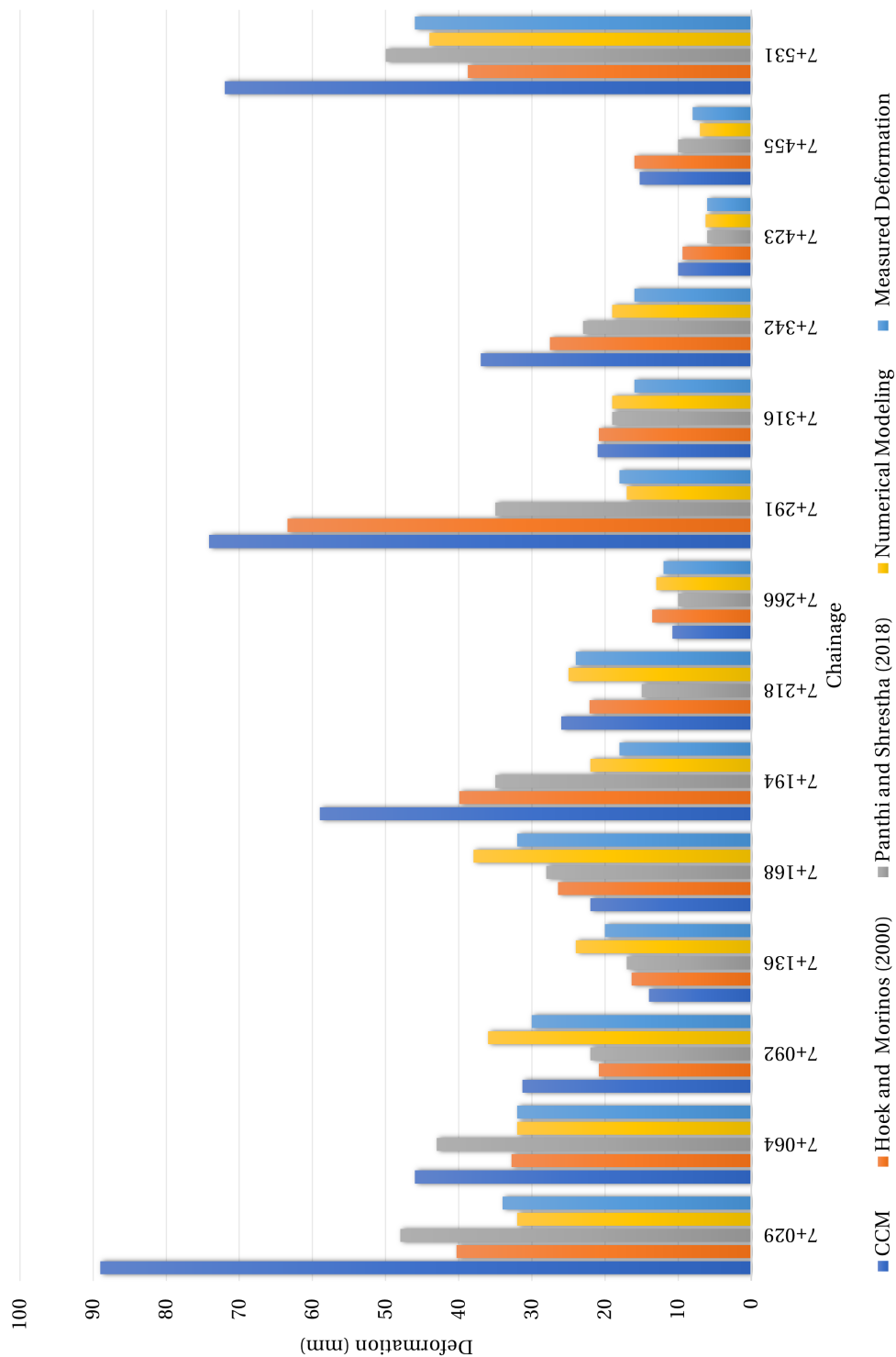


Figure 12.2: Comparison of estimated deformations using different methods with measured deformation

CCM Carranza-Torres and Fairhurst (2000) and Hoek and Marinos (2000) methods are useful tools and can be utilized to get preliminary information. Despite the deviation of estimation from measured values of deformation, information such as how rock mass conditions and in situ stress affect the convergence of the tunnel can be accessed. On the

other hand, Panthi and Shrestha (2018) method found useful for the estimation of tunnel deformation. Many of the drawbacks of the other methods as discussed before have been overcome by Panthi and Shrestha (2018) method. Panthi and Shrestha (2018) method overcomes the drawback of CCM and Hoek and Marinos (2000) methods, as this method can be used for all tunnels despite their shape and size. Also, the effect of anisotropy has been considered in this method. Panthi and Shrestha (2018) estimation values are more close to measured deformation in comparison to estimation from CCM and Hoek and Marinos (2000). Numerical Modeling proves to be the best method for estimation deformation. However, while performing the numerical modeling, one must be careful with the input parameters. If garbage is feed as input the results will also be garbage, "Garbage-In- Garbage- Out". Hence, the quality of input parameters should be higher.

12.4 Discussion on impact of swelling pressure on rock support

The La-Higuera tunnel fails as rock support yields due to swelling pressure exerted by rock mass containing swelling minerals. The impact of swelling pressure on installed rock support of La-Higuera headrace tunnel is studied using numerical modeling in Chapter 6.10.4. In RS2 for the elastic reinforced concrete liner, a factor of support capacity plot based on a factor of support can be generated. Thus the shotcrete is considered to be an elastic reinforced concrete liner and the swelling pressure of varying magnitude is applied. The support yields at swelling pressure 1.22 MPa. However, the assumption of support as elastic is not true. Therefore, the analysis is carried out considering liner as plastic. The results thus obtained suggest that the extent of deformation due to swelling pressure in the plastic liner is significantly higher even at swelling pressure lower than 1.22 MPa. The number of yielded liners increases with the increase in the magnitude of swelling pressure as shown in Table 6.17 along with the magnitude of deformation. The increase in the number of yielded liner and deformation ultimately leads the support to fail to cause a collapse of the tunnel.

For the assessment of impact of swelling pressure on rock support installed at the Moglice headrace tunnel passing through flysch rock mass, the support is considered to be plastic. The analysis is performed using numerical modeling as described in Chapter 11.4. The same model used for plastic deformation analysis is used in which swelling pressure of varying magnitude has been applied. In Table 10.7, the details of yielded liner and bolts during plastic deformation analysis has been shown. All the bolts are yielded due to shear force as shown in Figure 10.9, Figure 10.10, Figure 10.11 and Figure 10.12. The details of yielded support after applying different swelling pressure for chainages 7+029, 7+423, 7+455 and 7+531 are shown in Table 11.5, Table 11.6, Table 11.7, and Table 11.8 respectively. The comparison of these results with the result of plastic deformation analysis shows that no additional bolts have been yielded and the number of yielded liner elements is non significant.

12.5 Discussion on long term deformation due to rock swelling

The deformation pressure will act on the installed rock support due to rock swelling. The deformation thus caused by swelling pressure has been estimated using analytical and numerical methods as discussed in Chapter 4.3. The semi-empirical and analytical

methods used for plastic deformation analysis has been modified to predict the extent of deformation due to swelling pressure.

The assessment of the La-Higuera headrace tunnel shows how the increase in long-term deformation due to swelling pressure may cause failure. In Table 6.11, Table 6.13, Table 6.15 and Table 6.17, the magnitude of increase in deformation due to varying swelling pressure estimated using CCM, Hoek and Marinos (2000) method, Panthi and Shrestha (2018) method and numerical modeling respectively has been shown. The magnitude of swelling pressure has been varied from 5% to 55% of maximum swelling pressure obtained from laboratory tests. The analytical methods predict that there is a substantial increase in deformation as the magnitude of swelling pressure increases. The increase in deformation from no swelling pressure to deformation due to maximum swelling pressure of magnitude 1.49 MPa by CCM, Hoek and Marinos (2000) method, Panthi and Shrestha (2018) method is 98 mm, 13 mm, and 46 mm respectively. But the results from the numerical analysis show the extent of deformation is much worst. The presence of the weakness zone and the swelling pressure from the rock mass causes more deformation and the support yields causing the failure.

The lesson learned from the La-Higuera tunnel collapse is that the deformation of underestimated rock support will cause failure. Hence the assessment is carried out to estimate the long-term deformation of the Moglice headrace tunnel passing through flysch in Chapter 11. The swelling pressures have been varied from 25% to 55% of the maximum swelling pressure measures at the laboratory to simulate the possible worst-case scenarios. The results of long-term deformation estimated using CCM, Hoek and Marinos (2000) method, Panthi and Shrestha (2018) and numerical modeling have been compared as shown in Figure 12.3 and Figure 12.4. In a comparison of the increase in the extent of deformation due to swelling pressure is compared with the results from plastic deformation analysis of each chainage, the magnitude of deformation estimated by each method is very less. The maximum deformation is estimated by numerical modeling for chainage 7+029 is 9 mm due to maximum swelling pressure of 0.14 MPa. The analyses of long-term deformation using different methods show no significant increase in deformation due to swelling pressure at the Moglice headrace tunnel. The installed rock support can withstand the swelling pressure exerted by the rock mass assuring the safety of the tunnel during the long operational period of the hydropower plant.

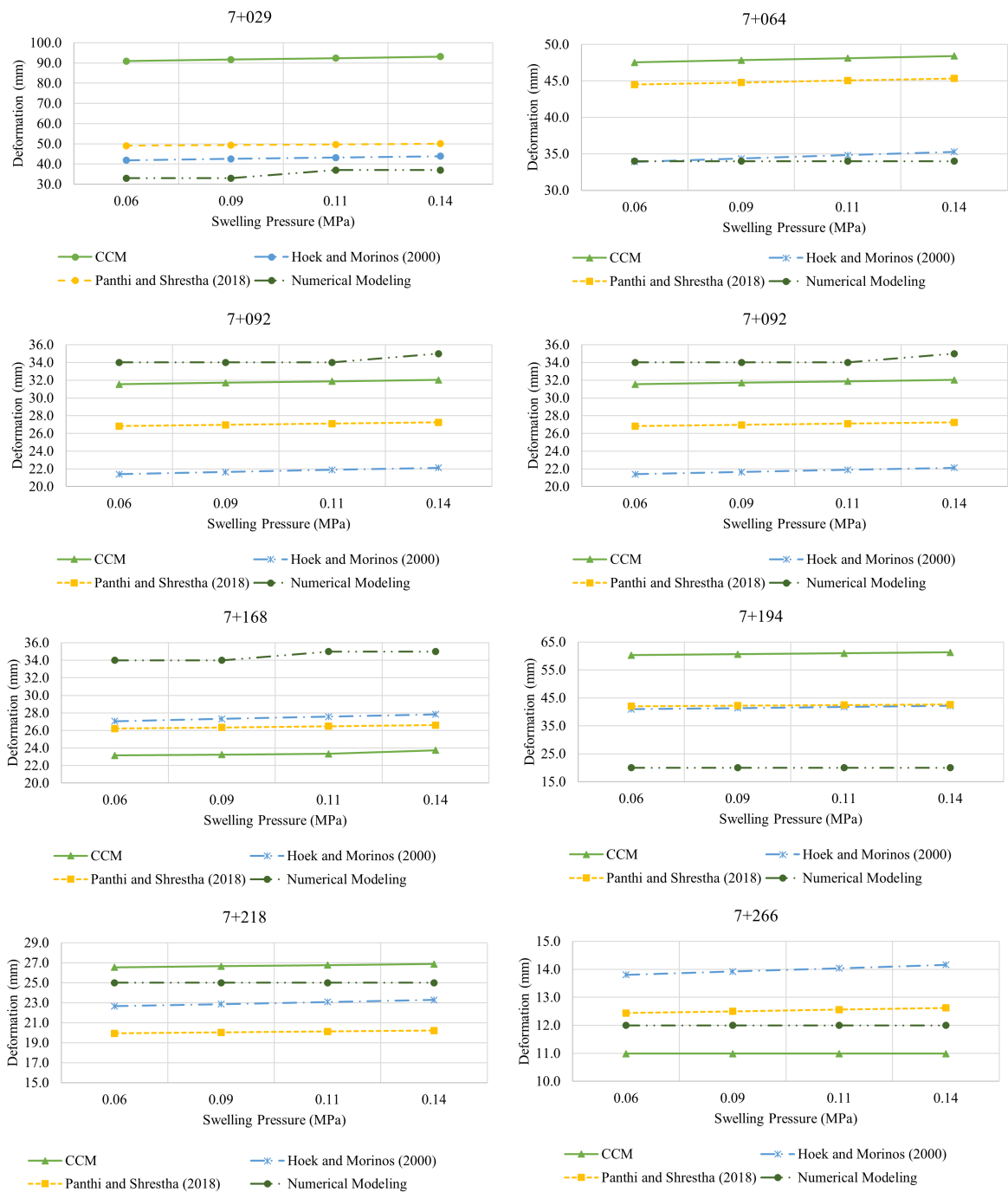


Figure 12.3: Comparison of estimated Long term deformations due to swelling pressure at Moglice head-race tunnel from chainage 7+069 to 7+266 using different methods

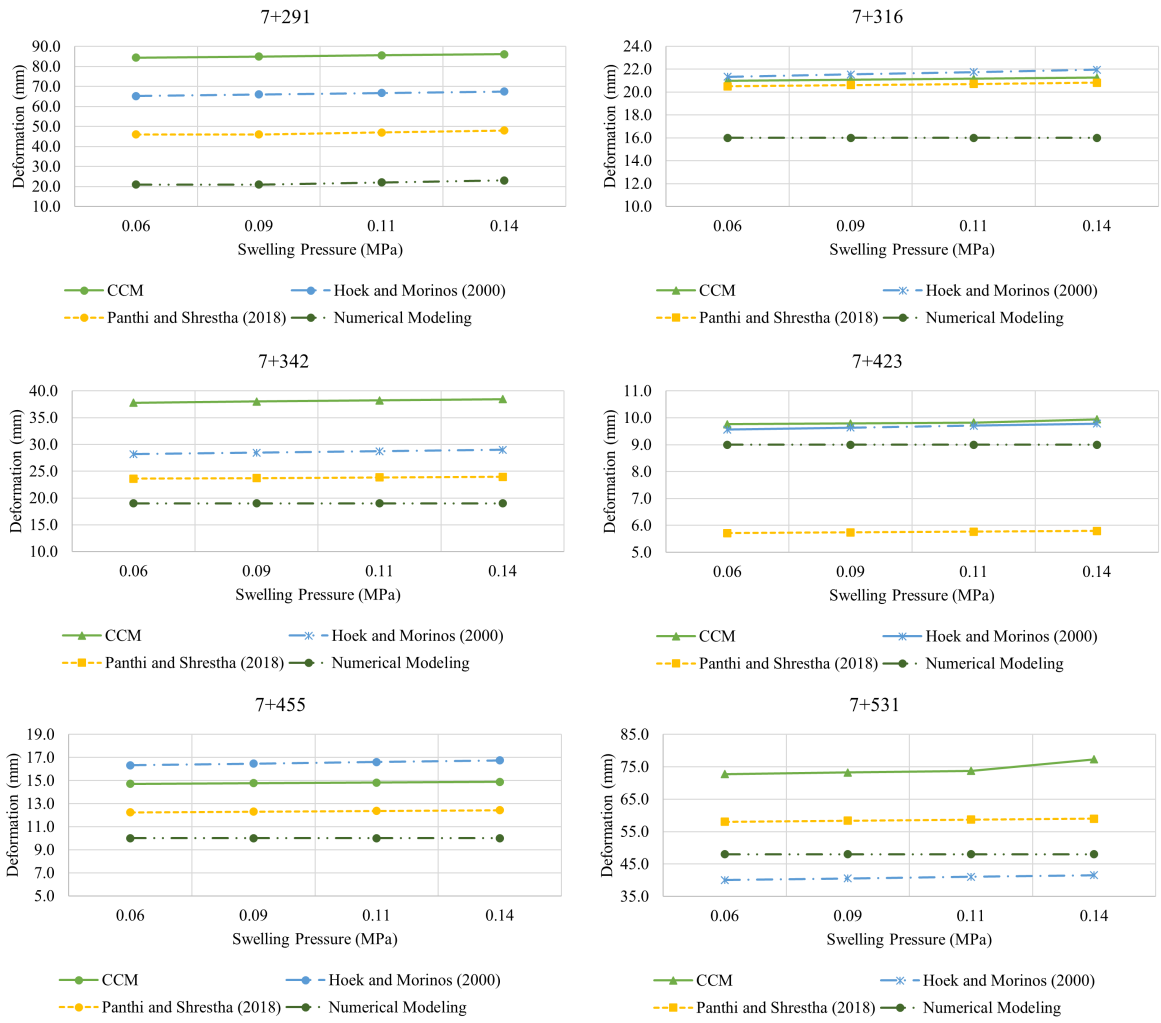


Figure 12.4: Comparison of estimated Long term deformations due to swelling pressure at Moglice head-race tunnel from chainage 7+291 to 7+531 using different methods

13 Conclusion and Recommendation

13.1 Conclusion

For the Moglice headrace tunnel passing through flysch formation, plastic deformation analysis has been carried out using semi-empirical, analytical, and numerical methods. The same methods are modified and used for the evaluation of long-term deformation due to rock swelling pressure. The semi-empirical and analytical methods are modified by adding the in-situ swelling pressure with in-situ gravitational stress. The methods are based on in-situ stress and rock mass quality which makes it necessary to have a good estimation of these parameters. Along with the evaluation of the plastic deformation analysis and deformation due to rock swelling for the Moglice headrace tunnel, the assessment is carried out for the design of the inclined portion of the Moglice headrace tunnel based on the Norwegian design principle. Also, a detailed evaluation of the La-Higuera tunnel collapse has been done in this thesis. Based on these studies following conclusions are drawn:

- The inclined portion of the Moglice headrace tunnel designed based on the Norwegian design principle is found to be safe based on the results of the assessment carried out to evaluate the factor of safety for Norwegian confinement criteria and minimum principal stress.
- The in-situ swelling pressure is lower than the swelling pressure measured at laboratory and may vary from 5% to 55% of the swelling pressure measured at laboratory.
- The La-Higuera headrace tunnel collapses due to the underestimated rock support to withstand the swelling pressure exerted by the surrounding rock mass.
- The field stress measurement is not carried out at flysch formation at the Moglice headrace tunnel. However, the stress measurement is done at section 7+844 which lies in a different rock formation using the hydraulic fracturing method. The results of field stress measurement cannot be used for the analysis at flysch rock but the results can be used to estimate the tectonic stress prevailing at the project location using misfit criteria.
- The CCM, Hoek and Marinos method, and Panthi and Shrestha method can be used for plastic deformation analysis and proven to be useful and reliable tools during planning and design of the project.
- The use of the numerical method is best for plastic deformation analysis in comparison to semi-empirical and analytical methods. It provides a larger possibility to simulate real ground conditions and can be used for any shape of underground excavation. In addition, the numerical method provides information on the yielding of supports.
- The numerical modeling method provides the best result for stability analysis of headrace tunnel due to swelling pressure. The semi-empirical and analytical methods such as CCM, Hoek and Marinos method, and Panthi and Shrestha method can be used to estimate deformation due to swelling pressure by adding the in situ

swelling pressure with induced gravitational stress.

- The stability assessment carried out using different methods for varying magnitude of swelling pressure from 25% to 55% of maximum swelling pressure measured at lab shows that there is no substantial increase in deformation at the Moglice headrace tunnel. In addition, the numerical modeling shows the increase in an additional number of yielding bolts and liners are none to very less. The installed support is of enough capacity to withstand the possible worst case of maximum swelling pressure.

13.2 Recommendation

Following are the recommendation for the plastic deformation analysis and stability analysis against swelling of tunnels constructed in weak rock mass:

- The analyses using either analytical or numerical methods demand the accurate estimation of input parameters. Therefore, it is recommended to conduct laboratory testing and field observations to get reliable and accurate information on rock mass properties and geological conditions of the field.
- The information on the induced in situ stress condition is always important. If possible the field stress measurement should be done, if not numerical modeling should be carried out.
- The empirical and analytical methods can be used for both plastic deformation analysis and stability analysis against swelling to get the preliminary information during planning and design. However, it is recommended to use numerical modeling for the analyses, as it incorporates more complexities such as including the effect of weakness zone, groundwater, etc.
- For the stability analysis of tunnel against swelling it is recommended to perform sensitivity analysis by varying the magnitude of in situ swelling pressure from 25% to 55% of maximum laboratory swelling pressure so that possible worst-case scenarios can be assessed.

Following are the recommendation for future study, design and monitoring of the hydropower tunnels passing through the swelling rock mass:

- Swelling is caused due to the interaction of minerals with water. The thesis has not considered the effect of groundwater. Therefore, the effect of groundwater can be studied for the stability assessment of the headrace tunnel.
- The complexity of cases like La-Higuera requires more extensive assessment, therefore 3D analysis is recommended to analyze the problem.
- In swelling rock mass the monitoring of deformation should be extended for some time after commissioning of the project during the operation of the tunnel.
- While designing the rock support for the hydropower tunnel in the swelling rock mass, possible maximum swelling pressure should be considered during design.

References

- Aasen, O., Ødegaard, H., and Palmstrom, A. (2013). Planning of pressurized headrace tunnel in albania. *Norwegian Hydropower Tunnelling II. Oslo: Norwegian tunnelling society NFF*.
- Almenara, J. M. T. (2021). Analysis of plastic deformations in weak rock masses of flysch. an evaluation based on a hydropower tunnel in albania. Unpublished paper.
- Arikan, F. and Aydin, N. (2012). Influence of weathering on the engineering properties of dacites in northeastern turkey. *International Scholarly Research Notices*, 2012.
- Aydan, Ö., Akagi, T., and Kawamoto, T. (1993). The squeezing potential of rocks around tunnels; theory and prediction. *Rock mechanics and rock engineering*, 26(2):137–163.
- Barton, N. (2002). Some new q-value correlations to assist in site characterisation and tunnel design. *International journal of rock mechanics and mining sciences*, 39(2):185–216.
- Barton, N. et al. (1978). Suggested methods for the quantitative description of discontinuities in rock masses. In *International Journal of Rock Mechanics and Mining Sciences and Geomechanics Abstracts*, volume 15, pages 319–368.
- Barton, N., Lien, R., and Lunde, J. (1974). Engineering classification of rock masses for the design of tunnel support. *Rock mechanics*, 6(4):189–236.
- Basnet, C. B. (2013). Evaluation on the squeezing phenomenon at the headrace tunnel of chameliya hydroelectric project, nepal. Master's thesis, Institutt for geologi og bergteknikk.
- Basnet, C. B. and Panthi, K. K. (2018). Analysis of unlined pressure shafts and tunnels of selected norwegian hydropower projects. *Journal of Rock Mechanics and Geotechnical Engineering*, 10(3):486–512.
- Basnet, C. B. and Panthi, K. K. (2019). Evaluation on the minimum principal stress state and potential hydraulic jacking from the shotcrete-lined pressure tunnel: A case from nepal. *Rock Mechanics and Rock Engineering*, 52(7):2377–2399.
- Basnet, C. B. and Panthi, K. K. (2020). Detailed engineering geological assessment of a shotcrete lined pressure tunnel in the himalayan rock mass conditions: a case study from nepal. *Bulletin of Engineering Geology and the Environment*, 79(1):153–184.
- Bell, F. and Haskins, D. (1997). A geotechnical overview of katse dam and transfer tunnel, lesotho, with a note on basalt durability. *Engineering geology*, 46(2):175–198.
- Bieniawski, Z. and Bernede, M. (1979). Suggested methods for determining the uniaxial compressive strength and deformability of rock materials: Part 1. suggested method for determining deformability of rock materials in uniaxial compression. In *International journal of rock mechanics and mining sciences & geomechanics abstracts*, volume 16, pages 138–140. Elsevier.
- Bieniawski, Z. T. (1989). *Engineering rock mass classifications: a complete manual for*

- engineers and geologists in mining, civil, and petroleum engineering*. John Wiley & Sons.
- Brady, B. and Brown, E. (2007). Rock strength and deformability. In *Rock mechanics for underground mining*, pages 85–141. Springer.
- Brattli, B. and Broch, E. (1995). Stability problems in water tunnels caused by expandable minerals. swelling pressure measurements and mineralogical analysis. *Engineering Geology*, 39(3-4):151–169.
- Broch, E. (1983). Estimation of strength anisotropy using the point-load test. In *International Journal of Rock Mechanics and Mining Sciences & Geomechanics Abstracts*, volume 20, pages 181–187. Elsevier.
- Broch, E. (1984). Development of unlined pressure shafts and tunnels in norway.
- Broch, E. and Palmstrom, A. (2017). The design of unlined hydropower tunnels and shafts: 100 years of norwegian experience. *Hydropower & Dams*, (3).
- Brown, E. and Hoek, E. (1980). *Underground excavations in rock*. CRC Press.
- Brox, D. (2019). Hydropower tunnel failures: Risks and causes. In *Tunnels and Underground Cities: Engineering and Innovation meet Archaeology, Architecture and Art*, pages 4386–4396. CRC Press.
- Cai, M., Kaiser, P., Tasaka, Y., and Minami, M. (2007). Determination of residual strength parameters of jointed rock masses using the gsi system. *International Journal of Rock Mechanics and Mining Sciences*, 44(2):247–265.
- Cao, C., Shi, C., Lei, M., Yang, W., and Liu, J. (2018). Squeezing failure of tunnels: a case study. *Tunnelling and Underground Space Technology*, 77:188–203.
- Carlos Lang, M. B. and Salazar, P. (2017). High cover tbm tunneling in the andes mountains—a comparative study of two challenging tunnel projects in chile. *RAPID EXCAVATION and TUNNELING CONFERENCE 2017 PROCEEDINGS*, pages 269–283.
- Carranza-Torres, C. and Fairhurst, C. (2000). Application of the convergence-confinement method of tunnel design to rock masses that satisfy the hoek-brown failure criterion. *Tunnelling and underground space technology*, 15(2):187–213.
- Castro, S., Van Sint Jan, M., Gonzalez, R., Lois, P., Velasco, L., et al. (2003). Dealing with expansive rocks in the los quilos and chacabuquito water tunnels-andes mountains of central chile. In *10th ISRM Congress*. International Society for Rock Mechanics and Rock Engineering.
- Chaudhary, B. (2020). Assessment on plastic deformation at the powerhouse cavern and tailrace tunnel of andhikhola hydroelectric project. Master's thesis, NTNU.
- Chauhan, K. (2020). Planning and rock engineering design of the underground structures of the tamakoshi v hydroelectric project. Master's thesis, NTNU.
- Chern, J., Shiao, F., and Yu, C. (1998). An empirical safety criterion for tunnel con-

- struction. In *Proceedings of the regional symposium on sedimentary rock engineering, Taipei, Taiwan*, pages 222–227.
- Devoll (2015). Devoll hydropower project - moglicë dam / albania hydraulic fracturing stress measurements in the headrace tunnel (hrt3) at chainage 7+884.
- Dick, J. C., Shakoor, A., and Wells, N. (1994). A geological approach toward developing a mudrock-durability classification system. *Canadian Geotechnical Journal*, 31(1):17–27.
- Dilek, Y., Furnes, H., and Shallo, M. (2008). Geochemistry of the jurassic mirdita ophiolite (albania) and the morb to ssz evolution of a marginal basin oceanic crust. *Lithos*, 100(1-4):174–209.
- Dyke, C. and Dobereiner, L. (1991). Evaluating the strength and deformability of sandstones.
- Einstein, H. (1996). Tunnelling in difficult ground—swelling behaviour and identification of swelling rocks. *Rock mechanics and rock engineering*, 29(3):113–124.
- Erguler, Z. A. and Shakoor, A. (2009). Quantification of fragment size distribution of clay-bearing rocks after slake durability testing. *Environmental & Engineering Geoscience*, 15(2):81–89.
- FAMA, M. E. D. (1993). Numerical modeling of yield zones in weak rock. In *Analysis and design methods*, pages 49–75. Elsevier.
- Flåten, M. (2015). Stress induced stability assessment of the underground caverns for moglicë hydropower project, albania. Master's thesis, NTNU.
- Franklin, J. (1985). Suggested method for determining point load strength. In *International Journal of Rock Mechanics and Mining Sciences & Geomechanics Abstracts*, volume 22, pages 51–60. Elsevier.
- Franklin, J. and Chandra, R. (1972). The slake-durability test. In *International Journal of Rock Mechanics and Mining Sciences & Geomechanics Abstracts*, volume 9, pages 325–328. Elsevier.
- Frashëri, A. (2005). Geothermal regime and hydrocarbon generation in the albanides. *Petroleum Geoscience*, 11(4):347–352.
- Frashëri, A., Nishani, P., Bushati, S., and Hyseni, A. (1996). Relationship between tectonic zones of the albanides, based on results of geophysical studies. *Mémoires du Muséum national d'histoire naturelle (1993)*, 170:485–511.
- Frengen, R. B. (2020). Assessment of swelling pressure on sprayed concrete lining at the headrace tunnel of moglice hydropower project. Master's thesis, NTNU.
- Goodman, R. (1993). Engineering geology: rock in engineering construction.
- Goodman, R. E. (1989). *Introduction to rock mechanics*, volume 2. Wiley New York.

- Grimstad, E. (1993). Updating the q-system for nmt. In *Proceedings of the International Symposium on Sprayed Concrete-Modern use of wet mix sprayed concrete for underground support, Fagemes, Oslo, Norwegian Concrete Association, 1993*.
- Hawkins, A. and McConnell, B. (1992). Sensitivity of sandstone strength and deformability to changes in moisture content. *Quarterly Journal of Engineering Geology and Hydrogeology*, 25(2):115–130.
- Heidbach, O., Barth, A., Müller, B., Reinecker, J., Stephansson, O., Tingay, M., and Zang, A. (2016a). Wsm quality ranking scheme, database description and analysis guidelines for stress indicator.
- Heidbach, O., Rajabi, M., Reiter, K., Ziegler, M., Team, W., et al. (2016b). World stress map database release 2016. *GFZ Data Services*, 10.
- Hoek, E. (2000). Practical rock engineering.
- Hoek, E. and Brown, E. T. (1997). Practical estimates of rock mass strength. *International journal of rock mechanics and mining sciences*, 34(8):1165–1186.
- Hoek, E., Carranza-Torres, C., Corkum, B., et al. (2002). Hoek-brown failure criterion-2002 edition. *Proceedings of NARMS-Tac*, 1(1):267–273.
- Hoek, E. and Diederichs, M. S. (2006). Empirical estimation of rock mass modulus. *International journal of rock mechanics and mining sciences*, 43(2):203–215.
- Hoek, E. and Marinos, P. (2000). Predicting tunnel squeezing problems in weak heterogeneous rock masses. *Tunnels and tunnelling international*, 32(11):45–51.
- Hudson, J. A. and Harrison, J. P. (2000). *Engineering rock mechanics: an introduction to the principles*. Elsevier.
- Hveding, V., Haga, I., Helland-Hansen, E., Holtedahl, T., Lye, K. A., Hillestad, K. O., et al. (1992). Hydropower development. *Trondheim: Norwegian Institute of Technology, Dept. of Hydraulic Engineering*.
- ISRM (1977). *Suggested methods for determining tensile strength of rock materials* International Society for Rock Mechanics. Commission on Standardization of Laboratory and Field Tests. Committee on Laboratory Tests. The Society.
- ISRM (1979a). Suggest methods for determining water content, porosity, density, absorption and related properties and swelling and slake-durability index properties Franklin, John A. *Int. J. Rock Mech. Min. Sci. & Geomech. Abstr.*, 16:141–156.
- ISRM (1979b). Suggested methods for determining the uniaxial compressive strength and deformability of rock materials. *Rock Characterisation Testing and Monitoring—ISRM Suggested Methods*.
- Jethwa, J., Singh, B., and Singh, B. (1984). Estimation of ultimate rock pressure for tunnel linings under squeezing rock conditions—a new approach. In *Design and Performance of Underground Excavations: ISRM Symposium—Cambridge, UK, 3–6 September 1984*, pages 231–238. Thomas Telford Publishing.

- Kovári, K. (1998). Tunneling in squeezing rock. *Tunnel 5/98*.
- Labasse, H. (1949). Les pressions de terrains dans les mines de huiles. *Revue Universelle des Mines*, 5(3):78–88.
- Malaj, A., Rusi, I., Meço, A., Faca, D., and Allkja, S. (2017). The characterization of flysch rock in albania with field and laboratory testing. *Procedia Engineering*, 191:104–111.
- Manchao, H. and Xiaoming, S. (2020). Engineering view of soft rocks. In *Soft Rock Mechanics and Engineering*, pages 7–17. Springer.
- Mandl, G. (2005). *Rock joints*. Springer.
- Marinos, P. and Hoek, E. (2001). Estimating the geotechnical properties of heterogeneous rock masses such as flysch. *Bulletin of engineering geology and the environment*, 60(2):85–92.
- Marroni, M., Pandolfi, L., Onuzi, K., Palandri, S., and Xhomo, A. (2009). Ophiolite-bearing vermishi flysch (albanian alps, northern albania): elements for its correlation in the frame of dinaric-hellenic belt. *Ofioliti*, 34(2):95–108.
- Mehranpour, M. H. and Kulatilake, P. H. (2016). Comparison of six major intact rock failure criteria using a particle flow approach under true-triaxial stress condition. *Geomechanics and Geophysics for Geo-Energy and Geo-Resources*, 2(4):203–229.
- Myrvang, A. (2001). Rock mechanics. *Norway University of Technology (NTNU), Trondheim (in Norwegian)*.
- Neupane, B. (2010). Engineering geological evaluation of underground works at upper tamakoshi hydroelectric project, nepal. Master's thesis, Norges teknisk-naturvitenskapelige universitet, Fakultet for
- NGI (2015). Using q-system-rock mass classification and support design, technical report. *NGI, Oslo*.
- NGI (2019). Documentation of installation of flatjacks and measurements in the headrace tunnel.
- Nickmann, M., Spaun, G., and Thuro, K. (2006). Engineering geological classification of weak rocks. In *Proceedings of the 10th International IAEG Congress*, volume 492, pages 1–9. Citeseer.
- Nilsen, B. and Palmström, A. (2000). Engineering geology and rock engineering. *Norwegian Group for Rock Mechanics, Oslo*.
- Nilsen, B. and Palmstrom, A. (2000). *Engineering Geology and Rock Engineering - Handbook No 2*. Norwegian Group of Rock Mechanics.
- Nilsen, B. and Thidemann, A. (1993). *Rock engineering*. Norwegian Institute of Technology, Division of Hydraulic Engineering.
- Palmstrom, A. (1995). *RMI-a rock mass characterization system for rock engineering purposes*. na.

- Palmstrom, A. and Broch, E. (2006). Use and misuse of rock mass classification systems with particular reference to the q-system. *Tunnelling and underground space technology*, 21(6):575–593.
- Palmström, A. and Singh, R. (2001). The deformation modulus of rock masses—comparisons between in situ tests and indirect estimates. *Tunnelling and Underground Space Technology*, 16(2):115–131.
- Panet, M. (1995). *Le calcul des tunnels par la méthode convergence-confinement*. Number BOOK. Presses ENPC.
- Panthi, K. K. (2006). Analysis of engineering geological uncertainties related to tunnelling in himalayan rock mass conditions.
- Panthi, K. K. (2012). Evaluation of rock bursting phenomena in a tunnel in the himalayas. *Bulletin of Engineering Geology and the Environment*, 71(4):761–769.
- Panthi, K. K. (2014). Norwegian design principle for high pressure tunnels and shafts: its applicability in the himalaya. *Hydro Nepal: Journal of Water, Energy and Environment*, 14:36–40.
- Panthi, K. K. (2017). Review on the prevailing methods for the prediction of potential rock burst/rock spalling in tunnels. *Fjellsprengningsdagen, Bergmekanikkdagen, Geoteknikkdagen*.
- Panthi, K. K. and Basnet, C. B. (2016). Review on the major failure cases of unlined pressure shafts/tunnels of norwegian hydropower projects. *Hydro Nepal: Journal of Water, Energy and Environment*, 18:6–15.
- Panthi, K. K. and Basnet, C. B. (2021). Fluid flow and leakage assessment through an unlined/shotcrete lined pressure tunnel: A case from nepal himalaya. *Rock Mechanics and Rock Engineering*, 54(4):1687–1705.
- Panthi, K. K., Basnet, C. B., et al. (2018). State-of-the-art design guidelines in the use of unlined pressure tunnels/shafts for hydropower scheme. In *ISRM International Symposium-10th Asian Rock Mechanics Symposium*. International Society for Rock Mechanics and Rock Engineering.
- Panthi, K. K. and Shrestha, P. K. (2018). Estimating tunnel strain in the weak and schistose rock mass influenced by stress anisotropy: An evaluation based on three tunnel cases from nepal. *Rock mechanics and rock engineering*, 51(6):1823–1838.
- Peranić, J. and Arbanas, Ž. (2020). Impact of the wetting process on the hydro-mechanical behavior of unsaturated residual soil from flysch rock mass: preliminary results. *Bulletin of Engineering Geology and the Environment*, 79(2):985–998.
- PowerTechnology (2021). Devoll hydropower project. <https://www.power-technology.com/projects/devoll-hydropower-project/>. Accessed: 2021-05-09.
- Rocscience (2007). *Phase2 2D finite element program for calculating stresses and estimating support around underground excavations*. Rocscience.

- Rusi, M. (2016). Estimating rock mass parameters in block and matrix rocks in devoll valley.
- Sakurai, S. (1984). Displacement measurements associated with the design of underground openings. In *Field measurements in geomechanics. International symposium*, pages 1163–1178.
- Selen, L. (2017). Study on material properties and testing of various rock types, development of investigation procedure and test methodology for future projects. Master's thesis, NTNU.
- Selen, L. (2020). Assessment on the swelling and disintegration potential of weak and weathered rocks in water tunnels of hydropower projects-a contribution based on use of laboratory testing methods.
- Selen, L., Panthi, K. K., and Vistnes, G. (2020). An analysis on the slaking and disintegration extent of weak rock mass of the water tunnels for hydropower project using modified slake durability test. *Bulletin of Engineering Geology and the Environment*, 79(4):1919–1937.
- Selmer, R. and Palmstrom, A. (1989). Tunnel collapses in swelling clay zones. *Tunnels & tunnelling*, pages 49–58.
- Selmer-Olsen, R. (1969). Experience with unlined pressure shafts in norway. In *Proc. Int. Symposium on large permanent underground openings, Oslo*.
- Selmer-Olsen, R. (1974). Underground openings filled with high-pressure water or air. *Bulletin of the International Association of Engineering Geology-Bulletin de l'Association Internationale de Géologie de l'Ingénieur*, 9(1):91–95.
- Selmer-Olsen, R. (1988). General engineering design procedures. *Norwegian Tunnelling Today, Tapir*, pages 53–58.
- Serafim, J. (1983). Consideration of the geomechanical classification of bieniawski. In *Proc. int. symp. on engineering geology and underground construction*, volume 1, pages 33–44.
- Shallo, M. and Vranaj, A. (1994). On the geology of korca-kolonja region in albania= επί της γεωλογίας της περιοχής korca-kolonja στην αλβανία. *Δελτίον της Ελληνικής Γεωλογικής Εταιρίας*, 30(2):449–458.
- Shrestha, G. L. (2006). Stress induced problems in himalayan tunnels with special reference to squeezing.
- Shrestha, N. (2020). Evaluation on stability condition along the headrace tunnel of kulekhani-iii hydroelectric project. Master's thesis, NTNU.
- Shrestha, P. K. (2014). *Stability of tunnels subject to plastic deformation-a contribution based on the cases from the Nepal Himalaya*. PhD thesis.
- Shrestha, P. K. and Panthi, K. K. (2014). Groundwater effect on faulted rock mass: an evaluation of modi khola pressure tunnel in the nepal himalaya. *Rock mechanics and rock engineering*, 47(3):1021–1035.

- Singh, B., Jethwa, J., Dube, A., and Singh, B. (1992). Correlation between observed support pressure and rock mass quality. *Tunnelling and Underground Space Technology*, 7(1):59–74.
- Singh, T., Kainthola, A., and Venkatesh, A. (2012). Correlation between point load index and uniaxial compressive strength for different rock types. *Rock Mechanics and Rock Engineering*, 45(2):259–264.
- Skrede, S.-E. (2017). Stability assessment of hydropower tunnel in swelling and slaking rock mass. Master's thesis, NTNU.
- Smith, H. J. (1997). The point load test for weak rock in dredging applications. *International Journal of Rock Mechanics and Mining Sciences*, 34(3-4):295–e1.
- SNPower (2012). Hlh tunnel collapse. Presentation.
- Statkraft (2021). Moglicë hydropower plant. <https://www.statkraft.com/about-statkraft/where-we-operate/albania/moglice-hydropower-plant/>. Accessed: 2021-05-09.
- Steiner, W. (1993). Swelling rock in tunnels: rock characterization, effect of horizontal stresses and construction procedures. In *International journal of rock mechanics and mining sciences & geomechanics abstracts*, volume 30, pages 361–380. Elsevier.
- Taylor, R. (1988). Coal measures mudrocks: composition, classification and weathering processes. *Quarterly Journal of Engineering Geology and Hydrogeology*, 21(1):85–99.
- Theng, B. K. G. (2012). *Formation and properties of clay-polymer complexes*. Elsevier.
- Udpa, L., Sun, Y., Lord, W., and Shin, Y. (1989). Mesh and boundary considerations in the numerical modeling of large 3-d electromagnetic ndt geometries. In *Review of Progress in Quantitative Nondestructive Evaluation*, pages 793–800. Springer.
- Ulusay, R. et al. (2013). Harmonizing engineering geology with rock engineering on stability of rock slopes. In *ISRM SINOROCK 2013*. International Society for Rock Mechanics and Rock Engineering.
- UNFCCC (2004). Clean development mechanism project design document form (cdm-pdd) version 02 - in effect as of: 1 july 2004). Report, United Nations Framework Convention on Climate Change.
- Vallejo, L. E., Welsh Jr, R. A., Robinson, M. K., et al. (1989). Correlation between unconfined compressive and point load strengths for appalachian rocks. In *The 30th US Symposium on Rock Mechanics (USRMS)*. American Rock Mechanics Association.
- Vásárhelyi, B. (2003). Some observations regarding the strength and deformability of sandstones in dry and saturated conditions. *Bulletin of Engineering Geology and the Environment*, 62(3):245–249.
- Vegvesen, S. (2014). Laboratorieundersøkelser, håndbok r210. Oslo: Statens vegvesen.







- Vergara, M. R. and Triantafyllidis, T. (2016). Influence of water content on the mechanical properties of an argillaceous swelling rock. *Rock mechanics and rock engineering*, 49(7):2555–2568.
- Vlachopoulos, N. and Diederichs, M. (2009). Improved longitudinal displacement profiles for convergence confinement analysis of deep tunnels. *Rock mechanics and rock engineering*, 42(2):131–146.
- Wood, A. M. M. (1972). Tunnels for roads and motorways. *Quarterly Journal of Engineering Geology and Hydrogeology*, 5(1-2):111–126.
- Zhai, H., Canbulat, I., Hebblewhite, B., and Zhang, C. (2017). Review of current empirical approaches for determination of the weak rock mass properties. *Procedia engineering*, 191:908–917.
- Zhang, H., Adoko, A. C., Meng, Z., Wang, H., and Jiao, Y. (2017). Mechanism of the mudstone tunnel failures induced by expansive clay minerals. *Geotechnical and Geological Engineering*, 35(1):263–275.

A Standard Charts and Figures

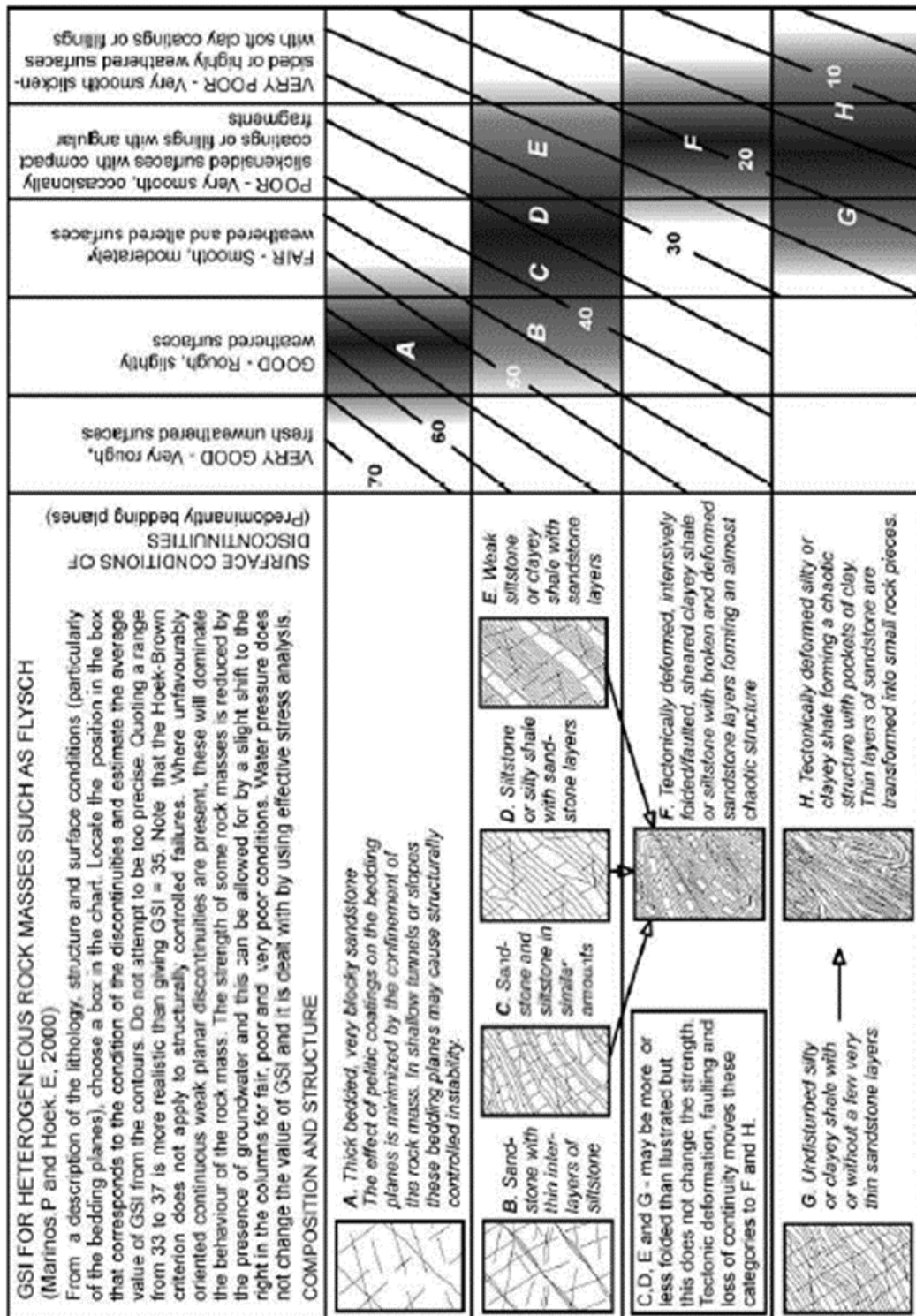
A.1 Determination of mi Hoek and Marinos (2000)

Rock type	Class	Group	Texture			
			Coarse	Medium	Fine	Very fine
SEDIMENTARY	Clastic		Conglomerates (21 ± 3) Breccias (19 ± 5)	Sandstones 17 ± 4	Siltstones 7 ± 2 Greywackes (18 ± 3)	Claystones 4 ± 2 Shales (6 ± 2) Marls (7 ± 2)
		Non-Clastic	Carbonates	Crystalline Limestone (12 ± 3)	Sparitic Limestones (10 ± 2)	Micritic Limestones (9 ± 2)
	Evaporites			Gypsum 8 ± 2	Anhydrite 12 ± 2	
	Organic					Chalk 7 ± 2
METAMORPHIC	Non Foliated		Marble 9 ± 3	Hornfels (19 ± 4) Metasandstone (19 ± 3)	Quartzites 20 ± 3	
	Slightly foliated		Migmatite (29 ± 3)	Amphibolites 26 ± 6	Gneiss 28 ± 5	
	Foliated*			Schists 12 ± 3	Phyllites (7 ± 3)	Slates 7 ± 4
IGNEOUS	Plutonic	Light	Granite 32 ± 3 Granodiorite (29 ± 3)	Diorite 25 ± 5		
		Dark	Gabbro 27 ± 3 Norite 20 ± 5	Dolerite (16 ± 5)		
	Hypabyssal			Porphyries (20 ± 5)	Diabase (15 ± 5)	Peridotite (25 ± 5)
	Volcanic	Lava		Rhyolite (25 ± 5) Andesite 25 ± 5	Dacite (25 ± 3) Basalt (25 ± 5)	
		Pyroclastic	Agglomerate (19 ± 3)	Breccia (19 ± 5)	Tuff (13 ± 5)	




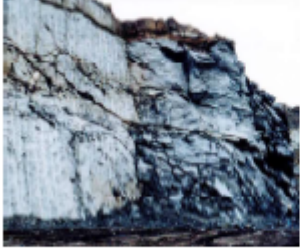

A.2 GSI for Jointed Rock Hoek and Marinos (2000)

<p>GEOLOGICAL STRENGTH INDEX FOR JOINTED ROCKS (Hoek and Marinos, 2000)</p> <p>From the lithology, structure and surface conditions of the discontinuities, estimate the average value of GSI. Do not try to be too precise. Quoting a range from 33 to 37 is more realistic than stating that GSI = 35. Note that the table does not apply to structurally controlled failures. Where weak planar structural planes are present in an unfavourable orientation with respect to the excavation face, these will dominate the rock mass behaviour. The shear strength of surfaces in rocks that are prone to deterioration as a result of changes in moisture content will be reduced if water is present. When working with rocks in the fair to very poor categories, a shift to the right may be made for wet conditions. Water pressure is dealt with by effective stress analysis.</p>		<p>SURFACE CONDITIONS</p> <p>VERY GOOD Very rough, fresh unweathered surfaces</p> <p>GOOD Rough, slightly weathered, iron stained surfaces</p> <p>FAIR Smooth, moderately weathered and altered surfaces</p> <p>POOR Slackensided, highly weathered surfaces with compact coatings or fillings or angular fragments</p> <p>VERY POOR Slackensided, highly weathered surfaces with soft clay coatings or fillings</p>				
<p>STRUCTURE</p>		<p>DECREASING SURFACE QUALITY →</p>				
 <p>INTACT OR MASSIVE - intact rock specimens or massive in situ rock with few widely spaced discontinuities</p>	90			N/A	N/A	
 <p>BLOCKY - well interlocked undisturbed rock mass consisting of cubical blocks formed by three intersecting discontinuity sets</p>	80	70				
 <p>VERY BLOCKY - interlocked, partially disturbed mass with multi-faceted angular blocks formed by 4 or more joint sets</p>		60	50			
 <p>BLOCKY/DISTURBED/SEAMY - folded with angular blocks formed by many intersecting discontinuity sets. Persistence of bedding planes or schistosity</p>			40	30		
 <p>DISINTEGRATED - poorly interlocked, heavily broken rock mass with mixture of angular and rounded rock pieces</p>				20		
 <p>LAMINATED/SHEARED - Lack of blockiness due to close spacing of weak schistosity or shear planes</p>	N/A	N/A			10	
<p>↓ DECREASING INTERLOCKING OF ROCK PIECES</p>						

A.3 GSI for Heterogeneous masses such as flysch Hoek and Marinos (2000)

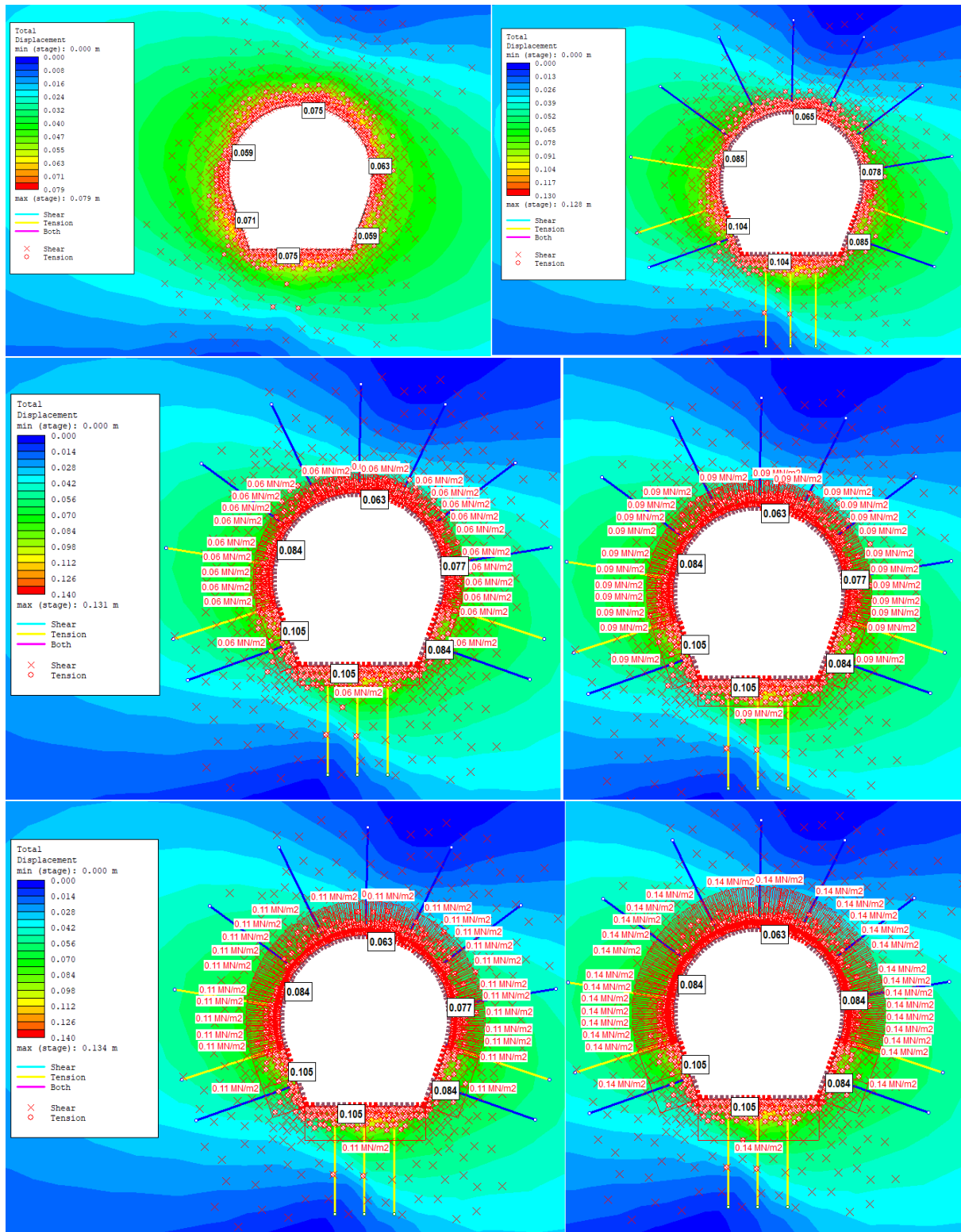


A.4 Disturbance factor Hoek et al. (2002)

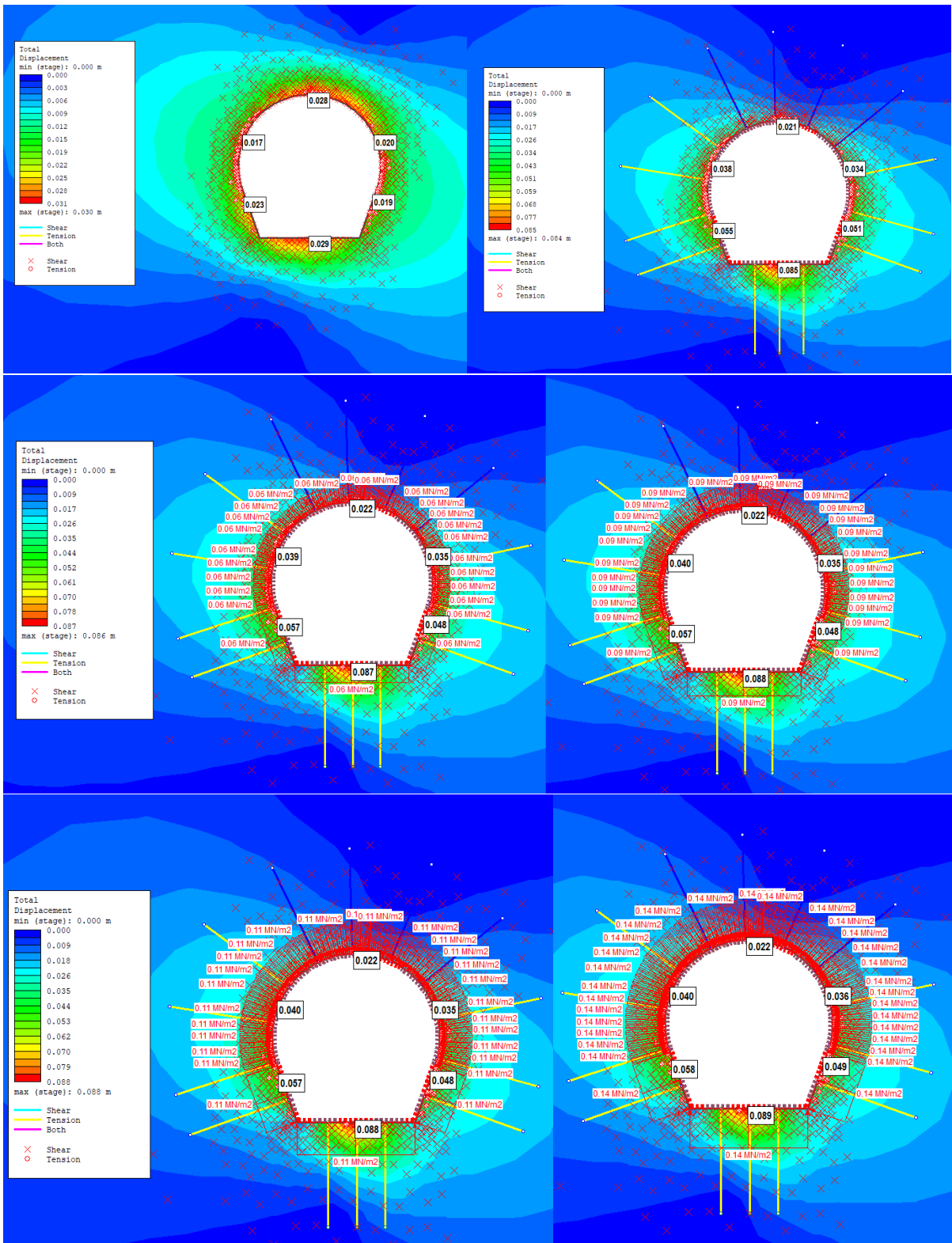
Appearance of rock mass	Description of rock mass	Suggested value of <i>D</i>
	Excellent quality controlled blasting or excavation by Tunnel Boring Machine results in minimal disturbance to the confined rock mass surrounding a tunnel.	<i>D</i> = 0
	Mechanical or hand excavation in poor quality rock masses (no blasting) results in minimal disturbance to the surrounding rock mass. Where squeezing problems result in significant floor heave, disturbance can be severe unless a temporary invert, as shown in the photograph, is placed.	<i>D</i> = 0 <i>D</i> = 0.5 No invert
	Very poor quality blasting in a hard rock tunnel results in severe local damage, extending 2 or 3 m, in the surrounding rock mass.	<i>D</i> = 0.8
	Small scale blasting in civil engineering slopes results in modest rock mass damage, particularly if controlled blasting is used as shown on the left hand side of the photograph. However, stress relief results in some disturbance.	<i>D</i> = 0.7 Good blasting <i>D</i> = 1.0 Poor blasting
	Very large open pit mine slopes suffer significant disturbance due to heavy production blasting and also due to stress relief from overburden removal. In some softer rocks excavation can be carried out by ripping and dozing and the degree of damage to the slopes is less.	<i>D</i> = 1.0 Production blasting <i>D</i> = 0.7 Mechanical excavation

B Numerical Modeling Results

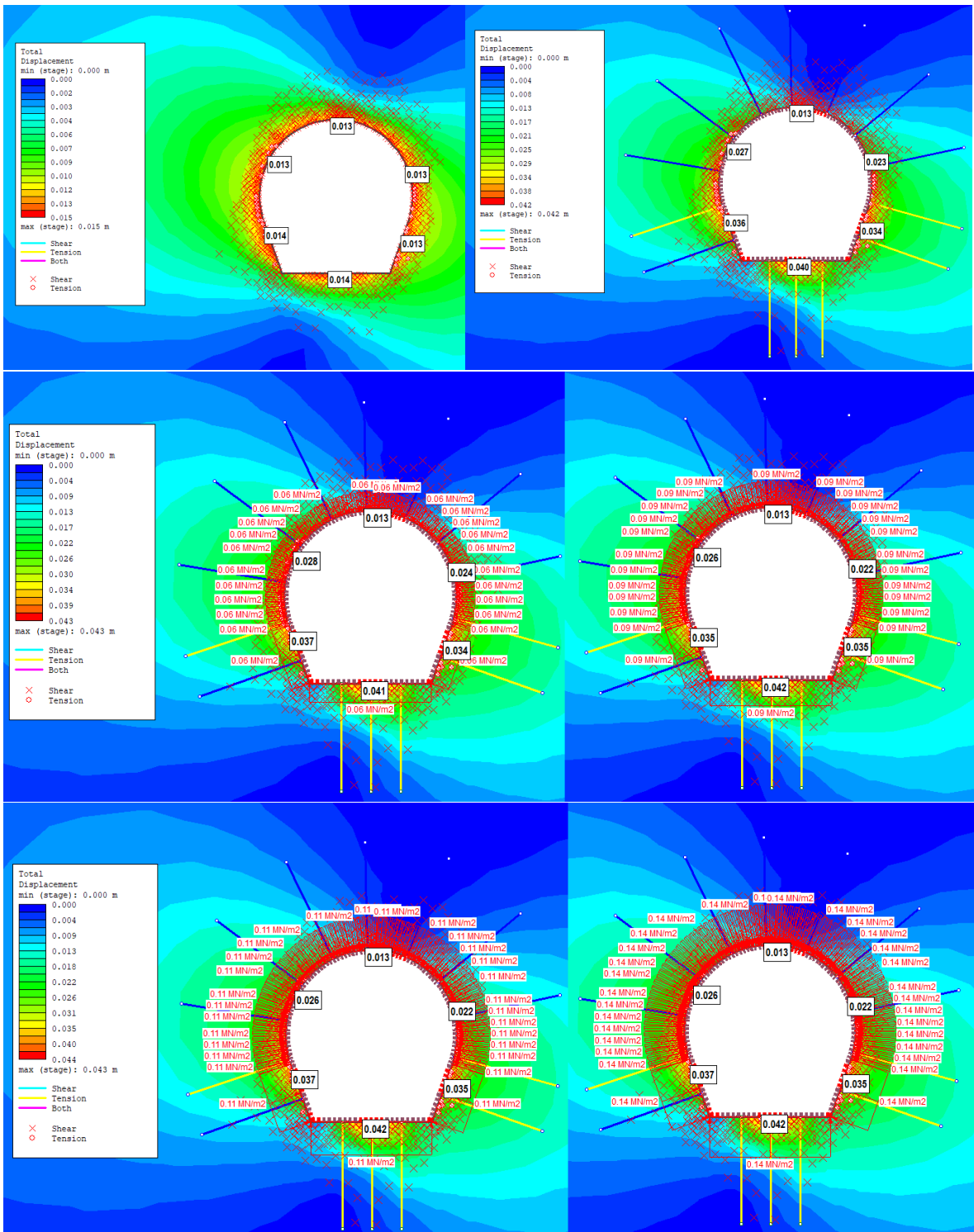
B.1 Plastic deformation and long-term deformation due to swelling pressure at Chainage 7+064



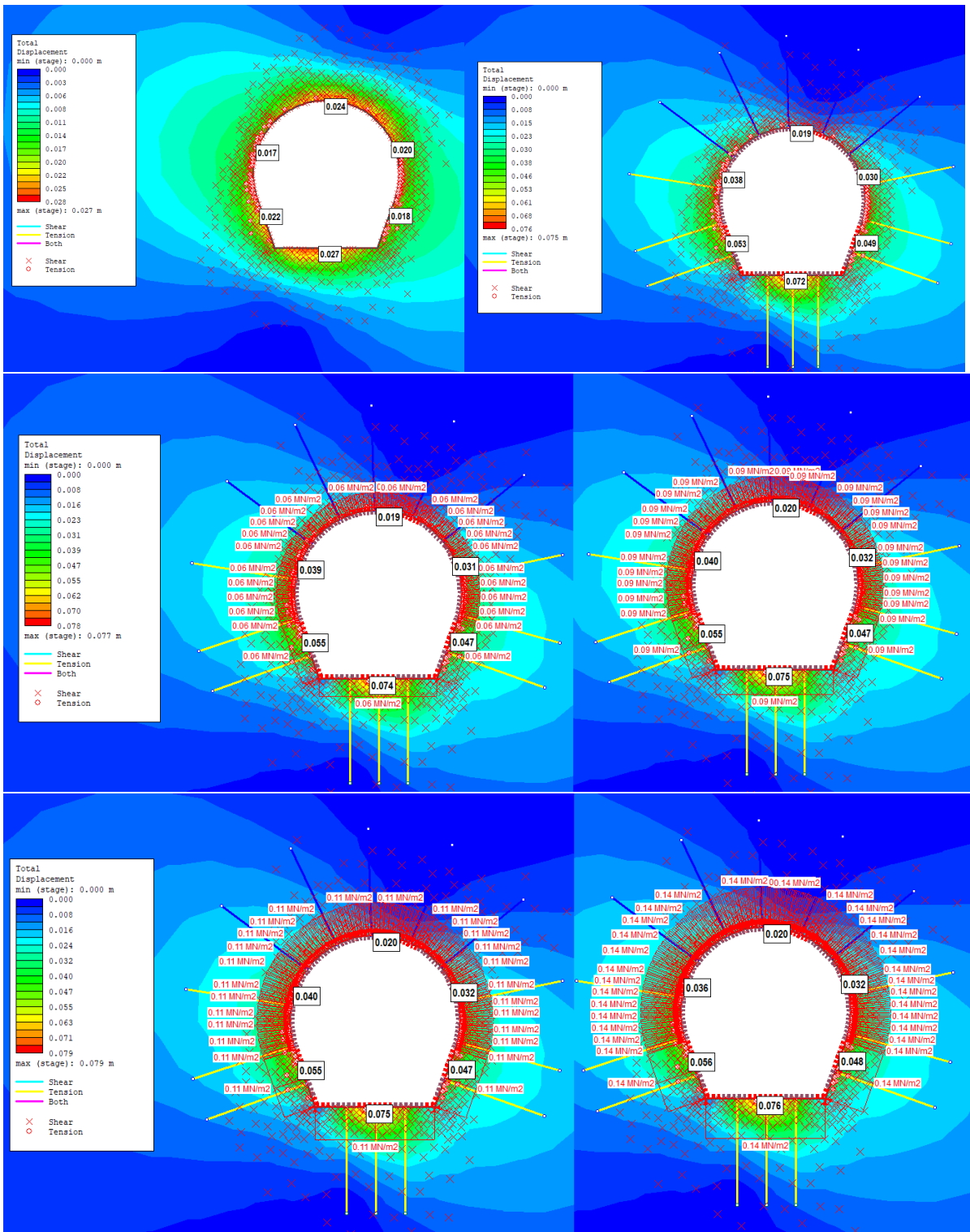
B.2 Plastic deformation and long-term deformation due to swelling pressure at Chainage 7+092



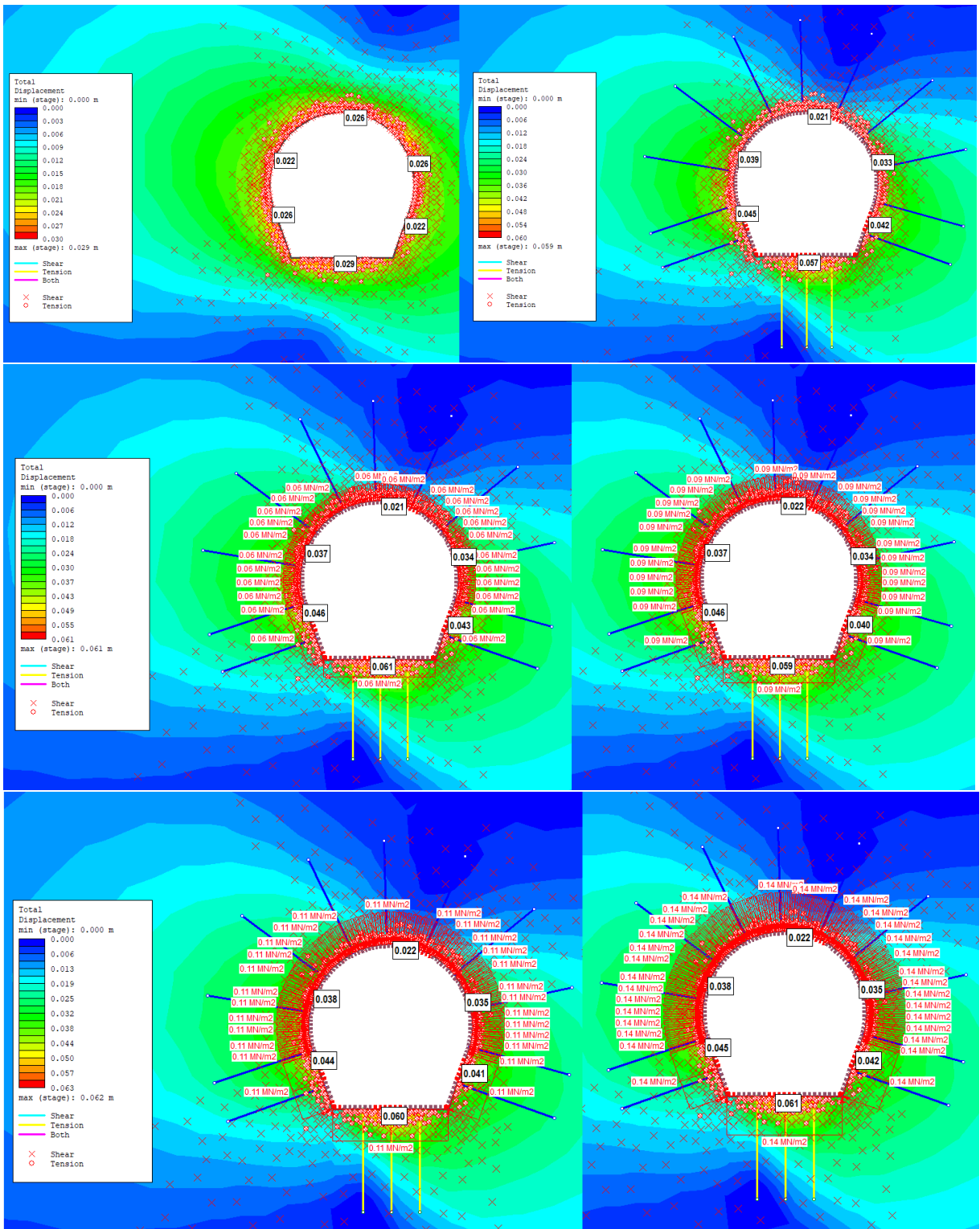
B.3 Plastic deformation and long-term deformation due to swelling pressure at Chainage 7+136



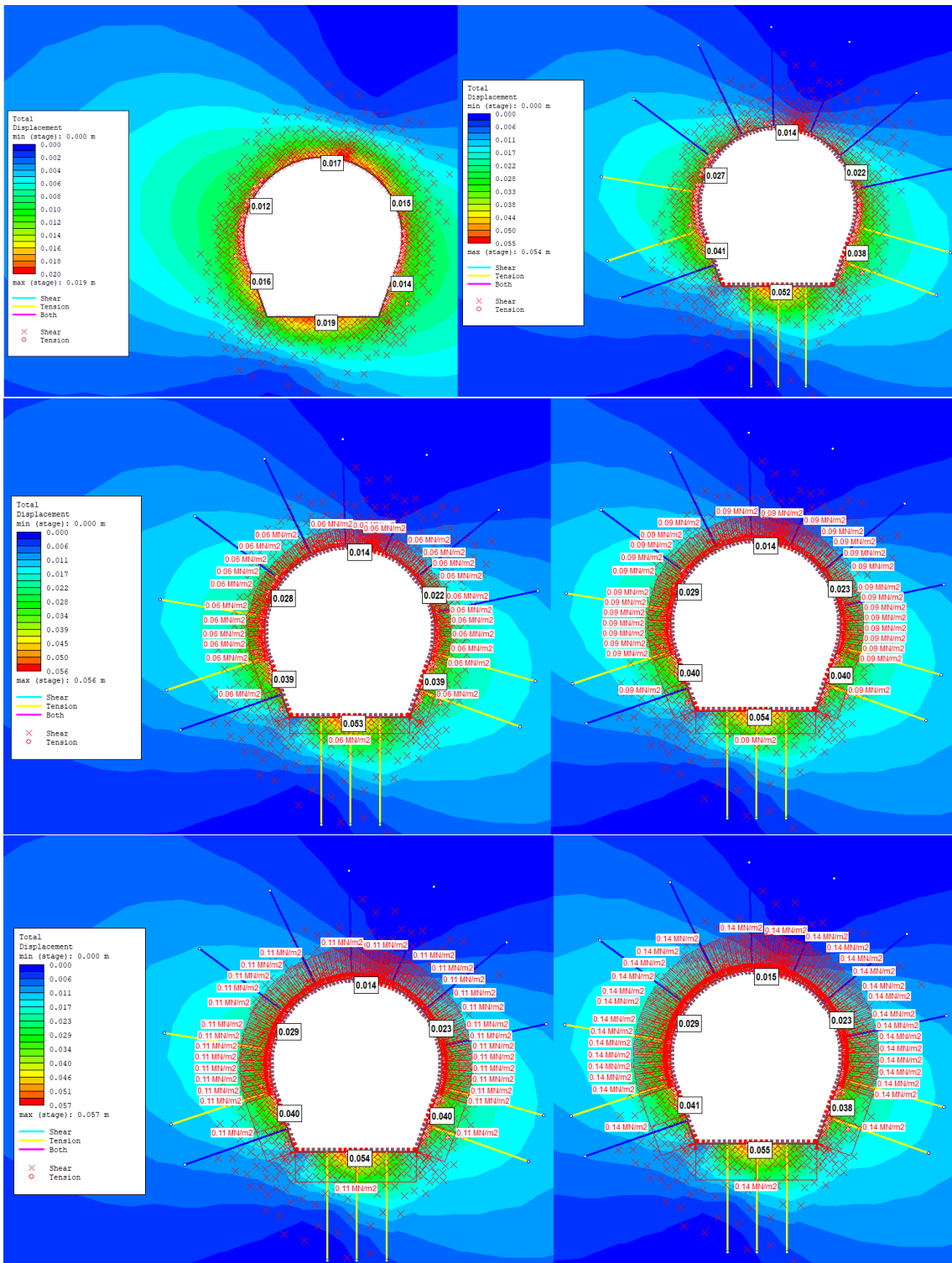
B.4 Plastic deformation and long-term deformation due to swelling pressure at Chainage 7+168



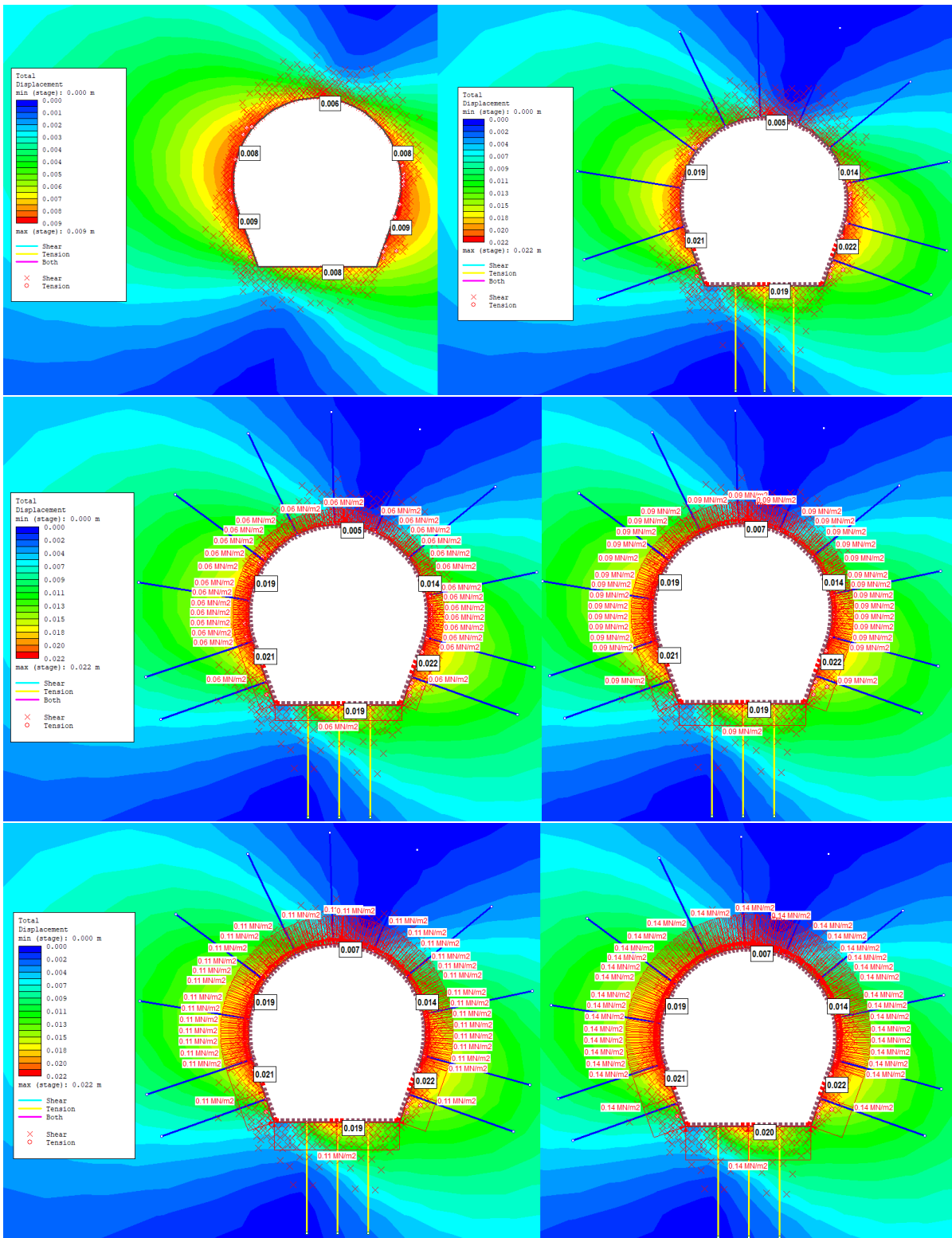
B.5 Plastic deformation and long-term deformation due to swelling pressure at Chainage 7+194



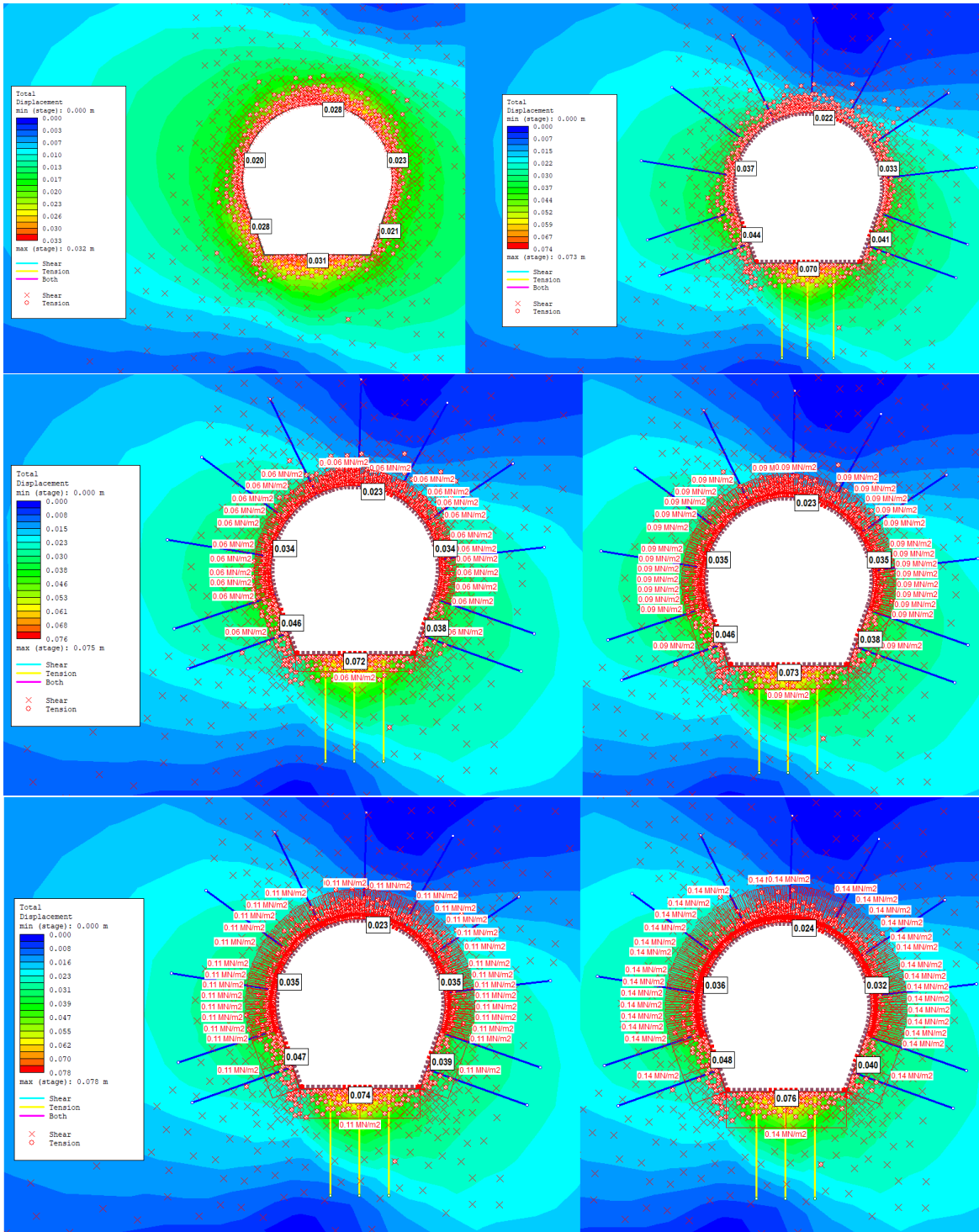
B.6 Plastic deformation and long-term deformation due to swelling pressure at Chainage 7+218



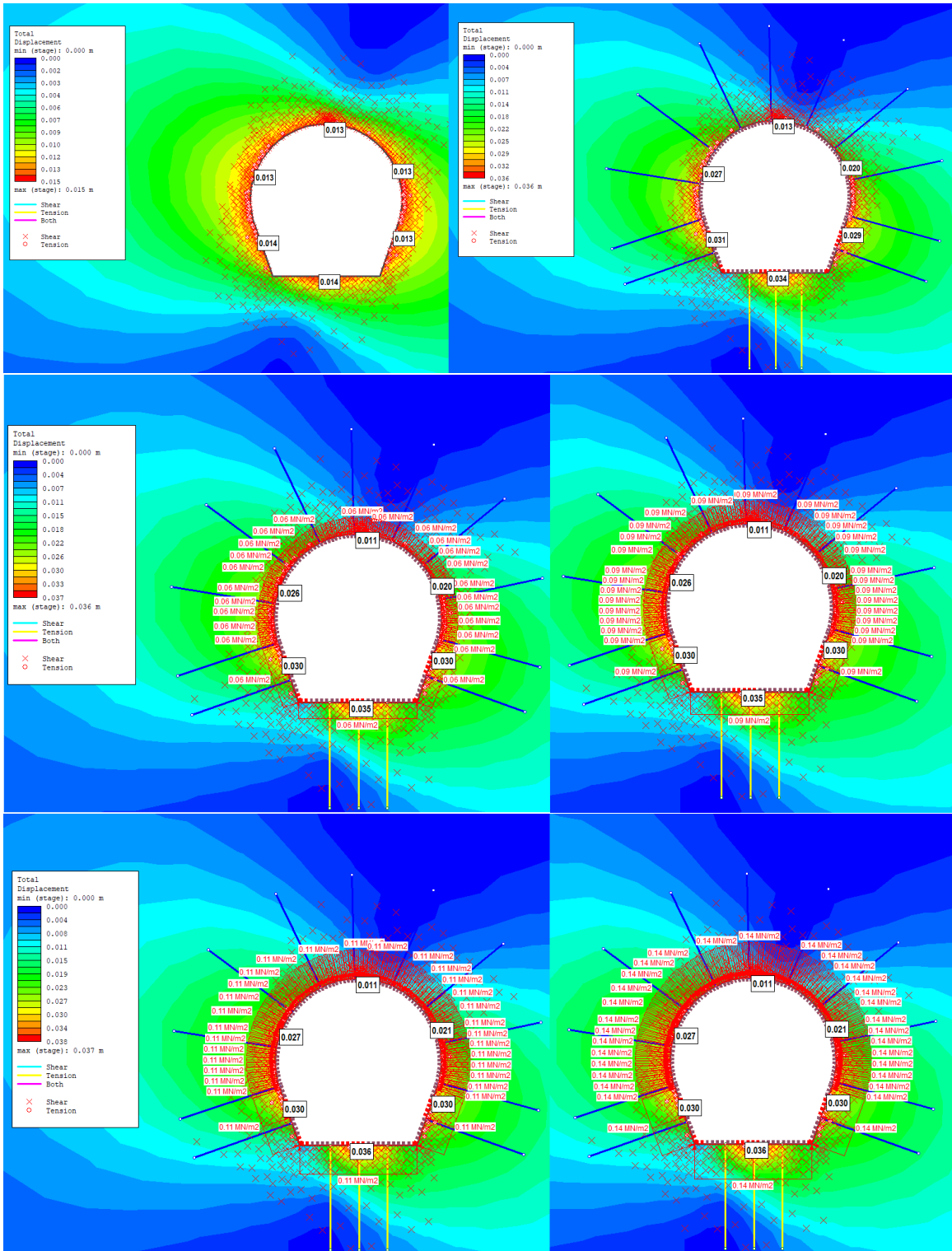
B.7 Plastic deformation and long-term deformation due to swelling pressure at Chainage 7+266



B.8 Plastic deformation and long-term deformation due to swelling pressure at Chainage 7+291



B.9 Plastic deformation and long-term deformation due to swelling pressure at Chainage 7+316



B.10 Plastic deformation and long-term deformation due to swelling pressure at Chainage 7+342

